



# Brain network estimation from dense EEG signals : application to neurological disorders

Aya Kabbara

## ► To cite this version:

Aya Kabbara. Brain network estimation from dense EEG signals : application to neurological disorders. Neurons and Cognition [q-bio.NC]. Université de Rennes; Université Libanaise, 2018. English. NNT : 2018REN1S028 . tel-01943768

**HAL Id: tel-01943768**

**<https://theses.hal.science/tel-01943768>**

Submitted on 4 Dec 2018

**HAL** is a multi-disciplinary open access archive for the deposit and dissemination of scientific research documents, whether they are published or not. The documents may come from teaching and research institutions in France or abroad, or from public or private research centers.

L'archive ouverte pluridisciplinaire **HAL**, est destinée au dépôt et à la diffusion de documents scientifiques de niveau recherche, publiés ou non, émanant des établissements d'enseignement et de recherche français ou étrangers, des laboratoires publics ou privés.

**THÈSE / UNIVERSITÉ DE RENNES 1**

*sous le sceau de l'Université Bretagne Loire*

En cotutelle internationale avec  
**L'Université libanaise, Liban**

pour le grade de

**DOCTEUR DE L'UNIVERSITÉ DE RENNES 1**

*Mention : Signal, Image, Vision*

**Ecole doctorale MathSTIC**

présentée par

**Aya Kabbara**

Préparée à l'unité de recherche LTSI-Inserm U1099  
Laboratoire Traitement du Signal et de l'Image- Université de rennes1  
ISTIC informatique-électronique

---

**Estimation des  
réseaux cérébraux à  
partir de l'EEG-hr:  
application sur les  
maladies  
neurologiques**

**Thèse soutenue au Liban  
le 19 juin 2018**

devant le jury composé de :

**Olaf SPORNS**

Professeur, Indiana University / *rapporteur*

**Fadi KARAME**

Professeur associé, American University of Beirut /  
*rapporteur*

**Sophie ACHARD**

Chercheur au CNRS, GIPSA-Lab / *examineur*

**Arij DAOU**

Professeur assistant, American University of Beirut /  
*examineur*

**Fabrice WENDLING**

Directeur de recherche Inserm, Université de  
Rennes1/ *directeur de thèse*

**Mohamad KHALIL**

Professeur, Université libanaise/ *directeur de thèse*

**Mahmoud HASSAN**

Post-doc, Université de Rennes1/ *co-directeur de  
thèse*

**Wassim EL FALOU**

Professeur, Université libanaise/ *co-directeur de  
thèse*



# Résumé en français

Le cerveau humain est un système interconnecté très complexe. L'identification de réseaux cérébraux fonctionnels et l'analyse de leurs dynamiques est un enjeu important non seulement pour comprendre le fonctionnement normal du cerveau mais aussi pour développer des méthodes diagnostiques dans les désordres neurologiques. Les études récentes montrent que de tels désordres sont le plus souvent associés à des anomalies dans la connectivité cérébrale qui entraînent des altérations dans des réseaux cérébraux «large-échelle» impliquant des régions distantes. C'est particulièrement le cas pour l'épilepsie et les maladies neurodégénératives (Alzheimer, Parkinson) qui constituent, selon l'OMS, un enjeu majeur de santé publique. Dans ce contexte, la demande clinique est très forte pour de nouvelles méthodes capables d'identifier des réseaux pathologiques, simple à mettre en œuvre et surtout non invasives.

**L'objectif principal de cette thèse est de développer des méthodes d'identification de réseaux pathologiques à partir de l'électroencéphalographie à haute résolution spatiale (EEG-hr, 256 électrodes) qui bénéficie, par ailleurs, et intrinsèquement, de l'excellente résolution temporelle de l'EEG (~1ms).**

Durant cette thèse, deux questions principales ont été abordées :

- 1- **Comment suivre la dynamique spatio-temporelle des réseaux cérébraux ?** Tout d'abord, des données EEG enregistrées chez des sujets sains en états de repos (resting-state) ont été analysées. Une méthode développée dans l'équipe dite « connectivité de sources » a été utilisée pour identifier les réseaux cérébraux au niveau cortical à partir des enregistrements EEG de scalp. Nous avons eu une attention particulière pour l'aspect dynamique de ces réseaux et leur reconfiguration en fonction du temps à une échelle temporelle très courte (centaine de millisecondes). En profitant de la résolution temporelle offerte par l'EEG (milliseconde), nous avons pu développer des méthodes pour suivre les dynamiques spatiotemporelles des réseaux cérébraux fonctionnels. Cela a été fait en étendant la méthode « connectivité de sources » afin de générer des réseaux dynamiques en utilisant une approche basée sur des fenêtres glissantes. Ensuite, nous avons exploité la topologie de ces réseaux dynamiques en utilisant la théorie de graphe. Les résultats ont montré la capacité de l'approche proposée pour suivre les



dynamiques spatio-temporelles des réseaux cérébraux impliqués à l'état de repos. La présence des régions cérébrales considérées comme des « Hubs » a été aussi abordée. Les résultats ont également révélé que les mêmes régions cérébrales peuvent alterner dynamiquement et jouer le rôle de hubs provinciaux (locaux) ou de connecteurs (globaux).

Ensuite, une nouvelle méthode, qui vise à explorer les changements dynamiques des structures modulaires du cerveau, a été aussi proposée. La méthode proposée peut être appliquée pendant l'état de repos ou pendant une tâche cognitive. La méthode a été validée sur des données simulées, et des données d'électroencéphalographie (EEG) et magnétoencéphalographie (MEG) enregistrées pendant le repos et pendant l'exécution d'une tâche cognitive (dénomination d'objet et tâche motrice). Les résultats ont montré la capacité de l'algorithme proposé à identifier les structures modulaires avec une bonne précision spatio-temporelle.

- 2- **Comment élaborer de nouveaux neuromarqueurs?** Les méthodes développées et testées sur des sujets sains en états de repos ont été évaluées dans le contexte des troubles neurologiques.

La première application clinique est la maladie d'Alzheimer. L'objectif ici est de proposer des nouveaux neuromarqueurs du déclin cognitif calculés sur les réseaux cérébraux identifiés à l'état de repos. Nous avons commencé par analyser les changements topologiques qui se produisent dans les réseaux dynamiques des patients qui souffrent d'Alzheimer. Des données EEG ont été enregistrées chez 20 participants (10 patients et 10 sujets sains) à l'état de repos.

Les résultats ont démontré que les réseaux pathologiques, sont caractérisés par un traitement global de l'information (intégration) plus faible et un traitement de l'information locale (ségrégation) plus élevé comparés aux réseaux normaux. Les résultats ont également montré une corrélation entre les altérations des réseaux cérébraux des patients souffrants d'Alzheimer et leurs scores cognitifs.

La 2<sup>ème</sup> application clinique est l'épilepsie. L'objectif ici est d'identifier les réseaux épileptogènes à partir des signaux EEG-hr de scalp. Les réseaux identifiés à partir de l'EEG-hr ont été comparés aux enregistrements intracérébraux (stéréo-EEG, SEEG) enregistrés chez les mêmes patients. L'approche appliquée ici est principalement basée sur des paramètres de graphe qui quantifient les réseaux cérébraux locaux. Inspirée de la compréhension actuelle des réseaux épileptogènes,

notre approche soutient l'hypothèse suivante: une région cérébrale, qui montre une fonctionnalité locale significativement élevée, joue un rôle central dans le réseau épileptogène. Les résultats ont été validés par la comparaison entre les positions des régions cérébrales détectées par l'EEG de scalp à la position des électrodes intracérébrales.

# Abstract

The brain is organized into large-scale functional networks that can flexibly reconfigure their connectivity patterns. Thus, the identification and the analysis of their dynamic functional connectivity can help to better understand the neurological diseases, the general functioning of the brain and to develop new diagnostic methods. It is now recognized that neurological pathologies are due to alterations in these brain networks. Today, a number of modalities and techniques are proposed to identify and analyze these networks to observe their alterations. **The main objective of my thesis is to develop methods to identify these pathological networks from electroencephalography (EEG)** with high spatial resolution (dense-EEG, 256 electrodes) in addition to the excellent temporal resolution (~1ms).

In this thesis, two main challenges were addressed:

## **1- Tracking dynamics of functional brain networks**

First, dense-EEG data recorded in healthy subjects at rest were analyzed. A recently developed method called “EEG source connectivity” was used to identify brain networks at the cortical level from scalp EEG recordings.

I was more interested in studying the dynamic behaviors of brain networks and their reconfiguration on a very short time-scale (sub-second). This was done by extending the "source connectivity" method to generate dynamic networks using a sliding window approach. The topology of the obtained networks was then analyzed using graph theory. Results showed the ability of the method to follow the spatiotemporal dynamics of brain networks involved in the resting state. The existence of brain regions considered as "Hubs" has been investigated. Results also revealed that the same brain regions can alternate dynamically and play the role of provincial (local) hubs or (global) connectors.

In addition, a new method, which aims to explore the dynamic changes of the modular structures of the brain, was proposed. The method presents two algorithms that can be applied during a resting state paradigm, or during a task-directed paradigm (cognitive task). The method was validated on simulated data, and EEG/ MEG) data recorded at rest and during cognitive tasks. Results showed the capacity of the proposed algorithm to identify fast modular structures with good space/time accuracies.

## **2- Developing EEG network-based neuromarkers of brain disorders**

The first clinical application is in the context of Alzheimer's disease (AD). The main objective of this work was to explore the topological changes that occur in the dynamic networks of AD patients. EEG data were recorded in 20 participants (10 patients and 10 healthy subjects) at rest. Results revealed that pathological networks are characterized by lower global information processing (integration) and higher local information processing (segregation) compared to healthy networks. Results also showed a significant correlation between the alterations of the brain networks of AD patients and their cognitive scores.

The second clinical application is epilepsy. The objective of this work was to identify epileptogenic networks from scalp EEG signals. The networks identified from dense-EEG were compared to intracerebral recordings (stereo-EEG, SEEG) recorded for the same patients. The approach applied here was mainly based on graph parameters that quantify the local functional networks. Inspired by the current understanding of epileptogenic networks, our approach supports the following hypothesis: a brain region, which shows significantly high local functionality, plays a central role in the epileptogenic network. Results justify the utility of our hypothesis by comparing the positions of the nodes detected using EEG to that of intracerebral recordings. We showed that the proposed approach is very promising in matching cortical brain regions located in the neighborhood of the SEEG implementation.

## TABLE OF CONTENTS

<b>CHAPTER 1. INTRODUCTION.....</b>	<b>9</b>
<b>1.1.CONCEPT: THE BRAIN AS A DYNAMIC NETWORK .....</b>	<b>9</b>
<b>1.2.NETWORKS AND GRAPHS: DEFINITION .....</b>	<b>10</b>
<b>1.3.NETWORK MEASURES.....</b>	<b>11</b>
1.3.1.DEGREE, IN-DEGREE, OUT-DEGREE AND STRENGTH: .....	11
1.3.2.CLUSTERING COEFFICIENT: .....	12
1.3.3.PATH LENGTH, DISTANCE AND GLOBAL EFFICIENCY: .....	12
1.3.4.MODULARITY, WITHIN-DEGREE MODULE, PARTICIPATION COEFFICIENT: .....	13
1.3.5.HUBS: 13	
<b>1.4.BRAIN CONNECTIVITY .....</b>	<b>15</b>
<b>1.5.NEUROIMAGING TECHNIQUES .....</b>	<b>17</b>
1.5.1.FUNCTIONAL MAGNETIC RESONANCE IMAGING (fMRI): .....	17
1.5.2.ELECTRO-ENCEPHALOGRAPHY/ MAGNETO-ENCEPHALOGRAPHY (EEG/MEG): .....	17
<b>1.6.EEG/MEG SOURCE CONNECTIVITY .....</b>	<b>20</b>
1.6.1.SOLVING THE INVERSE PROBLEM: .....	22
1.6.2.FUNCTIONAL CONNECTIVITY ESTIMATION .....	23
<b>1.7.DYNAMIC FUNCTIONAL NETWORKS .....</b>	<b>24</b>
<b>1.8.THESIS OBJECTIVE.....</b>	<b>25</b>
<b>CHAPTER 2. RESULTS .....</b>	<b>28</b>
<b>STUDY 1: IDENTIFICATION OF INTERICTAL EPILEPTIC NETWORKS FROM DENSE-EEG 28</b>	
<b>STUDY 2: THE DYNAMIC FUNCTIONAL CORE NETWORK OF THE HUMAN BRAIN AT REST</b>	
<b>.....</b>	<b>29</b>
<b>STUDY 3: REDUCED INTEGRATION AND IMPROVED SEGREGATION OF FUNCTIONAL</b>	
<b>BRAIN NETWORKS IN ALZHEIMER'S DISEASE .....</b>	<b>30</b>
<b>STUDY 4: DENSE SCALP-EEG SOURCE CONNECTIVITY PREDICTS DEPTH-EEG</b>	
<b>EXPLORATION IN EPILEPSY .....</b>	<b>31</b>
<b>STUDY 5: TRACKING FAST MODULAR BRAIN STATES IN REST AND TASK .....</b>	<b>32</b>
<b>CHAPTER 3. DISCUSSION .....</b>	<b>33</b>
<b>3.1. DYNAMIC FUNCTIONAL NETWORKS AT REST AND TASK .....</b>	<b>34</b>
<b>3.2. TOWARD EEG NETWORK-BASED NEUROMARKERS OF BRAIN DISORDERS .....</b>	<b>36</b>
<b>3.3. METHODOLOGICAL CONSIDERATION .....</b>	<b>37</b>
3.3.1. SOURCE LEAKAGE: .....	37
3.3.2. THE ILL-POSED INVERSE PROBLEM.....	38
3.3.3. EFFECT OF THE INVERSE/CONNECTIVITY MEASURE: .....	39
3.1.4. SELECTING THE SLIDING WINDOW LENGTH: .....	40
3.1.5. THRESHOLDING THE CONNECTIVITY MATRIX: .....	41
<b>3.4. FUTURE DIRECTIONS .....</b>	<b>41</b>

# Chapter 1.

## INTRODUCTION

*“Everything appears to be connected in ways that were absolutely unpredictable just ten years ago, or even five years ago”.*

*-Professor Marc Vidal*

We are all part of multiple complex networks: a network of interacting particles in the universe, a network of city streets on the Earth’s surface and a network of friends, co-workers, neighbors and family. Interestingly, one of the most important networks that we engage with, in our everyday life, is the network of the brain.

It is now well recognized that the brain is a coherent connective system composed of multiple individual units (from cells to areas) interacting with each other.

### **1.1. Concept: The brain as a dynamic network**

Emerging evidence show that most cognitive states and behavioral functions depend on the activity of many brain regions operating as a large-scale network (1–9). To understand this network, it is insufficient to study the activity of a brain region in isolation, but to study the ways in which the brain regions interact and communicate. As many brain responses only last on the order of milliseconds to seconds (10–12), the brain dynamically reconfigures its network organization at sub-second temporal scale to guarantee an efficient cognitive function. Accordingly, several studies have been conducted to assess the spatiotemporal dynamics of functional brain networks during cognitive processes (13–18). This dynamical behavior is even present in the pattern of intrinsic or spontaneous brain activity (i.e when the person is at rest) (17,19–23). Relying on this conceptual understanding, network neuroscientists endeavor to explore the dynamics of the brain connectivity patterns and how they are linked to cognitive and resting conditions. Still, an accurate tracking of the spatiotemporal dynamics of large-scale networks remain an unsolved issue (13).

On the other hand, a large body of studies revealed that neurological disorders (including Epilepsy, Alzheimer, Parkinson...etc.) are associated with disruptions in the structural and

functional organization of the brain (24,25). The identification of the related brain networks alterations will help to better understand the neural mechanisms underlying brain disorders, and hence to better monitor and treat patients. From a clinical perspective, the demand is high for non-invasive and easy-to-use methods to identify the pathological networks. More precisely, novel ‘neuromarkers’ able to characterize network alterations and associated cognitive deficits are needed.

In this thesis, two main challenges are addressed:

- 1- Tracking the dynamic changes of brain networks during rest and task at sub-second time scale.
- 2- Characterizing and identifying the pathological brain networks using a non-invasive technique.

To address both issues, we made use of the electro-encephalography (EEG) which is a non-invasive technique offering an excellent temporal resolution that is not reachable using other techniques such as the fMRI (26–28). The approach adapted is based on a recently developed method called “EEG source connectivity” combined with graph theory.

This chapter presents the background for the understanding of the work, and is organized as follows. First, we start by defining the networks and describing some of the most important network measures derived from graph theory. We then move on to the concept of brain connectivity, focusing on the key distinction between functional, structural and effective brain networks. Afterwards, we introduce the non-invasive neuroimaging techniques used to reconstruct the functional brain networks. Finally, the approach based on “EEG/MEG source connectivity” is described.

## **1.2. Networks and graphs: Definition**

By rendering the brain into a network, network science offers a powerful framework to infer the quantitative organizational properties of brain networks using a branch of mathematics known as graph theory.

A graph is the mathematical representation of a network. It is basically composed of nodes interconnected with edges. Nodes constitute the elementary components of the system such as airports in the airline network. Edges represent the connections or the interactions

between the nodes such as flights between airports. Two connected nodes are often named as “neighbors” (29). Depending on the nature of edges, a graph can be categorized into one of four types: directed/undirected and weighted/binary graph (Figure 1.A).

A Graph can be also represented by a connectivity matrix, referred to as “adjacency matrix” where nodes are represented by rows or columns, and edges are represented by matrix elements. In weighted networks, matrix elements are continuous values and can range from strong (highest number) to weak (lowest number). In contrast, in binary matrix, elements are either 0 (connection does not exist) or 1 (connection exists). The undirected graphs are illustrated by a symmetrical matrix. Figure 1.B presents the adjacency matrices of each graph type.

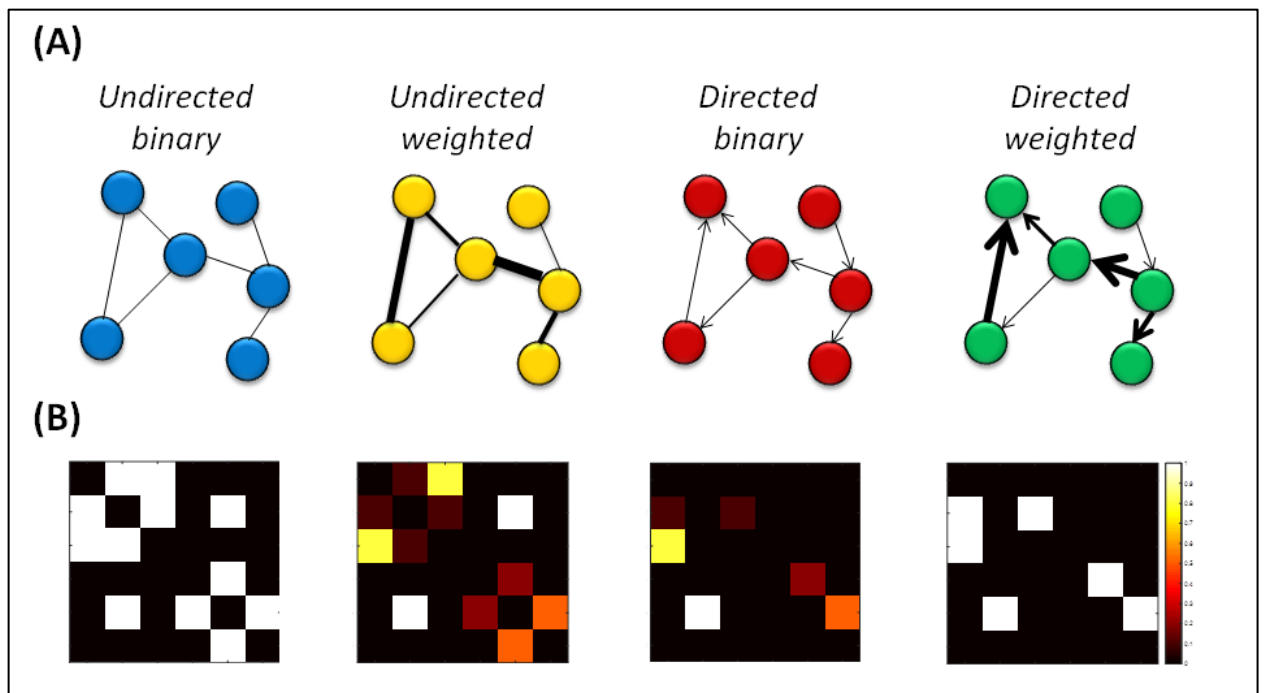


Figure 1. The four types of graph and their corresponding adjacency matrix.

### 1.3. Network measures

In practice, graph theory offers many quantitative tools to characterize global and local network properties. In this section, we describe the most used graph or network measures in the context of brain networks analysis (Figure 2).

#### 1.3.1. Degree, in-degree, out-degree and strength:

The simplest measure that can be captured is the node’s degree, which is the number of edges attached to a particular node (30). In directed graphs, the in-degree and out-degree are the number of incoming and outgoing connections, respectively (29). For weighted



networks, another measure can be examined which is the node's strength (31). It is defined as the sum of all edges weights connected to a node. These four measures indicate how influential an element is with respect to other elements. Generally, nodes with high degree or strength values are considered to have high number of interconnected nodes. High in-degree nodes are influenced by many other nodes while high out-degree nodes are interpreted as influencer elements in the system.

### ***1.3.2. Clustering coefficient:***

The clustering coefficient of a node evaluates the density of connections formed by its neighbors (32). It is calculated by dividing the number of existing edges between the node's neighbors to the number of possible edges that can exist between them. The average of all nodes' clustering coefficients is the mean clustering coefficient of the whole network. The clustering coefficient is one of the measures used to quantify the local neighborhood and the specialization information in a network, often referred to "local segregation" (33).

### ***1.3.3. Path length, distance and global efficiency:***

In a network, a node can be directly linked to another node using an edge, or indirectly linked using one or many intermediate nodes. Thus, the communication between each pair of nodes is underlined by either short or long path length. In a binary network, the path length between two nodes is the number of connecting edges. In a weighted network, the length of a path represents the sum of the edge weights. The topological distance between two nodes is the length of the shortest path length linking them. Generally, the communication along short paths is thought to be more effective since it is faster, more direct, and less corrupted by noise effects. The global efficiency is the average of the inverse of the distance matrix (34). A network with high global efficiency indicates that, on average, nodes are reached by short communications. The efficiency is then used to quantify the global communication of a network, often referred to "global integration" (33).

#### ***1.3.4. Modularity, within-degree module, participation coefficient:***

The modularity shows the tendency of a network to be partitioned into modules or communities of high internal connectivity and low external connectivity (35,36). Once a network is composed into modules, many graph metrics can be derived. One of the interesting measures is the within-degree module that assesses the connectivity of each node within its same community. Another measure is the participation coefficient that computes how much a node is connected to nodes of other communities. The within-degree module and the participation coefficient illuminate about the extent to which information is segregated and specialized into modules, and the extent to which information is distributed and shared between modules (37).

#### ***1.3.5. Hubs:***

Hubs are components or nodes that play a key role in establishing and maintaining an efficient communication in a network (38). The identification of hubs can infer from many graph measures including the degree, the strength, the betweenness-centrality and the vulnerability (39–42). In addition, hubs can be classified into provincial and connector hubs (37,38,43–45). The main difference is that provincial hubs are mostly connected to nodes within their own module while connector hubs attempt to connect several modules.

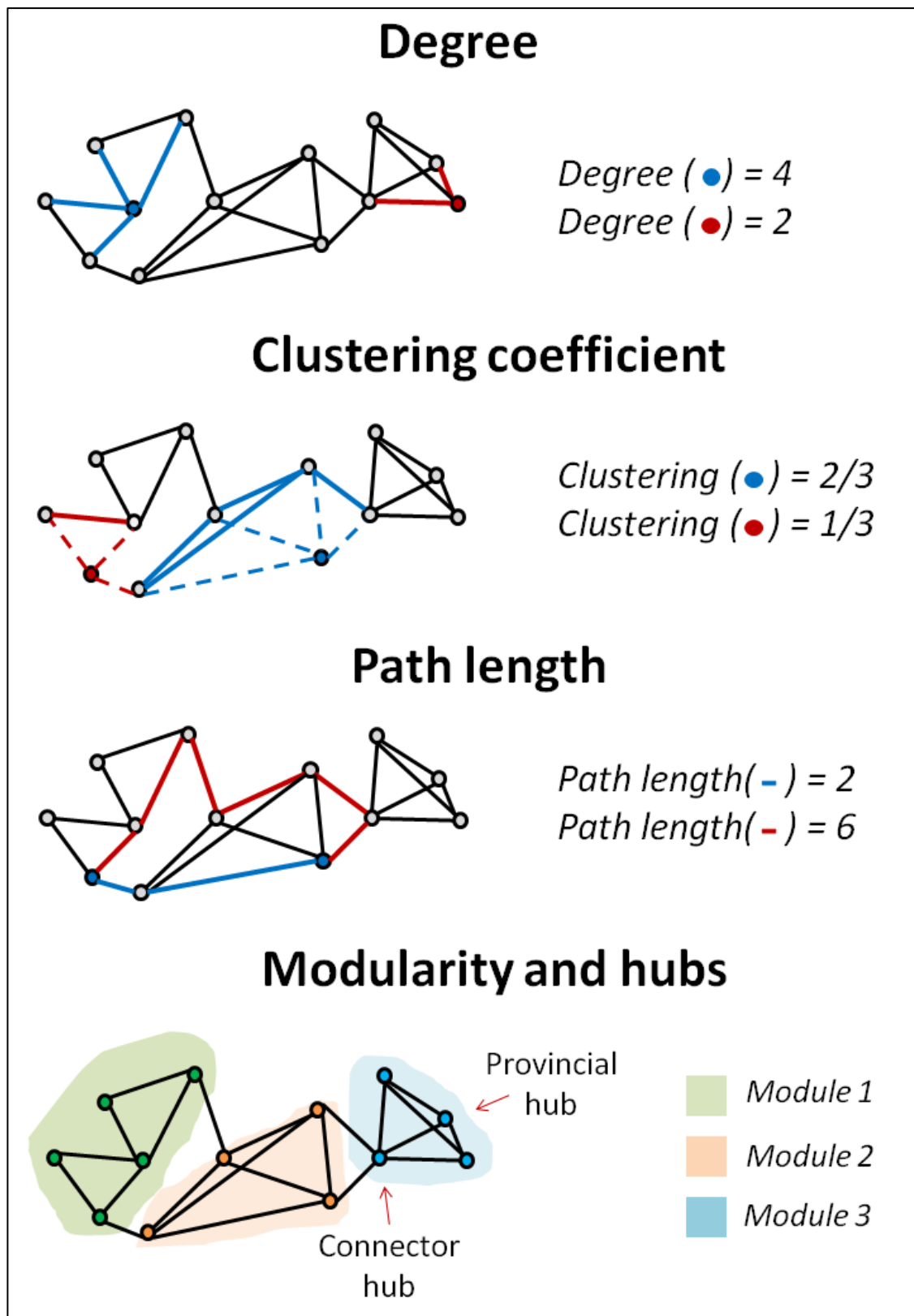


Figure 2. Some of the network measures used to quantify the characteristics of an undirected binary graph: degree, clustering coefficient, path length, modularity and hubs.

## 1.4. Brain connectivity

Brain connectivity refers to a set of connections linking neural elements. Given the broad range of neuroimaging techniques used to record the brain activity, it is expected to have different ways to analyze the brain connectivity. Mainly, the major distinction is between the structural connectivity, the functional connectivity and the effective connectivity (33,46–48).

Structural connectivity is defined as the physical or anatomical connections between units of the brain. This type of connectivity is generally inferred by the white matter tracts imaged using the diffusion tensor imaging. Structural networks are static networks at the short time scale (seconds to minutes), but can be dynamic at longer time scale (from hours to years). Numerous studies have analyzed the brain topology of structural brain networks at rest (49–53). It has been also revealed that structural connectivity analysis is sensitive to detect alterations of brain networks associated with brain disorders (54–60).

Functional connectivity refers to the statistical dependencies between neuronal populations. Functional brain networks are derived from electrophysiological time-series using electro-encephalography (EEG), magneto-encephalography (MEG) and functional magnetic resonance (fMRI). This type of network is time-dependent and modifies on short time scale. The temporal correlation can be measured using linear correlation, non-linear correlation, coherence, phase locking value and many other metrics (see Section 1.6.2). The functional connectivity was shown as a powerful tool to understand the mechanism underlying the information processing during rest (19,21,22,61–66) and task (14,16,67–71). Many studies have also explored the functional disruption of the brain networks in brain disorders (72–84).

The way in which the functional networks are computed in our work will be fully described in section 1.6.

Effective connectivity describes the direct interactions between neural elements. Many methods are proposed to construct the effective networks based such as granger-causality (85) and Dynamic Causal Modeling (86). Like functional connectivity, effective connectivity is dynamic and is derived from time-series data.

Figure 3 illustrates the difference between structural and functional/effective connectivity.

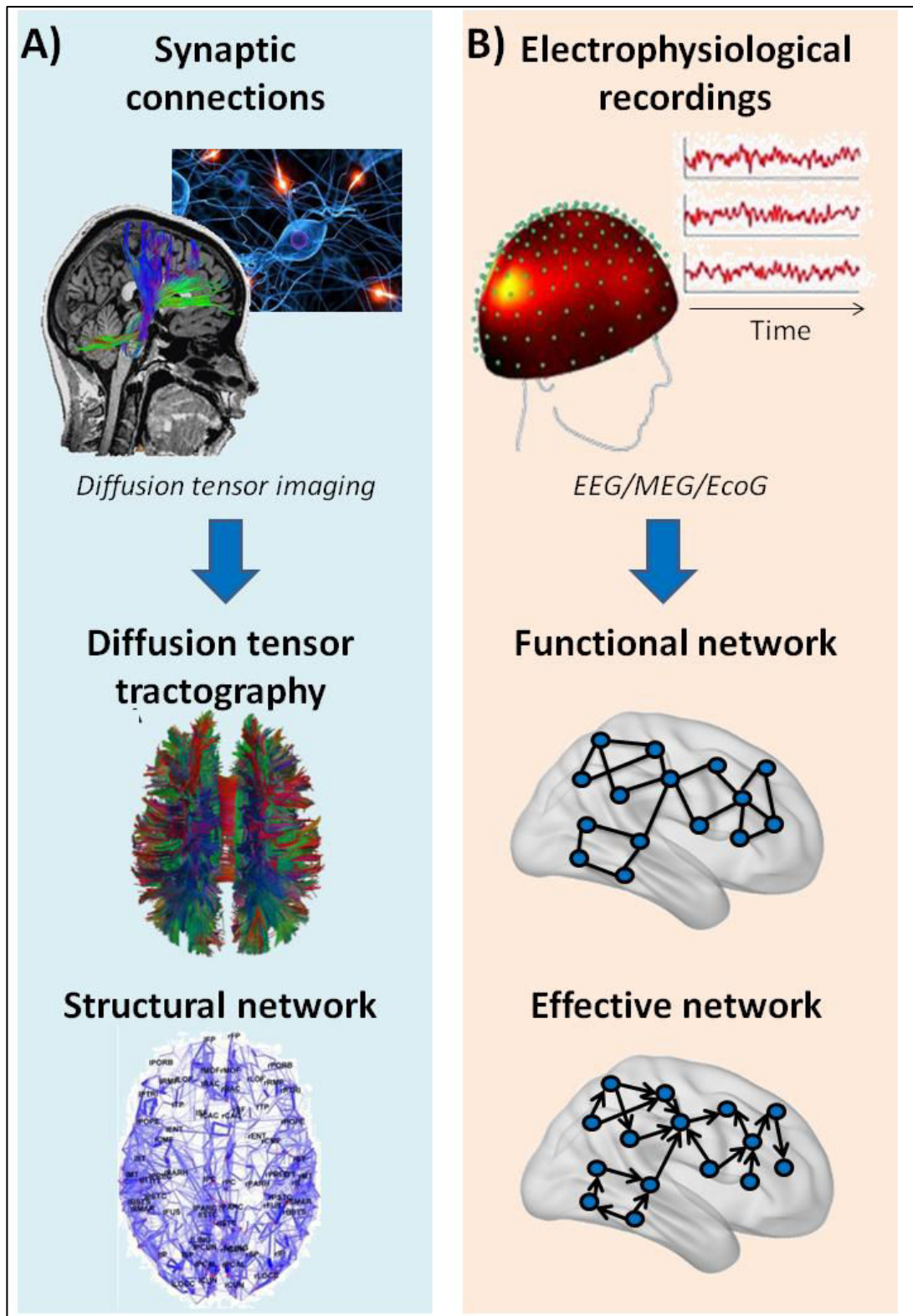


Figure 3. Principal elements of the connectivity analysis. A) structural networks refer to anatomical connections between neural elements, such as synapses linking neurons, or fiber tracts connecting large brain regions. B) functional networks as well as effective networks are derived from electrophysiological data time series. Functional networks present statistical dependencies between brain areas while effective networks show causal interactions between brain areas.

## **1.5. Neuroimaging techniques**

As we are interested in studying the dynamic changes of the brain at very short time-scale, we particularly focus in this section on the neuroimaging techniques used to construct the functional brain networks.

### ***1.5.1. Functional magnetic resonance imaging (fMRI):***

fMRI is a neuroimaging technique used to map the brain activity by detecting changes of the blood oxygenation (87). In other words, fMRI measures the “blood oxygen level-dependent” (BOLD) signals based on the fact that increased activity in a particular part of the brain increases oxygenated blood flow. This technique is characterized by an excellent spatial resolution. However, its temporal resolution is limited since the BOLD response inferred from the hemodynamic changes takes time (in the order of seconds) (88). In addition, although this technique is based on the correlation between blood flow and the neuronal activity, it is considered as a non-direct measure of the neural activity. Figure 4.A shows example of fMRI acquisition.

### ***1.5.2. Electro-encephalography/ Magneto-encephalography (EEG/MEG):***

EEG and MEG are non-invasive techniques used to record the brain activity using sensors placed on or near the scalp of the head (27,89), as illustrated in Figure 4.B and Figure 4.C. These techniques provide direct observation of the neuronal activity by recording signals corresponding to the electrical/magnetic activity generated by the large neuronal population.

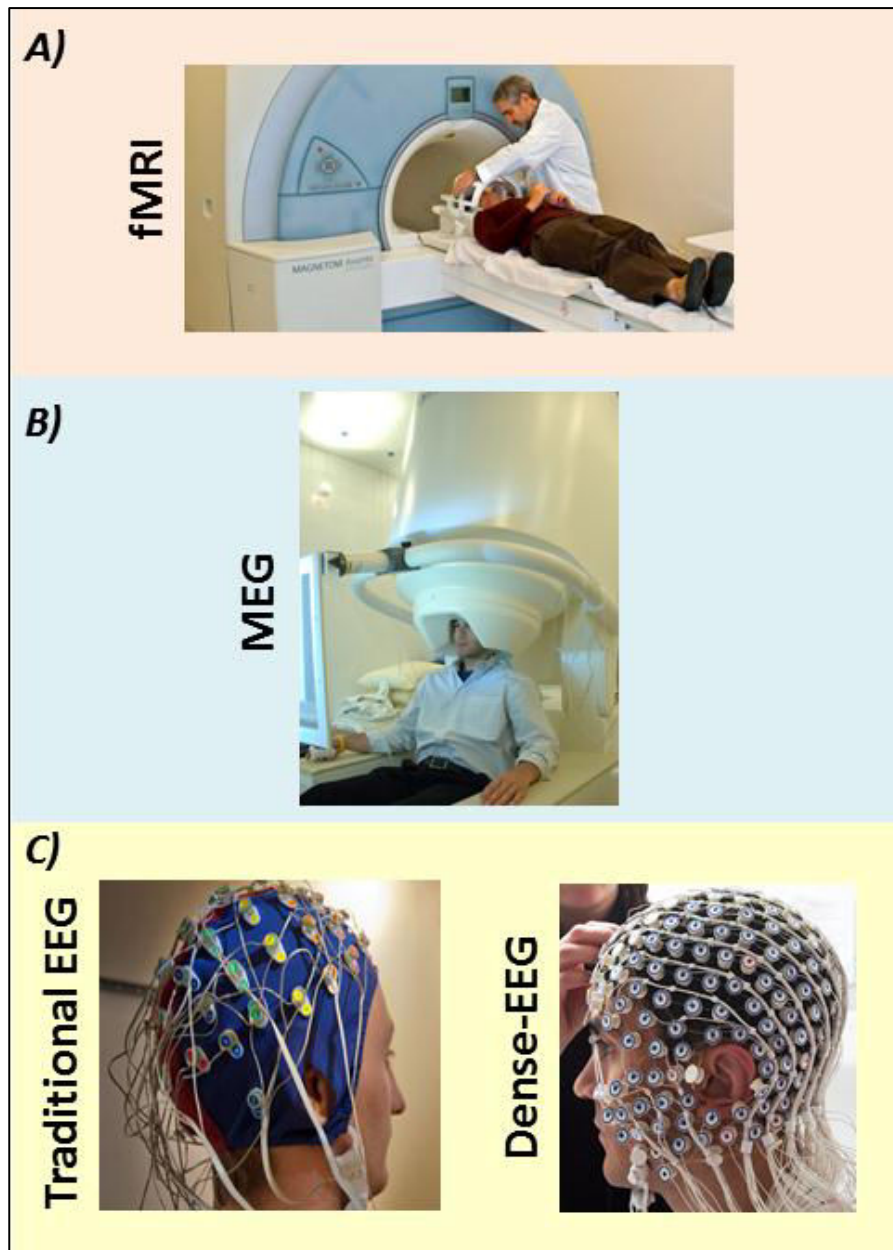


Figure 4. Examples of brain activity recordings. A) fmri acquisition. B) meg acquisition. C) traditional EEG and dense-EEG acquisitions (>128 channels)

EEG/MEG signals can be composed to different oscillations named rhythms (90). These rhythms have distinct properties in terms of spatial and spectral localization. There are six classical brain rhythms as illustrated in Figure 5:

- Delta rhythm: It is a slow rhythm (1-4 Hz), with relatively large amplitude, and is mainly observed during deep sleep.
- Theta rhythm: It is a slightly faster rhythm (4-7 Hz), found during drowsiness.
- Alpha rhythm: Alpha rhythms are oscillations, located between 8-12 Hz. It appears when the subject has closed eyes or is in a relaxation state.

- d. Beta rhythm: This is a relatively fast rhythm, belonging to the 13-30 Hz frequency band. It is observed in awoken and conscious persons. This rhythm is affected by the performance of movements.
- e. Gamma rhythm: This rhythm concerns frequencies above 30 Hz. Gamma rhythm is characterized by a maximal frequency around 80 Hz or 100 Hz. It is associated to various cognitive and motor functions.






Rhythm name	Frequency range	State associated	Examples of rhythms
Delta	1 → 4 Hz	Deep sleep	
Theta	4 → 7 Hz	Drowsy	
Alpha	8 → 12 Hz	Relaxed	
Beta	13 → 30 Hz	Engaged	
Gamma	30 → 45 Hz	Conscious and active	

Figure 5. Characteristics of EEG/MEG rhythms

The main advantages of using EEG/MEG techniques are: i) the non-invasiveness, ii) the direct recording of brain activity, iii) the excellent temporal resolution (at millisecond time scale) and iv) the ease of use. On the other hand, they are characterized by a relatively low spatial resolution compared to fMRI. Recently, a method known as “EEG/MEG source connectivity” has been proposed in order to increase the spatial resolution when applied on dense-EEG (Figure 4.C) and MEG data (91).



## **1.6. EEG/MEG source connectivity**

Most MEG/EEG functional connectivity studies were performed at the sensor/electrode level. However, the interpretation of the sensor based recorded signals is not straightforward due to the volume conduction effect as well as the field spread problem (review in (91)). Interestingly, the past years have seen a noticeable increase of interest for functional connectivity at the level of cortical sources reconstructed from EEG/MEG signals. In this context, EEG/MEG source connectivity is an emerging technique that allows overcoming the problem of the volume conduction that corrupts the sensor-level recordings. It also helps to reduce the effect of the field spread (review in (92)).

The method involves two main steps: i) solving the EEG inverse problem in order to estimate the cortical sources and reconstruct their temporal dynamics and ii) measuring the functional connectivity between the reconstructed time-series. Figure 6 illustrates the different steps that should be performed to obtain the functional cortical networks from scalp EEG.

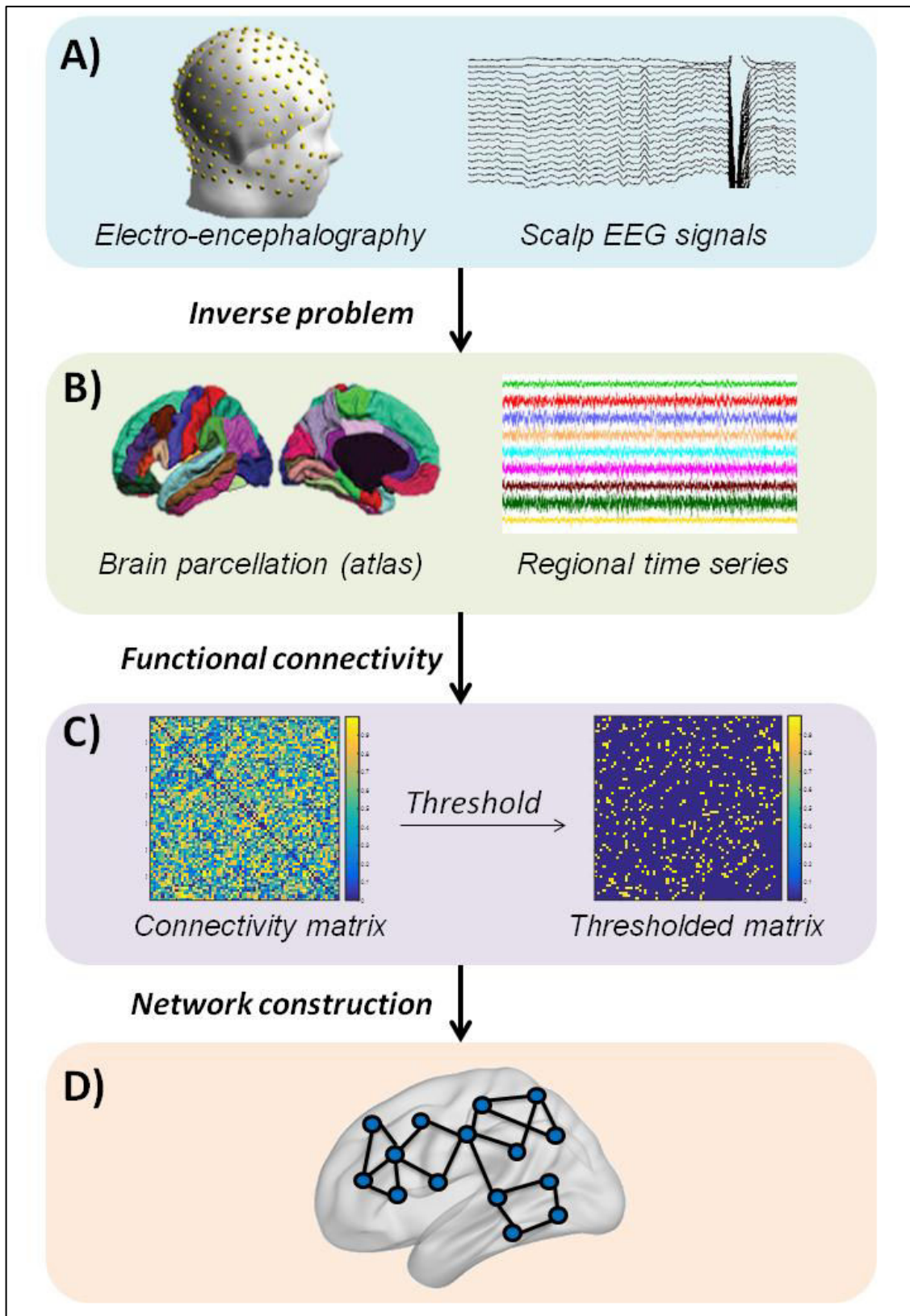


Figure 6. The full pipeline that shows the different steps performed to obtain a functional network from EEG data. A) EEG time series recorded at the level of the scalp. B) solving the inverse problem to obtain the regional time series. C) computing the functional connectivity matrix. The matrix can be thresholded to remove spurious connections. D) the resulted adjacency matrix will be presented as a graph composed of nodes (where nodes represent the brain regions) and edges (where edges represent the functional connectivity values).

### ***1.6.1. Solving the inverse problem:***

According to the dipole theory, EEG/MEG signals,  $S(t)$ , measured from  $Q$  sensors can be expressed as linear combinations of time-varying current dipole sources  $D(t)$ :

$$S(t) = G.D(t) + B(t).$$

$\hat{D}(t)$  is the estimation of dipolar source parameters (typically, the position, orientation and magnitude), where  $G$  and  $B(t)$  are respectively the matrix containing the lead fields of the dipolar sources and the additive noise. Generally, the lead field matrix can be computed using a multiple layer head model (volume conductor) and the electrodes positions. The head model explains how the electric currents or the magnetic fields flow from the electric generators in the brain (source space) through the different tissues of the head (brain, skull and skin), to finally reach the sensors. The simplest head models are the spherical head models that consider that the head is composed of concentric spheres, where each sphere represents a specific tissue type (93). To compute more accurate and realistic head models, many numerical methods have been proposed such as the Boundary Element Model (BEM) (94,95) and the Finite Element Model (FEM) (96). In brief, these methods compute the individual specific head model by taking into account detailed features of the head anatomy.

Mathematically, the inverse problem is an ill-posed problem as the solution is not unique ( $P \gg Q$ ). For this reason, solving such problems will imply the use of a priori information to limit the approximate solutions. This means that some constraints on the cortical sources properties (amplitude, position, orientation) should be added. See review in (97) for more detailed comparison between inverse solution's assumptions and constraints. Overall, two families of solutions were proposed in the past decade: i) the dipole fitting methods (these methods estimate the position and the amplitude of a limited number of dipoles) and ii) the distributed methods (these methods consist of defining of a priori dense grid of dipoles and then estimating their activity from the recordings).

Once the sources are computed on a high resolution mesh surface (usually between 8000 and 15000 vertices), one should estimate the time courses of a set of predefined brain regions or regions of interests (ROIs). A typical way is to use one of the available

anatomical and/or functional brain atlases such as Desikan Killiany composed of 68 ROIs (98), the Destrieux composed of 148 ROIs (99) or the Brainnetome composed of 246 ROIs (100). Then, the regional time series can be computed by averaging the source time series across ROIs. Besides averaging, many other strategies can be applied to estimate the activity associated with a ROI. Some proposed to extract the time series from a single representative dipole within the ROI (101,102). The selection of the representative dipole is mainly based on ground truth data (103), or data driven methods (selecting the dipole with the highest power (104), or the largest singular value based on a row singular vector (102), or the highest cross-talk function (CTF) index in the regions (105), or the resolution index closest to 1 in the ROI (106). Others also proposed the use of dimensionality reduction methods such as the principal component analysis. The connectivity analysis will be ultimately performed between the estimated regional time series.

### ***1.6.2. Functional connectivity estimation***

Measures of functional connectivity compute statistical dependencies between signals. These measures can be linear or non-linear, phase or amplitude-based, and time or spectral measures. Table 1 shows the properties of the most used functional connectivity metrics.

<b>Linear</b>	Amplitude coupling	Linear correlation coefficient
		Partial correlation
		Amplitude envelope correlation
		Leakage controlled amplitude envelope correlation
	Phase coupling	Phase difference derivative
		Weighted phase lag index (WPLI)
	Spectral coherence	Imaginary coherence
		Magnitude squared coherence
		Partial coherence

<b>Non Linear</b>	Amplitude coupling	Non-linear correlation coefficient
	Phase coupling	Phase-lag index
		Phase-locking value
	Phase or amplitude coupling	Mutual information

Table 1. Overview of the properties of different functional connectivity measures.

Connectivity values are estimated between all pairs of ROIs using one of the connectivity measurements.

This leads to an adjacency matrix (i.e connectivity matrix) of dimension  $N \times N$  where  $N$  denotes the number of ROIs. In order to remove the spurious connections, a threshold is generally applied on the obtained matrix. Empirical, proportional or statistical threshold can be applied. This procedure will enhance the contrast between relevant and irrelevant connectivity values. However, one should be prudent in choosing the threshold approach depending on the data treated. It is recommended to choose a proportional threshold when comparing connectivity between two or more groups (107), and to choose a statistical threshold in other cases (108). Network measures are shown to be stable across statistical and proportional thresholds contrary to absolute thresholds (109).

The adjacency matrix can be considered as a weighted undirected graph composed of nodes representing the brain regions, and edges representing the functional connectivity values.

## 1.7. Dynamic functional networks

To generate dynamic functional networks, we adopted a sliding window approach. This approach was widely used by many studies (13,19–21,23,68,110–112). The connectivity dynamics are assessed as follows:

- The regional time series are segmented into overlapping or non-overlapping time windows of length  $L$ .
- At each window, a functional matrix is computed..
- The window is moved forward to compute the connectivity in the next window.

Finally, the process will generate the dynamic connectivity tensor ( $N \times N \times L$  matrix).

Figure 7 illustrates the steps performed to generate the dynamic functional connectivity.

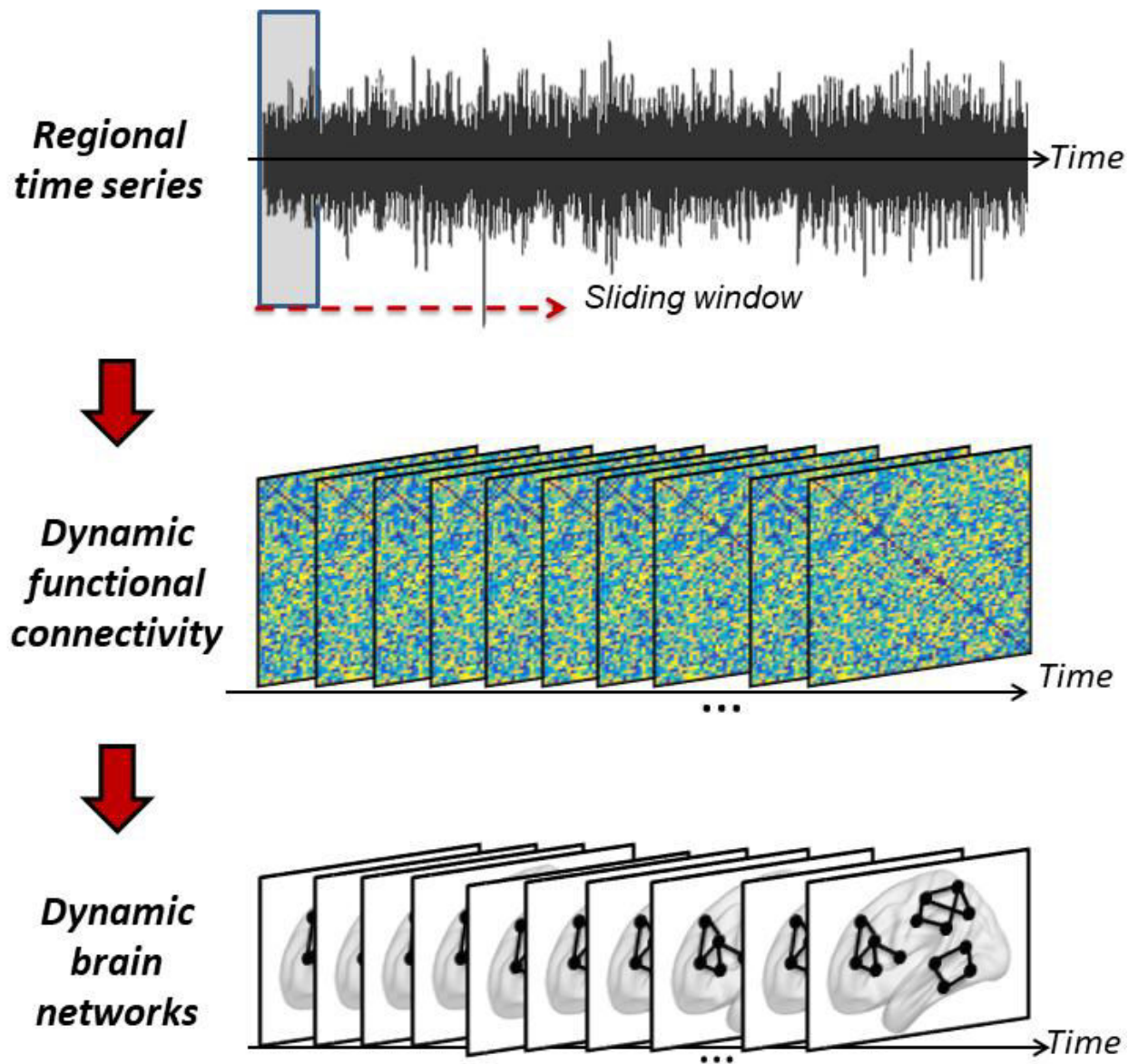


Figure 7. The steps performed to assess the dynamic functional connectivity of the regional time series using a sliding window approach.

## 1.8. Thesis objective

Many previous studies have successfully constructed valuable brain networks using EEG/MEG source connectivity method. However, most of these studies have analyzed the brain in a stationary way. Recently, many studies have been elaborated to study the brain networks in a dynamic way, benefiting from the high temporal resolution provided by EEG and MEG (Cohen, 1972; Penfield & Jasper, 1954). Some have proposed to group the

temporal networks into states, where each state reflect unique spatial connectivity pattern. These brain states were generated using Hidden Markov model approaches (17,21), K-means clustering (14,15,19,113), or independent component analysis (114). Other studies have tried to investigate the dynamic topological changes using graph theoretical analysis (23).

Our objective in this thesis is to more investigate to what extent the dynamic behavior of the brain can uncover insights about its characteristics during rest and task, in healthy and pathological brain networks. For this end, we extend the use of EEG source connectivity to track dynamic functional brain networks at a short temporal scale.

First, we started by assessing the performance of the EEG source connectivity in “re-estimating” reference large-scale networks modeled at neocortical level in the context of epilepsy. The different combinations of inverse solutions/connectivity measures were evaluated using a biophysical/physiological model and real epileptic data. Based on the previous work in addition to the findings obtained in (14,115), the wMNE/PLV combination was chosen to construct the cortical network in the following works. Second, we investigated the dynamic behavior of the functional brain networks during rest over a very short time scale (sub-second). This was done by combining the EEG source connectivity analysis with graph theoretical study to explore the dynamics of node’s characteristics (centrality, vulnerability, strength and clustering), networks and modules over hundreds of milliseconds. We also showed that the same regions can play the same role (provincial or integrator) during a given time period. In a third step, the previous approach was applied to explore the disruptions in the functional networks of Alzheimer’s disease (AD) patients. Using EEG data recorded during resting state paradigm, we studied the dynamic topological changes of AD networks in terms of integration and segregation. The correlation between the brain network disruption and the cognitive score of the AD patients was also assessed. Third, the dynamic functional connectivity was used to identify the epileptogenic networks from EEG signals recorded from spontaneous brain activity regardless of the presence/absence of epileptiform events. Intracerebral SEEG recordings were used to evaluate the accuracy of epileptogenic networks identified from scalp EEG data. Finally, we proposed an algorithm aiming to elucidate the main modular brain structures that fluctuate over time during rest and task conditions. These modular structures can be considered as modular states (MS). The method is based on categorizing the

modular structures that share the same topology by quantifying the similarity between the temporal modular structures. Our algorithm was tested on simulated data, and on three datasets recorded from real EEG and MEG acquisitions.



## Chapter 2.

# RESULTS

In this chapter, we present a brief resume of our studies. In the end of this manuscript, the complete version of the corresponding articles will be provided.

### **Study 1: Identification of interictal epileptic networks from dense-EEG**

Mahmoud Hassan, Isabelle Merlet, Ahmad Mheich, [Aya Kabbara](#), Arnaud Biraben, Anca Nica, Fabrice Wendling

Article published in Brain Topography (2017), 30(1):60-76

#### **Abstract:**

Epilepsy is a network disease. The epileptic network usually involves spatially distributed brain regions. In this context, noninvasive M/EEG source connectivity is an emerging technique to identify functional brain networks at cortical level from noninvasive recordings. In this paper, we analyze the effect of the two key factors involved in EEG source connectivity processing: (i) the algorithm used in the solution of the EEG inverse problem and (ii) the method used in the estimation of the functional connectivity. We evaluate four inverse solutions algorithms (dSPM, wMNE, sLORETA and cMEM) and four connectivity measures ( $r^2$ ,  $h^2$ , PLV, and MI) on data simulated from a combined biophysical/physiological model to generate realistic interictal epileptic spikes reflected in scalp EEG. We use a new network-based similarity index to compare between the network identified by each of the inverse/connectivity combination and the original network generated in the model. The method will be also applied on real data recorded from one epileptic patient who underwent a full presurgical evaluation for drug-resistant focal epilepsy. In simulated data, results revealed that the selection of the inverse/connectivity combination has a significant impact on the identified networks. Results suggested that nonlinear methods (nonlinear correlation coefficient, phase synchronization and mutual information) for measuring the connectivity are more efficient than the linear one (the cross correlation coefficient). The wMNE inverse solution showed higher performance than dSPM, cMEM and sLORETA. In real data, the combination (wMNE/PLV) led to a

very good matching between the interictal epileptic network identified from noninvasive EEG recordings and the network obtained from connectivity analysis of intracerebral EEG recordings. These results suggest that source connectivity method, when appropriately configured, is able to extract highly relevant diagnostic information about networks involved in interictal epileptic spikes from non-invasive dense-EEG data.

## **Study 2: The dynamic functional core network of the human brain at rest**

A. Kabbara, W. EL Falou, M. Khalil, F. Wendling & M. Hassan

Article published in Scientific reports 7 (1), 2936

### **Abstract:**

The human brain is an inherently complex and dynamic system. Even at rest, functional brain networks dynamically reconfigure in a well-organized way to warrant an efficient communication between brain regions. However, a precise characterization of this reconfiguration at very fast time-scale (hundreds of millisecond) during rest remains elusive. In this study, we used dense electroencephalography data recorded during task-free paradigm to track the fast temporal dynamics of spontaneous brain networks. Results obtained from network-based analysis methods revealed the existence of a functional dynamic core network formed of a set of key brain regions that ensure segregation and integration functions. Brain regions within this functional core share high betweenness centrality, strength and vulnerability (high impact on the network global efficiency) and low clustering coefficient. These regions are mainly located in the cingulate and the medial frontal cortex. In particular, most of the identified hubs were found to belong to the Default Mode Network. Results also revealed that the same central regions may dynamically alternate and play the role of either provincial (local) or connector (global) hubs.

### **Study 3: Reduced integration and improved segregation of functional brain networks in Alzheimer's disease**

A Kabbara, H Eid, W El Falou, M Khalil, F Wendling, M Hassan

Article published in Journal of neural engineering 15 (2), 026023

#### **Abstract:**

**Objective:** Emerging evidence shows that cognitive deficits in Alzheimer's disease (AD) are associated with disruptions in brain functional connectivity. Thus, the identification of alterations in AD functional networks has become a topic of increasing interest. However, to what extent AD induces disruption of the balance of local and global information processing in the human brain remains elusive. The main objective of this study is to explore the dynamic topological changes of AD networks in terms of brain network segregation and integration. **Approach:** We used electroencephalography (EEG) data recorded from 20 participants (10 AD patients and 10 healthy controls) during resting state. Functional brain networks were reconstructed using EEG source connectivity computed in different frequency bands. Graph theoretical analyses were performed to assess differences between both groups. **Main results:** Results revealed that AD networks, compared to networks of age-matched healthy controls, are characterized by lower global information processing (integration) and higher local information processing (segregation). Results showed also significant correlation between the alterations in the AD patients' functional brain networks and their cognitive scores. **Significance:** These findings may contribute to the development of EEG network-based test that could strengthen results obtained from currently-used neurophysiological tests in neurodegenerative diseases.

## Study 4: Dense scalp-EEG source connectivity predicts depth-EEG exploration in epilepsy

Aya Kabbara, Mahmoud Hassan, Mohamad Khalil, Arnaud Biraben, Anca Nica, Isabelle Merlet and Fabrice Wendling

*Submitted*

### **Abstract:**

**Objective:** Most brain disorders, including drug-resistant epilepsies, are network diseases. Thus, from a clinical perspective, the demand is high for non-invasive, network-based and easy-to-use methods to identify these pathological brain networks.

**Methods:** In this paper, we introduce a novel methodological framework to identify epileptogenic networks from scalp dense-electroencephalography (EEG). The proposed approach combines the emerging technique called ‘EEG source connectivity’ with graph theory. We used depth-EEG and scalp dense-EEG data at rest (regardless of the presence/absence of epileptiform activity) from 18 patients. Depth-EEG data were used to evaluate the accuracy of epileptogenic networks identified from scalp data. The method performance was quantified by its capacity to identify pathological brain networks in the region explored by depth-EEG in epileptic patients. This quantification was done using hemispherical and lobar accuracies as well as the distance between depth-EEG electrode positions and estimated networks.

**Results:** Results showed that the proposed approach was able to predict the brain hemisphere (accuracy=  $97\pm 9\%$ ) and the lobe (accuracy= $91\pm 19\%$ ) where SEEG exploration was performed a posteriori (averagedistance=  $13\pm 11$  mm). Results showed also the high advantage of network segregation measures (local functional connectivity) compared to global measures ( $p<0.01$ , corrected) in revealing epileptogenic networks.

**Interpretation:** These results may promote the noninvasive dense-EEG as a complementary tool in pre-surgical evaluation in order i) to define of the best depth-electrode placement (hemisphere and lobe) and ii) to highlight cortical regions that may be overlooked during pre-surgical planning.

## **Study 5: Tracking fast modular brain states in rest and task**

A. Kabbara, M. Khalil, F. Wendling & M. Hassan

*Submitted*

### **Abstract:**

The human brain is a dynamic networked system that permanently reconfigures its connectivity patterns during time. Thus, developing approaches able to adequately detect the fast brain dynamics is critical. Of particular interest are the methods that study the modular structure of brain networks, i.e. the presence of clusters of regions that are densely inter-connected. In this paper, we propose a novel framework to identify fast modular states that dynamically fluctuate over time during rest and task. We validate our method using MEG data recorded during a finger movement task, identifying modular states linking somatosensory and primary motor regions. The algorithm was also validated on dense-EEG data recorded during picture naming task, revealing the transition between several modular states which relate to visual processing, semantic processing and language. Next, we validate our method on a dataset of resting state dense-EEG data recorded from 124 parkinsonians patients of different cognitive phenotypes. Results disclosed the brain modular states that differentiate cognitively intact patients, patients with moderate cognitive deficits and patients with severe cognitive deficits. Our new approach tracks the brain modular states on an adequate task-specific timescale.

## Chapter 3.

# DISCUSSION

There is growing evidence suggesting that the brain is a networked system of interacting functional regions. This complex system is dynamic and flexibly changes its functional organization of resting (21,23,113,116) and task-evoked connectivity (13,14,114,117).

In addition, progress in the field of network science field has revealed that brain disorders are related to alterations in the functional brain connectivity, disrupting the large-scale network organization and function (Stam 2014, Fornito, Zalesky et al. 2015). Therefore, from a clinical perspective, the demand is high for novel ‘neuromarkers’ able to characterize the pathological networks using direct, non-invasive, and easy-to-use methods. We also speculate that an accurate description of the dynamics of brain networks over time not only helps to understand the cognitive functions, but also allow to investigate subtle alterations related to brain disorders.

Among the neuroimaging techniques that allow for extracting relevant information about functional brain networks, Electro-encephalography (EEG) has significantly progressed over the past years. This promising technique offers the opportunity to non-invasively track the temporal resolution of the brain networks. To generate accurate results, EEG signals should be carefully processed.

For many years, functional connectivity analyses using EEG were performed at the sensor level. However, scalp EEG signals are severely corrupted by i) the ‘volume conduction’ effect due to the conduction properties of the head and ii) the ‘field spread’ problem caused by the fact that many sensors may collect the same activity of a single brain source (Nolte, Bai et al. 2004, Van Diessen, Numan et al. 2015). These two limitations make the interpretation of scalp-based networks a difficult issue.

Recently, an emerging method named “EEG source connectivity” has seen a considerable progress (91). It was shown that this method can successfully identify the brain networks at the level of cortex with a good spatial resolution and an excellent temporal resolution. It also helps to reduce the effects of the volume conduction and the field spread problems.

Still, several methodological issues should be considered when reconstructing the brain sources from scalp signals, and assessing their connectivity.

The main achievements of the thesis can be summarized as follows:

- The dynamic analysis of the resting state networks at sub-second time-scale revealed several new characteristics of functional brain networks in terms of centrality and hubness. We showed that the human brain holds a dynamic functional core network of a set of central brain regions that dynamically warrant both segregation and integration processes. By classifying the brain regions into local and global hubs, we showed that the same brain region can dynamically switch its function between provincial (segregation) and connector (integration) hubs.
- A novel framework to explore reconfiguration of fast modular brain structures was developed in order to extract functional modular states during both task-free and task-related paradigms. We validate the new framework using MEG data recorded during a finger movement task, identifying modular states linking somatosensory and primary motor regions. The algorithm was also validated on dense-EEG data recorded during picture naming task, revealing the sub-second transition between several modular states which relate to visual processing, semantic processing and language.
- By investigating the dynamic topological alterations in Alzheimer's disease networks, we showed that AD networks are characterized by lower global information processing (integration) and higher local information processing (segregation), compared to networks of age-matched healthy controls.
- In the context of epilepsy, results showed that network segregation measures (local functional connectivity) compared to global measures in matching intracerebral EEG sites. The local network measures were able to match the brain hemisphere (accuracy=  $97\pm 9\%$ ) and the lobe (accuracy=  $91\pm 19\%$ ) where SEEG exploration was performed posteriori (average distance=  $13\pm 11$  mm).

### **3.1. Dynamic functional networks at rest and task**

Tracking the temporal dynamics of brain networks is an important issue that helps to improve our knowledge about the cognitive and behavioral tasks, and the

neuropathological diseases. Studying the dynamic brain networks reconfiguration can include longitudinal studies aiming to explore the slow changes of brain topology with the normal aging. It also includes the investigation of fast spontaneous or evoked changes in response to external stimuli. In particular, tracking the spatiotemporal dynamics of large scale networks over a very short time duration is a very challenging issue in task and rest (13,19). Thanks to the excellent temporal resolution of electrophysiological modalities (such as EEG and MEG), we have a unique opportunity to access how the functional connectivity evolves in short-time (sub-second) and how it may be perturbed by brain disease.

The use of the dynamic functional connectivity has revealed potential impact for basic neuro-scientific and clinical studies. Importantly, several resting studies showed that some crucial regions play a key role in maintaining efficient temporal communication in the whole brain (23,116). Other studies focused on assessing the temporal transitions between resting state networks (21). The importance of uncovering the dynamic behavior of the brain was also demonstrated in many cognitive tasks (14,17,18,45). While these studies differ in the way in which the functional networks were analysed, they succeeded to characterize the temporally-evolving networks that rapidly dissolve during tasks. According to clinical applications, dynamic connectivity was important to relate brain behavior to pathology in anesthesia (118), epilepsy (119), Parkinson (82), and depression (120).

To measure the dynamics of large scale functional networks using EEG and MEG, several methods have been developed and proposed during the last decade. Some of these studies proposed to group the temporal networks into states, where each state represent a distinctive connectivity pattern. These brain states were mainly generated using Hidden Markov model approaches (17,21), K-means clustering (15,19,113) or independent component analysis (114). However, a precise characterization of the dynamic reconfiguration of the brain at very fast time-scale has rarely been studied. To tackle this issue, we developed methods to track the dynamic aspects using graph theoretical analysis, in order to investigate the dynamic topological changes during rest (Study 2, Study 3, Study 4) and task (Study 5). Particularly, the sliding window approach was used. The key contribution of the developed methods is that they went beyond the state of the art techniques by looking at the temporal transition between brain regions, network hubs, and



modules over sub-second time scale. Results obtained from the resting state study revealed the existence of a functional dynamic core network formed of a set of key brain regions that ensure segregation and integration functions. One of the primary benefits of the method is that it was capable to show that the same central regions dynamically alternate its function between provincial (local) or connector (global) hub. In addition, the method proposed to elucidate the main modular brain structures that fluctuate over time has revealed applicability in rest and task paradigms. In particular, it was able to automatically decipher functional modular brain states i.e. subset of brain modules implicated in a given brain function at adapted time period.

A challenge that future studies may need to address is how to dynamically regulate the sliding window width instead of predefining it. Another important issue that could be tracked in the future is the development of electrophysiological models that allow researchers to compare experimental results to computational results, and to more relate the functional networks to the mechanism that drive brain connectivity.

### **3.2. Toward EEG network-based neuromarkers of brain disorders**

Brain disorders are often associated with alterations of large-scale functional brain networks. Methods able to identify these pathological networks from easy-to-use and non-invasive techniques are clinically needed. From theoretical point of view, network neuroscience has offered the opportunity to more understand and quantitatively assess the characteristics of brain networks. Hence, multiple studies have explored the functional connectivity in brain disorders using MEG/EEG (121). However, most of these studies were performed at the sensor-based level where signals are corrupted by the volume conduction and the field spread problems. As an emerging technique, MEG/EEG source connectivity allows reconstructing the functional brain networks at the level of cortical sources from sensor level recordings (91). The main key advantages of MEG/EEG systems is the non-invasiveness, the ease of use and the excellent temporal resolution that help to analyze fast dynamical changes that may occur in brain disorders such as epileptic seizures. In addition, MEG and EEG directly measure the neuronal activity in contrast with blood-oxygen-level-dependent (BOLD) signals.

Recently, MEG/EEG source connectivity has revealed valuable information about the functional networks involved in brain disorders. Promising results were obtained in characterizing the networks involved in epilepsy (77,80,122–128), Alzheimer and Parkinson diseases (82,84,129–131). Besides identifying the pathological brain networks, many studies were interested in assessing an association between the degree of cognitive deficits and the alterations of functional connectivity in the context of neurodegenerative diseases (82,129). Thus, we speculate that this potential technique will have high clinical impact not only for accurately identifying pathological networks, which is crucial in some disorders like epilepsy, but also offering the possibility to develop neuromarker for neurodegenerative diseases (neuromarker for cognitive impairment in Parkinson's disease and Alzheimer's disease). The reported results showed that this objective can be achieved by appropriate processing techniques and sufficient database. This can offer the opportunity to develop new start-ups in order to provide easy to use tools for clinicians.

In the context of epilepsy, MEG/EEG source connectivity could be used to help in developing new therapeutic approaches based on neurostimulation by optimizing the brain stimulation protocols. Indeed, the technique could aid to know when and where the stimulations should be applied (central node or 'hubs' may be the major target to be stimulated).

### **3.3. Methodological consideration**

#### **3.3.1. Source leakage:**

While the functional connectivity at the source level reduces the effect of the field spread, it doesn't totally suppress its effects (91). The main outcome of the source leakage is that spurious connections can occur between adjacent regions. To overcome this problem, several techniques have been initially proposed to solve the problem at the sensor level, such as the imaginary coherence (132) and the phase lag index (133). Others have suggested to track the problem at the source level before performing any connectivity analysis (134,135). All the proposed approaches are based generally on ignoring zero-lag interactions among signals, by supposing that their contributions are only due to the source leakage. Other studies proposed to only keep the long-range connections (22,23,116). Although these approaches have some advantages, they may suppress important correlations that occur at zero-lag (67) or even among close regions (136).

Since “EEG source connectivity” is a relatively young field, such problems are still under discussion and more efforts are needed to completely address the source leakage problem.

It is also noteworthy that the number of regions of interests (ROIs) may be related to the effect of the “mixing sources”, as the reconstructed signals that belong to a single ROI will be averaged. This means that choosing a low number of large ROIs could help in removing spurious links that occur between spatially adjacent sources. However, it may cause a low spatial resolution. There is, so far, no clear consensus about how to select the appropriate number of nodes that represent the large-scale networks. Hence, one should adapt a compromise between low and high number of ROIs to attempt good spatial resolution and reduced spatial leakage between the regional time series.

In this thesis, we used 68 anatomical ROIs (Study2, Study3 and Study5) to define the nodes in the brain network. We assume that 68 regions were sufficient to investigate the global characteristics of the brain networks while minimizing the problem of spurious connections between ‘very close sources’. As defining epileptogenic networks from dense-EEG requires higher “granularity”, i.e. spatial precision and accurate characterization of the network local properties, the number of anatomical ROIs was increased to 221 ROIs.

### ***3.3.2. The ill-posed inverse problem***

It is likely that the selection of a source imaging method to solve the inverse problem has a remarkable effect on the accuracy of the reconstructed source signals, and ultimately on the brain networks obtained. From a methodological point of view, as the number of source dipoles (in thousands) is much larger than the number of sensors (in hundreds), the inverse problem is ill-posed. This implies that adding physical and mathematical constraints is necessary to solve the inverse problem. These constraints can be applied on the spatial, temporal, or spatio-temporal properties of dipoles distributions (97). Thus, depending on the imposed hypothesis, each brain imaging method has its strengths and weaknesses. A detailed comparison between different brain imaging methods developed in the context of EEG/MEG source connectivity was reported by (97). The review describes the hypotheses, the advantages and drawbacks of seven algorithms (sLORETA, MCE, MNE, VB-SCCD, STWV-DA, Champagne, and 4-ExSo-MUSIC). It also provides a quantitative evaluation of the seven methods performance tested on simulated data for an example of epileptic EEG activity, by assessing the distance of Localization Error and the CPU runtime.

In this thesis, we used the weighted minimum norm estimate (wMNE) as an inverse solution. Based on (97), the main assumption of the weighted minimum norm estimate was to find a solution with lowest energy. This assumption can be generally explained by the economic energy cost of the brain during information processing. Compared to other inverse solutions, the wMNE implies relatively few hypotheses and presents acceptable distance of localization error and CPU runtime (97).

### ***3.3.3. Effect of the inverse/connectivity measure:***

Extracting valuable information about brain networks from noninvasive neuroimaging techniques such as MEG and EEG is challenging but reachable. Using “EEG source connectivity”, one should select one of several inverse solutions and connectivity measures to construct the functional brain networks. In this context, the obvious question that is raised is: what is the best inverse/connectivity combination that allows constructing accurate brain networks that actually correspond to those activated during considered brain processes?

For this purpose, previous studies performed in the team have been conducted to compare different combinations of inverse/connectivity methods in situations where ground truth data is available. The objective was to determine the optimal combination providing brain networks, from dense-EEG, as close as possible to reference networks. . In the first study, real data recorded during a cognitive task was used (14,115). Interestingly, a large number of combinations between the inverse solution and functional connectivity measures were tested. The objective was to estimate the networks involved during a picture naming task for which a solid background was available regarding activated brain regions and networks. In brief, a comprehensive literature review on these networks was mainly obtained from neuroimaging techniques such as fMRI, MEG, depth EEG and PET. From this review, a “reference” network was determined and used as a ground truth to define a performance criterion about the accuracy of networks obtained from “EEG source connectivity” combinations. For one combination (wMNE/PLV), the estimated network, activated during the cognitive task (500-700 ms), was found to spatially match the reference network. The above described work was then extended from static to dynamic analysis during the same cognitive task. EEG source connectivity method applied using

wMNE/PLV combination was able to track the spatiotemporal dynamics of activated brain networks from the onset (presentation of the visual stimuli) to the reaction time (articulation). Estimated dynamic networks were also found to match previously-reported regions/networks, as identified with other techniques such as depth-EEG and MEG.

In this thesis, a study was performed in the context of epilepsy where a physiologically-plausible computational model of epileptogenic networks was used as a ground truth (Study 1). Simulated scalp-EEG signals were used to evaluate the performance of EEG source connectivity methods in term of “re-estimating” reference large-scale networks modelled at neocortical level. Again, the combination that showed the highest similarity between reference and estimated networks was the wMNE/PLV, used in our following works.

Nevertheless, other combinations or strategies that showed accurate construction of cortical networks from sensor level recordings could be also investigated and compared such as the use of beamforming combined with amplitude correlation between band-limited power envelopes as reported in several studies (18,134,135,137,138).

#### ***3.1.4. Selecting the sliding window length:***

Choosing the suitable window width is a crucial issue in constructing the dynamic functional networks. On one hand, choosing short windows may underlie errors in the generated networks. On the other hand, large windows may fail to capture the temporal changes of the brain networks. Hence, the ideal is to choose the shortest window that guarantees a sufficient number of data points over which the connectivity is calculated. This depends on the frequency band of interest that affects the degree of freedom in time series.

In this thesis, we are mainly quantifying the phase synchronization using the phase locking value metric (PLV). Hence, we adapted the recommendation of Lachaux et al. (139) in selecting the smallest appropriate window length that is equal to  $\frac{6}{\text{central frequency}}$  where 6 is the number of ‘cycles’ at the given frequency band. We also validated the reproducibility of resting state results whilst changing the size of the sliding window (Study 2).

### ***3.1.5. Thresholding the connectivity matrix:***

A threshold is commonly applied to remove weak connections from functional connectivity data. However, there is no current consensus on what threshold to use on the functional connectivity matrix. Thresholds can be absolute (correlation-based), proportional (density-based) or statistical (sparsity-based). Each threshold approach has its advantages and disadvantages depending on the data treated.

Absolute thresholds consist on setting a value for the connectivity matrix, above which the connections are considered and below which the connections are removed. The absolute thresholding is the simplest approach to apply. However, absolute thresholds may eliminate strong and significant connections in low-average connectivity networks, or overemphasize weak connections in high-average connectivity networks (140).

Proportional thresholds keep a percentage of the strongest connections (edges), such as maintaining only the top 10% of correlation values of the connectivity matrix. (109) showed that network measures are stable across proportional thresholds. In group comparison, a proportional threshold ensures equal density between groups (same number of nodes and edges, network size (107)).

Statistical thresholds require converting the connectivity matrix to a  $p$ -value map. The connectivity values whose  $p$ -values passed the statistical FDR threshold are then retained (40,108,141). Such thresholds are beneficial as they perform multiple testing to adjust thresholds by controlling false-positive rate.

In this thesis, we used a proportional threshold (highest 10% of the edge's weights) in studying the resting state networks characteristics (Study 2), and in group comparison analysis (Study 3 and Study 5). According to previous studies, the 10% threshold provides an optimal trade-off between retaining the true connections and reducing spurious connections (142). The consistency of results across a range of proportional thresholds (ranging from 5 to 20%) was considered in this work. The statistical threshold was also applied on the functional connectivity matrices of epileptogenic networks (Study 4).

## **3.4. Future directions**

In this thesis, we investigated the capability of “EEG source connectivity” to track the fast dynamic changes of brain networks at very short time scale. This investigation was performed by extracting dynamic characteristics and topologies of networks using graph theory. The proposed methods were applied on three clinical applications (Epilepsy, Alzheimer’s disease and Parkinson’s disease).

In future works, a new clinical application will be also considered. We are going to study the functional alterations occurred in the brain networks of patients with major depression. EEG data will be collected in Mazloun Hospital in Tripoli, Lebanon

Second, in this thesis, we only investigated the functional connectivity methods. We speculate that effective connectivity could add additional information about the directionality of the functional interactions between brain regions. This issue could be addressed by testing various effective connectivity measures derived from Granger causality as already reported in a number of studies (101,123)

Third, one can notice that the presented studies used to consider a predefined frequency range depending on the analyzed data (motor task, naming task, resting state). However, multiple studies indicate that network integration exists across a wide range of frequencies (143–145). Using MEG, recent studies reported that frequency band specific networks aren’t wholly identical, but share a common mode of connection patterns due to inter-bands coupling (145). Our ongoing work is to investigate the dynamic changes of modular network organization spanning over hundreds of millisecond time scale within and between EEG frequency bands. We hypothesized that the brain modular networks are reshaping during transitions between frequency bands whilst some common characteristics remain unchangeable over all bands. To extract both the individual and the common characteristics over the classically defined EEG bands, we are going to use the multi-slice modularity technique (Figure 8).

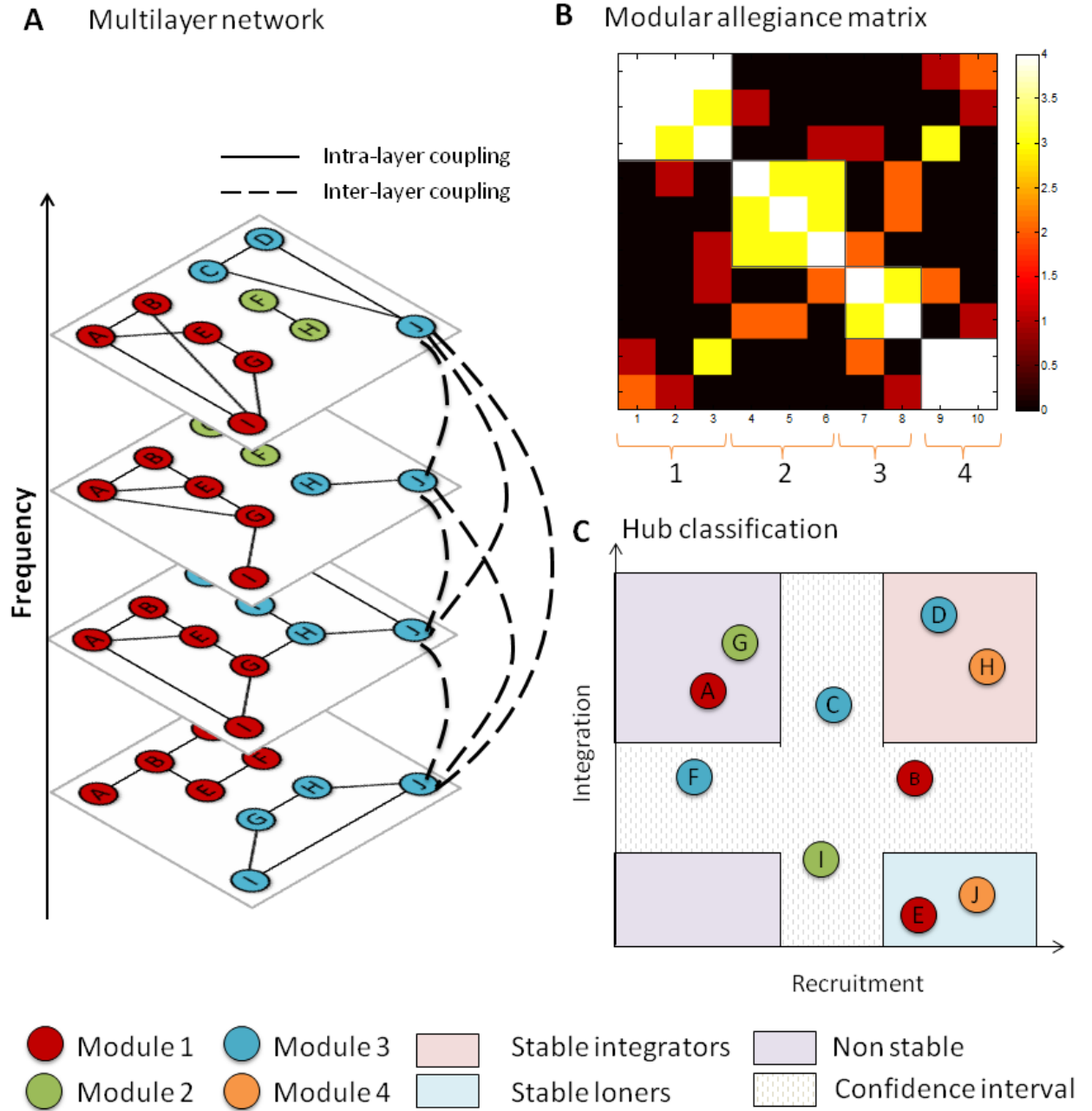


Figure 8. The proposed pipeline for the study of the frequency-dependant properties of brain networks. A) multi-slice modularity will be applied, where each slice will represent a frequency band. B) the modular allegiance will be formed. C) nodes will be classified into three main classes: 1) stable integrators, 2) stable loners, 3) non stable.

Further work will be also to evaluate the effect of the number of channels and the number of ROIs on the identified networks properties. This evaluation will be performed on simulated and real data.





# References

1. Fuster JM. Cortex and Mind: Unifying Cognition. Cortex and Mind: Unifying Cognition. 2010. 1-314 p.
2. Sporns O, Chialvo DR, Kaiser M, Hilgetag CC. Organization, development and function of complex brain networks. Trends Cogn Sci. 2004;8(9):418–25.
3. Greicius MD, Krasnow B, Reiss AL, Menon V. Functional connectivity in the resting brain: a network analysis of the default mode hypothesis. Proc Natl Acad Sci U S A . 2003;100(1):253–8.
4. McIntosh AR. Towards a network theory of cognition. Vol. 13, Neural Networks. 2000. p. 861–70.
5. Bressler SL. Large-scale cortical networks and cognition. Vol. 20, Brain Research Reviews. 1995. p. 288–304.
6. Goldman-Rakic PS. Topography of Cognition: Parallel Distributed Networks in Primate Association Cortex. Annu Rev Neurosci. 1988;11(1):137–56.
7. Mesulam M - M. Large- scale neurocognitive networks and distributed processing for attention, language, and memory. Ann Neurol. 1990;28(5):597–613.
8. Mountcastle V. An organizing principle for cerebral function: the unit model and the distributed system. The Mindful Brain. 1978. p. 7–50.
9. Edelman GM. Neural Darwinism: Selection and reentrant signaling in higher brain function. Vol. 10, Neuron. 1993. p. 115–25.
10. Pfurtscheller G, Lopes Da Silva FH. Event-related EEG/MEG synchronization and desynchronization: Basic principles. Vol. 110, Clinical Neurophysiology. 1999. p. 1842–57.
11. Pfurtscheller G, Aranibar A. Event-related cortical desynchronization detected by power measurements of scalp EEG. Electroencephalogr Clin Neurophysiol. 1977;42(6):817–26.
12. O'Neill GC, Tewarie P, Vidaurre D, Liuzzi L, Woolrich MW, Brookes MJ. Dynamics of large-scale electrophysiological networks: A technical review. NeuroImage. 2017;
13. Hutchison RM, Womelsdorf T, Allen EA, Bandettini PA, Calhoun VD, Corbetta M, et al. Dynamic functional connectivity: Promise, issues, and interpretations. Neuroimage. 2013;80:360–78.
14. Hassan M, Benquet P, Biraben A, Berrou C, Dufor O, Wendling F. Dynamic

- reorganization of functional brain networks during picture naming. *Cortex*. 2015;73:276–88.
15. Allen EA, Damaraju E, Eichele T, Wu L, Calhoun VD. EEG Signatures of Dynamic Functional Network Connectivity States. *Brain Topography*. 2017;1–16.
  16. Bassett DS, Wymbs NF, Porter MA, Mucha PJ, Carlson JM, Grafton ST. Dynamic reconfiguration of human brain networks during learning. *Proc Natl Acad Sci U S A*. 2011;108(18):7641–6.
  17. Vidaurre D, Abeysuriya R, Becker R, Quinn AJ, Alfaro-Almagro F, Smith SM, et al. Discovering dynamic brain networks from big data in rest and task. *NeuroImage*. 2017.
  18. O'Neill GC, Tewarie PK, Colclough GL, Gascoyne LE, Hunt BAE, Morris PG, et al. Measurement of Dynamic Task Related Functional Networks using MEG. *Neuroimage*. 2016;in press.
  19. Allen EA, Damaraju E, Plis SM, Erhardt EB, Eichele T, Calhoun VD. Tracking whole-brain connectivity dynamics in the resting state. *Cereb Cortex*. 2014;24:663–76.
  20. O'Neill GC, Bauer M, Woolrich MW, Morris PG, Barnes GR, Brookes MJ. Dynamic recruitment of resting state sub-networks. *Neuroimage*. 2015;115:85–95.
  21. Baker AP, Brookes MJ, Rezek IA, Smith SM, Behrens T, Smith PJP, et al. Fast transient networks in spontaneous human brain activity. *Elife*. 2014;2014.
  22. de Pasquale F, Della Penna S, Snyder AZ, Lewis C, Mantini D, Marzetti L, et al. Temporal dynamics of spontaneous MEG activity in brain networks. *Proc Natl Acad Sci U S A*. 2010;107:6040–5.
  23. de Pasquale F, Penna S Della, Sporns O, Romani GL, Corbetta M. A Dynamic Core Network and Global Efficiency in the Resting Human Brain. *Cereb Cortex*. 2015;bhv185.
  24. Fornito A, Zalesky A, Breakspear M. The connectomics of brain disorders. *Nat Rev Neurosci*. 2015;16(3):159–72.
  25. Fornito A, Bullmore ET. Connectomics: A new paradigm for understanding brain disease. *Eur Neuropsychopharmacol*. 2015;25(5):733–48.
  26. Nunez PL, Srinivasan R. Electroencephalogram. *Scholarpedia*. 2007;2(2):1348.
  27. Cohen D. Magnetoencephalography: Detection of the Brain's Electrical Activity with a Superconducting Magnetometer. *Science* (80- )
  28. Penfield W, Jasper H. Epilepsy and the Functional Anatomy of the Human Brain.

- JAMA J Am Med Assoc. 1954;155:86–86.
29. Sporns O. Networks of the brain. 2010.
  30. Diestel R. Graph Theory . Vol. 173, New York. 2005. 803-6 p.
  31. Barrat A, Barthélemy M, Pastor-Satorras R, Vespignani A. The architecture of complex weighted networks. *Proc Natl Acad Sci U S A*. 2004;101(11):3747–52.
  32. Watts DJ, Strogatz SH. Collective dynamics of “small-world” networks. *Nature*. 1998;393(6684):440–2.
  33. Bullmore E, Sporns O. Complex brain networks: graph theoretical analysis of structural and functional systems. *Nat Rev Neurosci*. 2009;10(3):186–98.
  34. Latora V, Marchiori M. Efficient Behavior of Small World Networks. *Phys Rev Lett*. 2001;87:198701.
  35. Eickhoff SB, Stephan KE, Mohlberg H, Grefkes C, Fink GR, Amunts K, et al. A new SPM toolbox for combining probabilistic cytoarchitectonic maps and functional imaging data. *Neuroimage*. 2005;25(4):1325–35.
  36. Sporns O, Betzel RF. Modular Brain Networks. *Annu Rev Psychol*. 2016;67(1):613–40.
  37. Guimerà R, Nunes Amaral LA. Functional cartography of complex metabolic networks. *Nature* . 2005;433(7028):895–900.
  38. van den Heuvel MP, Sporns O. Network hubs in the human brain. Vol. 17, *Trends in Cognitive Sciences*. 2013. p. 683–96.
  39. Sporns O, Honey CJ, Kotter R. Identification and classification of hubs in brain networks. *PLoS One*. 2007;2(10).
  40. Achard S, Salvador R, Whitcher B, Suckling J, Bullmore E. A resilient, low-frequency, small-world human brain functional network with highly connected association cortical hubs. *J Neurosci*. 2006;26(1):63–72.
  41. Zuo XN, Ehmke R, Mennes M, Imperati D, Castellanos FX, Sporns O, et al. Network centrality in the human functional connectome. *Cereb Cortex*. 2012;22(8):1862–75.
  42. Gol'dshtein V, Koganov GA, Surdutovich GI. Vulnerability and Hierarchy of Complex Networks. *Physics (College Park Md)*. 2004;16:4.
  43. Power JD, Schlaggar BL, Lessov-Schlaggar CN, Petersen SE. Evidence for hubs in human functional brain networks. *Neuron*. 2013;79(4):798–813.
  44. van den Heuvel MP, Sporns O. An anatomical substrate for integration among functional networks in human cortex. *J Neurosci*. 2013;33:14489–500.

45. Moussa MN, Vechlekar CD, Burdette JH, Steen MR, Hugenschmidt CE, Laurienti PJ. Changes in Cognitive State Alter Human Functional Brain Networks. *Front Hum Neurosci.* 2011;5(August):1–15.
46. Friston KJ. Functional and Effective Connectivity: A Review. *Brain Connect.* 2011;1(1):13–36.
47. Rubinov M, Sporns O. Complex network measures of brain connectivity: Uses and interpretations. *Neuroimage.* 2010;52:1059–69.
48. Collin G, Sporns O, Mandl RCW, van den Heuvel MP. Structural and Functional Aspects Relating to Cost and Benefit of Rich Club Organization in the Human Cerebral Cortex. *Cereb Cortex.* 2013;24:2258–67.
49. Hagmann P, Cammoun L, Gigandet X, Meuli R, Honey CJ, Van Wende J, et al. Mapping the structural core of human cerebral cortex. *PLoS Biol.* 2008;6:1479–93.
50. Gong G, He Y, Concha L, Lebel C, Gross DW, Evans AC, et al. Mapping anatomical connectivity patterns of human cerebral cortex using in vivo diffusion tensor imaging tractography. *Cereb Cortex.* 2009;19:524–36.
51. Iturria-Medina Y, Sotero RC, Canales-Rodriguez EJ, Aleman-Gomez Y, Melie-Garcia L. Studying the human brain anatomical network via diffusion-weighted MRI and Graph Theory. *Neuroimage.* 2008;40:1064–76.
52. Li L, Hu X, Preuss TM, Glasser MF, Damen FW, Qiu Y, et al. Mapping putative hubs in human, chimpanzee and rhesus macaque connectomes via diffusion tractography. *Neuroimage.* 2013;80:462–74.
53. Nijhuis EHJ, van Cappellen van Walsum AM, Norris DG. Topographic Hub Maps of the Human Structural Neocortical Network. *PLoS One.* 2013;8.
54. Lo C, Wang P-N, Chou K, Wang J, He Y, Lin C. Diffusion tensor tractography reveals abnormal topological organization in structural cortical networks in Alzheimer's disease. *J Neurosci.* 2010;30(50):16876–85.
55. Mallio CA, Schmidt R, de Reus MA, Vernieri F, Quintiliani L, Curcio G, et al. Epicentral Disruption of Structural Connectivity in Alzheimer's Disease. *CNS Neurosci Ther.* 2015;21(10):837–45.
56. Lo C-Y, Wang P-N, Chou K-H, Wang J, He Y, Lin C-P. Diffusion Tensor Tractography Reveals Abnormal Topological Organization in Structural Cortical Networks in Alzheimer's Disease. *J Neurosci.* 2010;30(50):16876–85.
57. Zhang Z, Liao W, Chen H, Mantini D, Ding JR, Xu Q, et al. Altered functional-structural coupling of large-scale brain networks in idiopathic generalized epilepsy.

- Brain. 2011;134(10):2912–28.
58. Liu M, Chen Z, Beaulieu C, Gross DW. Disrupted anatomic white matter network in left mesial temporal lobe epilepsy. *Epilepsia*. 2014;55(5):674–82.
  59. Zhang Y, Schuff N, Du A-T, Rosen HJ, Kramer JH, Gorno-Tempini ML, et al. White matter damage in frontotemporal dementia and Alzheimer’s disease measured by diffusion MRI. *Brain*. 2009;132(Pt 9):2579–92.
  60. Fornito A, Zalesky A, Breakspear M. The connectomics of brain disorders. Vol. 16, *Nature Reviews Neuroscience*. 2015. p. 159–72.
  61. Fox MD, Raichle ME. Spontaneous fluctuations in brain activity observed with functional magnetic resonance imaging. *Nat Rev Neurosci*. 2007;8:700–11.
  62. Cordes D, Haughton VM, Arfanakis K, Wendt GJ, Turski PA, Moritz CH, et al. Mapping functionally related regions of brain with functional connectivity MR imaging. *Am J Neuroradiol*. 2000;21:1636–44.
  63. Biswal BB, Van Kylen J, Hyde JS. Simultaneous assessment of flow and BOLD signals in resting-state functional connectivity maps. *NMR Biomed*. 1997;10:165–70.
  64. De Luca M, Beckmann CF, De Stefano N, Matthews PM, Smith SM. fMRI resting state networks define distinct modes of long-distance interactions in the human brain. *Neuroimage*. 2006;29(4):1359–67.
  65. Xiong J, Parsons LM, Gao JH, Fox PT. Interregional connectivity to primary motor cortex revealed using MRI resting state images. *Hum Brain Mapp*. 1999;8:151–6.
  66. Yuan H, Zotev V, Phillips R, Drevets WC, Bodurka J. Spatiotemporal dynamics of the brain at rest - Exploring EEG microstates as electrophysiological signatures of BOLD resting state networks. *Neuroimage*. 2012;60(4):2062–72.
  67. Brookes MJ, O’Neill GC, Hall EL, Woolrich MW, Baker A, Palazzo Corner S, et al. Measuring temporal, spectral and spatial changes in electrophysiological brain network connectivity. *Neuroimage*. 2014;91:282–99.
  68. O’Neill GC, Tewarie PK, Colclough GL, Gascoyne LE, Hunt BAE, Morris PG, et al. Measurement of dynamic task related functional networks using MEG. *Neuroimage*. 2016;
  69. Bassett DS, Yang M, Wymbs NF, Grafton ST. Learning-Induced Autonomy of Sensorimotor Systems. *Nat Neurosci*. 2015;18(5):744–51.
  70. Lehmann D, Faber PL, Galderisi S, Herrmann WM, Kinoshita T, Koukkou M, et al. EEG microstate duration and syntax in acute, medication-naïve, first-episode

- schizophrenia: A multi-center study. *Psychiatry Res - Neuroimaging*. 2005;138(2):141–56.
71. Pascual-Marqui RDD, Michel CMM, Lehmann D. Segmentation of brain electrical activity into microstates: model estimation and validation. *Biomed Eng IEEE Trans* . 1995;42(7):658–65.
  72. Van Diessen E, Zweiphenning WJEM, Jansen FE, Stam CJ, Braun KPJ, Otte WM. Brain network organization in focal epilepsy: A systematic review and meta-analysis. *PLoS One*. 2014;9(12):1–21.
  73. Engels MMA, van der Flier WM, Stam CJ, Hillebrand A, Scheltens P, van Straaten ECW. Alzheimer's disease: The state of the art in resting-state magnetoencephalography. *Clin Neurophysiol*. 2017;128(8):1426–37.
  74. Montez T, Poil S-S, Jones BF, Manshanden I, Verbunt JPA, van Dijk BW, et al. Altered temporal correlations in parietal alpha and prefrontal theta oscillations in early-stage Alzheimer disease. *Proc Natl Acad Sci* . 2009;106(5):1614–9.
  75. Stam CJ, Jones BF, Nolte G, Breakspear M, Scheltens P. Small-world networks and functional connectivity in Alzheimer's disease. *Cereb Cortex*. 2007;17(1):92–9.
  76. De Haan W, Van der Flier WM, Koene T, Smits LL, Scheltens P, Stam CJ. Disrupted modular brain dynamics reflect cognitive dysfunction in Alzheimer's disease. *Neuroimage*. 2012;59(4):3085–93.
  77. Dai Y, Zhang W, Dickens DL, He B. Source connectivity analysis from MEG and its application to epilepsy source localization. *Brain Topogr*. 2012;25(2):157–66.
  78. Bartolomei F, Wendling F, Bellanger JJ, Régis J, Chauvel P. Neural networks involving the medial temporal structures in temporal lobe epilepsy. *Clin Neurophysiol*. 2001;112(9):1746–60.
  79. Bartolomei F, Lagarde S, Wendling F, McGonigal A, Jirsa V, Guye M, et al. Defining epileptogenic networks: Contribution of SEEG and signal analysis. Vol. 58, *Epilepsia*. 2017. p. 1131–47.
  80. Jmail N, Gavaret M, Bartolomei F, Chauvel P, Badier JM, Bunar CG. Comparison of Brain Networks During Interictal Oscillations and Spikes on Magnetoencephalography and Intracerebral EEG. *Brain Topogr*. 2016;29(5):752–65.
  81. Hassan M, Mheich A, Biraben A, Merlet I, Wendling F. Identification of epileptogenic networks from dense EEG: A model-based study. In: *Proceedings of the Annual International Conference of the IEEE Engineering in Medicine and*

- Biology Society, EMBS. 2015. p. 5610–3.
82. Hassan M, Chaton L, Benquet P, Delval A, Leroy C, Plomhause L, et al. Functional connectivity disruptions correlate with cognitive phenotypes in Parkinson's disease. *NeuroImage Clin.* 2017;14:591–601.
  83. Utianski RL, Caviness JN, van Straaten ECW, Beach TG, Dugger BN, Shill HA, et al. Graph theory network function in parkinson's disease assessed with electroencephalography. *Clin Neurophysiol.* 2016;127(5):2228–36.
  84. Bosboom JLW, Stoffers D, Wolters EC, Stam CJ, Berendse HW. MEG resting state functional connectivity in Parkinson's disease related dementia. *J Neural Transm.* 2009;116(2):193–202.
  85. Granger CWJ. Investigating Causal Relations by Econometric Models and Cross-spectral Methods. *Econometrica* .1969;37(3):424.
  86. Friston K, Moran R, Seth AK. Analysing connectivity with Granger causality and dynamic causal modelling. Vol. 23, *Current Opinion in Neurobiology*. 2013. p. 172–8.
  87. Scott A. Huettel; Allen W. Song; Gregory McCarthy, Huettel, Scott; Song A, Beckmann CF, Smith SM, Huettel S a., Song AW, et al. *Functional Magnetic Resonance Imaging*. Vol. 23, Book. 2004. 137-152 p.
  88. Logothetis NK, Pauls J, Augath M, Trinath T, Oeltermann A. Neurophysiological investigation of the basis of the fMRI signal. *Nature*. 2001;412(6843):150–7.
  89. Berger H, Gloor P. Hans Berger on the electroencephalogram of man. *Electroencephalography and Clinical Neurophysiology, Supplement no. 28*. 1969. p. 350.
  90. Niedermeyer E, Silva FL Da. *Electroencephalography*. Vol. 65, Obstetrical gynecological survey. 2005. 1256 p.
  91. Schoffelen JM, Gross J. Source connectivity analysis with MEG and EEG. Vol. 30, *Human Brain Mapping*. 2009. p. 1857–65.
  92. Hassan M, Wendling F. Electroencephalography source connectivity : toward high time / space resolution brain networks. *IEEE Signal Process Mag.* 2018;1–25.
  93. Ermer JJ, Mosher JC, Baillet S, Leahy RM. Rapidly recomputable EEG forward models for realistic head shapes. *Phys Med Biol.* 2001;46(4):1265–81.
  94. Fuchs M, Drenckhahn R, Wischmann HA, Wagner M. An improved boundary element method for realistic volume-conductor modeling. *IEEE Trans Biomed Eng.* 1998;45(8):980–97.



95. Oostenveld R, Oostendorp TF. Validating the boundary element method for forward and inverse EEG computations in the presence of a hole in the skull. *Hum Brain Mapp.* 2002;17(3):179–92.
96. Zhang Y, Ding L, van Drongelen W, Hecox K, Frim DM, He B. A cortical potential imaging study from simultaneous extra- and intracranial electrical recordings by means of the finite element method. *Neuroimage.* 2006;31(4):1513–24.
97. Becker H, Albera L, Comon P, Gribonval R, Wendling F, Merlet I. Brain-source imaging: From sparse to tensor models. *IEEE Signal Process Mag.* 2015;32(6):100–12.
98. Desikan RS, Sugonne F, Fischl B, Quinn BT, Dickerson BC, Blacker D, et al. An automated labeling system for subdividing the human cerebral cortex on MRI scans into gyral based regions of interest. *Neuroimage.* 2006;31:968–80.
99. Destrieux C, Fischl B, Dale A, Halgren E. Automatic parcellation of human cortical gyri and sulci using standard anatomical nomenclature. *Neuroimage.* 2010;53(1):1–15.
100. Yu C, Zhou Y, Liu Y, Jiang T, Dong H, Zhang Y, et al. Functional segregation of the human cingulate cortex is confirmed by functional connectivity based neuroanatomical parcellation. *Neuroimage.* 2011;54(4):2571–81.
101. Coito A, Michel CM, Van Mierlo P, Vulliemoz S, Plomp G. Directed Functional Brain Connectivity Based on EEG Source Imaging: Methodology and Application to Temporal Lobe Epilepsy. *IEEE Trans Biomed Eng.* 2016;63(12):2619–28.
102. Sohrabpour A, Ye S, Worrell GA, Zhang W, He B. Noninvasive Electromagnetic Source Imaging and Granger Causality Analysis: An Electrophysiological Connectome (eConnectome) Approach. *IEEE Trans Biomed Eng.* 2016;63(12):2474–87.
103. Babiloni F, Babiloni C, Carducci F, Romani GL, Rossini PM, Angelone LM, et al. Multimodal Integration of EEG and MEG Data: A Simulation Study with Variable Signal-to-Noise Ratio and Number of Sensors. *Hum Brain Mapp.* 2004;22(1):52–62.
104. Rueda-Delgado LM, Solesio-Jofre E, Mantini D, Dupont P, Daffertshofer A, Swinnen SP. Coordinative task difficulty and behavioural errors are associated with increased long-range beta band synchronization. *Neuroimage.* 2017;146:883–93.
105. Farahibozorg SR, Henson RN, Hauk O. Adaptive cortical parcellations for source reconstructed EEG/MEG connectomes. *Neuroimage.* 2018;169:23–45.
106. Stenroos M, Hauk O. Minimum-norm cortical source estimation in layered head

- models is robust against skull conductivity error. *Neuroimage*. 2013;81:265–72.
107. van den Heuvel MP, de Lange SC, Zalesky A, Seguin C, Yeo BTT, Schmidt R. Proportional thresholding in resting-state fMRI functional connectivity networks and consequences for patient-control connectome studies: Issues and recommendations. *Neuroimage*. 2017;152:437–49.
  108. Genovese CR, Lazar NA, Nichols T. Thresholding of statistical maps in functional neuroimaging using the false discovery rate. *Neuroimage*. 2002;15(4):870–8.
  109. Garrison KA, Scheinost D, Finn ES, Shen X, Constable RT. The (in)stability of functional brain network measures across thresholds. *Neuroimage*. 2015;118:651–61.
  110. Chang C, Liu Z, Chen MC, Liu X, Duyn JH. EEG correlates of time-varying BOLD functional connectivity. *Neuroimage*. 2013;72:227–36.
  111. Brookes MJ, Woolrich MW, Price D. An Introduction to MEG connectivity measurements. In: *Magnetoencephalography: From Signals to Dynamic Cortical Networks*. 2014. p. 321–58.
  112. Dujardin K, Moonen AJH, Behal H, Defebvre L, Duhamel A, Duits AA, et al. Cognitive disorders in Parkinson’s disease: Confirmation of a spectrum of severity. *Park Relat Disord*. 2015;21(11):1299–305.
  113. Damaraju E, Allen EA, Belger A, Ford JM, McEwen S, Mathalon DH, et al. Dynamic functional connectivity analysis reveals transient states of dysconnectivity in schizophrenia. *NeuroImage Clin*. 2014;5:298–308.
  114. O’Neill GC, Tewarie PK, Colclough GL, Gascoyne LE, Hunt BAE, Morris PG, et al. Measurement of dynamic task related functional networks using MEG. *Neuroimage*. 2017;146:667–78.
  115. Hassan M, Dufor O, Merlet I, Berrou C, Wendling F. EEG source connectivity analysis: From dense array recordings to brain networks. *PLoS One*. 2014;9.
  116. de Pasquale F, Della Penna S, Snyder AZ, Marzetti L, Pizzella V, Romani GL, et al. A Cortical Core for Dynamic Integration of Functional Networks in the Resting Human Brain. *Neuron*. 2012;74:753–64.
  117. Bola M, Sabel BA. Dynamic reorganization of brain functional networks during cognition. *Neuroimage*. 2015;114:398–413.
  118. Lee H, Noh GJ, Joo P, Choi BM, Silverstein BH, Kim M, et al. Diversity of functional connectivity patterns is reduced in propofol-induced unconsciousness. *Hum Brain Mapp*. 2017;38(10):4980–95.

119. Khambhati AN, Bassett DS, Oommen BS, Chen, Stephanie H, Lucas TH, Davis KA, et al. Recurring functional interactions predict network architecture of interictal and ictal states in neocortical epilepsy. *Revis eNeuro*. 2016;
120. Lu Q, Bi K, Liu C, Luo G, Tang H, Yao Z. Predicting depression based on dynamic regional connectivity: A windowed Granger causality analysis of MEG recordings. *Brain Res*. 2013;1535:52–60.
121. Uhlhaas PJ, Singer W. Neural Synchrony in Brain Disorders: Relevance for Cognitive Dysfunctions and Pathophysiology. Vol. 52, *Neuron*. 2006. p. 155–68.
122. Nissen IA, Stam CJ, Reijneveld JC, van Straaten IE, Hendriks EJ, Baayen JC, et al. Identifying the epileptogenic zone in interictal resting-state MEG source-space networks. *Epilepsia* . 2016;1–12.
123. Coito A, Plomp G, Genetti M, Abela E, Wiest R, Seeck M, et al. Dynamic directed interictal connectivity in left and right temporal lobe epilepsy. *Epilepsia*. 2015;56(2):207–17.
124. Ding L, Worrell GA, Lagerlund TD, He B. Ictal source analysis: Localization and imaging of causal interactions in humans. *Neuroimage*. 2007;34(2):575–86.
125. Lu Y, Yang L, Worrell GA, He B. Seizure source imaging by means of FINE spatio-temporal dipole localization and directed transfer function in partial epilepsy patients. *Clin Neurophysiol*. 2012;123(7):1275–83.
126. Song J, Tucker DM, Gilbert T, Hou J, Mattson C, Luu P, et al. Methods for examining electrophysiological coherence in epileptic networks. *Front Neurol*. 2013;4 MAY.
127. Vecchio F, Miraglia F, Quaranta D, Granata G, Romanello R, Marra C, et al. Cortical connectivity and memory performance in cognitive decline: A study via graph theory from EEG data. *Neuroscience*. 2016;316:143–50.
128. Hassan M, Merlet I, Mheich A, Kabbara A, Biraben A, Nica A, et al. Identification of Interictal Epileptic Networks from Dense-EEG. *Brain Topography*. 2016;1–17.
129. Hata M, Kazui H, Tanaka T, Ishii R, Canuet L, Pascual-Marqui RD, et al. Functional connectivity assessed by resting state EEG correlates with cognitive decline of Alzheimer's disease - An eLORETA study. *Clin Neurophysiol*. 2016;127(2):1269–78.
130. Baggio HC, Segura B, Sala-Llloch R, Marti MJ, Valldeoriola F, Compta Y, et al. Cognitive impairment and resting-state network connectivity in Parkinson's disease. *Hum Brain Mapp*. 2015;36(1):199–212.

131. Bertrand J-A, McIntosh R, Postuma RB, Kovacevic N, Latreille V, Panisset M, et al. Brain connectivity alterations are associated with dementia in Parkinson's disease. *Brain Connect.* 2015;1–27.
132. Nolte G, Bai O, Wheaton L, Mari Z, Vorbach S, Hallett M. Identifying true brain interaction from EEG data using the imaginary part of coherency. *Clin Neurophysiol.* 2004;115(10):2292–307.
133. Stam CJ, Nolte G, Daffertshofer A. Phase lag index: Assessment of functional connectivity from multi channel EEG and MEG with diminished bias from common sources. *Hum Brain Mapp.* 2007;28(11):1178–93.
134. Brookes MJ, Woolrich MW, Barnes GR. Measuring functional connectivity in MEG: A multivariate approach insensitive to linear source leakage. *Neuroimage.* 2012;63(2):910–20.
135. Colclough GL, Brookes MJ, Smith SM, Woolrich MW. A symmetric multivariate leakage correction for MEG connectomes. *Neuroimage.* 2015;117:439–48.
136. Finger H, Bönstrup M, Cheng B, Messé A, Hilgetag C, Thomalla G, et al. Modeling of Large-Scale Functional Brain Networks Based on Structural Connectivity from DTI: Comparison with EEG Derived Phase Coupling Networks and Evaluation of Alternative Methods along the Modeling Path. *PLoS Comput Biol.* 2016;12(8).
137. Brookes MJ, Hale JR, Zumer JM, Stevenson CM, Francis ST, Barnes GR, et al. Measuring functional connectivity using MEG: Methodology and comparison with fMRI. *Neuroimage.* 2011;56:1082–104.
138. Colclough GL, Woolrich MW, Tewarie PK, Brookes MJ, Quinn AJ, Smith SM. How reliable are MEG resting-state connectivity metrics? *Neuroimage.* 2016;138:284–93.
139. Lachaux J-P, Rodriguez E, Le van Quyen M, Lutz A, Martinerie J, Varela FJ. Studying single-trials of phase synchronous activity in the brain. *Int J Bifurc Chaos.* 2000;10(10):2429–39.
140. van Wijk BCM, Stam CJ, Daffertshofer A. Comparing brain networks of different size and connectivity density using graph theory. *PLoS One.* 2010;5(10).
141. Bassett DS, Porter MA, Wymbs NF, Grafton ST, Carlson JM, Mucha PJ. Robust detection of dynamic community structure in networks. *Chaos.* 2013;23(1).
142. Lord A, Horn D, Breakspear M, Walter M. Changes in community structure of resting state functional connectivity in unipolar depression. *PLoS One.* 2012;7(8).
143. Watrous AJ, Deuker L, Fell J, Axmacher N. Phase-amplitude coupling supports


- phase coding in human ECoG. *Elife*. 2015;4(AUGUST2015).
144. Jiang H, Bahramisharif A, van Gerven MAJ, Jensen O. Measuring directionality between neuronal oscillations of different frequencies. *Neuroimage*. 2015;118:359–67.
  145. Tewarie P, Hillebrand A, van Dijk BW, Stam CJ, O'Neill GC, Van Mieghem P, et al. Integrating cross-frequency and within band functional networks in resting-state MEG: A multi-layer network approach. *Neuroimage*. 2016;142:324–36.

# **Study 1: Identification of interictal epileptic networks from dense-EEG**

Mahmoud Hassan, Isabelle Merlet, Ahmad Mheich, Aya Kabbara, Arnaud Biraben, Anca Nica, Fabrice Wendling

Article published in Brain Topography (2017), 30(1):60-76

# Identification of Interictal Epileptic Networks from Dense-EEG

Mahmoud Hassan<sup>1,2</sup>  · Isabelle Merlet<sup>1,2</sup> · Ahmad Mheich<sup>1,2,4</sup> · Aya Kabbara<sup>1,2,4</sup> ·  
Arnaud Biraben<sup>1,2,3</sup> · Anca Nica<sup>3</sup> · Fabrice Wendling<sup>1,2</sup>

Received: 14 March 2016 / Accepted: 16 August 2016  
© Springer Science+Business Media New York 2016

**Abstract** Epilepsy is a network disease. The epileptic network usually involves spatially distributed brain regions. In this context, noninvasive M/EEG source connectivity is an emerging technique to identify functional brain networks at cortical level from noninvasive recordings. In this paper, we analyze the effect of the two key factors involved in EEG source connectivity processing: (i) the algorithm used in the solution of the EEG inverse problem and (ii) the method used in the estimation of the functional connectivity. We evaluate four inverse solutions algorithms (dSPM, wMNE, sLORETA and cMEM) and four connectivity measures ( $r^2$ ,  $h^2$ , PLV, and MI) on data simulated from a combined biophysical/physiological model to generate realistic interictal epileptic spikes reflected in scalp EEG. We use a new network-based similarity index to compare between the network identified by each of the inverse/connectivity combination and the original network generated in the model. The method will be also applied on real data recorded from one epileptic patient who underwent a full presurgical evaluation for drug-resistant focal epilepsy. In simulated data, results revealed that the selection of the inverse/connectivity combination has a significant impact on the identified

networks. Results suggested that nonlinear methods (non-linear correlation coefficient, phase synchronization and mutual information) for measuring the connectivity are more efficient than the linear one (the cross correlation coefficient). The wMNE inverse solution showed higher performance than dSPM, cMEM and sLORETA. In real data, the combination (wMNE/PLV) led to a very good matching between the interictal epileptic network identified from noninvasive EEG recordings and the network obtained from connectivity analysis of intracerebral EEG recordings. These results suggest that source connectivity method, when appropriately configured, is able to extract highly relevant diagnostic information about networks involved in interictal epileptic spikes from non-invasive dense-EEG data.

**Keywords** Epilepsy · Dense-EEG source connectivity · Epileptic networks

## Introduction

Epilepsy is a network disease (Engel Jr et al. 2013). Over the two past decades, the concept of “epileptic focus” has progressively evolved toward that of “epileptic network” (Kramer and Cash 2012; Laufs 2012). Indeed, with the progress of functional neuroimaging techniques, many studies confirmed that the epileptic zone (EZ) can rarely be reduced to a circumscribed brain area (Bartolomei et al. 2001) as it very often involves distinct brain regions generating both interictal (Bourien et al. 2005) and ictal activity (Bourien et al. 2004). Among the investigation techniques classically used in the diagnostic of epilepsy, electrophysiological recordings (typically, magneto- and electro-encephalography including depth-EEG, referred to

**Electronic supplementary material** The online version of this article (doi:10.1007/s10548-016-0517-z) contains supplementary material, which is available to authorized users.

✉ Mahmoud Hassan  
mahmoud.hassan@univ-rennes1.fr

<sup>1</sup> INSERM, U1099, Rennes 35000, France

<sup>2</sup> LTSI, Université de Rennes 1, Rennes 35000, France

<sup>3</sup> Neurology Department, CHU, Rennes 35000, France

<sup>4</sup> AZM Center-EDST, Lebanese University, Tripoli, Lebanon

as M/EEG) are still extensively used to localize and delineate the EZ in a patient-specific context. Regarding the numerous methods proposed to process the recorded data; those aimed at characterizing brain connectivity are particularly suitable to identify networks involved during epileptiform activity (both interictal and ictal).

In the context of invasive EEG signals (intracranial EEG, stereo-EEG and electrocorticography –EcoG-) recorded in patients candidate to surgery, these “connectivity” methods have been a topic of extensive research [see van Mierlo et al. (2014) for recent review]. For instance, the coherence function was shown to localize the seizure onset (Gotman 1987), similarity indexes were used to distinguish a preictal state from the ongoing interictal activity (Le Van Quyen et al. 2005; Mormann et al. 2000). Nonlinear regression analysis was applied to intracerebral signals to characterize connectivity patterns at the seizure onset (Bourien et al. 2004). Readers may refer to previous reviews for more detailed information about brain connectivity methods applied to non-invasive (van Mierlo et al. 2014) and invasive EEG signals (Wendling et al. 2010) in drug-resistant focal epilepsies.

In the context of scalp M/EEG recording, connectivity methods have received less attention as compared with invasive EEG. A number of studies performed at the level of electrodes and focused on ictal periods have been reported aiming at analyzing seizure propagation (Gotman 1983) or to determine the seizure onset side (Caparos et al. 2006), for instance. For interictal periods, few connectivity studies made use of dense EEG and phase synchronization (Ramon and Holmes 2013) to identify epileptic sites. One reason for this paucity of studies may lie in the intricate interpretation of connectivity measures obtained from scalp recordings. Indeed, this interpretation is not straightforward as signals are severely corrupted by the effects of volume conduction (Schoffelen and Gross 2009).

Interestingly, some recent studies showed how to overcome this limitation. In line with previous cognitive studies (Astolfi et al. 2007; Babiloni et al. 2005; Betti et al. 2013; Bola and Sabel 2015; David et al. 2003; David et al. 2002; de Pasquale et al. 2010; Hassan et al. 2015a; Hassan et al. 2014; Hassan and Wendling 2015; Hipp et al. 2011; Hoechstetter et al. 2004; Liljeström et al. 2015; Schoffelen and Gross 2009), the basic principle is to estimate functional connectivity at the level of brain sources reconstructed from scalp signals. These methods, referred to as “source connectivity” were applied to both interictal EEG (Coito et al. 2015; Song et al. 2013; Vecchio et al. 2014) and MEG signals (Dai et al. 2012; Malinowska et al. 2014) as well as to EEG signals recorded during seizures (Ding et al. 2007; Jiruska et al. 2013; Lu et al. 2012) or resting states (Adebimpe et al. 2016; Coito et al. 2016).

Although these approaches all include two steps (M/EEG inverse problem followed by source connectivity estimation), they strongly differ from a methodological viewpoint. Indeed, various algorithms were used to reconstruct brain sources and both functional and effective connectivity measures were utilized to assess statistical couplings among time series associated with reconstructed sources. Therefore, a central issue is the impact of selected methods (EEG inverse solution and connectivity measure) on the topological/statistical properties of identified epileptic networks activated during paroxysmal activity.

In this paper, we report a quantitative comparison of methods aimed at identifying cortical epileptic networks from scalp EEG data. The novelty of this work is twofold. First, our comparative study includes simulated dense EEGs generated from physiologically- and biophysically-plausible models of distributed and coupled epileptic sources. To our knowledge, no previous study has reported results on the performance of source connectivity methods based on a “ground truth” provided by realistic computational models of interictal EEG signals (recorded later in time than the dense EEG recordings). Second, in line with a recent analysis performed on MEG data (Malinowska et al. 2014), networks estimated from real scalp dense EEG are compared with those obtained from depth-EEG recordings (SEEG).

## Materials and Methods

### Inverse Solution Algorithms

Given the equivalent current dipole model, EEG signals  $X(t)$  recorded from  $M$  channels can be considered as linear combinations of  $P$  time-varying current dipole sources  $S(t)$ :

$$X(t) = GS(t) + N(t)$$

where  $G[M, P]$  is the lead field matrix and  $N(t)$  is the noise. As  $G$  is known, the EEG inverse problem consists of estimating the unknown sources  $\hat{S}(t)$  from  $X(t)$ . Several algorithms have been proposed to solve this problem based on different assumptions about spatial and temporal properties of sources and regularization constraints. Here, we chose to evaluate the four algorithms implemented in Brainstorm (Tadel et al. 2011).

#### *Weighted Minimum Norm Estimate (wMNE)*

Minimum norm estimates (MNE) originally proposed by (Hämäläinen and Ilmoniemi 1994) are based on a search for the solution with minimum power using the L2 norm to regularize the problem. A common expression for MNE resolution matrix is



$$\hat{S}_{\text{MNE}} = G^T(GG^T + \lambda C)^{-1}G$$

where  $\lambda$  is the regularization parameter and  $C$  represents the noise covariance matrix. The weighted MNE (wMNE) algorithm compensates for the tendency of MNE to favor weak and surface sources (Hämäläinen 2005). This is achieved by introducing a weighting matrix  $W_X$  in

$$\hat{S}_{\text{wMNE}} = (G^T W_X G + \lambda C)^{-1} G^T W_X X$$

that adjusts the properties of the solution by reducing the bias inherent to the standard MNE solution. Classically,  $W_X$  is a diagonal matrix built from matrix  $G$  with non-zero terms inversely proportional to the norm of the lead field vectors.

#### *Dynamical Statistical Parametric Mapping (dSPM)*

The dSPM is based on the MNE solution (Dale et al. 2000). For dSPM, the normalization matrix contains the minimum norm estimates of the noise at each source (Caparos et al. 2006), derived from the noise covariance matrix, defined as:

$$\hat{S}_{\text{dSPM}} = W_{\text{dSPM}} \hat{S}_{\text{MNE}}$$

where  $W_{\text{dSPM}}^2 = \text{diag}(\hat{S}_{\text{MNE}} C \hat{S}_{\text{MNE}}^T)$ .

#### *Standardized Low Resolution Brain Electromagnetic Tomography (sLORETA)*

sLORETA uses the source distribution estimated from MNE and standardizes it a posteriori by the variance of each estimated dipole source:

$$\hat{S}_{\text{sLORETA}} = W_{\text{sLORETA}} \hat{S}_{\text{MNE}}$$

where  $W_{\text{sLORETA}}^2 = \text{diag}(\hat{S}_{\text{MNE}} G) = \text{diag}(\hat{S}_{\text{MNE}} (GG^T + C) \hat{S}_{\text{MNE}}^T)$ . The sLORETA inverse method has been originally described using the whole brain volume as source space (Pascual-Marqui 2002). For the present study, in order to ease the comparison with other methods, we restricted the source space to the neocortical surface.

#### *Standard Maximum Entropy on the Mean (cMEM)*

The Maximum Entropy on the Mean (MEM) solver is based on a probabilistic method where inference on the current source intensities is estimated from the data, which is the basic idea of the maximum of entropy. The first application of MEM to electromagnetic source localization was reported in (Clarke and Janday 1989). The main feature of this method is its ability to recover the spatial extent of the underlying sources. Its solution is assessed by finding the closest distribution of source intensities to a

reference distribution in which source intensities are organized into cortical parcels showing homogeneous activation state (parallel cortical macro-columns with synchronized activity). In addition a constraint of local spatial smoothness in each parcel can be introduced (Chowdhury et al. 2013).

#### **Connectivity Measures**

We selected four methods that have been widely used to estimate functional brain connectivity from electrophysiological signals (local field potentials, depth-EEG or EEG/MEG) (see (Wendling et al. 2009) for review). These measures were chosen to cover the main families of connectivity methods (linear and nonlinear regression, phase synchronization and mutual information).

Briefly, concerning the regression approaches, the linear cross-correlation coefficient is only limited to the detection of the linear properties of the relationships between time series. However, mechanisms at the origin of EEG signals were shown to have strong nonlinear behaviors (Pereda et al. 2005). Thus, we have selected three nonlinear connectivity measures. The nonlinear regression where the basic idea is to evaluate the dependency of two signals from signal samples only and independently of the type of relation between the two signals. Concerning the phase synchronization measure, the method estimates the instantaneous phase of each signal and then computes a quantity based on co-variation of extracted phases to determine the degree of relationship. Finally, the mutual information method is based on the probability and information theory to measures mutual dependence between two variables. More technical details about the four methods are presented hereafter:

#### *Cross-Correlation Coefficient ( $r^2$ )*

The cross-correlation coefficient measures the linear correlation between two variables  $x$  and  $y$  as a function of their time delay ( $\tau$ ). Referred to as the linear correlation coefficient, it is defined as:

$$r_{xy}^2 = \max_{\tau} \frac{\text{cov}^2(x(t), y(t + \tau))}{(\sigma_{x(t)} \sigma_{y(t+\tau)})^2}$$

where  $\sigma$  and cov denote the standard deviation and the covariance, respectively.

#### *Nonlinear Correlation Coefficient ( $h^2$ )*

The nonlinear correlation coefficient ( $h^2$ ) is a non-parametric measure of the nonlinear relationship between two time series  $x$  and  $y$ . In practice, the nonlinear relation

between the two time series is approximated by a piecewise linear curve.

$$h_{xy}^2 = \max_{\tau} \left( 1 - \frac{\text{var}(y(t + \tau)/x(t))}{\text{var}(y(t + \tau))} \right)$$

where  $\text{var}(y(t + \tau)/x(t)) \triangleq \arg \min_f (E[y(t + \tau) - f(x(t))]^2)$  and  $f(x)$  is the linear piecewise approximation of the non-linear regression curve.

### Mutual Information (MI)

The mutual information (MI) between signal  $x$  and  $y$  is defined as:

$$MI_{xy} = \sum p_{ij}^{xy} \log \frac{p_{ij}^{xy}}{p_i^x p_j^y}$$

where  $p_{ij}^{xy}$  is the joint probability of  $x = x_i$  and  $y = y_j$ . In the case of no relationship between  $x$  and  $y$ ,  $p_{ij}^{xy} = p_i^x p_j^y$ , so that the MI is zero for independent processes. Otherwise,  $MI_{xy}$  will be positive, attaining its maximal value for identical signals.

### Phase Locking Value (PLV)

For two signals  $x$  and  $y$ , the phase locking value is defined as:

$$PLV_{xy} = \left| \langle e^{i[\varphi_x(t) - \varphi_y(t)]} \rangle \right|$$

where  $\varphi_x(t)$  and  $\varphi_y(t)$  are the unwrapped phases of the signals  $x$  and  $y$  at time  $t$ . The  $\langle \cdot \rangle$  denotes the average over time. The Hilbert transform was used to extract the instantaneous phase of each signal.

The  $h^2$ , PLV and  $r^2$  values range from 0 (independent signals) to 1 (fully correlated signals).

## Data

### Simulations

In order to quantitatively assess the performance of source connectivity approaches, we generated simulated EEG signals following the procedure described in (Cosandier-Rim    et al. 2008), see Fig. 1a. The distributed source space consisted in a mesh of the cortical surface (8000 vertices, ~5 mm inter-vertex spacing) that was obtained by segmenting the grey-white matter interface from a normal subject's structural T1-weighted 3D-MRI with Freesurfer (Fischl 2012). Dipoles were located at each vertex of this mesh and oriented radially to the surface at the midway between the white/grey matter interface and the pial surface. The time-course of each dipole of the source space was generated from a modified version of the

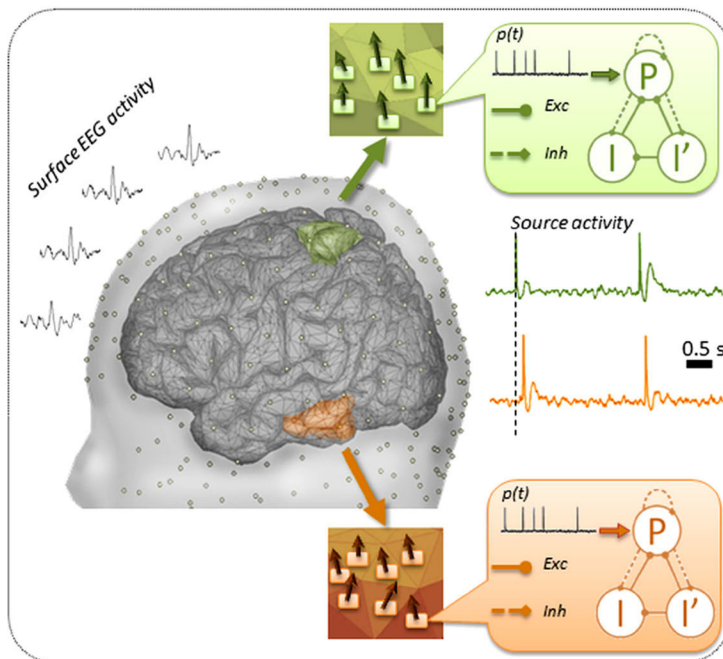
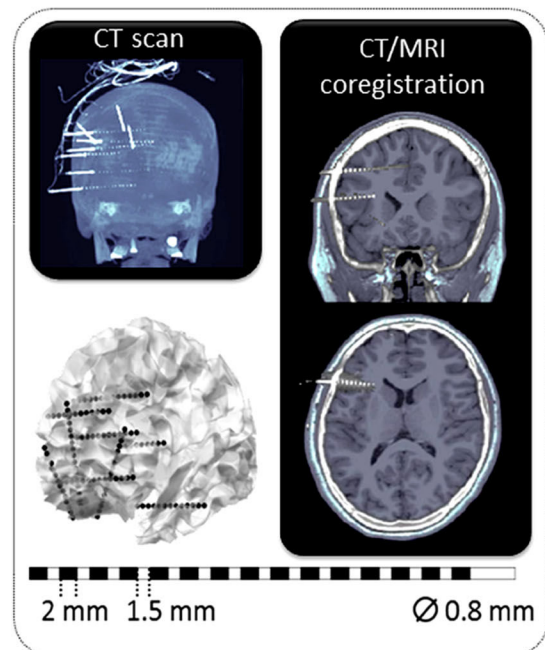
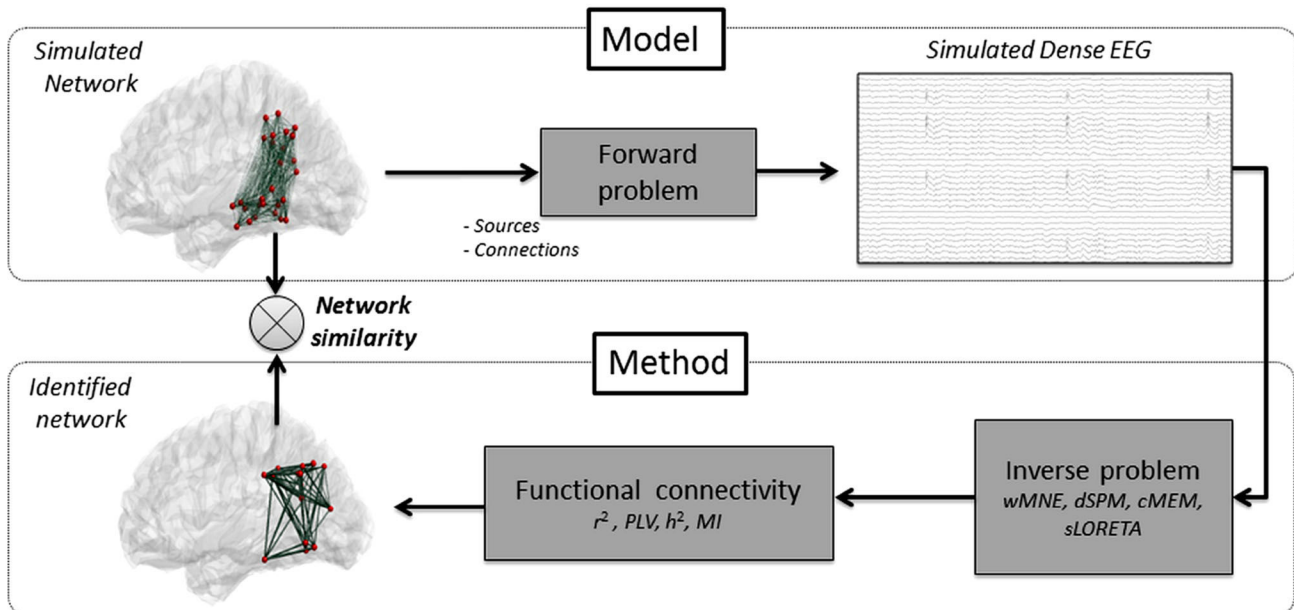
**Fig. 1** Structure of the investigation. **a** Simulated epileptic spikes: model used to generate epileptic spikes (see "Simulations" section for detailed description), **b** Identification of interictal epileptic network: first, a network is generated by the model and considered as the 'ground truth'. By solving the forward problem, synthetic dense EEG data are generated. These signals are then used to solve the inverse problem in order to reconstruct the dynamics of sources using three different inverse solutions (wMNE, sLORETA, dSPM and cMEM). The statistical couplings are then computed between the reconstructed sources using three different methods ( $r^2$ , PLV,  $h^2$  and MI). The identified network by each combination (inverse/connectivity) was then compared with the original network using a 'network similarity' algorithm [13] and **c** Intracerebral recordings: the positions of the intracerebral SEEG signals used in the real application. The coordinates of the electrode's contacts was obtained by the CT/MRI coregistration. wMNE weighted minimum norm estimate, sLORETA standardized low resolution brain electromagnetic tomography, dSPM dynamical statistical parametric mapping, cMEM standard maximum entropy on the mean,  $r^2$  linear correlation coefficient, PLV phase locking value,  $h^2$  nonlinear correlation coefficient, MI mutual information,  $P$  pyramidal cells,  $I$  inhibitory interneurons

physiologically relevant neural mass model reported in (Bourien et al. 2005; Wendling et al. 2000, 2002).

In brief, this computational model was designed to represent a neuronal population with three subsets of neurons (pyramidal cells  $P$  and interneurons  $I$  and  $I'$ ) interacting via synaptic transmission (Fig. 1a). Pyramidal cells ( $P$ ) receive endogenous excitatory drive (AMPAergic collateral excitation) from other local pyramidal cells and exogenous excitatory drive from distant pyramidal cells (via external noise input  $p(t)$ ). They also receive inhibitory drive (GABAergic feedback inhibition) from both subsets of local interneurons ( $I$  and  $I'$ ). In turn, interneurons receive excitatory input (AMPA) from pyramidal cells.

A Gaussian noise was used as external input to neuronal population. The mean ( $m = 90$ ) and standard deviation ( $\sigma = 30$ ) were adjusted to represent randomly varying density of incoming action potentials (Aps). However, for the purpose of this study, a modification was made to this noise model. Indeed, abrupt increase/decrease of the density of Aps can occur in the external input noise at user-defined times to mimic transient AP volleys from other brain regions involved in the generation of interictal events. Thus, in this model, a simulated IES can be viewed as the responses of a nonlinear dynamical system (comprising positive and negative feedback loops) to transient pulses superimposed on a Gaussian noise (classically used in the neural mass modeling approaches).

As in the standard implementation, the shape (spike component followed by a wave component) can still be controlled by adjusting excitation and inhibition parameters of each population (gains in feedback loops). However, the aforementioned modification offers one major advantage: as pulses in the noise input are user-defined, the occurrence times of simulated IESs are controlled, in

**A Simulated epileptic spikes****C Intracerebral recordings****B Identification of epileptogenic network**

contrast with the standard implementation where IESs simply result from random fluctuations of the noise. The consequence is that this new model feature allows for simulation multi-focal IESs with well-controlled time shifts. Indeed, as illustrated in Fig. 1a, we could generate delayed epileptiform activity in multiple distant patches just by introducing short delays between the pulses superimposed on the respective input noises of neuronal populations at each patch.

Finally, from appropriate setting of the input noise, as well as excitation and inhibition-related parameters at each neural mass included in simulated epileptic sources, a set of epileptiform temporal dynamics was obtained. These dynamics were assigned to a source made of contiguous vertices (active source) manually outlined with a mesh visualization software (Paraview, Kitware Inc., NY, US). Uncorrelated background activities were attributed to the other vertices. Once the amplitude of each elementary dipole was known, EEG simulations were obtained by solving the forward problem in a 3-layer realistic head model (inner skull, outer skull and the scalp with conductivity values of 0.33, 0.0042, 0.33 S/m respectively) using the Boundary Element Method (BEM) with the OpenMEEG (Gramfort et al. 2010) implemented in Brainstorm software.

We considered two different scenarios. In the first one (single network), EEG simulations were generated from a single source located in the inferior parietal region ( $\sim 1000 \text{ mm}^2$ ). In the second one (two interconnected networks) an additional source ( $\sim 1000 \text{ mm}^2$ ) was placed in the middle temporal gyrus. In that case, the temporal dynamics of the second source were highly correlated with those of the first source, but with a minor delay (30 ms). This delay of 30 ms was in the range of 10–50 ms delays that are often observed during interictal spikes at different intracranial recording location (Alarcon et al. 1994, 1997; Emerson et al. 1995; Merlet and Gotman 1999) or at different surface sensors (Barth et al. 1984; Ebersole 1994) or between the peaks of dipole source activity (Baumgartner et al. 1995; Merlet and Gotman 1999). This delay was usually interpreted as reflecting propagation between distant regions in the brain. For each scenario, 20 epochs of 60 s at 512 Hz containing 30 epileptic spikes were simulated. Each epoch was obtained for a new realization of the input random noise leading to a new realization of epileptic spikes occurring in background activity. Simulated data were imported in Brainstorm for further analysis.

### Real Data

Real data were selected from a patient who underwent presurgical evaluation for drug-resistant focal epilepsy.

Seizures were stereotyped, with a sudden start, febrile motor automatisms of the upper limb, stretching of the neck and torso and no post-ictal motor deficit. The patient had a comprehensive evaluation including detailed history and neurological examination, neuropsychological testing, structural MRI, standard 32-channels (Micromed, Italy) as well as Dense-EEG 256-channels (EGI, Electrical Geodesic Inc., Eugene, USA) scalp EEG with video recordings and intracerebral EEG recordings (SEEG). MRI showed a focal cortical dysplasia in the mesial aspect of the orbito-frontal region. Dense-EEG was recorded for 1 h, at 1000 Hz following the procedure approved by the National Ethics Committee for the Protection of Persons (CPP, agreement number 2012-A01227-36). The patient gave his written informed consent to participate in this study. This recording revealed sub-continuous spike activity at the most left frontopolar basal electrodes. From this interictal epileptic activity, 85 spikes were visually selected away from the occurrence of any artefacts (muscle activity, blood pulsation, eye blinks). Each spike was centered in a 2 s window and all 85 windows were concatenated for further analysis.

As part of his presurgical evaluation, the patient also underwent intracerebral SEEG recordings with 9 implanted electrodes ( $10 \pm 18$  contacts; length: 2 mm, diameter: 0.8 mm; 1.5 mm apart) placed intracranially according to Talairach's stereotactic method in the left frontal and temporal region, see Fig. 1c. The positioning of the electrodes was determined from available non-invasive information and hypotheses about the localization of his epileptic zone. From these data, subsets of 25 out of the 118 original leads were selected. This selection was made according to the following criteria: i) only contacts showing grey matter activity were retained and ii) among them, only the contact showing the maximal activity was kept when similar intracerebral activity was observed on several contacts.

### Data Analysis

#### *Scalp-EEG Based Interictal Epileptic Networks*

As illustrated in Fig. 1B, source activity was estimated using four inverse algorithms (dSPM, wMNE, sLORETA and cMEM, see “Materials and Methods” section). A baseline of 1 s length was used to estimate the noise covariance matrix both on simulated and real scalp EEG data. For real data, source localization was applied on averaged spikes, taking as time reference the maximum of the negative peak, while for simulated data the source localization was applied to non-averaged spikes. The cortical surface was anatomically parcellated into 148 regions of interest (ROI) (Destrieux et al. 2010) and then



re-subdivided into  $\sim 1500$  sub-ROIs using Brainstorm. The 148 ROIs provided initially by the Destrieux Atlas (using Freesurfer) were *quasi* equally subdivided to obtain the 1500 sub-ROIs with  $1 \text{ cm}^2$  average sizes. Time series of the reconstructed source activities were averaged over each of the 1500 ROIs.

After the reconstruction of sources (source localization and estimation of temporal dynamics), functional connectivity was estimated using four methods ( $r^2$ ,  $h^2$ , PLV, and MI, see “Materials and Methods” section). Each quantity was computed on the set of 2 s single spikes. All connectivity matrices ( $1500 \times 1500$ ) were thresholded as follows. We computed the strength of each node of the weighted undirected graph and we kept nodes with the highest 1 % strength values. The same threshold was applied on the adjacency matrices for all combinations (inverse/connectivity). The strength was defined as the sum of all edge weights for each node; all weights were positive and normalized between 0 and 1.

In order to define the reference networks, all the dipoles were supposed synchronized and the reference network reflected a fully connected undirected graph. In the case of double network scenario, a number of 37 sub-regions (nodes) were considered. The dynamics of the dipoles associated to these nodes were similar and resulting a  $37 \times 37$  fully connected network where connections (local and remote) between the 37 nodes have the same weight value.

#### *Quantification of Network Similarity*

In order to compare the reference brain network simulated in the model with the network identified from simulated scalp EEG by each of the inverse/connectivity combination (Fig. 1b), we used a network similarity algorithm recently developed in our team (Mheich et al. 2015a), see *supplementary materials* for more details about the algorithm. The main advantage of this algorithm is that it takes into account the spatial location (3D coordinates) of the nodes when comparing two networks, in contrast with other methods based on the sole statistical properties of compared graphs. The algorithm provides a normalized Similarity Index (SI): 0 for no similarity and 1 for two identical networks (same properties and topology). The connectivity analysis, the network measures and network visualization were performed using EEGNET (Hassan et al. 2015a, b).

#### *Depth-EEG Based Interictal Epileptic Networks*

Functional connectivity using  $h^2$  were directly computed from SEEG signals at the 25 selected intracerebral electrode contacts. Adjacency matrices ( $25 \times 25$ ) were obtained and thresholded using the same procedure than

that applied to the graphs obtained for scalp dense EEG (both simulated and real).

#### *Scalp-EEG-Based Versus Depth-EEG-Based Epileptic Network Matching*

In order to compare the graphs in the three-dimensional coordinates system of the cortex mesh, the 3D coordinates of the SEEG were first estimated by the co-registering the patient's CT scan and MRI. These points were then projected on the surface mesh. The transformation from MRIs (voxels) coordinates to surface (SCS/MNI) coordinates was realized in Brainstorm. The Scalp-EEG-based and depth-EEG-based epileptic networks were visually compared by matching the identified regions (nodes) in both networks.

#### *Statistical Analysis*

On the simulated data, a Wilcoxon rank-sum test was used to compare between the SIs obtained for each combination at each trial, corrected for multiple comparison using Bonferroni approach.

## **Results**

### **Simulated Data: Influence of the Source Reconstruction/Functional Connectivity Combination**

The results obtained in the case of the single network scenario are illustrated in Fig. 2, for the 16 different combinations of the source reconstruction and functional connectivity methods. The visual investigation of these results revealed that networks identified using the different combinations of methods were concordant with the reference network (Fig. 2b). Indeed none of the identified networks had nodes in a remote region (Fig. 2a). The qualitative analysis also showed that the number of nodes and the connections between them varied according to the combination of methods used. For a given connectivity approach, changing the localization method did not dramatically modify the network aspect, except for cMEM. Conversely, for a given source localization approach, changing the functional connectivity measure changed, qualitatively, the network. Although this was difficult to assess visually,  $h^2$  combined with MNE or sLORETA was giving the network that best matched the reference network while cMEM/MI provided a result that was different from the reference network.

Quantification of these differences is provided in Fig. 2c. Overall, values of network similarity were relatively high and ranged from 70 to 82 %. For a given

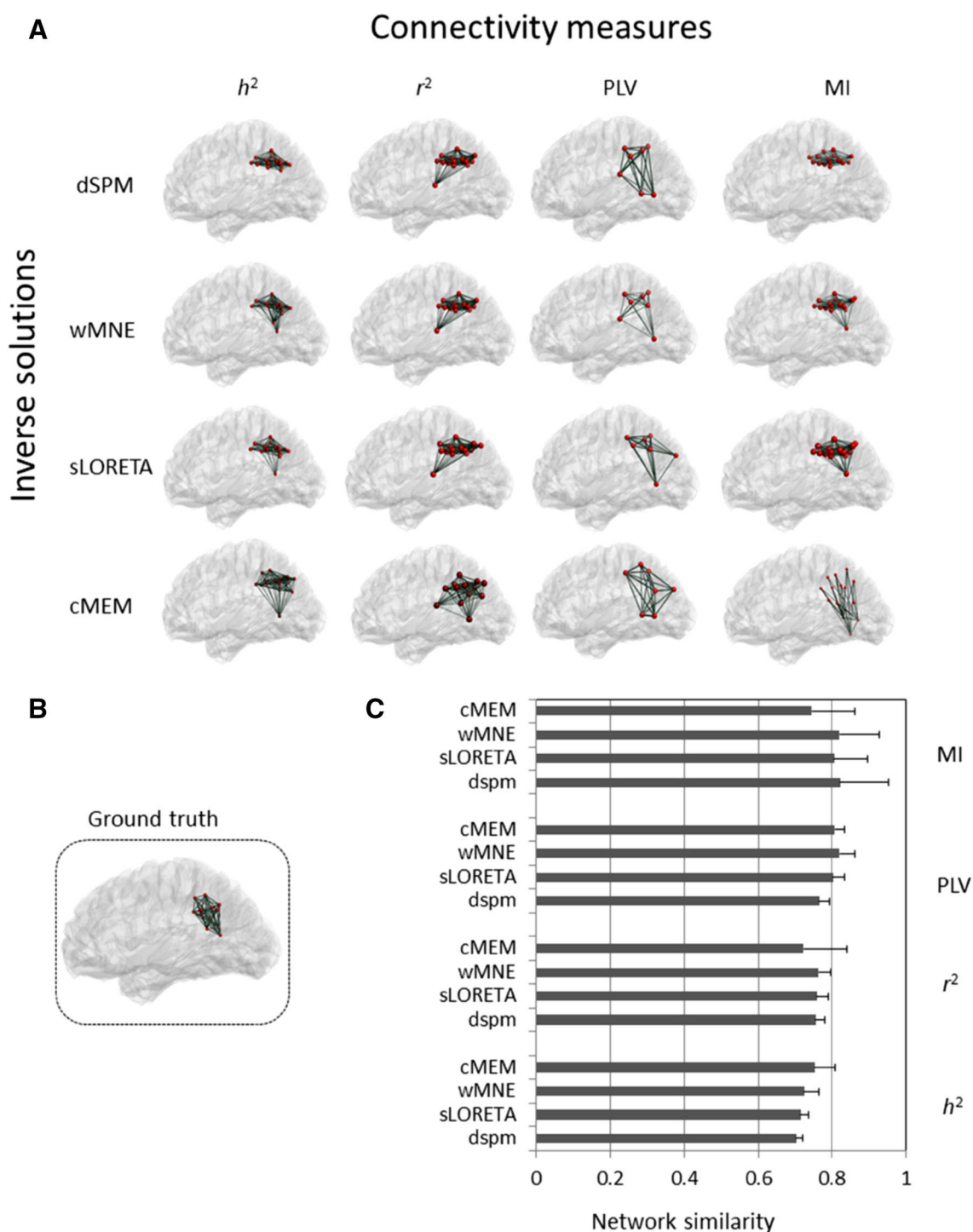


**Fig. 2** One network scenario. **a** Brain networks obtained by using the different inverse and connectivity methods. **b** The original network (ground truth) is shown and **c** values (mean  $\pm$  standard deviation) of

the similarity indices computed between the network identified by each combination and the model network

connectivity approach, changing only the localization algorithm slightly modified SI values by 3 % ( $h^2$ ) to 8 % (MI). For a given source localization approach, the SIs varied within 9 % (wMNE) to 12 % (dSPM). Results obtained using MI were on average better than PLV,  $r^2$  and

$h^2$ . The combination providing the highest similarity values between the estimated and the actual network was dSPM/MI (82.2 %) followed by wMNE/MI (82 %) and wMNE-PLV (82 %). The lowest similarity value was obtained with the dSPM/ $h^2$  combination. The Wilcoxon rank-sum test did

not reveal any significant difference between the similarity values obtained in this first study.

Results obtained in the case of two interconnected networks for the 16 combinations of the inverse/connectivity methods are reported in Fig. 3. Results indicate that the networks identified by all the combinations are relatively close to the model network (Fig. 3b) since, similarly to the previously scenario, there was no node in other distant regions or in the right hemisphere. The networks did not qualitatively change much for a given connectivity measure except for cMEM. Rather, as observed in the first scenario, the variability between the different combinations was more related to the choice of the connectivity measure, given a source localization approach. The results of PLV (whatever the inverse solution algorithm) provide the closest result to the reference network. cMEM/MI shows also a relatively close network to the reference network while cMEM/ $h^2$  indicated, visually, the farthest result from the reference network.

Values of network similarity are reported in Fig. 3c. These values were lower than those in the single network scenario, ranging from 57 to 73 %. For a particular connectivity measure, changing the inverse algorithm modified the SIs by 1 % ( $r^2$ ) to 8 % ( $h^2$ ) while for a given source reconstruction algorithm, the SIs varied between 6 % (dSPM) to 13 % (wMNE). The combination providing the result closest to the reference network was wMNE/PLV (73 %). High values were also obtained with sLORETA/PLV (68 %) and cMEM/PLV (66 %). The cMEM/ $h^2$  combination shows the lowest SI value (57 %).

Interestingly, for scenario 2 results obtained with wMNE/PLV were significantly closest to the actual network than the other ones (Wilcoxon rank-sum test,  $p < 0.01$ , corrected using Bonferroni).

### EEG Source Localization Versus Functional Connectivity

An essential issue that is addressed in this paper relates to the difference between the proposed “network-based” approach and the classical approach using source localization only. In Fig. 4, we show two typical examples of the difference between the proposed network-based analysis and the classical localization approach. The first example is for cMEM combined with MI vs. cMEM only. This Figure shows that the information extracted in both cases was noticeably different. The source connectivity approach identified a network close to the reference one (Fig. 4a), with nodes both in the parietal and in the temporal region (Fig. 4b). There were no spurious nodes in remote regions. In contrast, with the sole source localization, after averaging the results over a 50 ms interval around each of the epileptic peaks, the parietal source was

well retrieved while the temporal source remained almost unobserved. The second example was wMNE/PLV vs. wMNE, the figure shows that the network-based approach was able to identify a network close to the reference with no spurious connections in distant regions. The source localization approach identified the two regions different energies at. Moreover, many spurious sources were observed in remote regions. Similar results were observed for single network configuration.

### Real Data: Scalp-EEG-Based Versus Depth-EEG-Based Epileptic Network

The results obtained from real data recorded in a patient are described on Fig. 5. In this patient, the sources of scalp EEG interictal spikes were widespread over the left frontal and temporal regions. Sources with maximum activity were found in the left frontal pole and orbitofrontal regions but a substantial activation was also detected in the left temporal as well as right frontal poles (Fig. 5a, left). When combining wMNE and PLV on the same scalp EEG data, the source connectivity approach retrieved a 5-nodes network in the left frontal lobe, involving the mesial (rectus gyrus) and lateral orbitofrontal region as well as the anterior cingulate gyrus (Fig. 5a, right). This result was concordant with that the network identified directly from intracerebral recordings by computing the functional connectivity among SEEG signals (Fig. 5b right). Indeed, the depth-EEG based network involved six nodes in the left mesial orbito-frontal (rectus gyrus), and anterior cingulate region. All these nodes were also identified by the visual analysis (Fig. 5b, left) as regions involved in the main interictal activity (rectus gyrus) as well as in the propagated interictal activity (cingulate gyrus).

The similarity indices between networks identified by each of the combination with the depth-EEG-based network are presented in Fig. 5c. Results showed that the wMNE/PLV provides the highest SI value (70 %) followed by wMNE/ $h^2$  (47 %) and sLORETA/PLV (47 %). The cMEM method showed the lowest SI values whatever the connectivity measure (6, 1, 1 and 1 % for cMEM/MI, cMEM/PLV, cMEM/ $h^2$  and cMEM/ $r^2$  respectively).

### Discussion

Identifying epileptic brain networks from noninvasive M/EEG data is a challenging issue. Recently, source localization combined with functional connectivity analysis led to encouraging findings in the estimation of functional cortical brain networks from scalp M/EEG recordings (Coito et al. 2015; Jiruska et al. 2013; Malinowska et al. 2014). Nevertheless, the joint use of these

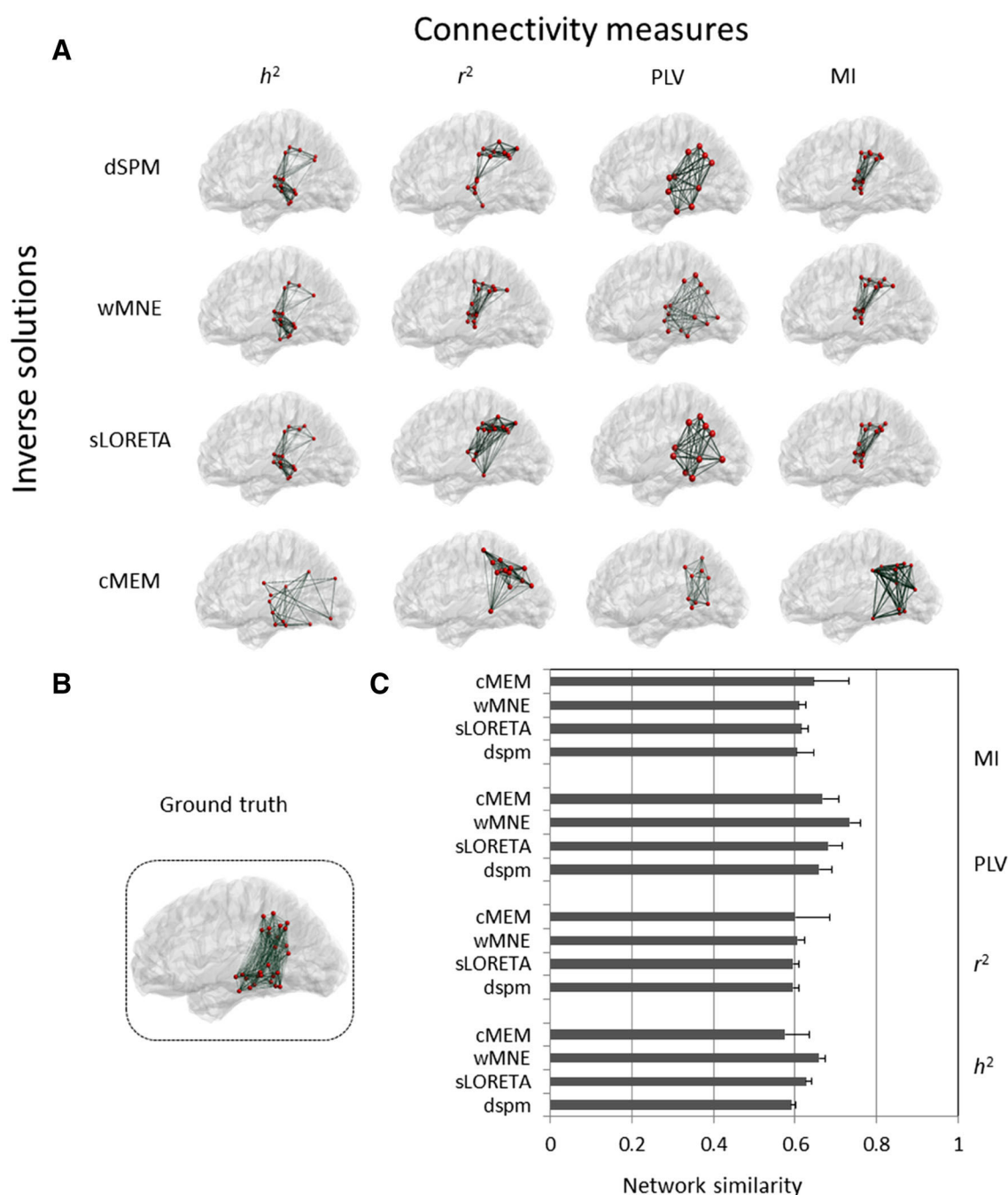


**Fig. 3** Two networks scenario. **a** Brain networks obtained by using the different inverse and connectivity methods. **b** The original network (ground truth) is shown and **c** values (mean  $\pm$  standard

deviation) of the similarity indices computed between the network identified by each combination and the model network

two approaches is still novel and raises a number of methodological issues that should be controlled in order to get appropriate and interpretable results. In this paper, we reported a comparative study -in the context of epilepsy- of the networks obtained from all possible combinations between four algorithms to solve the EEG inverse problem and four methods to estimate the functional connectivity. An originality of this study is related to the use of dense

EEG signals simulated data from a realistic model of multi-focal epileptic zone as a ground truth for comparing the performance of considered methods. To our knowledge, a model-based evaluation of source connectivity methods has not been performed yet. A second—and still novel—aspect is the use of depth-EEG signals (intracerebral recordings performed during presurgical evaluation of drug-resistant epilepsy) to evaluate the relevance of



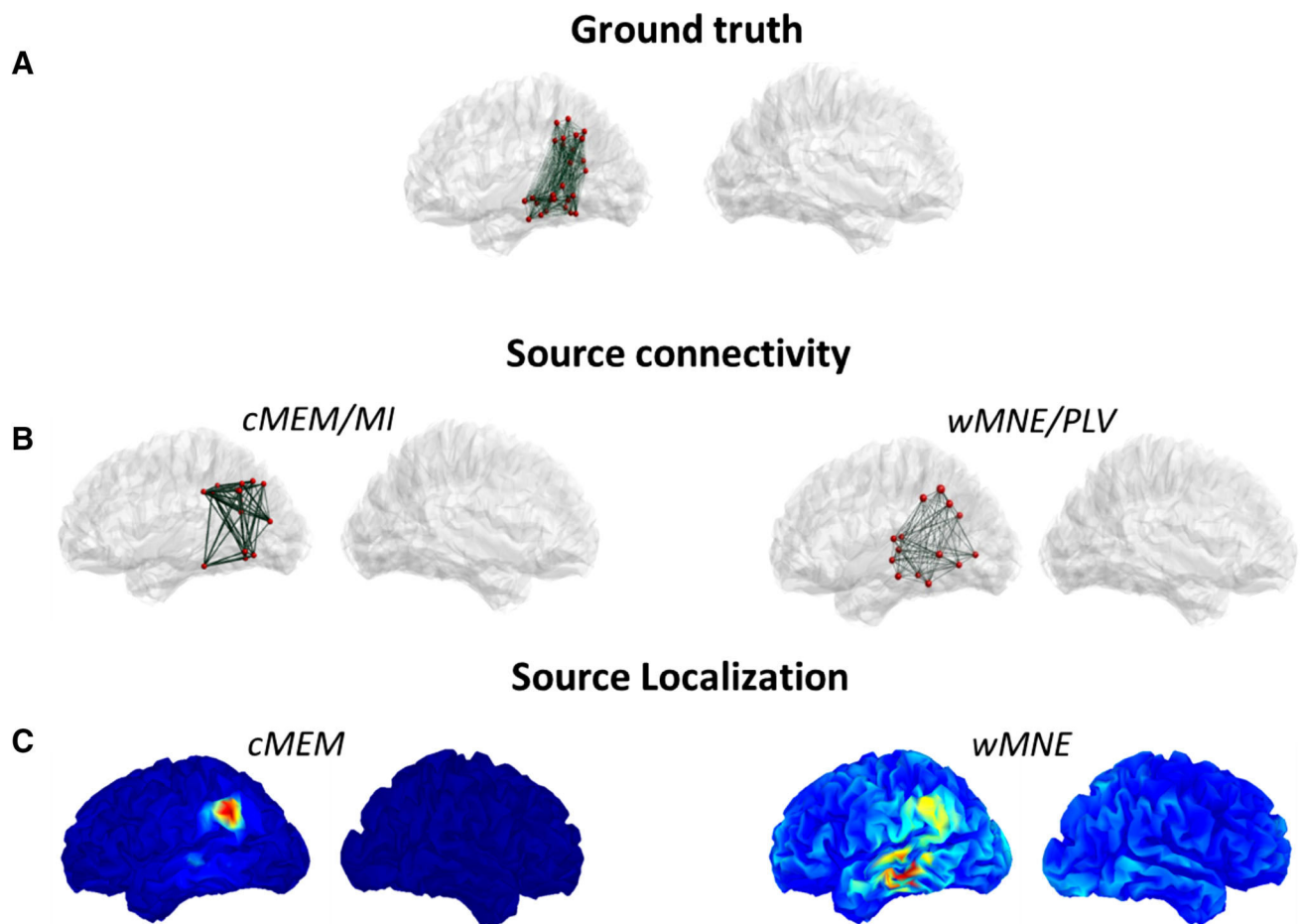


**Fig. 4** Source localization versus source connectivity. **a** the reference network. **b** Results obtained by the network-based approach (cMEM/MI and wMNE/PLV). **c**. Results obtained by the localization based approach (cMEM and wMNE) using same window of analysis.

networks identified from scalp EEG data. Overall results obtained on simulated as well on real data indicated that the combination of the wMNE and the PLV methods leads to the most relevant networks as compared with the ground-truth (simulations) or with the intracerebrally-identified networks (patient data). Results are more specifically discussed hereafter.

### Methodological Considerations

The connectivity matrices were thresholded by keeping the nodes with highest strength values (strongest 1 %). This procedure was used to standardize the comparison between all the combinations. We were aware about the effect of this threshold and we realized the comparative study using different threshold values. All threshold values were found to lead to the same differences between the method (inverse/connectivity) combinations.

In this paper, we have averaged the reconstructed sources within the same region of interest defined by the

Results were averaged over a 50 ms interval around each of the spike peaks. *Red* color represents the sources with the highest energy (Color figure online)

parcellation process based on Destrieux atlas. This approach was frequently used in the context of M/EEG source connectivity (de Pasquale et al. 2010; Fraschini et al. 2016; Hassan et al. 2015a). However, such an averaging procedure may increase the noise power since its computation is performed over sources that, with some probability, may not exhibit correlation (Brookes et al. 2014) where the need of alternative approaches such as flipping the sign of the sources in each ROIs before averaging the regional time series (Fraschini et al. 2016) or developing methods based on probabilistic maps, a widely approach used in the fMRI-based analysis, for instance.

Although EEG source connectivity reduced the problem of volume conduction as compared with scalp EEG connectivity, it does not yet provide a perfect solution. The volume conduction effect is a challenging issue when performing EEG/MEG inverse solution (Schoffelen and Gross 2009). In the connectivity context, the main effect of the volume conduction is the appearance of ‘artificial’ connections among close sources, a problem often referred

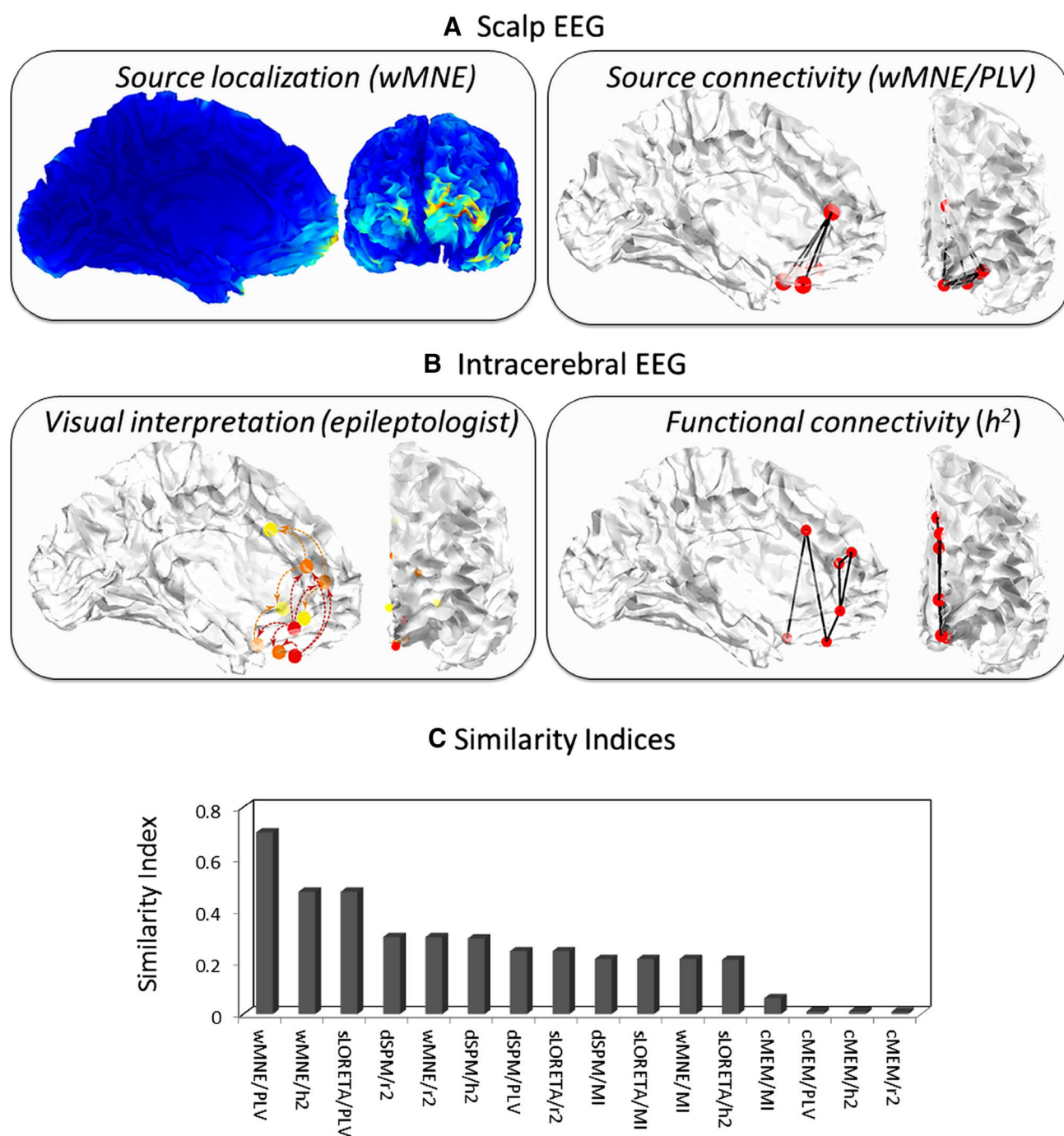


**Fig. 5** Application on real data. **a** Scalp EEG: results of the source localization approach using wMNE (*right*) and source connectivity using wMNE/PLV (*left*), **b** Intracerebral EEG: regions visually identified by the epileptologist (*right*) and the network obtained by

computing the functional connectivity between the intracerebral EEG signals (*left*), **c** Similarity indices: the SI values obtained between the network identified by each of the combination and the intracerebral-EEG-based network

to as ‘source leakage’. The use of a high spatial resolution (high number of ROIs) may increase this problem. A few approaches have been proposed recently to deal with the source leakage by either normalizing the edges weights by the distance between the nodes or removing the edges between very close sources. Although, these approaches

have some advantages, it was shown that, in most cases, they also remove ‘real’ connections (Schoffelen and Gross 2009). In this context, some connectivity methods such as PLV have been shown to reduce the volume conduction (Hipp et al. 2011). This may explain the good performance of this method. Indeed, in the double network scenario,

PLV was able to detect the long-range connections between parietal and temporal networks.

Four inverse/connectivity algorithms were evaluated in this paper. It is worth mentioning that some other inverse algorithms like MUSIC-based and beamforming as well as some connectivity measures such as power envelope correlation (O'Neill et al. 2015) were not included in this study. Moreover, we were focusing in this paper on evaluating different families of 'functional' connectivity methods regardless the directionality of these connections. Nevertheless, we consider that the analyses of the 'effective' connectivity methods that investigate the causality between brain regions may be of interest in the context of epilepsy (Coito et al. 2015, 2016). In this perspective, methods such as the granger causality, the transfer entropy could be added to expand this comparative study. In addition, all methods evaluated in the paper were bivariate, multivariate methods such as those based on the MVAR model were not included in our study. Different methodological questions appear when using MVAR-based approaches. First, the successful estimation of MVAR such as Partial Directed Coherence (PDC) or Directed Transfer Function (DTF) depends largely on the fitted MAR model, since all information is resulting from the estimated model parameters. In practice, this issue is difficult and directly related to the choice of an optimal model order and an optimal epoch length. Concerning the optimal model, most of the criteria were originally proposed for univariate AR modeling and no consensus was reported about multivariate ones. The second crucial question is how to choose the proper window size specially that MVAR model assumes that the underlying process is stationary, while neurophysiological activity are transient and may rapidly change their states representing high nonstationary behaviors (Pereda et al. 2005). Nevertheless the MVAR (when carefully applied) could provide complementary information not only about the link exists between two signals but also if one structure drive another or if there is feedback between these structures (Kuś et al. 2004). The directionality could be also defined as 'time-delay' between two regional time series which can be computed using linear or nonlinear correlation coefficients. As our main objective in this study was to compare inverse algorithms and 'functional' connectivity methods using same criteria (here we used similarity between reference and estimated undirected graphs), we didn't investigate the time-delays in the presented quantitative analysis. In addition this feature cannot be computed for all the selected methods (the case of the phase synchronization method for instance). We believe that the directionality, estimated from Granger causality or/and time delays, is indeed an interesting supplementary feature in the context of epileptic seizure propagation and will be a potential element for further analysis.

The head model used in this study was computed using the Boundary Element Method (BEM) with three layers (skin, skull and brain). This model was widely used in the context of M/EEG source estimation (Fuchs et al. 2007) as a compromise between computational cost and accuracy. Nevertheless, other methods exist to compute the head model such as the Finite Element Method (FEM) or adding other layers such as cerebrospinal fluid (CSF). These methods can possibly have effect of the resultant network (Cho et al. 2015). The evaluation of the above mentioned parameters/factors may be the topic of further investigation.

### Identification of Interictal Epileptic Networks from Scalp Dense-EEG Data

A salient feature of epilepsy in general and epileptic networks is the increased synchronization among interconnected neuronal populations distributed over distant areas. This "hyper"-synchronization often leads to an increase of brain connectivity, not only during the transition to seizures but also during interictal periods, as shown in many studies based on intracranial recordings (see (Wendling et al. 2010) for review). In this context, the combination of the M/EEG source imaging with the functional connectivity measures has recently disclosed promising findings to identify pathological brain networks, at the cortical level (Dai et al. 2012; Lu et al. 2012; Malinowska et al. 2014; Song et al. 2013).

However, two factors seem to be crucial for reliable estimation of EEG source connectivity: (i) the number of scalp electrodes and (ii) the combination between the inverse solution algorithm and the functional connectivity measure. Concerning the number of electrodes, it was reported that the increase of the spatial resolution by using dense EEG may dramatically improve the accuracy of the source localization analysis (Michel and Murray 2012; Song et al. 2015). In addition, the use of dense EEG, as compared to classical montages (32 or 64 electrodes), is needed to accurately identify functional brain networks from scalp EEG (Hassan et al. 2014). To overcome this issue, dense-EEG (256 electrodes) recordings were used in this study. The main feature of this system is the excellent coverage of the subject's head by surface electrodes allowing for improved reconstruction of the cortical activity from non-invasive scalp measurements, as compared with more standard 32-128 electrode systems (Song et al. 2015). Regarding the combination of inverse/connectivity methods, most of reported studies have empirically selected a combination while this selection was shown to have a dramatic impacts on results, in term of identified network topology (Hassan et al. 2014). The present analysis brings further confirmation of this high

variability observed when different inverse solutions and/or connectivity measures are being used in the pipeline leading to cortical networks from EEG signals.

A major advantage of the EEG source connectivity approach as presented here is that reconstructed sources and associated networks were identified for the whole brain. Then graph-based metrics (strength values) were computed to characterize the networks and the similarity index was used to compare the networks obtained from various method combinations. In addition, functional connectivity was applied directly to the reconstructed signals and not on derived components. In this regard, this study differs from (Malinowska et al. 2014) where connectivity was estimated on signals components obtained by ICA decomposition. Although the methodological issue of measuring connectivity between *independent* components still holds, a future interesting study will compare the results obtained from the ICA-based approach to those reported here from source connectivity.

### EEG Source Localization Versus Functional Connectivity

Source localization methods have been widely applied to interictal epileptic spikes (Becker et al. 2014). The goal of these approaches is the localization of brain generators of epileptic activity from scalp recordings. A fundamental question that is addressed in this paper relates to the difference between the source connectivity and the source localization approach. This study indicated that the information extracted from dense-EEG recordings in both cases can differ dramatically. First, the connectivity is an additional step to the simple source reconstruction/localization. Second, the fundamental difference between both methods is that the source localization ignores all possible communications between brain regions. When performing source localization analysis, the sources with highest amplitude (averaged at given time period or computed at the instant of peak amplitude of the signal) are classically kept. However, to some extent (depending on threshold), this approach may neglect the possible contribution of “low energy” sources participating into the network activity.

Conversely, the hypothesis behind the network-based approach (typically when phase synchronization methods are used as connectivity measure) is that sources can be synchronized regardless their amplitude. To this extent, we believe that the network-based approach allows for revealing networks that are more specific to epileptic networks, as hyper-synchronization phenomena constitute a typical hallmark of such networks. An illustrative example in this paper is the poor involvements of the temporal lobe region when the sole source localization approach (in the case of

cMEM) was applied while both parietal and temporal networks (as a priori introduced in the EEG generation model) are retrieved by the connectivity-based approach (cMEM/ $h^2$ ). Note that we have averaged the source localization results in a time window of 50 ms to cover the time delay of 30 ms set in the model between the two brain regions. Different time window were used to avoid the effect of the window length. All tested windows (30 ms, 40 ms, 50 ms and 60 ms) showed similar observations i.e. the absence of the temporal sources (not shown here). The fact that epilepsy is considered as a network disease can explain the low performance of some of the inverse methods as these methods were originally developed to localize ‘local’ epileptic foci characterized by high-energy sources regardless the interrelationships between brain regions. Our results show that EEG source connectivity methods are more suited in the case of multi-focal epileptic zone. More generally, they support the recent tendency in brain disorder research which is the necessity to move from localizing ‘pathological areas’ to identifying ‘altered networks’ (Diessen et al. 2013; Fornito et al. 2015).

### Epilepsy as a Network Disorder

There is increasing evidence that epileptic activity involves brain networks rather than a single well circumscribed region and that these dysfunctional networks contribute to both ictal and interictal activity (Bourien et al. 2004, 2005; Coito et al. 2015; Engel Jr et al. 2013; Hipp et al. 2011). Functional connectivity was widely applied to depth-EEG data to predict seizures (Mormann et al. 2000) and identify epileptic networks in partial epilepsies (Bartolomei et al. 2001). These studies showed alterations of synchronization in brain networks during interictal to ictal transition (Wendling et al. 2003) as well as during seizures (Diessen et al. 2013; Jiruska et al. 2013; Schindler et al. 2008). Most of these studies were performed using invasively-recorded data in patient’s candidate to surgery. Interestingly, our results show that pathological networks involved during epileptiform activity can also be identified from scalp EEG.

Indeed, we have evaluated the performance of a relatively new approach aiming at identifying epileptic brain networks from scalp EEG. The application of the method on real data showed the good performance of this method in term of network identified from scalp EEG as compared with those identified from intracerebral EEG. Note that the comparison was done only by computing  $h^2$  between the intracerebral signals based on a large number of studies showing that  $h^2$  is one of the most adapted metrics to compute functional connectivity between intracerebral recordings (Bettus et al. 2008; Wendling et al. 2010). Although it is obviously difficult to conclude on a single patient analysis, results showed good matching between



scalp-EEG based networks and both the depth-EEG based networks and the expert judgment. Therefore, future work will consist in the application of the EEG source connectivity on a big database of real dense EEG data recorded from epileptic patients. In these patients candidate to surgery, we plan to use also intracerebral EEG signals as a reference to validate the identified networks. In addition, due to the excellent temporal resolution of the EEG, the dynamic behaviors of the epileptic networks will be also explored (Hassan et al. 2015a; Mheich et al. 2015b).

Finally, the capacity to describe epileptic activity not only according to the sites where epileptiform activity is generated but also according to the abnormal functional relationships between these sites can definitively improve the surgical approach. We speculate that in order to better understand and ultimately prevent seizures, it is essential to identify and then remove/disconnect pathological nodes of the network (exhibiting abnormal hyper-synchronization capability). The proposed method contributes to this aim and reported results constitute a first step toward the development of more efficient non-invasive diagnostic methods for clinical epileptology.

**Acknowledgments** This work has received a French government support granted to the CominLabs excellence laboratory and managed by the National Research Agency in the “Investing for the Future” program under reference ANR-10-LABX-07-01. It was also financed by the Rennes University Hospital (COREC Project named conXion, 2012-14).

## References

- Adebimpe A, Aarabi A, Bourel-Ponchel E, Mahmoudzadeh M, Wallois F (2016) EEG resting state functional connectivity analysis in children with benign epilepsy with centrotemporal spikes. *Front Neurosci* 10:143
- Alarcon G, Guy C, Binnie C, Walker S, Elwes R, Polkey C (1994) Intracerebral propagation of interictal activity in partial epilepsy: implications for source localization. *Journal of Neurology, Neurosurg Psychiatry* 57:435–449
- Alarcon G et al (1997) Origin and propagation of interictal discharges in the acute electrocorticogram. Implications for pathophysiology and surgical treatment of temporal lobe epilepsy. *Brain* 120:2259–2282
- Astolfi L et al (2007) Comparison of different cortical connectivity estimators for high-resolution EEG recordings. *Hum Brain Mapp* 28:143–157
- Babiloni F et al (2005) Estimation of the cortical functional connectivity with the multimodal integration of high-resolution EEG and fMRI data by directed transfer function. *Neuroimage* 24:118–131
- Barth DS, Sutherling W, Engle J, Beatty J (1984) Neuromagnetic evidence of spatially distributed sources underlying epileptiform spikes in the human brain. *Science* 223:293–296
- Bartolomei F, Wendling F, Bellanger J-J, Régis J, Chauvel P (2001) Neural networks involving the medial temporal structures in temporal lobe epilepsy. *Clin Neurophysiol* 112:1746–1760
- Baumgartner C et al (1995) Propagation of interictal epileptic activity in temporal lobe epilepsy. *Neurology* 45:118–122
- Becker H et al (2014) EEG extended source localization: tensor-based vs. conventional methods. *NeuroImage* 96:143–157
- Betti V, Della Penna S, de Pasquale F, Mantini D, Marzetti L, Romani GL, Corbetta M (2013) Natural scenes viewing alters the dynamics of functional connectivity in the human brain. *Neuron* 79:782–797
- Bettus G, Wendling F, Guye M, Valton L, Régis J, Chauvel P, Bartolomei F (2008) Enhanced EEG functional connectivity in mesial temporal lobe epilepsy. *Epilepsy Res* 81:58–68. doi:10.1016/j.eplepsyres.2008.04.020
- Bola M, Sabel BA (2015) Dynamic reorganization of brain functional networks during cognition. *NeuroImage* 114:398–413
- Bourien J, Bellanger JJ, Bartolomei F, Chauvel P, Wendling F (2004) Mining reproducible activation patterns in epileptic intracerebral EEG signals: application to interictal activity. *IEEE Trans Bio-Med Eng* 51:304–315. doi:10.1109/TBME.2003.820397
- Bourien J, Bartolomei F, Bellanger JJ, Gavaret M, Chauvel P, Wendling F (2005) A method to identify reproducible subsets of co-activated structures during interictal spikes. Application to intracerebral EEG in temporal lobe epilepsy. *Clin Neurophysiol* 116:443–455. doi:10.1016/j.clinph.2004.08.010
- Brookes MJ et al (2014) Measuring temporal, spectral and spatial changes in electrophysiological brain network connectivity. *Neuroimage* 91:282–299
- Caparos M, Louis-Dorr V, Wendling F, Maillard L, Wolf D (2006) Automatic lateralization of temporal lobe epilepsy based on scalp EEG. *Clin Neurophysiol* 117:2414–2423
- Cho J-H, Vorwerk J, Wolters CH, Knösche TR (2015) Influence of the head model on EEG and MEG source connectivity analysis. *Neuroimage* 110:60–77
- Chowdhury RA, Lina JM, Kobayashi E, Grova C (2013) MEG source localization of spatially extended generators of epileptic activity: comparing entropic and hierarchical Bayesian approaches. *PLoS One* 8:e55969
- Clarke C, Janday B (1989) The solution of the biomagnetic inverse problem by maximum statistical entropy. *Inverse Prob* 5:483
- Coito A et al (2015) Dynamic directed interictal connectivity in left and right temporal lobe epilepsy. *Epilepsia* 56:207–217
- Coito A et al (2016) Altered directed functional connectivity in temporal lobe epilepsy in the absence of interictal spikes: A high density EEG study. *Epilepsia* 57(3):402–411
- Cosandier-Rimé D, Merlet I, Badier J-M, Chauvel P, Wendling F (2008) The neuronal sources of EEG: modeling of simultaneous scalp and intracerebral recordings in epilepsy. *NeuroImage* 42:135–146
- Dai Y, Zhang W, Dickens DL, He B (2012) Source connectivity analysis from MEG and its application to epilepsy source localization. *Brain Topogr* 25:157–166
- Dale AM, Liu AK, Fischl BR, Buckner RL, Belliveau JW, Lewine JD, Halgren E (2000) Dynamic statistical parametric mapping: combining fMRI and MEG for high-resolution imaging of cortical activity. *Neuron* 26:55–67
- David O, Garnero L, Cosmelli D, Varela FJ (2002) Estimation of neural dynamics from MEG/EEG cortical current density maps: application to the reconstruction of large-scale cortical synchrony. *IEEE Trans Biomed Eng* 49:975–987
- David O, Cosmelli D, Hasboun D, Garnero L (2003) A multitrial analysis for revealing significant corticocortical networks in magnetoencephalography and electroencephalography. *Neuroimage* 20:186–201
- de Pasquale F et al (2010) Temporal dynamics of spontaneous MEG activity in brain networks. *Proc Natl Acad Sci* 107:6040–6045

- Destrieux C, Fischl B, Dale A, Halgren E (2010) Automatic parcellation of human cortical gyri and sulci using standard anatomical nomenclature. *Neuroimage* 53:1–15
- Diessen E, Diederer SJ, Braun KP, Jansen FE, Stam CJ (2013) Functional and structural brain networks in epilepsy: what have we learned? *Epilepsia* 54:1855–1865
- Ding L, Worrell GA, Lagerlund TD, He B (2007) Ictal source analysis: localization and imaging of causal interactions in humans. *Neuroimage* 34:575–586
- Ebersole J (1994) Non-invasive localization of the epileptogenic focus by EEG dipole modeling. *Acta Neurol Scand* 89:20–28
- Emerson RG, Turner CA, Pedley TA, Walczak TS, Forgiione M (1995) Propagation patterns of temporal spikes. *Electroencephalogr Clin Neurophysiol* 94:338–348
- Engel J Jr, Thompson PM, Stern JM, Staba RJ, Bragin A, Mody I (2013) Connectomics and epilepsy. *Curr Opin Neurol* 26:186
- Fischl B (2012) FreeSurfer. *Neuroimage* 62:774–781
- Fornito A, Zalesky A, Breakspear M (2015) The connectomics of brain disorders. *Nat Rev Neurosci* 16:159–172
- Fraschini M, Demuru M, Crobe A, Marrosu F, Stam CJ, Hillebrand A (2016) The effect of epoch length on estimated EEG functional connectivity and brain network organisation. *J Neural Eng* 13:036015
- Fuchs M, Wagner M, Kastner J (2007) Development of volume conductor and source models to localize epileptic foci. *J Clin Neurophysiol* 24:101–119
- Gotman J (1983) Measurement of small time differences between EEG channels: method and application to epileptic seizure propagation. *Electroencephalogr Clin Neurophysiol* 56:501–514
- Gotman J (1987) Interhemispheric interactions in seizures of focal onset: data from human intracranial recordings. *Electroencephalogr Clin Neurophysiol* 67:120–133
- Gramfort A, Papadopoulos T, Olivi E, Clerc M (2010) OpenMEEG: opensource software for quasistatic bioelectromagnetics. *Biomed Eng Online* 9:45
- Hämäläinen M (2005) MNE software user's guide NMR Center. Mass Gen Hosp Harvard Univ 58:59–75
- Hämäläinen MS, Ilmoniemi R (1994) Interpreting magnetic fields of the brain: minimum norm estimates. *Med Biol Eng Comput* 32:35–42
- Hassan M, Wendling F (2015) Tracking dynamics of functional brain networks using dense EEG. *IRBM* 36:324–328
- Hassan M, Dufor O, Merlet I, Berrou C, Wendling F (2014) EEG source connectivity analysis: from dense array recordings to brain networks. *PLoS One* 9:e105041
- Hassan M, Benquet P, Biraben A, Berrou C, Dufor O, Wendling F (2015a) Dynamic reorganization of functional brain networks during picture naming. *Cortex* 73:276–288
- Hassan M, Shamas M, Khalil M, El Falou W, Wendling F (2015b) EEGNET: an open source tool for analyzing and visualizing M/EEG connectome. *PLoS One* 10:e0138297
- Hipp JF, Engel AK, Siegel M (2011) Oscillatory synchronization in large-scale cortical networks predicts perception. *Neuron* 69:387–396
- Hoehstetter K, Bornfleth H, Weckesser D, Ille N, Berg P, Scherg M (2004) BESA source coherence: a new method to study cortical oscillatory coupling. *Brain Topogr* 16:233–238
- Jiraska P, de Curtis M, Jefferys JG, Schevon CA, Schiff SJ, Schindler K (2013) Synchronization and desynchronization in epilepsy: controversies and hypotheses. *J Physiol* 591:787–797. doi:10.1113/jphysiol.2012.239590
- Kramer MA, Cash SS (2012) Epilepsy as a disorder of cortical network organization. *Neuroscientist* 18:360–372
- Kuś R, Kamiński M, Blinowska KJ (2004) Determination of EEG activity propagation: pair-wise versus multichannel estimate. *IEEE Trans Biomed Eng* 51:1501–1510
- Laufs H (2012) Functional imaging of seizures and epilepsy: evolution from zones to networks. *Curr Opin Neurol* 25:194–200
- Le Van Quyen M, Soss J, Navarro V, Robertson R, Chavez M, Baulac M, Martinerie J (2005) Preictal state identification by synchronization changes in long-term intracranial EEG recordings. *Clin Neurophysiol* 116:559–568
- Liljeström M, Kujala J, Stevenson C, Salmelin R (2015) Dynamic reconfiguration of the language network preceding onset of speech in picture naming. *Hum Brain Mapp* 36:1202–1216
- Lu Y, Yang L, Worrell GA, He B (2012) Seizure source imaging by means of FINE spatio-temporal dipole localization and directed transfer function in partial epilepsy patients. *Clin Neurophysiol* 123:1275–1283
- Malinowska U, Badier JM, Gavaret M, Bartolomei F, Chauvel P, Bénar CG (2014) Interictal networks in magnetoencephalography Human brain mapping 35:2789–2805
- Merlet I, Gotman J (1999) Reliability of dipole models of epileptic spikes. *Clin Neurophysiol* 110:1013–1028
- Mheich A, Hassan M, Gripon V, Dufor O, Khalil M, Berrou C, Wendling F (2015a) A novel algorithm for measuring graph similarity: application to brain networks. In: 7th international IEEE EMBS neural engineering conference, Montpellier, France
- Mheich A, Hassan M, Khalil M, Berrou C, Wendling F (2015b) A new algorithm for spatiotemporal analysis of brain functional connectivity. *J Neurosci Methods* 242:77–81
- Michel CM, Murray MM (2012) Towards the utilization of EEG as a brain imaging tool. *Neuroimage* 61:371–385
- Mormann F, Lehnertz K, David P, Elger CE (2000) Mean phase coherence as a measure for phase synchronization and its application to the EEG of epilepsy patients. *Physica D* 144:358–369
- O'Neill GC, Barratt EL, Hunt BA, Tewarie PK, Brookes MJ (2015) Measuring electrophysiological connectivity by power envelope correlation: a technical review on MEG methods. *Phys Med Biol* 60:R271
- Pascual-Marqui RD (2002) Standardized low-resolution brain electromagnetic tomography (sLORETA): technical details. *Methods Find Exp Clin Pharmacol* 24:5–12
- Pereda E, Quiroga RQ, Bhattacharya J (2005) Nonlinear multivariate analysis of neurophysiological signals. *Prog Neurobiol* 77:1–37
- Ramon C, Holmes MD (2013) Noninvasive localization of epileptic sites from stable phase synchronization patterns on different days derived from short duration interictal scalp dEEG. *Brain Topogr* 26:1–8
- Schindler KA, Bialonski S, Horstmann MT, Elger CE, Lehnertz K (2008) Evolving functional network properties and synchronizability during human epileptic seizures. *Chaos* 18:033119. doi:10.1063/1.2966112
- Schoffelen JM, Gross J (2009) Source connectivity analysis with MEG and EEG. *Hum Brain Mapp* 30:1857–1865
- Song J, Tucker DM, Gilbert T, Hou J, Mattson C, Luu P, Holmes MD (2013) Methods for examining electrophysiological coherence in epileptic networks. *Front Neurol* 4:55
- Song J et al (2015) EEG source localization: Sensor density and head surface coverage. *J Neurosci Methods* 256:9–21
- Tadel F, Baillet S, Mosher JC, Pantazis D, Leahy RM (2011) Brainstorm: a user-friendly application for MEG/EEG analysis. *Comput Intell Neurosci* 2011:8
- van Mierlo P, Papadopoulou M, Carrette E, Boon P, Vandenberghe S, Vonck K, Marinazzo D (2014) Functional brain connectivity from EEG in epilepsy: seizure prediction and epileptogenic focus localization. *Prog Neurobiol* 121:19–35
- Vecchio F et al (2014) Cortical connectivity in fronto-temporal focal epilepsy from EEG analysis: a study via graph theory. *Clin Neurophysiol* 126(6):1108–1116

- Wendling F, Bellanger J-J, Bartolomei F, Chauvel P (2000) Relevance of nonlinear lumped-parameter models in the analysis of depth-EEG epileptic signals. *Biol Cybern* 83:367–378
- Wendling F, Bartolomei F, Bellanger JJ, Chauvel P (2002) Epileptic fast activity can be explained by a model of impaired GABAergic dendritic inhibition. *Eur J Neurosci* 15:1499–1508
- Wendling F, Bartolomei F, Bellanger J-J, Bourien J, Chauvel P (2003) Epileptic fast intracerebral EEG activity: evidence for spatial decorrelation at seizure onset. *Brain* 126:1449–1459
- Wendling F, Ansari-Asl K, Bartolomei F, Senhadji L (2009) From EEG signals to brain connectivity: a model-based evaluation of interdependence measures. *J Neurosci Methods* 183:9–18
- Wendling F, Chauvel P, Biraben A, Bartolomei F (2010) From intracerebral EEG signals to brain connectivity: identification of epileptogenic networks in partial epilepsy. *Front Syst Neurosci* 4:154

## **Study 2: The dynamic functional core network of the human brain at rest**

A. Kabbara, W. EL Falou, M. Khalil, F. Wendling & M. Hassan

Article published in Scientific reports 7 (1), 2936



# SCIENTIFIC REPORTS

OPEN

## The dynamic functional core network of the human brain at rest

A. Kabbara<sup>1,2,3,4</sup>, W. EL Falou<sup>3,4</sup>, M. Khalil<sup>3,4</sup>, F. Wendling<sup>1,2</sup> & M. Hassan<sup>1,2</sup> 

Received: 10 August 2016

Accepted: 28 April 2017

Published online: 07 June 2017

The human brain is an inherently complex and dynamic system. Even at rest, functional brain networks dynamically reconfigure in a well-organized way to warrant an efficient communication between brain regions. However, a precise characterization of this reconfiguration at very fast time-scale (hundreds of millisecond) during rest remains elusive. In this study, we used dense electroencephalography data recorded during task-free paradigm to track the fast temporal dynamics of spontaneous brain networks. Results obtained from network-based analysis methods revealed the existence of a functional dynamic core network formed of a set of key brain regions that ensure segregation and integration functions. Brain regions within this functional core share high betweenness centrality, strength and vulnerability (high impact on the network global efficiency) and low clustering coefficient. These regions are mainly located in the cingulate and the medial frontal cortex. In particular, most of the identified hubs were found to belong to the Default Mode Network. Results also revealed that the same central regions may dynamically alternate and play the role of either provincial (local) or connector (global) hubs.

The human brain is a complex network. Even at rest, spatially distributed brain regions are functionally connected, in a very organized way, to continuously share information with each other<sup>1–4</sup>. The intrinsic connectivity networks (ICNs), also known as Resting State Networks (RSNs), are now widely recognized and found to be quite consistent across subjects<sup>1,5–13</sup> as well as neuroimaging techniques<sup>14–17</sup>. The most commonly known RSNs are the default mode network (DMN), the dorsal attention network (DAN), the ventral attention network (VAN), the motor network, the visual network (VIS), and the auditory network (AUD).

Several studies have reported the existence of few critical regions that may play a key role in establishing and maintaining an efficient brain communication at rest. The presence of central brain regions or ‘hubs’ at rest has been revealed for structural<sup>18–27</sup> and functional<sup>28–32</sup> connections. In addition to their highly central role, recent studies have shown that these brain hubs tend to be densely interconnected with each other more than expected by chance, forming the so called rich-club organization of the human brain<sup>33–35</sup>.

Using Magnetoencephalography (MEG) or/and Electroencephalography (EEG), it was shown that these RSNs have an electrophysiological basis<sup>16,36–41</sup>. In a preliminary study<sup>32</sup>, we used dense-EEG recordings to confirm the existence of brain regions playing the role of hubs in a static scenario. Yet, the main gain of using M/EEG is the excellent temporal resolution that allows the tracking of the temporal dynamics of RSNs at sub-second time scale, not reachable when using fMRI. Various MEG studies showed the crucial role of the DMN, and the cingulate cortex in particular, in maintaining efficient temporal communication in the whole brain<sup>16,42</sup>. Other studies focused on assessing the temporal transitions between RSNs<sup>40</sup>. However, none of them looked at the temporal transition between brain regions, networks and modules over hundreds of millisecond time scale.

To tackle this issue, we collected dense-EEG data from 20 subjects sitting without performing any particular task. We then reconstructed the functional networks using EEG source connectivity approach as described in previous work<sup>32,43,44</sup>. Topologies of the identified networks were characterized in terms of node’s strength, vulnerability, betweenness centrality and clustering coefficient. In the present study, we extend our previous static analysis<sup>32</sup> toward the study of the dynamic interactions between resting state networks. We have also explored the dynamic modularity and classified brain regions into provincial (intra-community) and connector (inter-community) hubs. Our results revealed the existence of a dynamic core network located mainly in the cingulate and the medial frontal cortex. We found that a large proportion of the brain hubs belong to the DMN. Results also revealed that the same brain hubs might dynamically change their actions and play the role of either provincial (segregation) or connector (integration) hubs.

<sup>1</sup>INSERM, U1099, F-35000, Rennes, France. <sup>2</sup>University of Rennes 1, LTSI, F-35000, Rennes, France. <sup>3</sup>Azm Center for Research in Biotechnology and its Application, EDST, Lebanese University, Beirut, Lebanon. <sup>4</sup>CRSI research center, Faculty of Engineering, Lebanese University, Beirut, Lebanon. Correspondence and requests for materials should be addressed to A.K. (email: [aya.kabbara7@gmail.com](mailto:aya.kabbara7@gmail.com))

## Results

The functional networks were estimated using dense EEG source connectivity method. As recommended in Hassan *et al.*<sup>44</sup>, we combined the weighted Minimum Norm Estimate (wMNE) and the Phase Locking Value (PLV) to reconstruct the dynamic of the cortical sources and compute the functional connectivity between these sources. This produced a fully connected, undirected and weighted networks (see Materials and Methods for details about the construction of the functional networks). In order to explore the advantages of the dynamic analysis, we performed our study in two ways: 'static' and 'dynamic'. For the static approach, the functional connectivity was computed over the entire noise-free epoch duration (40 seconds). To examine the dynamics of the RSNs, we used a sliding window of 300 milliseconds in which PLV was calculated over its data points (see Materials and Methods for more details). This value was chosen as it represents the minimal time window size required to adequately compute PLV as recommended by Lachaux *et al.*<sup>45</sup>. Other time window sizes (1 s, 2 s, 10 s and 40 s) were also explored and results are reported in Figures S2 and S4 in the Supplementary Materials.

We then identified the brain hubs by computing the centrality, vulnerability, strength and clustering coefficient measures of the different brain regions. These measures have been evaluated here since they represent the most commonly used metrics to detect brain hubs<sup>4, 21, 22, 28, 31, 34, 42, 46–54</sup>. In this context, Sporns *et al.*<sup>54</sup> showed that a node can be defined as hub if it has an unusually high strength (a large number of connections) and centrality (the node lies on a high number of shortest paths) and a low clustering coefficient (the neighbours of a hub are not directly connected with each other). We also speculate, based on previous studies<sup>19, 33, 48, 55, 56</sup>, that adding the vulnerability metric to the spectrum of network measures can provide new insights into the definition of the hubness. Indeed, a node with high vulnerability is supposed to have a high influence on the global efficiency of the network<sup>55</sup>. In addition, we have classified hubs into provincials and connectors based on a combination between the participation coefficient and the within-degree module<sup>24, 33, 54, 57–60</sup>. The full pipeline of our study is summarized in Fig. 1.

**Static analysis.** In this analysis, we computed the graph metrics (centrality, vulnerability, strength and clustering coefficient) using the entire signal length (40 s). We then quantified the difference between nodes distributions of each graph metric using a Wilcoxon test. Only nodes showing significant difference ( $p < 0.01$ , Bonferroni corrected) were retained, see Materials and Method section.

Figure 2A presents the results obtained for all subjects. It shows four circular barplots reflecting from the outside inward: centrality, vulnerability, strength and clustering coefficient. The outermost ring shows the 68 brain regions (obtained from the anatomical parcellation based on Desikan-Killiany atlas)<sup>61</sup> arranged by their assigned resting state network (see Table 1 in Supplementary Materials). The figure also shows that the central nodes are L/R iCC, L/R PCC, L/R paraH, L/R MOF, L/R rACC, L/R LOF, L pTRI, L pORB and R ENT. The vulnerable nodes are R iCC, L/R paraH, L/R MOF, L/R rACC, L LOF, L pTRI, L pORB and R ENT. The L/R iCC, L/R PCC, R paraH, L/R MOF, L/R rACC, L LOF are the regions with highest strength while L/R ITG and L/R rMFG are the regions with highest clustering coefficients.

Results also demonstrated that a large proportion of the identified brain regions in terms of centrality (12/13), vulnerability (10/11) and strength (8/8) belong to the DMN (Fig. 2B). In contrast, one can notice that the nodes that have the highest clustering coefficients were distributed across the DAN and the SAN, while no significant node was belonging to the DMN. Brain regions were also classified into provincial hubs, connector hubs and non-hubs by computing the participation coefficient combined with the within-degree z-score of the association matrix obtained for all subjects (Fig. 3A), refer to Materials and Methods section for more details about the modularity analysis. Figure 3B illustrates the spatial locations of the resultant hubs on the cortical surface. We observe that a large number of hubs belong to the DMN (9/12) with the presence of one node belonging to the DAN and two nodes not belonging to any of the five analyzed RSNs. The PCUN region was depicted as a provincial hub, while L PCC, R MOF, L/R paraH, L/R rACC, R paraC, R periCal, R iCC, L pORB and L LOF regions are classified as connector hubs.

**Dynamic analysis.** To investigate importance of the dynamic analysis, we applied the same above procedure for each sliding window. The centrality histogram depicts L/R iCC, R PCC, L MOF, and L/R paraH as significant regions. Concerning the vulnerability, the significant nodes are R iCC, R paraH, L/R MOF and L LOF. The nodes having the highest strength values are L/R iCC, L/R rACC, L/R paraH, L/R MOF, R ENT, L/R LOF and L FUS regions. Concerning the clustering parameter, L/R LOF, L/R ITG, L pTRI, L/R pORB, LFP, L/R postC, L FUS and L IPL regions showed the highest values (Fig. 4A). Very similar results were obtained using different time windows and thresholds (see Supplementary Materials, Figures S1 and S2).

We then investigated how the brain regions characteristics are fluctuating during time, and which regions are more frequently involved in the segregation/integration than others. To do that, we extracted at each time window the nodes with the highest centrality, vulnerability, strength and clustering coefficient values. We then computed the transition matrix which represents the number of changing times from one region to another for each of the graph metrics. The transition matrices illustrated in Fig. 4B demonstrate the significant (color-coded) columns ( $p < 0.01$ , Bonferroni corrected). One can state that the transition to nodes assigned to the DMN is very frequent compared to other RSNs. Importantly, results show that there is a high probability of transition to L/R iCC according to centrality, vulnerability and strength. According to vulnerability, the columns corresponding also to L pCC and R paraH are significant. Furthermore, the transitions to L LOF, the L/R MOF, L/R paraH are higher in the strength transition matrix. However, there is no significant transition to any of the DMN nodes concerning the clustering coefficient, and the single remaining column corresponding to L ITG.

We have also evaluated the fractional occupancy of RSNs during time. Initially we extracted the significant nodes at each time window and then we associated the considered window to the RSN that contains the majority of these nodes (see Table S1 for nodes affiliations). After that, we computed the occurrence rates of each RSN

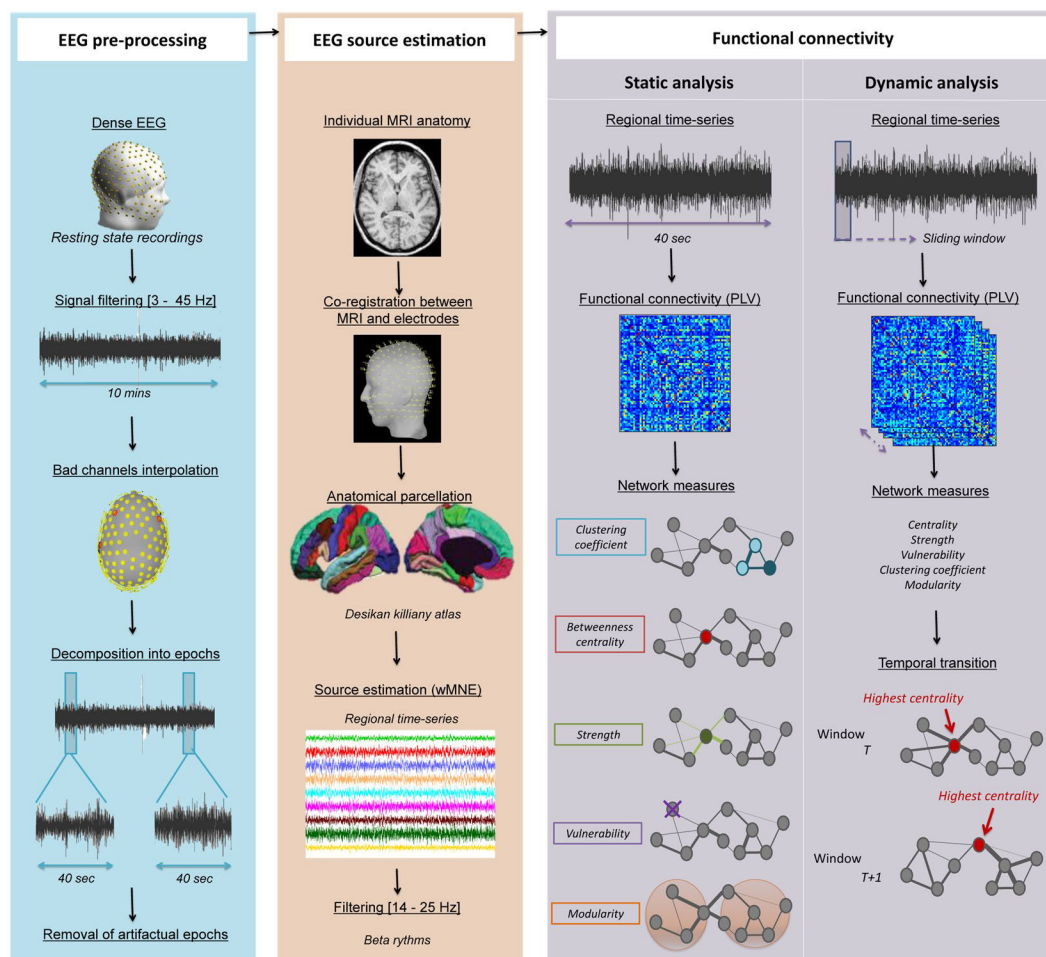


**Figure 1.** Structure of the investigation. *left:* Pre-processing of the dense-EEG data by interpolating channels and removing artifactual epochs, *middle:* Estimation of the EEG cortical sources using the weighted norm estimation method (wMNE). This step was followed by a projection of the source signals on the Desikan-killyan atlas, *right:* Quantification of the functional connectivity between the regional time series using the phase locking value (PLV). Two analyses were performed: (i) the static analysis in which PLV was computed over a segment of 40 s and (ii) the dynamic analysis in which PLV was computed over a 300 ms sliding window. The networks were then characterized by different graph measures (centrality, strength, vulnerability, clustering coefficient and modularity). The temporal transitions between networks/node's characteristic across time were also performed.

across all segments and all participants for the four measures. The statistical test using Wilcoxon demonstrates a significant difference between DMN and other RSNs with regard to centrality and strength ( $p < 0.01$ ). However, no significant difference was found between DMN and AUD according to the vulnerability measure. For the clustering coefficient, other RSNs occupancy rate is significantly different from that of DMN, DAN, SAN, AUD and VIS (Fig. 5A).

Interestingly, inspection of the transition matrices between RSNs reveals that there is a preference for the brain to move the centrality, vulnerability and strength characteristic to DMN rather than other networks (Fig. 5B). We also note that the vulnerability transition from the DMN to the AUD network is significantly considerable. Consistent with the previous results, the clustering coefficient transition to the DAN and 'Other' is the highest among the five known RSNs.

Finally, we have explored how a brain region can change its functional role (segregation/integration) over time. Thus, we assigned each of the 68 brain regions to one of the three classes (non-hub, provincial hub, connector hub) at each time window. Figure 6A illustrates the results for all subjects. A selected row in the matrix presents the role variations of a specific brain region across time windows. A simple examination of this figure reveals that the same node can change its type (provincial/connector) from one time to another. To extract the brain regions that are significantly behaving as connector or/and provincial hubs, we performed a chi-squared test and retained the significant nodes ( $p < 0.01$ , Bonferroni corrected). Ten out of the thirteen significant provincial hubs were found to be in the DMN, two are in the DAN and one was assigned to the VIS network. We also found a large proportion of connector hubs included in the DMN with the presence of two nodes in the DAN, three nodes in the VIS and three nodes assigned to none of the five RSNs. A considerable observation here is that some nodes

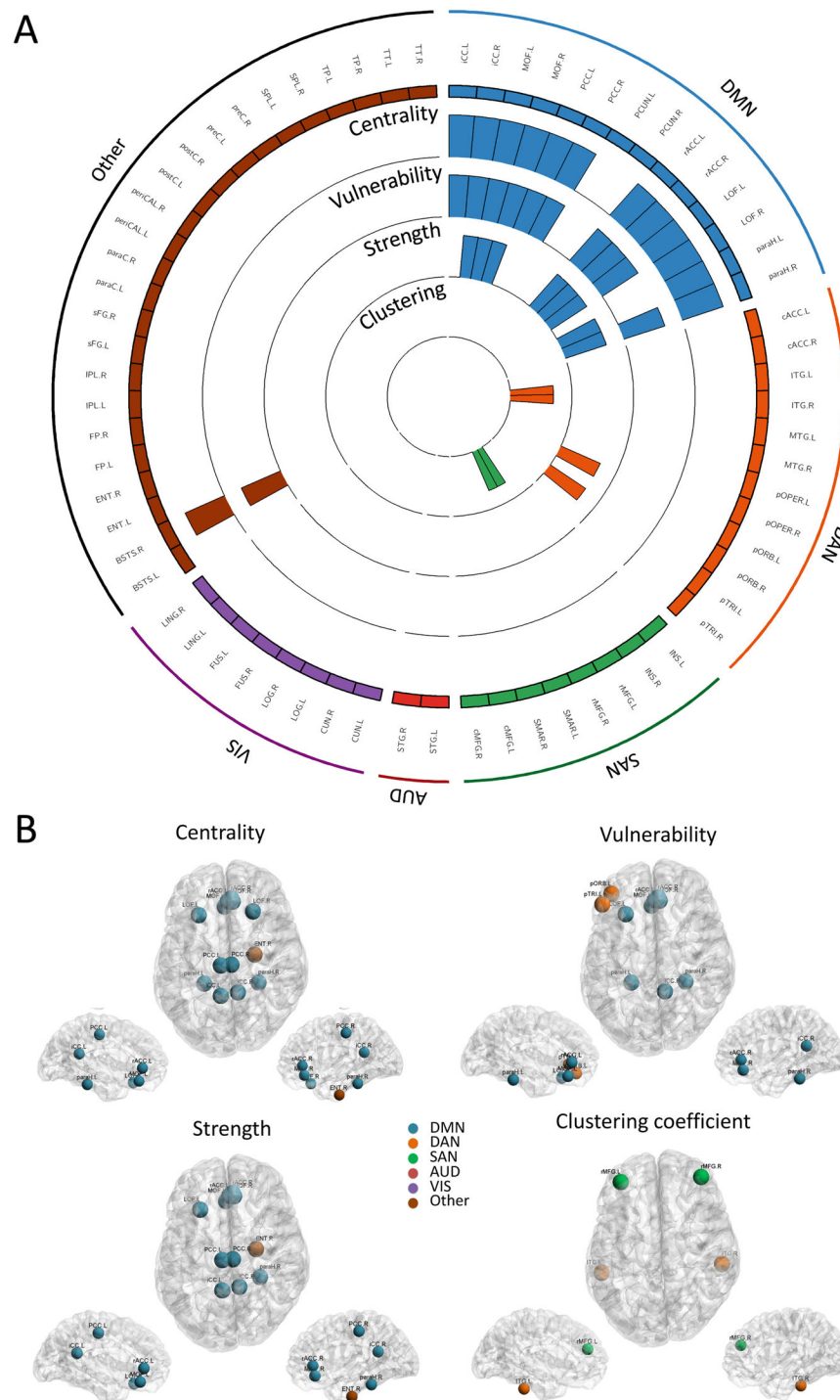


**Figure 2.** Static analysis: graph metrics. **(A)** The distribution of the four measures across the 68 brain regions. The circular barplots reflect from the outside inward: centrality, vulnerability, strength and clustering coefficient. The outermost ring shows the 68 brain regions obtained from the anatomical parcellation based on Desikan-Killiany atlas<sup>61</sup>, arranged by their assigned resting state networks: default mode network (DMN), dorsal attentional network (DAN), salience network (SAN), auditory network (AUD), visual network (VIS), see Table S1 in Supplementary Materials for more details about these assignments. We only showed the bars for significant nodes ( $p < 0.01$ , Bonferroni corrected). **(B)** The location of the significant brain regions on the cortical surface. The color of the node corresponds to which RSN is assigned. Names and abbreviations of the brain regions are listed in Table S1.

may change their function by dynamically alternating between provincial and connector hubs in the resting network across time. Among these nodes, we cite L/R iCC, L/R paraH, L FUS, L LOF, L/R MOF, L/R PCC, L pORB,



Detected as hub in our study		Detected as hub in literature	
Region	Graph measure	Graph measure	Technique
iCC	Str, BC, Vuln: static, dynamic	Deg: <sup>18, 47</sup> , Str: <sup>27</sup>	DTI
	P, Z: static, dynamic	BC: <sup>27, 53</sup> , PL: <sup>47</sup>	fMRI
PCC	BC, Vuln: static	Deg: <sup>22, 27, 47</sup> , Str: <sup>27, 29</sup>	DTI
	P, Z: static, dynamic	BC: <sup>21, 22, 27, 31, 42</sup>	fMRI
		RC: <sup>23</sup> , PL: <sup>47</sup>	MEG
rACC	Str: static, dynamic	Deg: <sup>22, 47</sup>	DTI
	BC, Vuln: static	BC: <sup>22, 31, 49, 53</sup>	fMRI
	P, Z: static, dynamic	RC: <sup>23, 24</sup> , P, Z: <sup>27</sup>	
MOF	Str, BC, Vuln: static, dynamic	Deg: <sup>22, 47</sup>	DTI
	P, Z: static, dynamic	BC: <sup>21, 22, 31, 42, 49</sup>	fMRI
		P, Z: <sup>27</sup> , PL: <sup>47</sup>	MEG
LOF	Str, Vuln: static, dynamic	Deg: <sup>22, 47</sup>	DTI
	BC: static	BC: <sup>21, 22</sup>	fMRI
	P, Z: static, dynamic		MEG
ParaH	Str, BC, Vuln: static, dynamic	BC: <sup>53</sup> , RC: <sup>52</sup>	DTI
	P, Z: static, dynamic	P, Z: <sup>53</sup>	fMRI
FUS	Strength: dynamic	Deg: <sup>47</sup>	fMRI
	P, Z: dynamic	BC: <sup>53</sup>	
		PL: <sup>47</sup>	
PCUN	P, Z: static, dynamic	Deg: <sup>18, 19, 22, 58</sup>	DTI
		Str: <sup>29</sup> , BC: <sup>18, 19, 22</sup>	fMRI
		RC: <sup>23, 24, 52</sup> , PL: <sup>47</sup>	
		Vuln: <sup>18</sup>	
		P, Z: <sup>27, 52, 58–60</sup>	
LING	P, Z: dynamic	Deg: <sup>47</sup> , PL: <sup>47</sup>	fMRI
ParaC	P, Z: static	Deg, Str, BC: <sup>27</sup>	DTI
		P, Z: <sup>27</sup>	
Cunues	P, Z: dynamic	Deg: <sup>47</sup> , PL: <sup>47</sup>	DTI
		P, Z: <sup>24</sup> , RC: <sup>24</sup>	fMRI
periCal	P, Z: static	Deg, Str, BC: <sup>27</sup>	DTI
		P, Z: <sup>27</sup>	
ENT	Str: dynamic	×	×
	BC, Vuln: static		
pORB	Str: static, dynamic	×	×
	P, Z: static, dynamic		
pTRI	Str, Vuln: static, dynamic	×	×
	P, Z: static		

**Table 1.** A comparison between the identified brain hubs in our study with structural and functional previous studies. Abbreviations. Deg: degree, Str: strength, PL: path length, BC: betweenness centrality, P: participation coefficient, Z: within degree module and Vuln: vulnerability.

and L pTRI. Results of significant provincial and connector nodes using different time windows are presented in Supplementary Materials, Figure S3.

## Discussion

There is growing evidence suggesting that the brain is a complex system of interacting functional units. This complex network was shown to be dynamic and network's behaviour changes over time. In this context, the recent past years have seen a significant increase of interest for dense-EEG analysis of functional brain networks at the level of cortical sources. This approach, called EEG source connectivity, is conceptually very attractive as high spatiotemporal resolution networks can be directly identified in the cortical source space. This method was recently evaluated for its capacity to reveal relevant networks in the context of cognitive tasks<sup>44</sup> and brain disorders<sup>62</sup>. It was then extended to track the spatiotemporal dynamics of functional brain networks<sup>43</sup>. More recently, we have performed a preliminary study using this technique combined with graph theory to explore the brain network architecture during rest in a static way<sup>32</sup>. However, the dynamic reconfiguration of resting brain network and its associated brain regions over short time scale (hundreds of millisecond) remains elusive. In this study, we used the dense-EEG data combined with graph theory analysis to characterize the fast dynamic reconfiguration of the brain networks at rest.

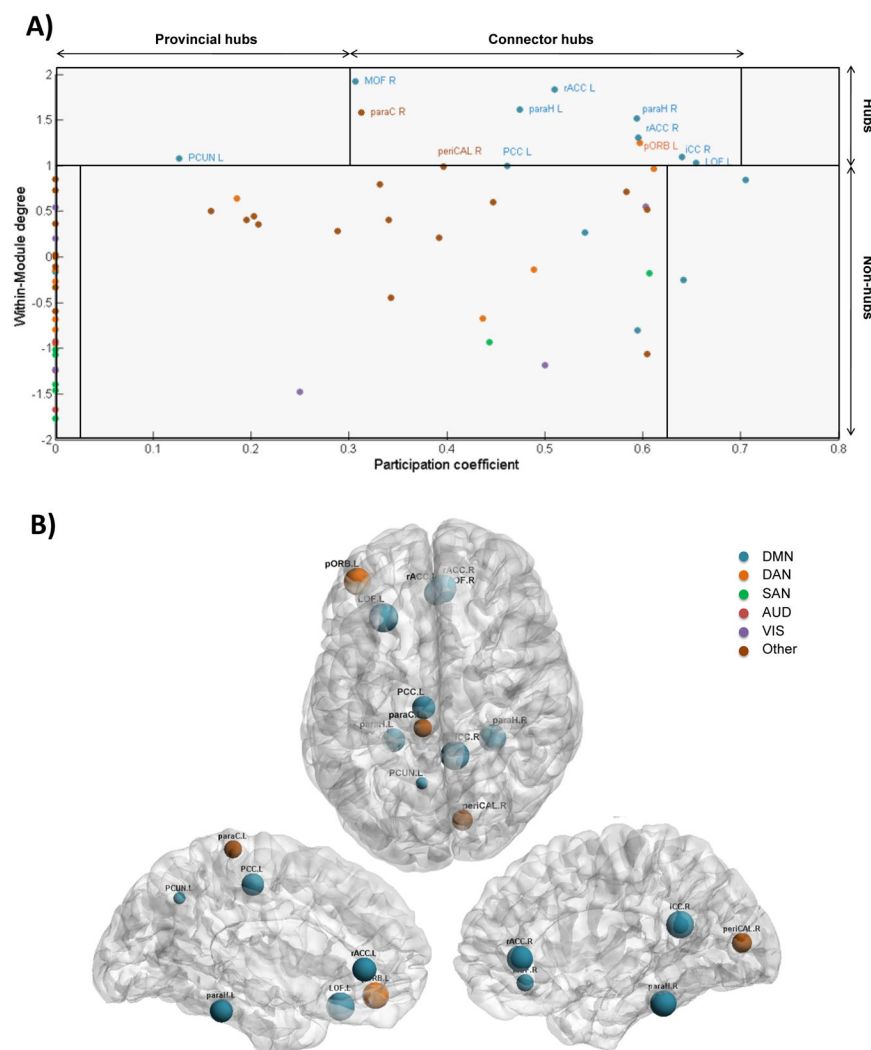


**Figure 3.** Static analysis: modularity. (A) The scatter plot of the participation coefficient and the within module degree for the 68 brain regions. Based on<sup>57</sup>, three main areas can be identified: Non-hubs, provincial and connector hubs. (B) The spatial locations of the identified hubs on the cortical surface. Names and abbreviations of the brain regions are listed in Table S1.

In this paper, we have investigated the dynamic behaviour of the functional brain networks during rest over a very short time scale (<second). This has never been done before. We have also quantified the modular architecture of the dynamic brain networks and have extracted the local (provincial) and global (integrator) brain regions that play a key role in maintaining the communication between brain regions. We also showed that the same regions can play the same role (provincial or integrator) during a given time period. Again, these methodological aspects and the results are novel.

The main originality of this work is the combination of source connectivity analysis with graph theoretical study to explore the dynamics of node's characteristics (centrality, vulnerability, strength and clustering), networks and modules over hundreds of milliseconds time scale which cannot be reached when using fMRI. Interestingly, the source connectivity method is a recently developed method used to identify functional networks at the cortical level from scalp dense-EEG recordings.

Our results showed mainly that the dynamic analysis of the RSNs at few hundreds of milliseconds time scale revealed valuable characteristics of the brain regions centrality and 'hubness'. We showed that the human brain holds a dynamic functional core network of a set of central brain regions that dynamically ensure both segregation and integration processes. By classifying the brain regions into local and global hubs using the participation coefficient and the within-module degree, we showed for the first time that same brain region can dynamically switch its function between provincial (segregation) and connector (integration) hubs. Results are further discussed hereafter.

**Network hubs in the brain.** Identifying brain regions that have a strong influence on information segregation and integration in the brain network is a key issue to characterize the brain functions. To the best of our

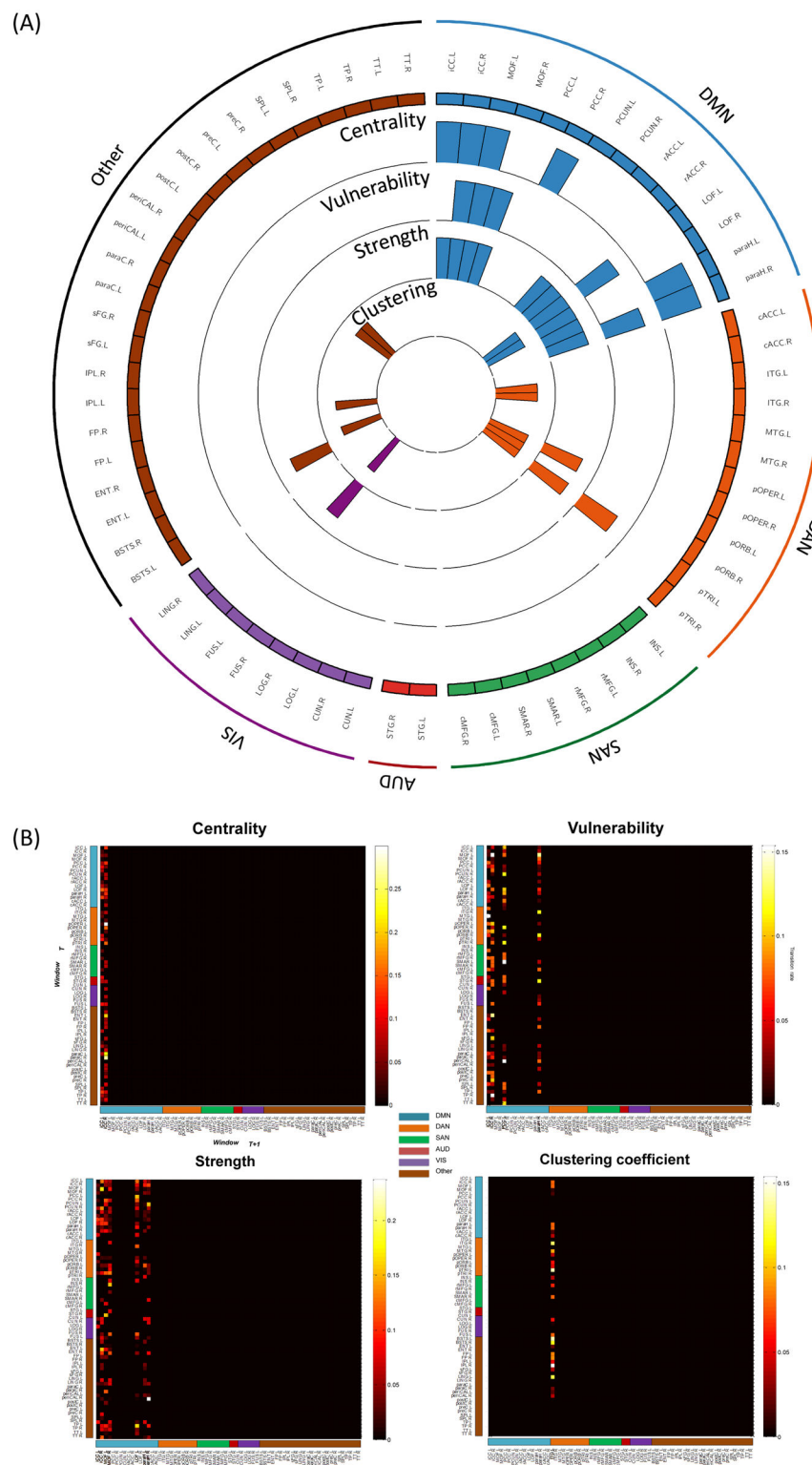


**Figure 4.** Dynamic analysis: graph metrics. (A) The distribution of the four measures across the 68 brain regions. The four circular barplots reflect (from the outside inward): centrality, vulnerability, strength and clustering coefficient. The outermost ring shows the 68 brain regions (obtained from the anatomical parcellation based on Desikan-Killiany atlas<sup>61</sup>), arranged by their assigned resting state networks: default mode network (DMN), dorsal attentional network (DAN), salience network (SAN), auditory network (AUD), visual network (VIS) (see Table S1 in Supplementary Materials). We only retain the bars for significant nodes ( $p < 0.01$ , Bonferroni corrected). (B) The temporal transitions between the 68 brain regions in terms of centrality, strength, vulnerability and clustering coefficient. Only significant columns are shown ( $p < 0.01$ , Bonferroni corrected). Names and abbreviations of the brain regions are listed in Table S1.

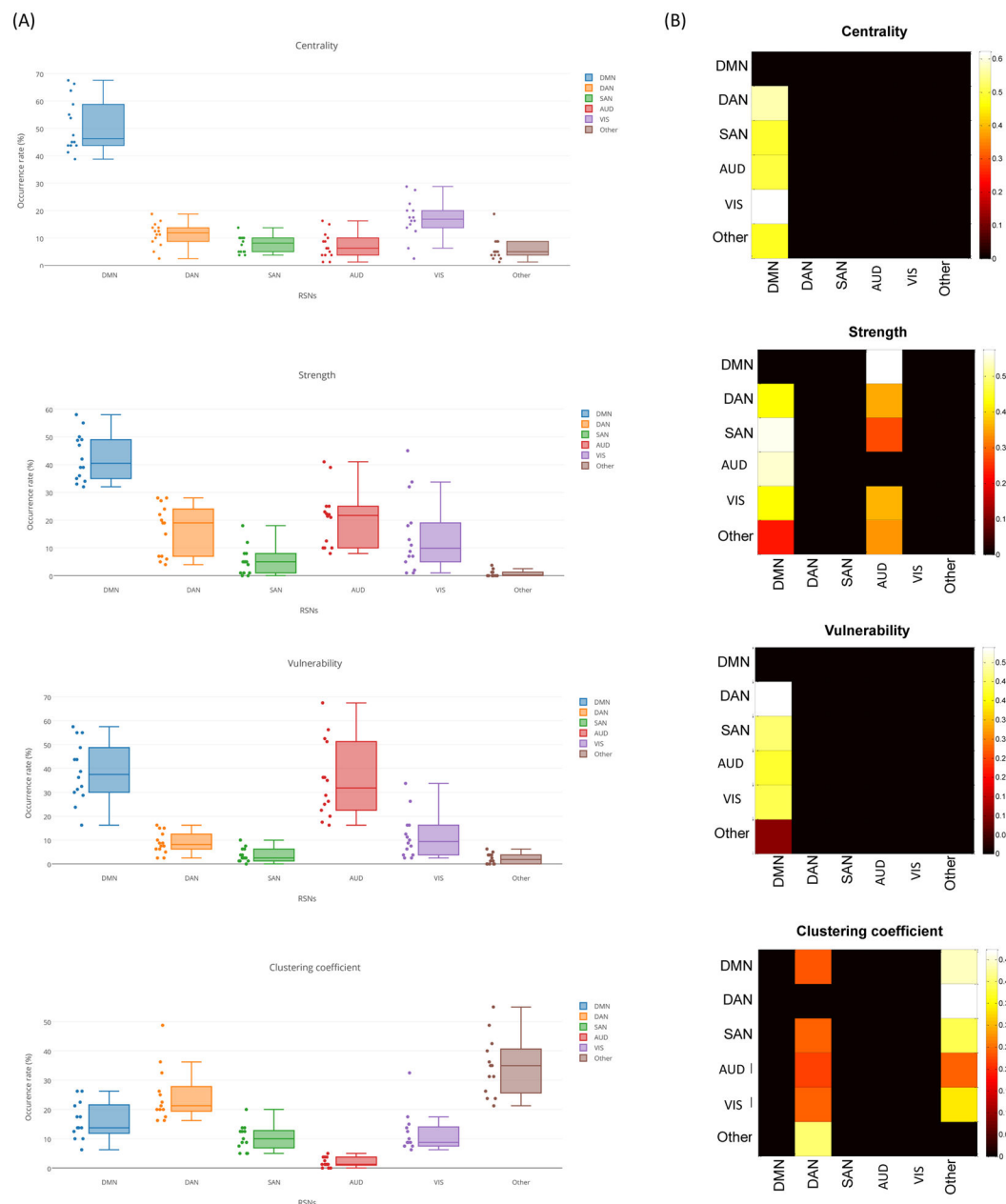


**Figure 5.** Dynamic analysis: networks transition. **(A)** The occurrence rates of the DMN, SAN, DAN, VIS, AUD and Other RSNs across time windows for all participants. **(B)** The temporal transitions between all networks across time windows for all participants. Only significant columns are shown ( $p < 0.01$ , Bonferroni corrected).

knowledge, this is the first attempt to identify functional hubs based on EEG source connectivity using graph theory approach. It is therefore essential to substantiate its usefulness by comparing the obtained results to prior studies. For this end, we have selected all the nodes detected here as hubs in terms of centrality, vulnerability, strength and/or modularity-based method, and compared them to those detected previously using other neuroimaging techniques (DTI, fMRI, and MEG). We found considerable overlapping between our results and previous results for most brain regions, while three brain regions were only detected as hubs in our study (Table 1). The Table 1 shows the brain regions identified as hubs in our study in both static and dynamic approach and the corresponding graph measures. The table shows also if these regions were identified as hubs previously using other neuroimaging techniques.

To identify brain hubs, many graph measures have been used. The simplest commonly used way is the detection of highest-degree nodes. This approach has been used by several studies<sup>13, 30, 63, 64</sup>. Others proposed to combine the degree and path length metrics<sup>31, 47, 53, 65, 66</sup>. Here, we evaluated the most commonly used graph measures in order to obtain a possible convergence between several measures. Interestingly, Table 1 shows that the iCC, paraH and MOF regions are detected in both static and dynamic analysis independently of the graph measure used.



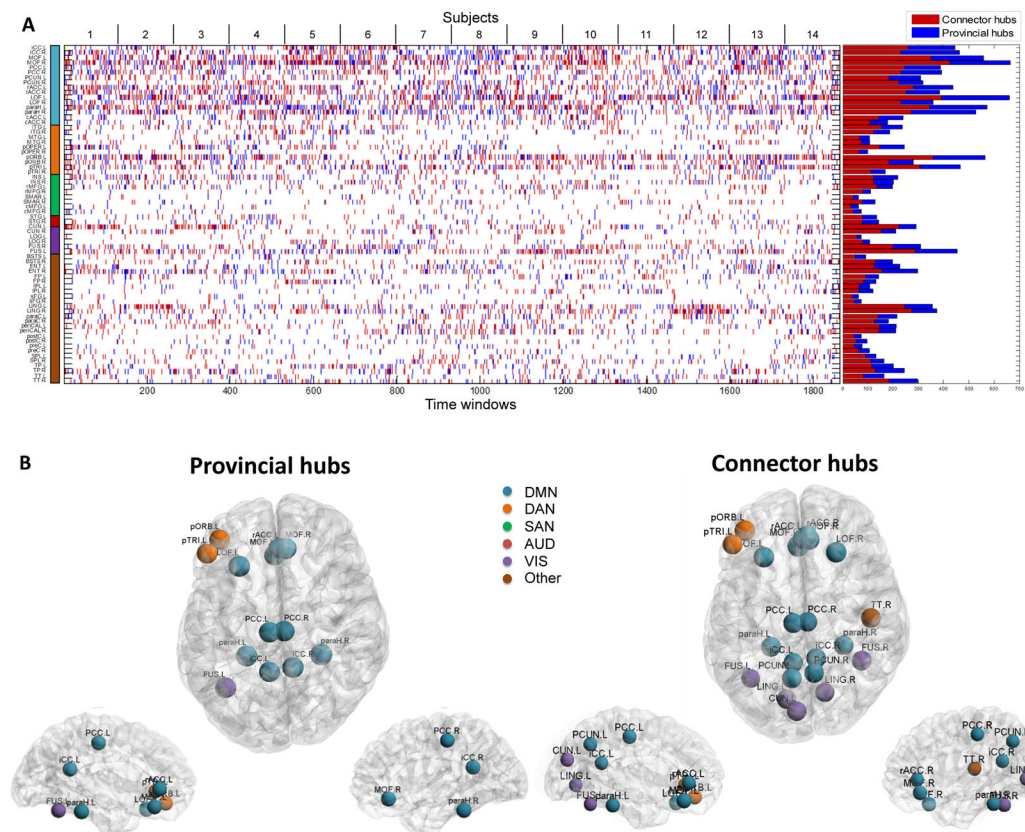


**Figure 6.** Dynamic analysis: modularity. **(A)** *left*: The variations of the node's type (provincial vs. connector) across time for each of the 68 brain regions, *right*: The bar plots represent the number of times a node is considered as provincial hub (blue color) and as connector hub (red color). **(B)** The spatial distributions of significant provincial hubs, and significant connector hubs. Names and abbreviations of the brain regions are listed in Table S1.

We hypothesized that a consistent hub node has a high centrality (the node lies a high number of shortest paths), high strength (the hub has a large number of connections), high vulnerability (the removal of the hub has a dramatic effect on the efficiency of the network) and low clustering coefficient (the neighbors of a hub are not directly connected with each other). Based on this definition of “hubness”, the R iCC, L/R MOF and R paraH regions are shown to be the strongest hubs as demonstrated in our static and dynamic analysis.

Several previous studies have also combined the participation coefficient and the within module degree to identify brain hubs<sup>24, 33, 54, 58–60</sup>. This method also allows the classification of hubs into two categories: provincial and connector. Using this approach, most of the hubs obtained in our study were intersecting with the already defined hubs using centrality, vulnerability and strength. Among these nodes, we list the L/R iCC, L/R paraH, L/R MOF, L/R PCC, L/R rACC, L/R pORB, L/R LOF, L/R FUS. Moreover, combining empirical results from structural and functional studies demonstrated a strong agreement between these hubs and the previously defined connector/provincial hubs. The PeriCal has also been detected as a provincial hub in Hagmann *et al.*<sup>27</sup>. The paraH was shown to play the role of connector hub in He *et al.*<sup>53</sup>. Similarly, the rACC region was identified as a connector in various studies<sup>27, 53</sup> and paraC was detected as a connector as reported in Hagmann *et al.*<sup>27</sup>. Additionally, while the PCUN was considered as a provincial hub in some studies<sup>58, 60</sup>, it was identified as a connector hub in others<sup>27, 34</sup>. The MOF was identified as provincial in Hagmann *et al.*<sup>27</sup> and as connector hub in Meunier *et al.*<sup>59</sup>.

**Hubs and RSNs.** There is a current debate whether the brain hubs are included in a single functional network, or are distributed among multiple RSNs serving as inter-links between these functional networks. While many studies support the first hypothesis<sup>16, 41, 58</sup>, others suggest that hubs form an infrastructure for communication between RSNs<sup>24, 33</sup>. Our results show that the brain hubs are distributed among the DMN (the cingulate, parahippocampal and prefrontal cortex regions), the DAN (parsorbitalis, and parstriangularis regions) and the VIS (cunues, lingual and fusiform). However, one can notice that the DMN regions provide the largest contribution to the network segregation/integration. This is revealed by a high fractional occupancy associated to the DMN compared to other RSNs, suggesting a frequent transition to this network in the centrality, vulnerability and strength temporal transition analysis. Having the majority of hubs included in the DMN corroborates with the fact that DMN is the most dominating RSN<sup>1, 10</sup>. Similar results were reported in the literature<sup>10, 67, 68</sup>, where an important overlap between hubs and the DMN was observed. Furthermore, a study that explored the rich club

organization of the human brain showed that the rich club nodes cross-link with the majority of RSNs and that the largest proportion belong to the DMN<sup>33</sup>.

**Dynamic core network.** Most studies in RSNs were performed in a static way i.e. networks were identified over the entire recording (called also ‘stationary’ analysis). The assumption that the connectivity between brain regions is static throughout the resting recording was criticized in several studies<sup>38</sup>. In particular, Allen *et al.*<sup>39</sup> reported that the functional connectivity states derived at rest from the dynamic analysis strongly differ from the patterns obtained using the static approach. Accordingly, Calhoun *et al.*<sup>69</sup> introduced the term “chroconnectome” to describe that the patterns of coupling among brain regions are dynamic and consistent over time.

Performing the analysis over the entire segment (40 s window length in our analysis) offered a global view about the characteristics of the RSNs. However, the sole static analysis prevents the exploration of how the brain regions/networks are reconfiguring at sub-second time scale. Moreover, examining the transition between nodes in terms of graph metrics allowed us to investigate how brain hubs are alternating between each other with time. Importantly, a unique finding has also been offered by tracking the dynamics, is the study of the hub’s type variations over time. In fact, a hub node has been usually considered as either provincial or connector hub<sup>23, 27, 34, 53, 58–60</sup>. However, we revealed that the same brain region can play the role of provincial hub or connector hub at two different times for same subject at rest. These findings are expected since the same regions have been detected as provincial hubs in some previous studies, and as connector hubs in others. For example, the PCUN was found to be a provincial hub in refs 60, 58 and a connector hub in refs 27, 34. Similarly for the MOF that was identified as provincial in ref. 27 and as connector hub in ref. 59. A possible explanation of these results is that these hub regions may participate in both the local segregation of the information and the global integration over the whole network.

**Methodological considerations.** In this study, we used a proportional threshold (highest 10% of the edge’s weights) to remove weak connections of the functional connectivity matrices. Garisson *et al.*<sup>70</sup> showed that network measures are stable across proportional thresholds contrary to absolute thresholds. Nevertheless and in order to ensure that the obtained results are not sensitive to the threshold value, we performed our analysis across a range of proportional thresholds (ranging from 5 to 20%) and realized the stability of our results across thresholds (see Supplementary Materials Figure S1). Results showed slight differences between the several threshold values. However, the overall conclusion of the study remains intact.

The time window used in the dynamic analysis corresponds to the minimal length that can be used to adequately compute PLV, as recommended by Lachaux *et al.*<sup>45</sup>. In order to verify the reproducibility of the obtained results, we repeated our analysis while changing the size of the selected window (300 ms - 1 s - 2 s-10 s). A high degree of agreement among these analyses was found, see Supplementary Materials Figures S2, S3. One can notice that most brain hubs were always located in the DMN for all time window sizes.

Here, we presented the results obtained by performing the study on beta rhythms based on previous findings<sup>16, 17, 71, 72</sup>. To verify the importance of beta band, we performed the same analysis on the broad-band (3–45 Hz), theta (3–7 Hz), alpha (7–13 Hz) and beta (14–25 Hz) frequency bands. We have evaluated the influence of the frequency band on the DMN occurrence, see Supplementary Materials Figure S4. The statistical test using Wilcoxon shows a significant difference between the DMN occurrences in beta, compared to theta and alpha ( $p < 0.01$ ). However, no significant difference was found between DMN’s occupancy in beta compared to the broad-band.

From a methodological point of view, several issues should be discussed when reconstructing the sources from scalp EEG signals. In fact, the number of source dipoles is much larger than the number of electrodes, making the inverse problem ill-posed. This required adding several physical and mathematical constraints to solve the inverse problem. In the case of choosing the wMNE as an inverse solution, the main assumption was to find a solution with lowest energy. This assumption is generally explained by the economic energy cost of the brain during information processing. However, compared to other inverse solutions, the wMNE implies relatively few hypotheses, (see review in Becker *et al.*<sup>73</sup> for more detailed comparison between inverse solution’s assumptions). Moreover, the lead-field matrix is underdetermined, and an accurate description of the head model will positively affect the quality of solutions. Here, we reduced the effect of this problem by computing a realistic subject-specific head model using each individual anatomical MRI image. In addition, the networks identified using EEG source connectivity are limited to the cortex as the sub-cortical regions are not easily accessible from scalp EEG recordings.

As an emerging technique, the evaluation of EEG source connectivity method is crucial. The question is to determine to what extent the functional brain networks identified from EEG source connectivity correspond to those that are actually activated during considered brain processes (resting state, cognitive task). For this purpose, we used (i) real data recorded during a cognitive task<sup>43, 44</sup> and (ii) simulated data using biophysical/physiological modelling and real epileptic data<sup>62</sup>. In Hassan *et al.*<sup>44</sup>, the method was used to estimate the networks involved during a picture naming task for which a solid background was available regarding activated brain regions and networks. In brief, we performed a comprehensive literature review on these networks mainly obtained from neuroimaging techniques such as fMRI, MEG, depth EEG and PET. From this review, a “reference” network could be determined. It was used as a ground truth to define a performance criterion about the accuracy of networks obtained from EEG source connectivity. Interestingly, we tested a large number of combinations between the inverse solution and functional connectivity measures. For one combination (wMNE/PLV), the estimated network, activating during the cognitive task (500–700 ms), was found to spatially match the reference network. The above described work was then extended from static to dynamic analysis during the same cognitive task. We showed that the EEG source connectivity method was able to track the spatiotemporal dynamics of activated brain networks from the onset (presentation of the visual stimuli) to the reaction time (articulation). Estimated dynamic networks were also found to match previously-reported regions/networks, as identified with other techniques such as depth-EEG and MEG. More recently, a study was performed in the context of epilepsy where a

physiologically-plausible computational model of epileptogenic networks was used as a ground truth. Simulated scalp-EEG signals were used to evaluate the performance of EEG source connectivity methods in term of “re-estimating” reference large-scale networks modelled at neocortical level. Again, the combination that showed the highest similarity between reference and estimated networks was the wMNE/PLV, used in the present paper.

Regarding the resting state data analyzed in the current paper, the only ‘ground-truth’ that could be considered are the fMRI recordings. Although fMRI data was not available for the healthy volunteers of our study, we didn’t ignore this issue and we have compared our results with those reported in literature using fMRI and DTI (Table 1). Qualitative comparison showed strong matching between brain hubs identified from our EEG-based methods, on the one hand, and brain hubs reported elsewhere and based on fMRI/DTI, on the other hand.

Furthermore, we assumed that by taking into account the whole atlas regions without any prior selection of particular region may give more straightforward results. Here, we used 68 anatomical ROIs to define the nodes in the brain network. There is no clear consensus about how to select the appropriate number of nodes that represent the large-scale networks. On one hand, choosing finer segmentation may increase the spatial resolution. On the other hand, keeping a reduced number of ROIs may help removing the spurious links that occur between spatially adjacent sources. In this regard, we assume that 68 regions were sufficient to investigate the global characteristics of the resting state networks while minimizing the problem of spurious connections between ‘very close sources’. Although the functional connectivity at the source level reduces the effect of the field spread, they do not suppress its effects completely. In this context, few strategies have been proposed to remove zero-lag correlations before performing any connectivity analyses<sup>72,74</sup>. Others suggest only keeping the long-range connections<sup>16,41,42</sup>. However, these methods suppress important correlations that may occur at zero-lag<sup>37</sup> or even among close regions.

In our study, we evaluated the possible effects of the field spread on our results by assessing the relationships between the average Euclidian distance of brain regions and their centrality, strength, clustering coefficient, participation index, and the within-module degree values. For each measure, the Euclidian distance of a node was calculated by averaging the distance between the node and all other nodes that affect the measurements. Our results showed that a large proportion of nodes have long connections with high metrics values. Furthermore, there was neither significant correlation between the betweenness centrality of a node and its average distance ( $\rho = -0.0627, p > 0.05$ ), neither for the clustering coefficient ( $\rho = -0.0374, p > 0.05$ ), the participation coefficient ( $\rho = -0.076, p > 0.05$ ) and the within degree module ( $\rho = 0.013, p > 0.05$ ). The correlation between the strength and the distance was statistically significant with a positive correlation value ( $\rho = 0.5, p < 0.01$ ). This implies that the used metrics were not affected by the spurious short connections and that a high number of long-range connections were presented.

## Materials and Methods

**Data acquisition and pre-processing.** The full pipeline of our study is summarized in Fig. 1. Data were recorded from twenty participants. All experiments were performed in accordance with the relevant guidelines and regulations of the National Ethics Committee for the Protection of Persons (CPP), (*BrainGraph* study, agreement number 2014-A01461-46, promoter: Rennes University Hospital), which approved all the experimental protocol and procedures. Written informed consents were obtained from all participants in the study.

Structural MRI and EEG dense recordings (256 channels, EGI, Electrical Geodesic Inc.) were collected for each subject. During the acquisition, the subjects were asked to relax for 10 minutes with their eyes closed without falling asleep. Electrodes impedances were kept below 10 k $\Omega$ . EEGs were sampled at 1000 Hz, band-pass filtered within 3–45 Hz, and segmented into non-overlapping 40 s long epochs. After visual inspection, the segments that have substantial noise not due to brain activity (amplitudes over  $\pm 80 \mu\text{V}$ ) have been marked and excluded from the analysis. For some subjects, few electrodes with poor signal quality have been identified and interpolated using the surrounding channels activities. The artifact-free segments (four segments per subject on average) were then used for source estimation. The preprocessing steps were performed using EEGLAB<sup>75</sup> and Brainstorm<sup>76</sup> open source toolboxes.

A realistic head model was constructed by segmenting the MRI using Freesurfer software package<sup>77</sup>. The individual MRI anatomy and EEGs data were co-registered through the identification of the same anatomical landmarks (left and right pre-auricular points and nasion). The lead field matrix was then computed for a cortical mesh with 15000 vertices using OpenMEEG<sup>78</sup>. The regional time series were filtered in the beta band [14–25 Hz], in which many previous studies have reported its importance in driving large-scale spontaneous neuronal interactions<sup>16,17,71,72</sup>. An atlas-based approach was used to project EEG signals onto an anatomical framework consisting of 68 cortical regions identified by means of the Desikan-Killiany<sup>61</sup> atlas using Freesurfer<sup>77</sup>, <http://freesurfer.net/>, see Table S1 for more details about the names and abbreviations of these regions.

**Brain networks construction.** Functional networks were computed using a recently proposed approach called ‘dense-EEG source connectivity’<sup>43,44</sup>. It included two main steps: (i) solving the EEG inverse problem to reconstruct the temporal dynamics of the cortical regions at source level and (ii) measuring the functional connectivity between these reconstructed regional time series.

**Source estimation.** According to the linear discrete equivalent dipole model, EEG signals  $X(t)$  recorded from  $Q$  channels ( $Q = 256$  in our case) can be expressed as linear combination of  $P$  time-varying current dipole sources  $S(t)$ :

$$X(t) = G \cdot S(t) + N(t) \quad (1)$$

where  $G$  is the lead field matrix and  $N(t)$  is the additive noise.  $G$  was computed from a multiple layer head model (volume conduction) and from the position of the  $Q$  electrodes. Here we used the Boundary Element Method (BEM) as a numerical method to compute realistic head models. We computed the lead field matrix using OpenMEEG<sup>78</sup>. In addition, the noise covariance matrix was calculated over a long segment of the resting recordings.

After calculating  $G$  and  $N(t)$ , the inverse problem consists of estimating the parameters of the dipolar sources  $\hat{S}(t)$  (notably the position, orientation and magnitude). As this problem is ill-posed ( $P \gg Q$ ), physical and mathematical constraints have to be added to find a single solution among the many solutions that minimize the residual term in the fitting of dense EEG signals. Using segmented MRI data, the source distribution can be constrained to a field of current dipoles homogeneously dispersed over the cortex and normal to the cortical surface. Precisely, in the source model, the electrical contribution of each macro-column to scalp electrodes can be represented by a current dipole located at the center of gravity of each triangle of the 3D mesh and oriented normally to the triangle surface. Using this source space, the weighted Minimum Norm Estimate (wMNE) method only estimates the moment of dipole sources. The wMNE compensates for the tendency of classical MNE to favor weak and surface sources (Hämäläinen and Ilmoniemi 1994). This is done by introducing a weighting matrix  $W_X$ :

$$\hat{S}_{wMNE} = (G^T W_X G + \lambda I)^{-1} G^T W_X X \quad (2)$$

where matrix  $W_X$  adjusts the properties of the solution by reducing the bias inherent to MNE solutions. Classically,  $W_X$  is a diagonal matrix built from matrix  $G$  with non-zero terms inversely proportional to the norm of the lead field vectors.  $\lambda$  is a regularization parameter computed relatively to the signal to noise ratio ( $\lambda = 0.2$  in our analysis).

**Functional connectivity.** We used the phase locking value metric to compute the functional connectivity between the 68 reconstructed regional time-series. The combination of wMNE/PLV was shown to be very efficient to precisely identify cortical brain networks from scalp EEG during cognitive activity<sup>43,44</sup>. As described in Lachaux *et al.*<sup>45</sup>, the phase locking value between two signals  $x$  and  $y$  is defined as:

$$PLV(t) = \left| \frac{1}{\delta} \int_{t-\delta/2}^{t+\delta/2} \exp(j(\varphi_y(t) - \varphi_x(t))) d\tau \right| \quad (3)$$

where  $\varphi_y(t)$  and  $\varphi_x(t)$  are the unwrapped phases of the signals  $x$  and  $y$  at time  $t$ . The Hilbert transform was used to extract the instantaneous phase of each signal.  $\delta$  denotes the size of the window in which PLV is calculated.

To explore the advantage of the dynamic analysis, we performed our study in both 'static' and 'dynamic' ways. For the static way, the functional connectivity was computed over the entire noise-free epoch duration (40 seconds). To examine the dynamics of the RSNs, we used a sliding window in which PLV was calculated over its data points. As recommended by Lachaux *et al.*<sup>45</sup>, the window length should be larger than  $\frac{6}{\text{central frequency}}$  where 6 is the number of 'cycles' at the given frequency band. Having a central frequency of 19.5 Hz for the beta band, the smallest window length can be used is 300 milliseconds. Other frequency bands and other time window size will also be described in the study.

**Network analysis.** Networks can be illustrated by graphs, which are sets of nodes (brain regions) and of edges (connectivity values) between those nodes. We constructed graphs of 68 nodes (i.e. the 68 previously identified cortical regions) and used all information from the functional connectivity (phase locking value) matrix<sup>79,80</sup>. This gave fully connected, weighted and undirected networks, in which the connection strength between each pair of vertices (i.e. the weight) was defined as their connectivity value.

We quantified the network's nodes using several graph metrics:

**Betweenness Centrality.** The importance of a node is proportional to the number of paths in which it participates<sup>51</sup>. Thus, a way to find the critical nodes is to calculate the betweenness centrality of each node:

$$BC_i = \sum_{i,j} \frac{\sigma(i, u, j)}{\sigma(i, j)} \quad (4)$$

where  $\sigma(i, u, j)$  is the number of shortest paths between nodes  $i$  and  $j$  that pass through node  $u$ ,  $\sigma(i, j)$  is the total number of shortest paths between  $i$  and  $j$ , and the sum is over all pairs  $i, j$  of distinct nodes.

**Vulnerability.** The vulnerability of a specific node can be defined as the reduction in performance when the node and all its edges are removed:

$$V_i = \frac{E - E_i}{E} \quad (5)$$

where  $E$  is the global efficiency of the network before any attack, and  $E_i$  is the global efficiency of the network after attacking the node  $i$ <sup>50</sup>.

**Strength.** The strength of a node is the sum of the weights of its corresponding edges:



$$S_i = \sum_j w_{ij} \quad (6)$$

where  $w_{ij}$  is the weight of the edge linking the node  $i$  to the node  $j$ <sup>81</sup>.

**Clustering coefficient.** The clustering coefficient of a node in a graph quantifies how close its neighbors are to being a clique<sup>82</sup>.

The network measures and visualization were performed using BCT<sup>83</sup> and BrainNet viewer<sup>84</sup>, respectively. The above-mentioned network measures were normalized, that is, they were expressed as a function of measures computed from random networks. We generated 500 surrogate random networks derived from the original networks by randomly reshuffling the edge weights. The normalized values were computed by dividing the original values by the average of the values computed on the randomized graphs.

**Modularity.** Several algorithms have been proposed to decompose a network into modules or communities of high intrinsic connectivity and low extrinsic connectivity (Simon 1962). Due to the so-called degeneracy problem<sup>85</sup>, the modules of a same network differ from a run to another and from a module detection algorithm to another. With the aim to assess the consistency of modules affiliation, we applied the consensus clustering process as follows:

- Generate a set of partitions of the same network using three community detection methods 100 times (Newman algorithm<sup>86</sup>, Louvain algorithm<sup>87</sup> and Infomap algorithm<sup>88</sup>).
- Compute the association matrix for all possible partitions<sup>89–91</sup>. This step results in a 68\*68 matrix where the element  $A_{i,j}$  represents the number of times the nodes  $i$  and  $j$  are assigned to the same module across the runs and algorithms.
- Compare the consensus matrix to a null model association matrix generated from a permutation of the original partitions<sup>92</sup> and keeping its significant values<sup>92</sup>.
- Re-cluster the resultant association matrix using Louvain method.

Once a network has been partitioned, we classify the 68 nodes into three main categories (non hubs, provincial and connector hubs) by considering the variations of two measures used to quantify nodes connectivity within and between modules. The first one is the within-module degree z-score that express the number of links a node makes to other nodes in the same module:

$$Z_i = \frac{K_i(m_i) - \overline{K(m_i)}}{\sigma_{k(m_i)}} \quad (7)$$

where  $K_i(m_i)$  is the within-module degree of the node  $i$ ,  $\overline{K(m_i)}$  is the mean of within module degree of nodes assigned to the same community as node  $i$ , and  $\sigma_{k(m_i)}$  is the standard deviation. Positive z-scores indicate that a node is highly connected to other members of the same community; negative z-scores indicate the opposite. In our study, nodes with  $Z_i > 1.5$  were considered as hubs, and nodes with  $Z_i < 1.5$  were considered as non-hubs.

We then focused on discriminating provincial and connector hubs based on a second metric known as participation coefficient. This metric characterizes how edges of a given node are distributed across modules:

$$P_i = 1 - \sum_{m=1}^M \left( \frac{K_i(m)}{K_i} \right)^2 \quad (8)$$

where  $M$  is the number of modules,  $K_i(m)$  is the number of edges between node  $i$  and nodes in module  $m$ . Based on the criteria proposed by ref. 57, a provincial hub having most of its links inside its own module has a  $P_i$  value lower than 0.3; while a connector hub has a  $P_i$  value greater than 0.3. This criterion was used in our study.

In addition to the evaluation of the difference between brain regions according to their hubness, we were also interested in examining the difference between RSNs. To do so, we associated each brain region in the Desikan-Killiany atlas to its corresponding RSN based on the study described by Shirer *et al.*<sup>93</sup> in which authors identified fourteen functional networks: anterior salience network, auditory network, basal ganglia network, dorsal default mode network, higher visual network, language network, left executive control network, sensorimotor network, posterior salience network, precuneus network, primary visual network, right executive control network, ventral default mode network, and visuospatial network. In our study, we focused on five RSNs: the DMN was obtained by combining the regions of the dorsal and the ventral default mode network, the SAN was obtained by associating all the regions in anterior and posterior salience networks. The combination of the higher and primary visual networks yields to our VIS network.

**Statistical tests.** To statistically identify the significant nodes in terms of each graph metric, we quantified the difference between nodes distributions using a Wilcoxon test for continuous data distribution (metrics distribution, transition matrices) and a chi-squared test for binary data distribution (affiliation of connector/non connector, provincial/non provincial hubs). All tests were corrected for multiple comparisons using Bonferroni correction method.

## References

1. Fox, M. D. & Raichle, M. E. Spontaneous fluctuations in brain activity observed with functional magnetic resonance imaging. *Nat Rev Neurosci* **8**, 700–711 (2007).
2. Raichle, M. E. *et al.* A default mode of brain function. *Proceedings of the National Academy of Sciences of the United States of America* **98**, 676–82 (2001).
3. Biswal, B., Yetkin, F. Z., Haughton, V. M. & Hyde, J. S. Functional connectivity in the motor cortex of resting human brain using echo-planar MRI. *Magn. Reson. Med.* **34**, 537–541 (1995).
4. Sporns, O. Networks of the Brain: Quantitative Analysis and Modeling. *Notes* (2010).
5. Biswal, B. B., Van Kylen, J. & Hyde, J. S. Simultaneous assessment of flow and BOLD signals in resting-state functional connectivity maps. *NMR Biomed.* **10**, 165–170 (1997).
6. Cordes, D. *et al.* Frequencies contributing to functional connectivity in the cerebral cortex in 'resting-state' data. *Am. J. Neuroradiol.* **22**, 1326–1333 (2001).
7. Cordes, D. *et al.* Mapping functionally related regions of brain with functional connectivity MR imaging. *Am. J. Neuroradiol.* **21**, 1636–1644 (2000).
8. Damoiseaux, J. S. *et al.* Consistent resting-state networks across healthy subjects. *Proc. Natl. Acad. Sci. USA* **103**, 13848–53 (2006).
9. De Luca, M., Smith, S., De Stefano, N., Federico, A. & Matthews, P. M. Blood oxygenation level dependent contrast resting state networks are relevant to functional activity in the neocortical sensorimotor system. *Exp. Brain Res.* **167**, 587–594 (2005).
10. Greicius, M. D., Krasnow, B., Reiss, A. L. & Menon, V. Functional connectivity in the resting brain: a network analysis of the default mode hypothesis. *Proc. Natl. Acad. Sci. USA* **100**, 253–8 (2003).
11. Lowe, M. J., Mock, B. J. & Sorenson, J. A. Functional Connectivity in Single and Multislice Echoplanar Imaging Using Resting-State Fluctuations. *Neuroimage* **7**, 119–132 (1998).
12. Xiong, J., Parsons, L. M., Gao, J. H. & Fox, P. T. Interregional connectivity to primary motor cortex revealed using MRI resting state images. *Hum. Brain Mapp.* **8**, 151–156 (1999).
13. van den Heuvel, M., Mandl, R. & Pol, H. H. Normalized cut group clustering of resting-state fMRI data. *PLoS One* **3** (2008).
14. Mantini, D., Perrucci, M. G., Del Gratta, C., Romani, G. L. & Corbetta, M. Electrophysiological signatures of resting state networks in the human brain. *Proc. Natl. Acad. Sci. USA* **104**, 13170–5 (2007).
15. Brookes, M. J. *et al.* Measuring functional connectivity using MEG: Methodology and comparison with fcMRI. *Neuroimage* **56**, 1082–1104 (2011).
16. de Pasquale, F. *et al.* A Cortical Core for Dynamic Integration of Functional Networks in the Resting Human Brain. *Neuron* **74**, 753–764 (2012).
17. Liu, Z., Fukunaga, M., de Zwart, J. A. & Duyn, J. H. Large-scale spontaneous fluctuations and correlations in brain electrical activity observed with magnetoencephalography. *Neuroimage* **51**, 102–111 (2010).
18. Gong, G. *et al.* Mapping anatomical connectivity patterns of human cerebral cortex using *in vivo* diffusion tensor imaging tractography. *Cereb. Cortex* **19**, 524–536 (2009).
19. Iturria-Medina, Y., Sotero, R. C., Canales-Rodriguez, E. J., Aleman-Gomez, Y. & Melie-Garcia, L. Studying the human brain anatomical network via diffusion-weighted MRI and Graph Theory. *Neuroimage* **40**, 1064–1076 (2008).
20. Jahanshad, N. *et al.* Genome-wide scan of healthy human connectome discovers SPON1 gene variant influencing dementia severity. *Proc. Natl. Acad. Sci. USA* **110**, 4768–73 (2013).
21. Li, L. *et al.* Mapping putative hubs in human, chimpanzee and rhesus macaque connectomes via diffusion tractography. *Neuroimage* **80**, 462–474 (2013).
22. Nijhuis, E. H. J., van Cappellen van Walsum, A. M. & Norris, D. G. Topographic Hub Maps of the Human Structural Neocortical Network. *PLoS One* **8** (2013).
23. van den Heuvel, M. P., Kahn, R. S., Goñi, J. & Sporns, O. High-cost, high-capacity backbone for global brain communication. *Proc. Natl. Acad. Sci. USA* **109**, 11372–77 (2012).
24. van den Heuvel, M. P. & Sporns, O. An anatomical substrate for integration among functional networks in human cortex. *J. Neurosci.* **33**, 14489–500 (2013).
25. van Horn, J. D. *et al.* Mapping connectivity damage in the case of phineas gage. *PLoS One* **7** (2012).
26. Zalesky, A. *et al.* Whole-brain anatomical networks: Does the choice of nodes matter? *Neuroimage* **50**, 970–983 (2010).
27. Hagmann, P. *et al.* Mapping the structural core of human cerebral cortex. *PLoS Biol.* **6**, 1479–1493 (2008).
28. Bola, M. & Sabel, B. A. Dynamic reorganization of brain functional networks during cognition. *Neuroimage* **114**, 398–413 (2015).
29. Tomasi, D. & Volkow, N. D. Association between Functional Connectivity Hubs and Brain Networks. *Cereb. Cortex* **21**, 2003–2013 (2011).
30. Tomasi, D. & Volkow, N. D. Functional connectivity density mapping. *Proc. Natl. Acad. Sci. USA* **107**, 9885–9890 (2010).
31. Zuo, X. N. *et al.* Network centrality in the human functional connectome. *Cereb. Cortex* **22**, 1862–1875 (2012).
32. Kabbara, A., Falou, W. El Khalil, M., Wendling, F. & Hassan, M. Graph analysis of spontaneous brain network using EEG source connectivity. *arXiv Prepr. arXiv1607.00952* (2016).
33. van den Heuvel, M. P. & Sporns, O. Rich-Club Organization of the Human Connectome. *J. Neurosci.* **31**, 15775–15786 (2011).
34. de Reus, M. & van den Heuvel, M. P. Rich club organization and intermodule communication in the cat connectome. *J. Neurosci.* **33**, 12929–39 (2013).
35. Collin, G., Sporns, O., Mandl, R. C. W. & van den Heuvel, M. P. Structural and Functional Aspects Relating to Cost and Benefit of Rich Club Organization in the Human Cerebral Cortex. *Cereb. Cortex* **24**, 2258–2267 (2013).
36. Chang, C., Liu, Z., Chen, M. C., Liu, X. & Duyn, J. H. EEG correlates of time-varying BOLD functional connectivity. *Neuroimage* **72**, 227–236 (2013).
37. Brookes, M. J. *et al.* Measuring temporal, spectral and spatial changes in electrophysiological brain network connectivity. *Neuroimage* **91**, 282–299 (2014).
38. Hutchison, R. M. *et al.* Dynamic functional connectivity: Promise, issues, and interpretations. *Neuroimage* **80**, 360–378 (2013).
39. Allen, E. A. *et al.* Tracking whole-brain connectivity dynamics in the resting state. *Cereb. Cortex* **24**, 663–676 (2014).
40. Baker, A. P. *et al.* Fast transient networks in spontaneous human brain activity. *Elife* **2014** (2014).
41. de Pasquale, F. *et al.* Temporal dynamics of spontaneous MEG activity in brain networks. *Proc. Natl. Acad. Sci. USA* **107**, 6040–6045 (2010).
42. de Pasquale, F. *et al.* A Dynamic Core Network and Global Efficiency in the Resting Human Brain. *Cereb. Cortex* bhw185, doi:10.1093/cercor/bhw185 (2015).
43. Hassan, M. *et al.* Dynamic reorganization of functional brain networks during picture naming. *Cortex* **73**, 276–288 (2015).
44. Hassan, M., Dufor, O., Merlet, I., Berrou, C. & Wendling, F. EEG source connectivity analysis: From dense array recordings to brain networks. *PLoS One* **9** (2014).
45. Lachaux, J.-P. *et al.* Studying single-trials of phase synchronous activity in the brain. *Int. J. Bifurc. Chaos* **10**, 2429–39 (2000).
46. Achard, S. *et al.* Hubs of brain functional networks are radically reorganized in comatose patients. *Proc. Natl. Acad. Sci. USA* **109**, 20608–13 (2012).
47. Achard, S., Salvador, R., Whitcher, B., Suckling, J. & Bullmore, E. A resilient, low-frequency, small-world human brain functional network with highly connected association cortical hubs. *J. Neurosci.* **26**, 63–72 (2006).

48. Alstott, J., Breakspear, M., Hagmann, P., Cammoun, L. & Sporns, O. Modeling the impact of lesions in the human brain. *PLoS Comput. Biol.* **5** (2009).
49. Cole, M. W., Pathak, S. & Schneider, W. Identifying the brain's most globally connected regions. *Neuroimage* **49**, 3132–3148 (2010).
50. Goldshtein, V., Koganov, G. A. & Surdutovich, G. I. Vulnerability and Hierarchy of Complex Networks. *Physics (College Park, Md.)* **16**, 4 (2004).
51. Freeman, L. C. A Set of Measures of Centrality Based on Betweenness. *Sociometry* **40**, 35–41 (1977).
52. Harriger, L., van den Heuvel, M. P. & Sporns, O. Rich Club Organization of Macaque Cerebral Cortex and Its Role in Network Communication. *PLoS One* **7** (2012).
53. He, Y. *et al.* Uncovering intrinsic modular organization of spontaneous brain activity in humans. *PLoS One* **4** (2009).
54. Sporns, O., Honey, C. J. & Kotter, R. Identification and classification of hubs in brain networks. *PLoS One* **2** (2007).
55. Costa, L. F., Rodrigues, F. A., Traverso, G. & Villas Boas, P. R. Characterization of complex networks: A survey of measurements. *Adv. Phys.* **56**, 167–242 (2007).
56. Kaiser, M. & Hilgetag, C. C. Edge vulnerability in neural and metabolic networks. *Biol. Cybern.* **90**, 311–317 (2004).
57. Guimerà, R. & Nunes Amaral, L. A. Functional cartography of complex metabolic networks. *Nature* **433**, 895–900 (2005).
58. Moussa, M. N. *et al.* Changes in Cognitive State Alter Human Functional Brain Networks. *Front. Hum. Neurosci.* **5**, 1–15 (2011).
59. Meunier, D., Achard, S., Morcom, A. & Bullmore, E. Age-related changes in modular organization of human brain functional networks. *Neuroimage* **44**, 715–723 (2009).
60. Power, J. D., Schlaggar, B. L., Lessov-Schlaggar, C. N. & Petersen, S. E. Evidence for hubs in human functional brain networks. *Neuron* **79**, 798–813 (2013).
61. Desikan, R. S. *et al.* An automated labeling system for subdividing the human cerebral cortex on MRI scans into gyral based regions of interest. *Neuroimage* **31**, 968–980 (2006).
62. Hassan, M. *et al.* Identification of Interictal Epileptic Networks from Dense-EEG. *Brain Topography* 1–17, doi:10.1007/s10548-016-0517-z (2016).
63. Buckner, R. L. *et al.* Cortical hubs revealed by intrinsic functional connectivity: mapping, assessment of stability, and relation to Alzheimer's disease. *J. Neurosci.* **29**, 1860–1873 (2009).
64. Cole, M. W., Yarkoni, T., Repovš, G., Anticevic, A. & Braver, T. S. Global Connectivity of Prefrontal Cortex Predicts Cognitive Control and Intelligence. *J. Neurosci.* **32**, 8988–8999 (2012).
65. Lohmann, G. *et al.* Eigenvector centrality mapping for analyzing connectivity patterns in fMRI data of the human brain. *PLoS One* **5** (2010).
66. Joyce, K. E., Laurienti, P. J., Burdette, J. H. & Hayasaka, S. A new measure of centrality for brain networks. *PLoS One* **5** (2010).
67. Raichle, M. E. & Snyder, A. Z. A default mode of brain function: A brief history of an evolving idea. *Neuroimage* **37**, 1083–1090 (2007).
68. Mason, M. F. *et al.* Wandering Minds: The Default Network and Stimulus-Independent Thought. *Science (80-)* **315**, 393–395 (2007).
69. Calhoun, V. D., Miller, R., Pearlson, G. & Adali, T. The Chronnectome: Time-Varying Connectivity Networks as the Next Frontier in fMRI Data Discovery. *Neuron* **84**, 262–274 (2014).
70. Garrison, K. A., Scheinost, D., Finn, E. S., Shen, X. & Constable, R. T. The (in)stability of functional brain network measures across thresholds. *Neuroimage* **118**, 651–661 (2015).
71. Brookes, M. J. *et al.* Investigating the electrophysiological basis of resting state networks using magnetoencephalography. *Proc. Natl. Acad. Sci. USA* **108**, 16783–8 (2011).
72. Hipp, J. F., Hawellek, D. J., Corbetta, M., Siegel, M. & Engel, A. K. Large-scale cortical correlation structure of spontaneous oscillatory activity. *Nat. Neurosci.* **15**, 884–890 (2012).
73. Becker, H. *et al.* Brain-source imaging: From sparse to tensor models. *IEEE Signal Process. Mag.* **32**, 100–112 (2015).
74. Brookes, M. J., Woolrich, M. W. & Barnes, G. R. Measuring functional connectivity in MEG: A multivariate approach insensitive to linear source leakage. *Neuroimage* **63**, 910–920 (2012).
75. Delorme, A. & Makeig, S. EEGLAB: An open source toolbox for analysis of single-trial EEG dynamics including independent component analysis. *J. Neurosci. Methods* **134**, 9–21 (2004).
76. Tadel, F., Baillet, S., Mosher, J. C., Pantazis, D. & Leahy, R. M. Brainstorm: A user-friendly application for MEG/EEG analysis. *Comput. Intell. Neurosci.* **2011** (2011).
77. Fischl, B. FreeSurfer. *NeuroImage* **62**, 774–781 (2012).
78. Gramfort, A., Papadopoulos, T., Olivi, E. & Clerc, M. OpenMEEG: opensource software for quasistatic bioelectromagnetics. *Biomed. Eng. Online* **9**, 45 (2010).
79. Hamalainen, M. S. & Ilmoniemi, R. J. Interpreting magnetic fields of the brain: minimum norm estimates. *Med. Biol. Eng. Comput.* **32**, 35–42 (1994).
80. Hassan, M., Shamas, M., Khalil, M., Falou, W. & El Wendling, F. EEGNET: An open source tool for analyzing and visualizing M/EEG connectome. *PLoS One* **10** (2015).
81. Barrat, A., Barthélemy, M., Pastor-Satorras, R. & Vespignani, A. The architecture of complex weighted networks. *Proc. Natl. Acad. Sci. USA* **101**, 3747–3752 (2004).
82. Watts, D. J. & Strogatz, S. H. Collective dynamics of 'small-world' networks. *Nature* **393**, 440–2 (1998).
83. Rubinov, M. & Sporns, O. Complex network measures of brain connectivity: Uses and interpretations. *Neuroimage* **52**, 1059–1069 (2010).
84. Xia, M., Wang, J. & He, Y. BrainNet Viewer: A Network Visualization Tool for Human Brain Connectomics. *PLoS One* **8** (2013).
85. Good, B. H., De Montjoye, Y. A. & Clauset, A. Performance of modularity maximization in practical contexts. *Phys. Rev. E - Stat. Nonlinear, Soft Matter Phys.* **81** (2010).
86. Girvan, M. & Newman, M. E. J. Community structure in social and biological networks. *Proc. Natl. Acad. Sci. USA* **99**, 7821–6 (2002).
87. Blondel, V. D., Guillaume, J.-L., Lambiotte, R. & Lefebvre, E. Fast unfolding of communities in large networks. *J. Stat. Mech. Theory Exp.* **10008**, 6 (2008).
88. Rosvall, M., Axelsson, D. & Bergstrom, C. T. The map equation. *Eur. Phys. J. Spec. Top.* **178**, 13–23 (2009).
89. Lancichinetti, A. & Fortunato, S. Consensus clustering in complex networks. *Sci. Rep.* **2**, 336 (2012).
90. Rubinov, M. & Sporns, O. Weight-conserving characterization of complex functional brain networks. *Neuroimage* **56**, 2068–2079 (2011).
91. Sales-Pardo, M., Guimerà, R., Moreira, A. A. & Amaral, L. A. N. Correction for Sales-Pardo *et al.*, Extracting the hierarchical organization of complex systems. *Proc. Natl. Acad. Sci. USA* **104**, 18874 (2007).
92. Bassett, D. S. *et al.* Robust detection of dynamic community structure in networks. *Chaos* **23** (2013).
93. Shirer, W. R., Ryali, S., Rykhlevskaia, E., Menon, V. & Greicius, M. D. Decoding subject-driven cognitive states with whole-brain connectivity patterns. *Cereb. Cortex* **22**, 158–165 (2012).

## Acknowledgements

This work was supported by the Rennes University Hospital (COREC Project named BrainGraph, 2015–17). The work has also received a French government support granted to the CominLabs excellence laboratory and

managed by the National Research Agency in the “Investing for the Future” program under reference ANR-10-LABX-07-01. It was also financed by Azm center for research in biotechnology and its applications. Authors would like to thank Olaf Sporns for his helpful discussion and comments that improved this work. We also thank Olivier Dufor for his help in the data acquisition. This work has been partially funded by the LUMINOUS Project, H2020-FETOPEN-2014-2015-RIA, agreement No. 686764.

### Author Contributions

Conceptualization: A.K., M.H.; Formal analysis: A.K., M.H., W.E.F.; Writing: A.K., M.H. and F.W.; Funding Acquisition: F.W., M.K.; Resources: F.W., M.H.

### Additional Information

**Supplementary information** accompanies this paper at doi:[10.1038/s41598-017-03420-6](https://doi.org/10.1038/s41598-017-03420-6)

**Competing Interests:** The authors declare that they have no competing interests.

**Publisher's note:** Springer Nature remains neutral with regard to jurisdictional claims in published maps and institutional affiliations.



**Open Access** This article is licensed under a Creative Commons Attribution 4.0 International License, which permits use, sharing, adaptation, distribution and reproduction in any medium or format, as long as you give appropriate credit to the original author(s) and the source, provide a link to the Creative Commons license, and indicate if changes were made. The images or other third party material in this article are included in the article's Creative Commons license, unless indicated otherwise in a credit line to the material. If material is not included in the article's Creative Commons license and your intended use is not permitted by statutory regulation or exceeds the permitted use, you will need to obtain permission directly from the copyright holder. To view a copy of this license, visit <http://creativecommons.org/licenses/by/4.0/>.

© The Author(s) 2017



**Supplementary materials for**

**The dynamic functional core network of the human brain at rest**

Kabbara A.<sup>1, 2, 3, 4, \*</sup>, EL Falou W.<sup>3, 4</sup>, Khalil M.<sup>3, 4</sup>, Wendling F.<sup>1, 2</sup>, Hassan M.<sup>1, 2</sup>

<sup>1</sup> INSERM, U1099, F-35000 Rennes, France

<sup>2</sup> University of Rennes 1, LTSI, F-35000 Rennes, France

<sup>3</sup> Azm research center in biotechnology, EDST, Lebanese University, Lebanon

<sup>4</sup> CRSI research center, Faculty of engineering, Lebanese University, Lebanon

\* Corresponding author: [aya.kabbara@etudiant.univ-rennes1.fr](mailto:aya.kabbara@etudiant.univ-rennes1.fr)

### Supplemental Data items

Acronyms	Name	RSN
iCC L	isthmuscingulate L	DMN
iCC R	isthmuscingulate R	DMN
MOF L	medialorbitofrontal L	DMN
MOF R	medialorbitofrontal R	DMN
PCC L	posteriorcingulate L	DMN
PCC R	posteriorcingulate R	DMN
PCUN L	precuneus L	DMN
PCUN R	precuneus R	DMN
rACC L	rostralanteriorcingulate L	DMN
rACC R	rostralanteriorcingulate R	DMN
LOF L	lateralorbitofrontal L	DMN
LOF R	lateralorbitofrontal R	DMN
paraH L	parahippocampal L	DMN
paraH R	parahippocampal R	DMN
cACC L	cAUDalanteriorcingulate L	DAN
cACC R	cAUDalanteriorcingulate R	DMN
ITG L	inferiortemporal L	DAN
ITG R	inferiortemporal R	DAN
MTG L	middletemporal L	DAN
MTG R	middletemporal R	DAN
pOPER L	parsopercularis L	DAN
pOPER R	parsopercularis R	DAN
pORB L	parsorbitalis L	DAN
pORB R	parsorbitalis R	DAN
pTRI L	parstriangularis L	DAN
pTRI R	parstriangularis R	DAN
INS L	insula L	SAN
INS R	insula R	SAN
rMFG L	rostralmiddlefrontal L	SAN
rMFG R	rostralmiddlefrontal R	SAN
SMAR L	supramarginal L	SAN
SMAR R	supramarginal R	SAN
cMFG L	caudalmiddlefrontal L	SAN
cMFG R	caudalmiddlefrontal R	SAN

Acronyms	Name	RSN
STG L	superiortemporal L	AUD
STG R	superiortemporal R	AUD
CUN L	cuneus L	VIS
CUN R	cuneus R	VIS
LOG L	lateraloccipital L	VIS
LOG R	lateraloccipital R	VIS
FUS R	fusiform R	VIS
FUS L	fusiform L	VIS
LING L	lingual L	VIS
LING R	lingual R	VIS
BSTS L	bankssts L	other
BSTS R	bankssts R	other
ENT L	entorhinal L	other
ENT R	entorhinal R	other
FP L	frontalpole L	other
FP R	frontalpole R	other
IPL L	inferiorparietal L	other
IPL R	inferiorparietal R	other
sFG L	superiorfrontal L	other
sFG R	superiorfrontal R	other
paraC L	paracentral L	other
paraC R	paracentral R	other
periCAL L	pericalcarine L	other
periCAL R	pericalcarine R	other
postC L	postcentral L	other
postC R	postcentral R	other
preC L	precentral L	other
preC R	precentral R	other
SPL L	superiorparietal L	other
SPL R	superiorparietal R	other
TP L	temporalpole L	other
TP R	temporalpole R	other
TT L	transversetemporal L	other
TT R	transversetemporal R	other

**Table S1.** Anatomic regions-of-interest (ROIs) included in the analysis, as derived from the Desikan Killiany atlas, and their affiliation to RSNs.

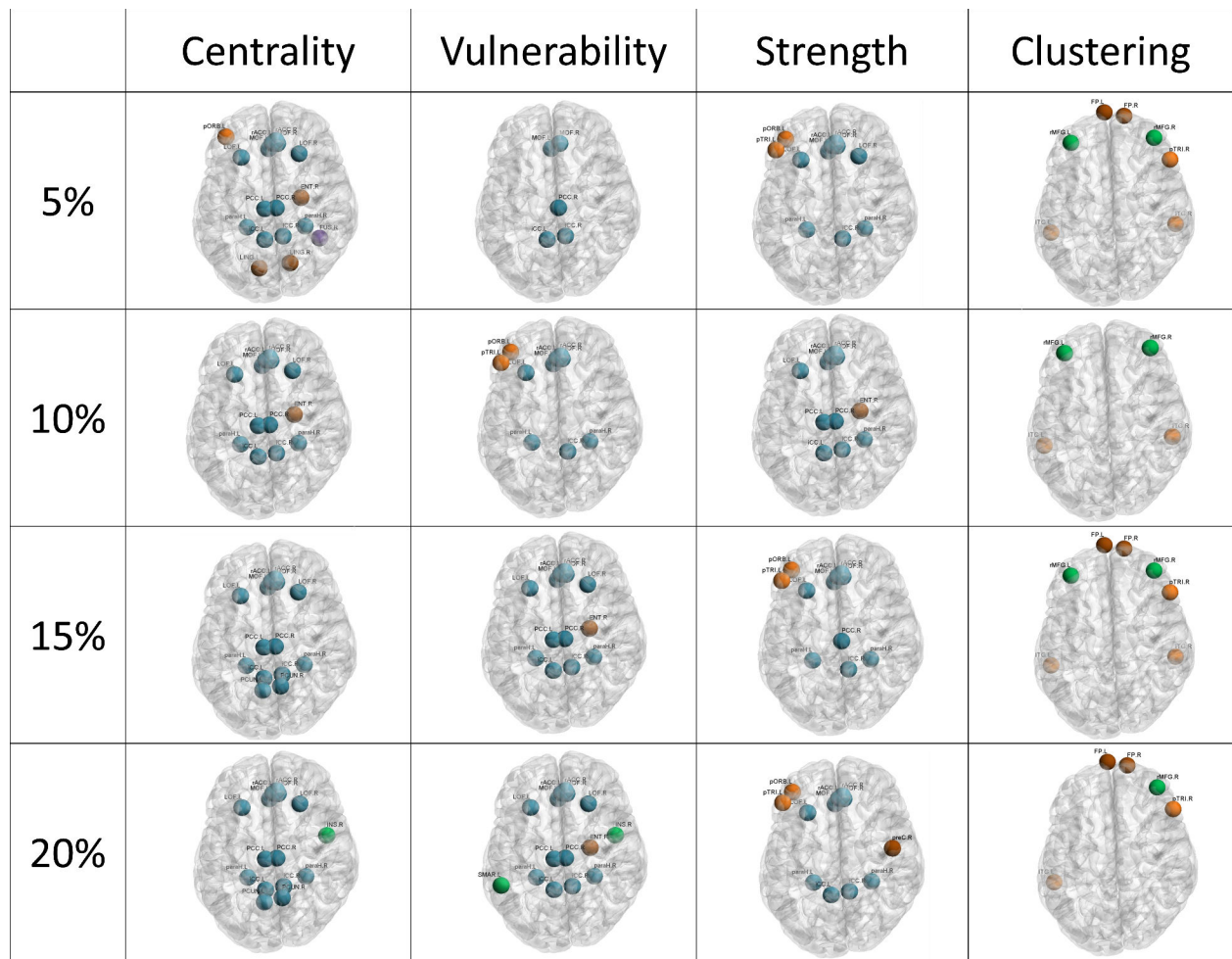


**Figure S1.** The locations of the significant brain regions on the cortical surface for the different thresholds (5%, 10%, 15%, 20%) in terms of centrality, vulnerability, strength and clustering coefficient. The color of the node corresponds to which RSN the region is assigned. Names and abbreviations of the brain regions are listed in table S1.

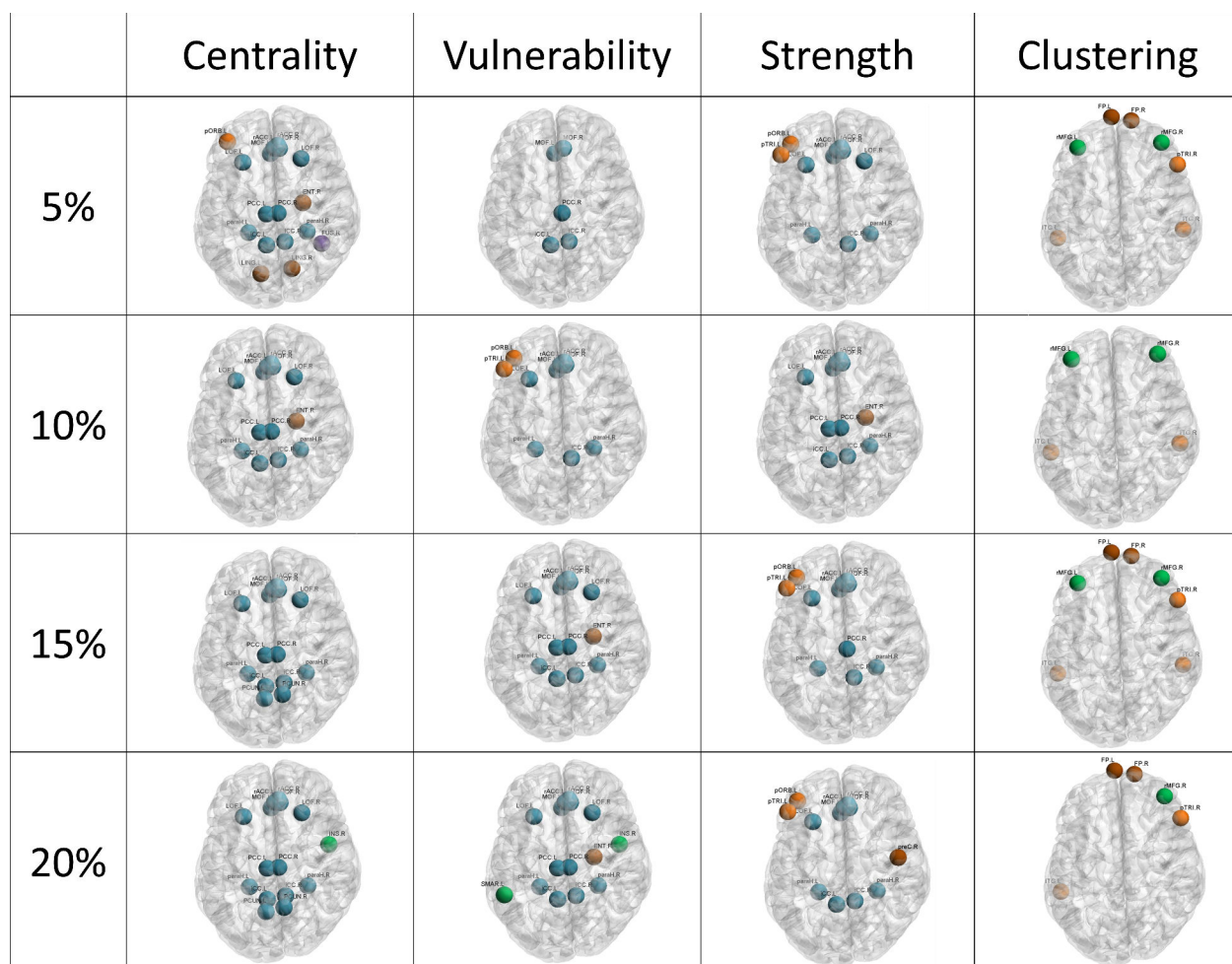


**Figure S2.** The locations of the significant brain regions on the cortical surface for different window size (300ms, 1s, 2s, 10s) in terms of centrality, vulnerability, strength and clustering coefficient. The color of the node corresponds to which RSN the region is assigned. Names and abbreviations of the brain regions are listed in table S1.

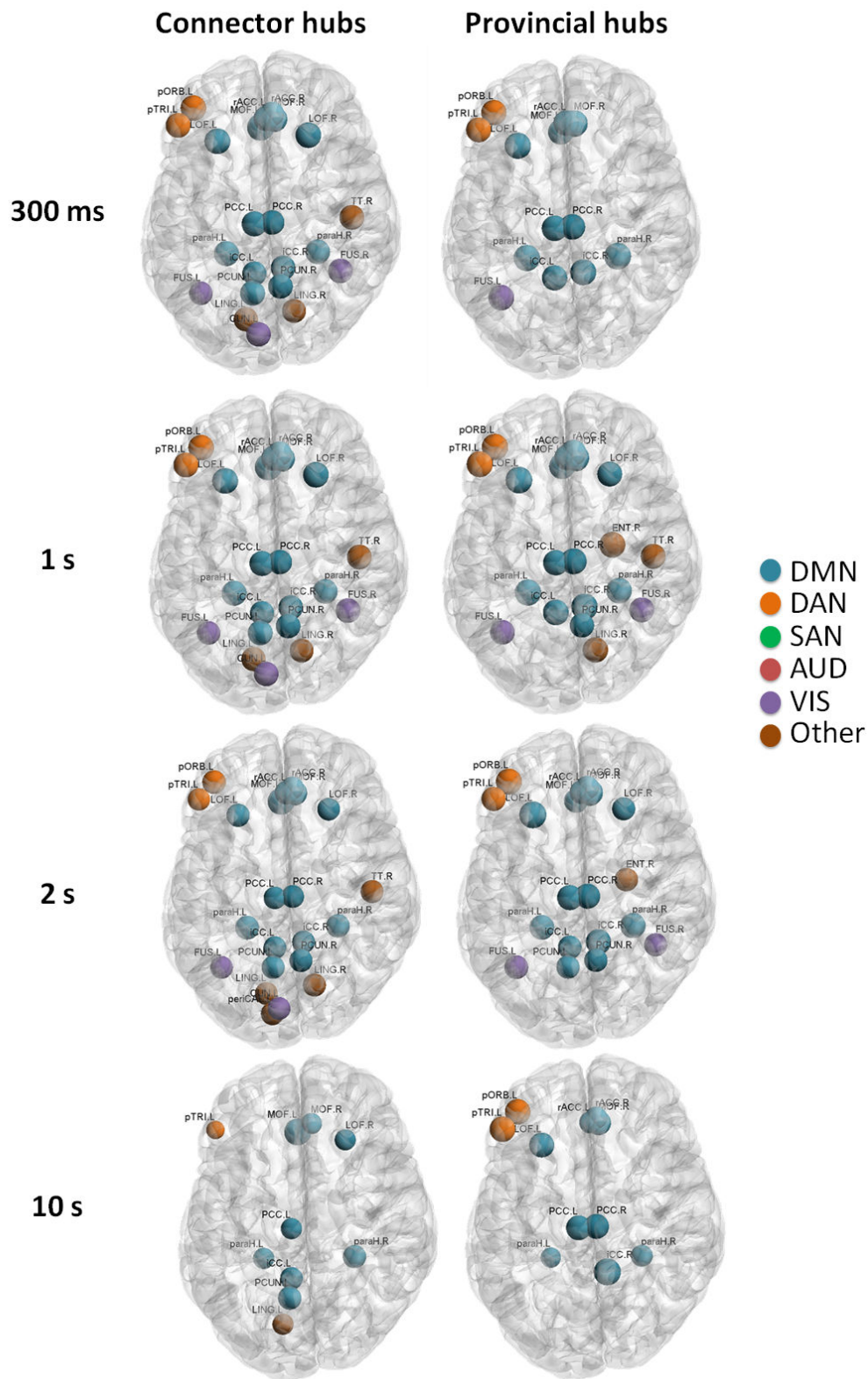


**Figure S3.** The spatial distributions of significant provincial hubs, and significant connector hubs for different window size. The color of the node corresponds to which RSN this node is assigned.

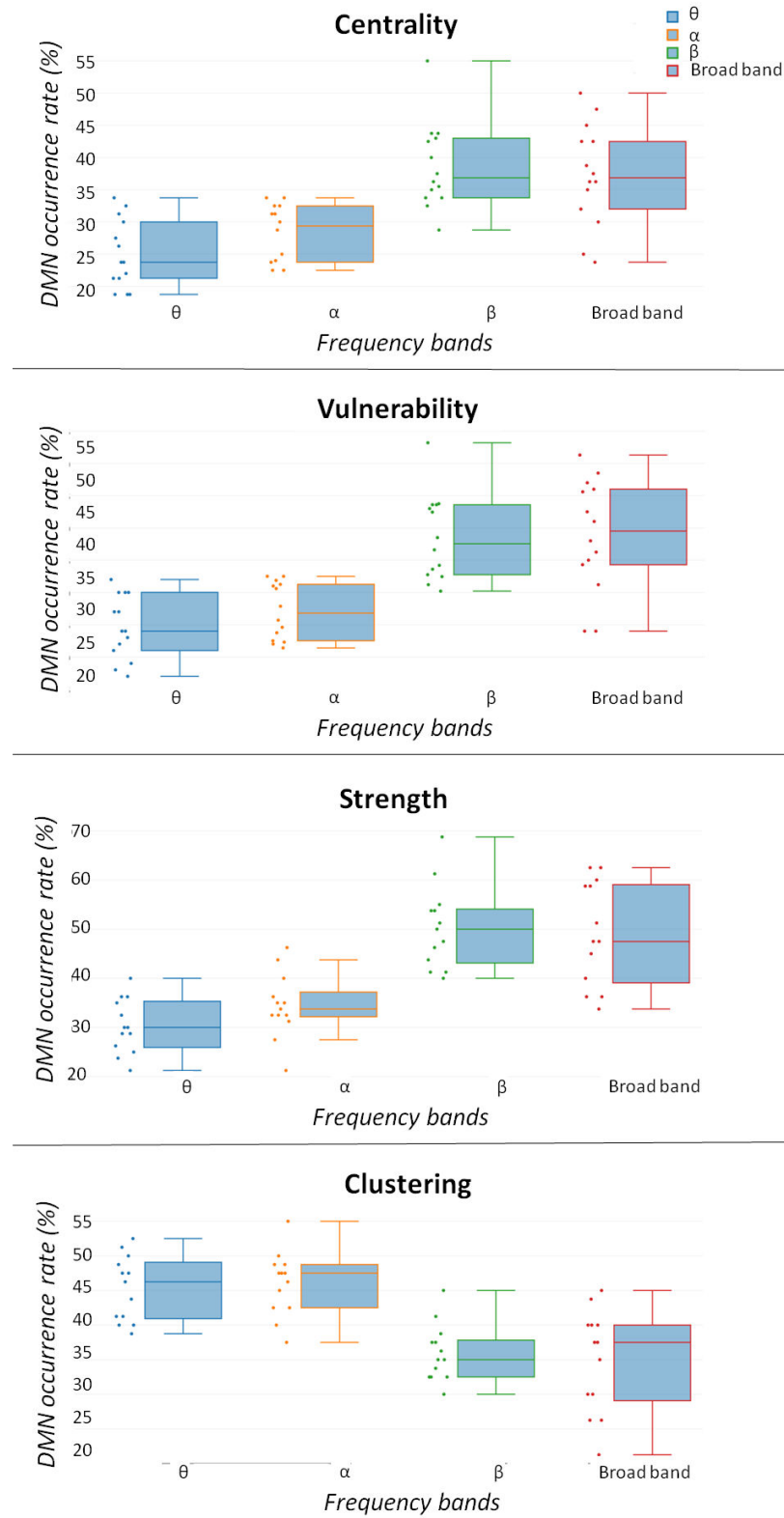


**Figure S4.** The fractional occupancy of DMN in each of  $\theta$  (3-7 Hz),  $\alpha$  (7-13 Hz),  $\beta$  (14-25 Hz) and broad-band (3-45 Hz) in term of centrality, strength, vulnerability and clustering.

# **Study 3: Reduced integration and improved segregation of functional brain networks in Alzheimer's disease**

A Kabbara, H Eid, W El Falou, M Khalil, F Wendling, M Hassan

Article published in Journal of neural engineering 15 (2), 026023

PAPER

## Reduced integration and improved segregation of functional brain networks in Alzheimer's disease

To cite this article: A Kabbara *et al* 2018 *J. Neural Eng.* **15** 026023

View the [article online](#) for updates and enhancements.



# Reduced integration and improved segregation of functional brain networks in Alzheimer's disease

A Kabbara<sup>1,2,3</sup>, H Eid<sup>4</sup>, W El Falou<sup>2,3</sup>, M Khalil<sup>2,3</sup>, F Wendling<sup>1,5</sup>  
and M Hassan<sup>1,5</sup> 

<sup>1</sup> Université Rennes, LTSI, F-35000 Rennes, France

<sup>2</sup> Azm Center for Research in Biotechnology and its Application, EDST, Lebanese University, Tripoli, Lebanon

<sup>3</sup> Faculty of Engineering, CRSI Research Center, Lebanese University, Tripoli, Lebanon

<sup>4</sup> Mazloum Hospital, Tripoli, Lebanon

E-mail: [mahmoud.hassan@univ-rennes1.fr](mailto:mahmoud.hassan@univ-rennes1.fr)

Received 6 October 2017, revised 29 December 2017

Accepted for publication 25 January 2018

Published 16 February 2018




## Abstract

**Objective.** Emerging evidence shows that cognitive deficits in Alzheimer's disease (AD) are associated with disruptions in brain functional connectivity. Thus, the identification of alterations in AD functional networks has become a topic of increasing interest. However, to what extent AD induces disruption of the balance of local and global information processing in the human brain remains elusive. The main objective of this study is to explore the dynamic topological changes of AD networks in terms of brain network segregation and integration.

**Approach.** We used electroencephalography (EEG) data recorded from 20 participants (10 AD patients and 10 healthy controls) during resting state. Functional brain networks were reconstructed using EEG source connectivity computed in different frequency bands. Graph theoretical analyses were performed assess differences between both groups. **Main results.** Results revealed that AD networks, compared to networks of age-matched healthy controls, are characterized by lower global information processing (integration) and higher local information processing (segregation). Results showed also significant correlation between the alterations in the AD patients' functional brain networks and their cognitive scores.

**Significance.** These findings may contribute to the development of EEG network-based test that could strengthen results obtained from currently-used neurophysiological tests in neurodegenerative diseases.

**Keywords:** EEG signal processing, brain networks, Alzheimer's disease

 Supplementary material for this article is available [online](#)

(Some figures may appear in colour only in the online journal)

## Introduction

Worldwide, about 35 million people are estimated to have dementia (World Health Organization 2012). Alzheimer's disease (AD), the most common cause of dementia, is a neurological disorder essentially characterized by progressive impairment of memory and other cognitive functions.

Emerging evidence show that the progressive evolution in AD is related to pathological changes in large-scale networks (Supekar *et al* 2008, Zhou *et al* 2010, Pievani *et al* 2011). Therefore, from a clinical perspective, the demand is high for non-invasive and easy-to-use methods to identify pathological alterations in brain networks. More precisely, novel 'neuro-markers' able to identify and characterize networks associated with cognitive deficits in AD patients, in particular at early stage, are needed.

<sup>5</sup> These authors contributed equally to this work.

In this context, electroencephalography (EEG) has some major assets since it is a non-invasive, easy to use and clinically available technique. A potential framework for advanced EEG analysis is the emerging technique called ‘MEG/EEG source connectivity’ (de Pasquale *et al* 2010, Hipp *et al* 2012, Mehrkanon *et al* 2014, Hassan *et al* 2015, Kabbara *et al* 2017). As shown by several recent studies (Hassan *et al* 2017a, 2017, Engels *et al* 2017), this technique could indeed respond to clinical demand, provided that appropriate information processing is performed. Previous results, using the EEG source connectivity methods, showed alterations in the functional connectivity at the theta and alpha2 bands in AD patients compared to controls (Canuet *et al* 2012). Relationships between the dysfunctional connections in AD patients and the cognitive decline progression were also observed (Hata *et al* 2016). Moreover, Vecchio *et al* showed, in a large group of AD patients, changes in topological brain network characteristics mainly in the clustering coefficient and the path length measures (Vecchio *et al* 2014).

However, to what extent the AD modifies the brain network segregation (local information processing) and integration (global information processing) remains unclear. This is the main objective of the paper. More precisely, we address two questions: (i) do the dynamic brain network segregation and integration changes in AD compared to controls? And (ii) is there a correlation between the network disruptions and the cognitive score of the AD patients? To tackle this issue, we combined the use of the EEG source connectivity with the graph theory based analysis. Resting state EEG data were recorded from 20 participants (10 AD patients and 10 age-matched controls). The functional networks were reconstructed at the cortical level from scalp EEG electrodes. The identified networks were then analyzed by graph measures that allow the characterization of these networks at different scales from high-level topology to low-level topology.

## Materials and methods

The full pipeline of this study is illustrated in figure 1.

### Participants

Ten healthy controls (6 males and 4 females, age 64–78 year) and ten patients diagnosed with AD (5 females and 5 males, age 66–81 year) participated in this study. All subjects provided informed consent in accordance with the local institutional review boards guidelines (CE-EDST-3-2017). Patients were recruited from the memory clinic of Dar al-Ajaza Hospital and from Mazloun Hospital, Tripoli, Lebanon. Age-matched healthy controls were recruited from Dar Al-Ajaza Hospital and the local community. For each subject medical history, a cognitive screening test and EEG recording were performed. The mini-mental state examination (MMSE) was used as an indicator of the global cognitive performance (Folstein *et al* 1975). This test has been widely used to characterize the overall cognitive level of AD patients and to estimate the severity and progression of cognitive impairment

(Ismail *et al* 2010). Based on Mungas (1991), any score greater than or equal to 24 points out of 30 (MMSE  $\geq$  0.8) indicates normal cognitive functions. Below this score indicate cognitive impairment.

### Data acquisition and preprocessing

EEG signals were recorded using a 32-channel EEG system (Twente Medical Systems International-TMSi-, Porti system) placed on the head according to the 10–20 system (Klem *et al* 1999). Signals were sampled at 500 Hz and band-pass filtered between 0.1–45 Hz. All subjects underwent 10 min of resting-state in which they were asked to relax and keep their eyes closed without falling asleep.

EEG signals are often contaminated by several sources of noise and artifacts. In order to clean raw signals, the pre-processing followed the same steps as described in several previous studies dealing with EEG resting state data (Onton *et al* 2006, Korjus *et al* 2015, Li *et al* 2015, Hassan *et al* 2017b, Kabbara *et al* 2017). Briefly, the bad channels (i.e. displaying signals that are either completely flat or are contaminated by movement artifacts) were first identified by visual inspection, complemented by the power spectral density, when needed. Then, these bad channels were recovered using an spherical interpolation procedure implemented in EEGLAB (Delorme and Makeig 2004). In addition, epochs with voltage fluctuation  $> +80 \mu\text{V}$  and  $< -80 \mu\text{V}$  were removed. Consequently, for each participant, four artifact-free epochs of 40 s lengths were selected. This epoch length was largely used previously and considered as a good compromise between the needed temporal resolution and the reproducibility of the results (Kabbara *et al* 2017). As the recorded EEG data used here has a very high temporal resolution ( $\sim 1$  ms), the number of available samples is largely sufficient to compute statistically-consistent functional networks. By using a sliding window approach while calculating the functional connectivity, a high number of networks were obtained for each 40 s-epoch and for different frequency bands.

The EEGs and MRI template (ICBM152) were co-registered after identifying the anatomical landmarks (left and right pre-auricular points and nasion) using Brainstorm (Tadel *et al* 2011). An atlas-based segmentation approach was used to project EEGs onto an anatomical framework consisting of 68 cortical regions identified by means of Desikan-Killiany (Desikan *et al* 2006) atlas, see table S1 (supplementary materials ([stacks.iop.org/JNE/15/026023/mmedia](https://stacks.iop.org/JNE/15/026023/mmedia))) for more details about the names and abbreviations of these regions. The lead field matrix was then computed for a cortical mesh of 15 000 vertices using OpenMEEG (Gramfort *et al* 2010).

**Brain networks construction.** Brain networks were constructed using the ‘EEG source connectivity’ method (Hassan *et al* 2014). It includes two main steps: (1) Reconstruct the temporal dynamics of the cortical sources by solving the inverse problem, and (2) Measure the functional connectivity between the reconstructed time series. Here, we used the weighted minimum norm estimate (wMNE) algorithm

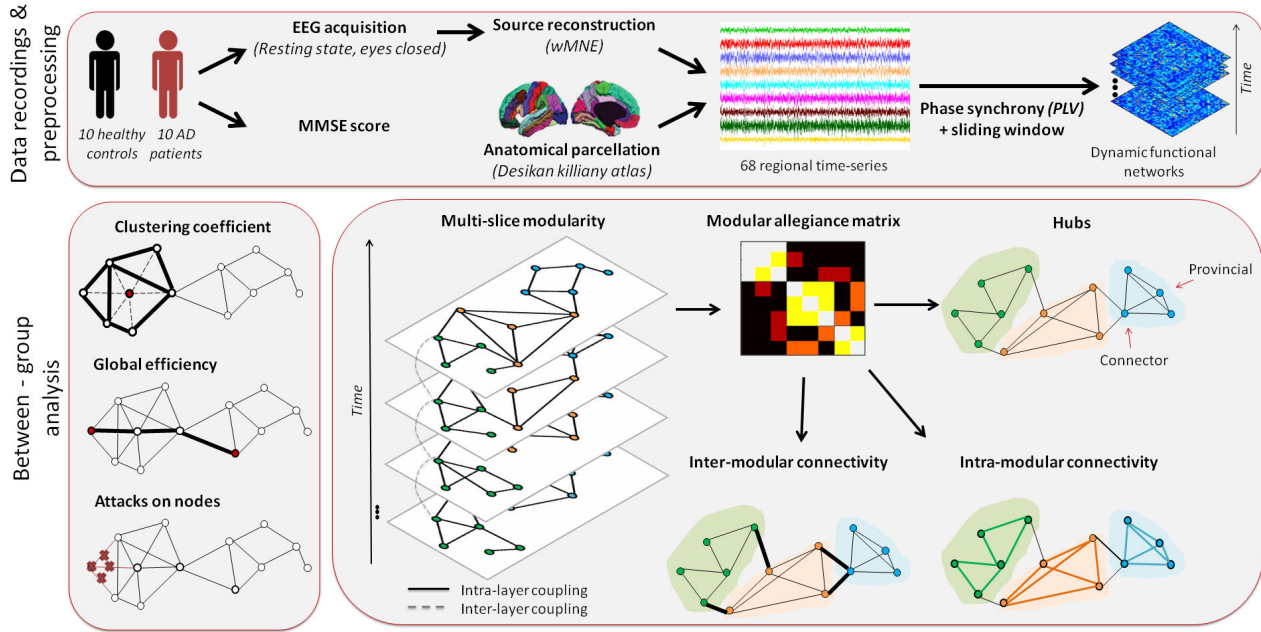


**Figure 1.** Design of the study. Data were recorded from 10 healthy controls and 10 AD patients during resting state condition (eyes closed). The cognitive performance was evaluated using MMSE score. The cortical sources were reconstructed using weighted minimum norm estimate (wMNE) inverse solution. Desikan Killiany atlas was used to anatomically parcellate the brain into 68 ROIs. The dynamic functional networks were then computed using phase synchrony method combined with a sliding window approach. In order to analyze the difference between healthy and AD networks, graph measures were extracted: clustering coefficient, global efficiency and vulnerability of each node (influence of each node's attack on the network global efficiency). Modularity-based parameters (mainly integration and segregation of networks) were also used. Moreover, the network hubs of each group were identified and compared.

as inverse solution (Hamalainen and Ilmoniemi 1994). The reconstructed regional time series were filtered in different frequency bands (theta (4–8 Hz); alpha1 (8–10 Hz); alpha2 (10–13 Hz); beta (13–30 Hz)). The functional connectivity was computed, for each frequency band, between the regional time series using the phase locking value (PLV) measure (Lachaux et al 1999). The PLV ranges between 0 (no phase locking) and 1 (full synchronization).

Using PLV, dynamic functional connectivity matrices were computed for each epoch using a sliding window technique (Kabbara et al 2017). It consists in moving a time window of certain duration  $\delta$  along the time dimension of the epoch, and then PLV is calculated within each window. As recommended in Lachaux et al (2000), we chose the smallest window length that is equal to  $\frac{6}{\text{central frequency}}$  where 6 is the number of 'cycles' at the given frequency band. In theta band, as the central frequency (Cf) equals to 6 Hz,  $\delta$  equals 1s. Likewise,  $\delta = 666$  ms in alpha1 band (Cf = 9 Hz), 521 ms in alpha2 band (Cf = 11.5 Hz), and 279 ms (Cf = 21.5 Hz) in beta band. Functional connectivity matrices were represented as graphs (i.e. networks) composed of nodes, represented by the 68 ROIs, and edges corresponding to the functional connectivity values computed over the 68 regions, pair-wise.

Considered  $\delta$  values yield, for each epoch, to 33 networks in theta band, 66 networks in alpha1 band, 76 networks in alpha2 band and 130 networks in beta band.

**Multi-slice networks modularity.** The modularity aims at decomposing a network into different communities of high intrinsic connectivity and low extrinsic connectivity (Eickhoff

et al 2005). To describe and quantify the evolution of brain networks as a function of time, we applied the multi-slice modularity (Bassett et al 2013). In this method, the nodes across network slices (time windows) are linked via a coupling parameter using a quality function given by the following formula:

$$Q_{ml} = \frac{1}{2\mu} \sum_{ijl} \left\{ \left( A_{ijl} - \gamma_l \frac{k_{il}k_{jl}}{2m_l} \right) \delta_{lr} + \delta_{ij} C_{jlr} \right\} \delta(M_{il}, M_{jr}). \quad (1)$$

Where nodes  $i$  and  $j$  are assigned to communities  $M_{il}$  and  $M_{jl}$  in slice  $l$ , respectively.  $A_{ijl}$  represents the weight of the edge between  $i$  and  $j$ .  $\gamma_l$  is the structural resolution parameter of slice  $l$ .  $C_{jlr}$  is the connection strength between the node  $j$  in slice  $r$  and the node  $j$  in slice  $l$ . The structural resolution parameter  $\gamma$  and the inter-slice coupling parameter are set to 1.  $k_{il}$  is the strength of the node  $i$  in slice  $l$ , the  $\delta$ -function  $\delta(x, y)$  is 1 if  $x = y$  and 0 otherwise,  $m = \frac{1}{2} \sum_{ij} A_{ij}$  and  $\mu = \frac{1}{2} \sum_{jr} k_{jr}$ .

The multi-slice modularity algorithm was applied with diagonal and ordinal inter-slice couplings. Diagonal and ordinal coupling means that each node is only connected to itself in the adjacent slices. Here, a slice corresponds to a network at a given time period. Hence, the number of slices equals the number of windows at a given frequency band.

To deal with the 'degeneracy' problem, we computed a  $68 \times 68$  association matrix (Sales-Pardo et al 2007, Rubinov and Sporns 2011, Lancichinetti and Fortunato 2012) where the element  $A_{ij}$  represents the number of times the nodes  $i$  and  $j$  are assigned to the same module across 200 runs using Louvain algorithm (Blondel et al 2008). The association

matrix was then compared to a null-model generated from 100 random permutations of the original partitions. That is, for each of the 100 partitions, we reassign nodes uniformly at random to the modules present in the partition. This generates a null model matrix whose element  $A_{ij}^r$  is the number of times the node  $i$  and  $j$  are randomly assigned to the same community. To remove randomness, we kept the significant values of the original association matrix by setting any element  $A_{ij}$  whose value is less than the maximum value of the random association matrix to 0 (Bassett et al 2013). Finally, the thresholded association matrix was re-clustered using Louvain algorithm.

### Network measures

The topological properties of identified networks were characterized using the following graph measures:

**Average clustering coefficient.** The clustering coefficient of a node represents how close its neighbors tend to cluster together (Watts and Strogatz 1998). Accordingly, the average clustering coefficient of a network is considered as a direct measure of its segregation (i.e. the degree to which a network is organized into local specialized regions) (Bullmore et al 2009). In brief, the clustering coefficient of a node is defined as the proportion of connections among its neighbors, divided by the number of connections that could possibly exist between them (Watts and Strogatz 1998).

**Global efficiency.** The global efficiency of a network is the average inverse shortest path length (Latora and Marchiori 2001). A short path length indicates that, on average, each node can reach other nodes with a path composed of only a few edges (Sporns 2010). Thus, the global efficiency is one of the most elementary indicators of network's integration (i.e. the degree to which a network can share information between distributed regions).

**Recruitment.** The recruitment of a node  $i$  corresponds to the average probability that the node is in the same module across runs and slices (i.e. time windows). It is calculated as follows:

$$\text{Recruitment}_i^M M_i = \frac{1}{n_M} \sum_{j \in M} A_{ij}. \quad (2)$$

Where  $M$  is the module of the node  $i$ .  $n_M$  denotes the number of nodes assigned to the module  $M$ .  $A_{ij}$  represents the number of times the nodes  $i$  and  $j$  are assigned to the same module across slices and runs. A region with high recruitment value tends to maintain itself in the same community across time (Bassett et al 2015).

**Integration.** It reflects how modules are interacting with each other. It is computed as the average number of links each node in a given module has with the nodes in the other modules across runs and slices (i.e. time windows). It is calculated as follows:

$$\text{Integration}_i^M M_i = \frac{1}{N - n_M} \sum_{j \notin M} A_{ij}. \quad (3)$$

Where  $M$  is the module of the node  $i$ .  $N$  denotes the total nodes number,  $n_M$  the number of nodes assigned to the module  $M$ .  $A_{ij}$  represents the number of times the nodes  $i$  and  $j$  are assigned to the same module across slices and runs. A region with high integration value tends to be present in communities other than its own across time (Bassett et al 2015).

### Hubs identification

**Hubness** is a key feature when exploring the brain network architecture due to the high influence of hub nodes on network dynamics and information processing (van den Heuvel and Sporns 2013). Once modules are identified, the 68 nodes were classified into three main categories (non hubs, provincial hubs and connector hubs) using combination of two measures. The first one is the within-module degree  $Z$  defined as:

$$Z_i = \frac{K_i(M_i) - \overline{K(M_i)}}{\sigma_{k(M_i)}}. \quad (4)$$

Where  $K_i(M_i)$  is the within-module degree of the node  $i$ ,  $\overline{K(M_i)}$  is the mean of within module degree of nodes assigned to the same community as node  $i$ , and  $\sigma_{k(M_i)}$  is the standard deviation. A positive  $Z$  value indicates that the node is highly connected to other members of the same community (Guimerà et al 2005). In our study, a node is considered as hub if the corresponding within module degree is greater than 1.5.

We then focused on classifying hubs into provincial and connector based on a second metric known as participation coefficient ( $P$ ). This metric characterizes how a node's edges are distributed across modules:

$$P_i = 1 - \sum_{c=1}^C \left( \frac{K_i(M)}{K_i} \right)^2. \quad (5)$$

Where  $C$  is the number of modules,  $K_i(m)$  is the number of edges between node  $i$  and nodes in module  $M$ . Based on the criteria proposed by Guimerà and Nunes Amaral (2005), a provincial hub having most of its links inside its own module has a  $P_i$  value lower than 0.3; while a connector hub has a  $P_i$  value greater than 0.3. These values were used in our study.

### Attacks on nodes

Like any other networked system, the brain network may lose some of its effectiveness as a result of an 'attack'. In particular, attacks on regions playing a key role will lead to significant network disruption. For this reason, we quantified the importance of each node in terms of its attack influence on the global network efficiency. This quantification is usually done using a graph measure known as 'vulnerability'. It is defined as the reduction in global efficiency of the network when the



**Table 1.** Differences among RSNs connectivity between healthy and AD networks in the different frequency bands. Abbreviations: default mode network = DMN, dorsal attention network = DAN, salience attention network = SAN, auditory network = AUD, visual network = VIS.

Frequency band	RSN	Healthy		Alzheimer		<i>p</i> -value
		Median	SD	Median	SD	
Theta	DMN	0.13	0.01	0.09	0.017	<b>0.02<sup>a</sup></b>
	DAN	0.09	0.009	0.08	0.11	0.82
	SAN	0.06	0.013	0.08	0.01	<b>0.047<sup>a</sup></b>
	AUD	0.012	0.017	0.03	0.02	0.14
	VIS	0.11	0.01	0.12	0.015	0.6
Alpha1	DMN	0.117	0.018	0.116	0.014	0.68
	DAN	0.087	0.0138	0.0975	0.008	0.21
	SAN	0.057	0.0101	0.07	0.014	0.17
	AUD	0.024	0.011	0.023	0.018	0.75
	VIS	0.15	0.017	0.13	0.018	0.11
Alpha2	DMN	0.12	0.008	0.11	0.005	<b>0.031<sup>a</sup></b>
	DAN	0.095	0.0037	0.091	0.009	0.35
	SAN	0.076	0.01	0.071	0.012	0.4
	AUD	0.036	0.006	0.033	0.012	0.4
	VIS	0.1311	0.1084	0.12	0.019	0.35
Beta	DMN	0.12	0.012	0.12	0.007	0.3
	DAN	0.091	0.044	0.086	0.011	0.25
	SAN	0.069	0.0075	0.074	0.0012	0.16
	AUD	0.033	0.013	0.02	0.012	0.09
	VIS	0.134	0.014	0.108	0.012	<b>0.003<sup>a</sup></b>

<sup>a</sup> Denotes for significant effects ( $p < 0.05$ ).

node and all its edges are removed (Gol'dshtein *et al* 2004). Thus, critical nodes can be identified from high vulnerability values as their attack (i.e. node and associated edges removal) leads to significant drop of the whole network efficiency.

### Statistical tests

To quantify the differences between healthy and AD networks in terms of RSNs connectivity, average clustering coefficient, global efficiency, integration/segregation measures and vulnerability, statistical tests were performed. For each subject, we averaged all the metrics values obtained from the different networks among all epochs and time windows for each subject. As data were not normally distributed, we assessed the statistical difference between the two groups using the Mann Whitney U Test also known as Rank-Sum Wilcoxon test (degree of freedom = 18).

For hubs identification, each group was considered separately. First, we concatenated the metrics values (participation coefficient and within-module degree  $Z$ ) from all group subjects, epochs and time windows. Based on the criteria of hubs classification (Guimerà and Nunes Amaral 2005), each node was assigned to its corresponding category (i.e. provincial, connector or non-hub) for each window. Then, the brain regions that are significantly behaving as connector or/and provincial hubs during time were extracted using a chi-squared test (as described in our previous work (Kabbara *et al* 2017)). To deal with the family-wise error rate, the statistical tests were corrected for multiple comparisons using Bonferroni method ( $p_{\text{Bonferroni adjusted}} < \frac{0.05}{N}$ ), with  $N$  (68) denotes the number of brain regions.

### The parcellation into RSNs

Each brain region of the Desikan-Killiany atlas was associated to its corresponding RSN based on Shirer *et al* (2012) in which authors identified fourteen functional networks: anterior salience network, auditory network, basal ganglia network, dorsal default mode network, higher visual network, language network, left executive control network, sensorimotor network, posterior salience network, precuneus network, primary visual network, right executive control network, ventral default mode network, and visuospatial network. Here, we focused on five RSNs: the default mode network (DMN) obtained by combining the regions of the dorsal and the ventral default mode network, the salience network (SAN) obtained by associating all the regions in anterior and posterior salience networks, the visual network (VIS) obtained by combining of the higher and primary visual networks. This same parcellation was also used in our previous study (Kabbara *et al* 2017).

## Results

### Intrinsic connectivity of RSNs

First, we were interested in evaluating the differences among the RSNs between healthy controls and AD patients. For this reason, we associated each brain region of the Desikan-Killiany atlas to its corresponding RSN according to Kabbara *et al* (2017). Results in table 1 show significant decreases in DMN connectivity in AD compared to healthy controls in the theta ( $p = 0.02$ ,  $U = 15$ ,  $r = 0.51$ ) and alpha2 ( $p = 0.031$ ,  $U = 17$ ,  $r = 0.47$ ) bands. Similarly, reduced visual network

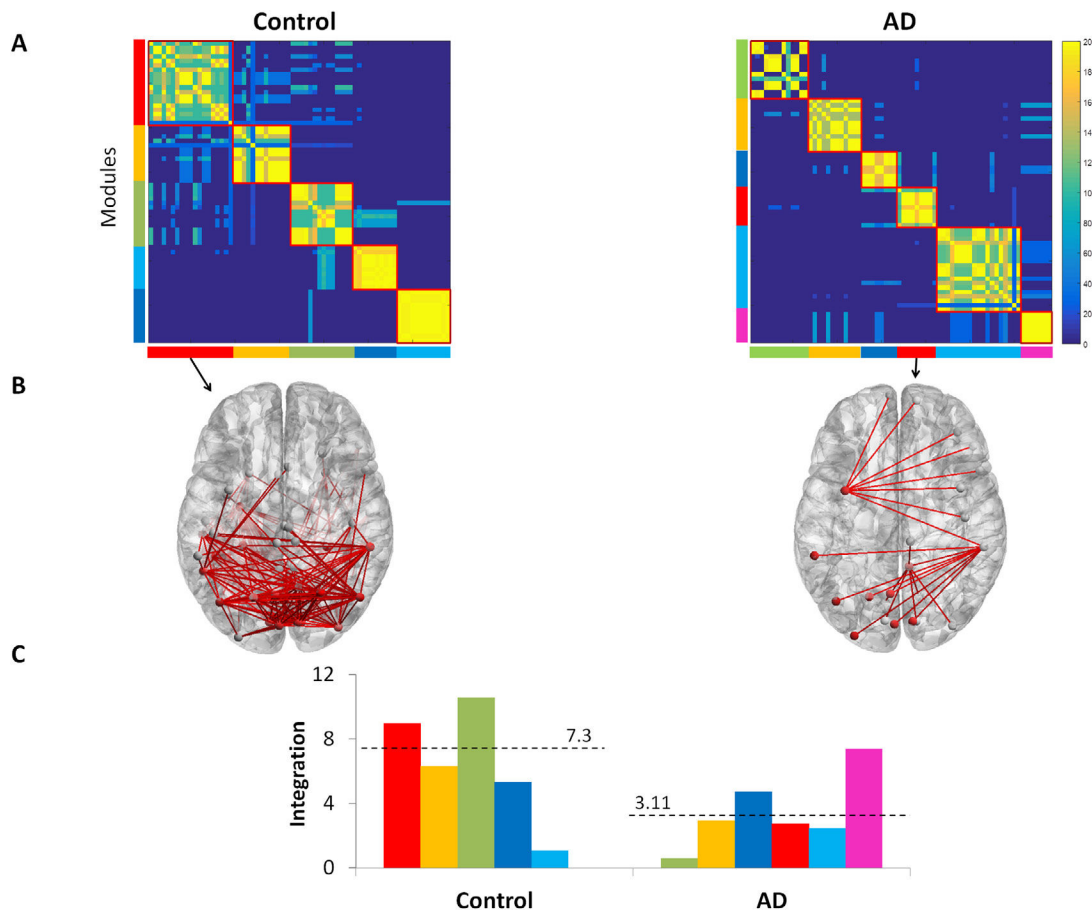


**Figure 2.** (A) The association matrices obtained by the multi-slice modularity method for healthy controls and AD patients. (B) A typical example showing the difference between the inter-module interactions obtained for the red module in both groups. (C) The bar plots show the integration values of each group's modules. The dotted line presents the average integration value across modules.

connectivity was found in beta band ( $p = 0.003$ ,  $U = 5$ ,  $r = 0.72$ ). Conversely, increased SAN connectivity was observed in the theta band ( $p = 0.047$ ,  $U = 15.5$ ,  $r = 0.5$ ).

#### Network integration and segregation

Here, we explored the difference of brain network dynamics between the two groups in terms of segregation using clustering coefficient and integration using the global efficiency measures. No group difference was observed in alpha1, alpha2 and beta bands. In contrast, in theta band, an increase in clustering coefficient ( $p = 0.006$ ;  $U = 9$ ,  $r = 0.57$ ) associated with a decrease in global efficiency ( $p = 0.03$ ;  $U = 16$ ,  $r = 0.49$ ) was found in AD networks.

To better explore the difference between the two groups, we clustered the networks into sub-networks (i.e. modules or communities) for which the integration and the segregation parameters were extracted. AD networks were characterized by a low inter-module activity (low integration) and high intra-module connectivity (high segregation) in theta (figure 2), alpha1 (figure S1, supplementary materials), and alpha2 (figure S2, supplementary materials) bands in contrast with results obtained in beta band (figure S3, supplementary materials).

#### Hubs identification

The cortical distributions of connector and provincial hubs identified in healthy subjects and AD patients are illustrated in figure 3. A loss in connector hubs number was observed in AD networks, while the number of provincial hubs was found to increase compared to healthy networks. Specifically, only the left middle orbito-frontal region was conserved in AD network as a connector hub, whereas the right middle orbito-frontal, the left rostral anterior cingulate, the right transverse temporal, the left posterior cingulate, the right posterior cingulate, the right isthmus cingulate and the left precuneus regions were present in healthy networks. In contrast, the left middle orbito-frontal, the right middle orbito-frontal and the right insula appeared as provincial hubs in AD networks.

We then investigated the influence of each node's removal on the global efficiency of the networks using the vulnerability metric. Results are shown in figure 4. We realized that 11 brain regions were more vulnerable in healthy networks versus AD networks ( $p < 0.05$ ). However, only the right middle orbito-frontal and the left lateral orbito-frontal regions have resisted the Bonferroni correction ( $p_{\text{Bonferroni adjusted}} < \frac{0.05}{68}$ ). While the 11 nodes are distributed across several RSNs, the majority of these regions corresponds to DMN (6/11) including mainly

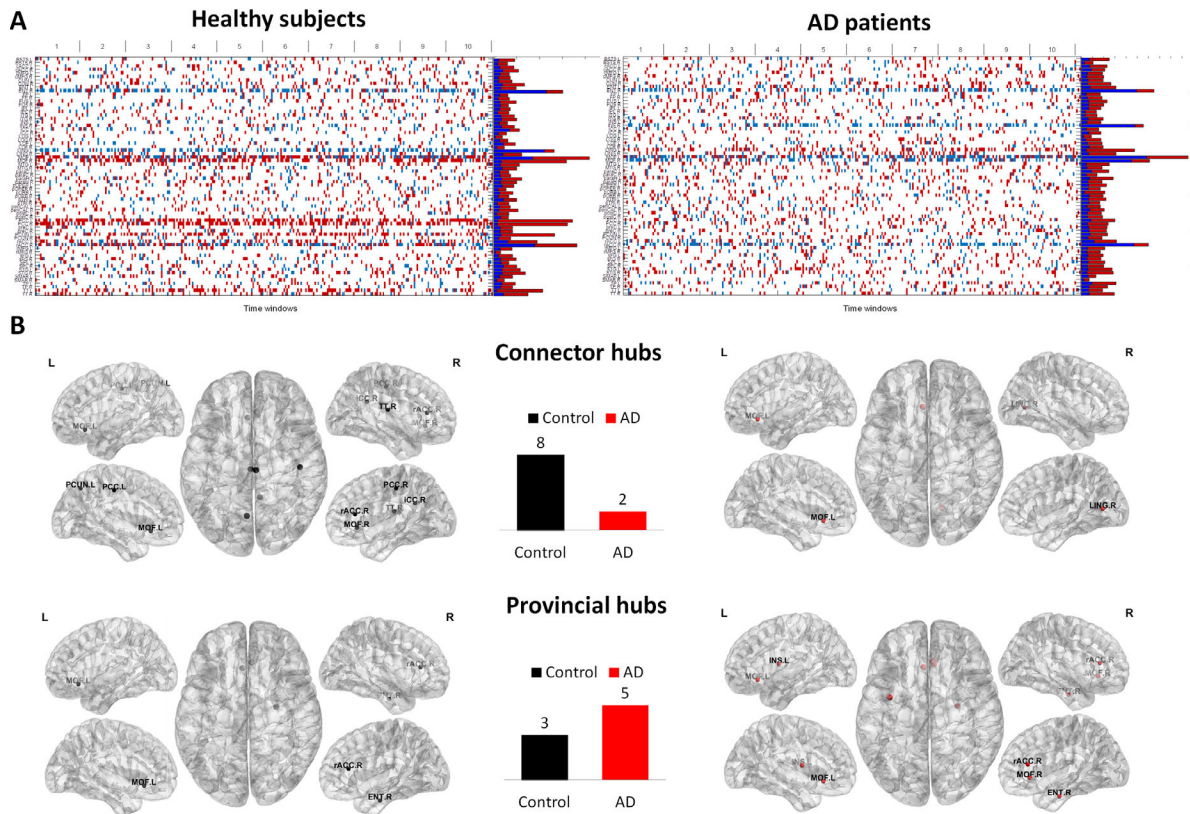


**Figure 3.** (A) Variations of the node type (provincial versus connector) across time and subjects for the 68 brain regions in both groups. Bar plots represent the number of times a node is considered as provincial hub (blue color) and as connector hub (red color). (B) The spatial distributions of significant provincial hubs, and significant connector hubs in both groups ( $p_{\text{Bonferroni adjusted}} < \frac{0.05}{68}$ ). Bar plots illustrate the difference in the number of connector and provincial hubs between the two groups.

the isthmus cingulate, the middle orbito-frontal and the rostral cingulate.

#### Correlation between network measures and cognitive scores

To assess the relationships between functional connectivity and the AD patient's cognitive impairment, we have estimated the correlation between the cognitive score (MMSE) and the network measures (clustering coefficient, global efficiency and vulnerability). A negative correlation between the average clustering coefficient and MMSE score ( $\rho = -0.95$ ;  $p < 0.001$ ) was found, while a positive correlation between the network global efficiency and MMSE score ( $\rho = 0.94$ ;  $p < 0.001$ ) was obtained (figure 5). Concerning the vulnerability, we focused on the two nodes that showed statistical difference between groups. Figure 5 shows that the MMSE score correlates positively with the left lateral orbito-frontal region ( $\rho = 0.84$ ;  $p = 0.002$ ), and the right middle orbito-frontal region ( $\rho = 0.87$ ;  $p = 0.001$ ).

#### Discussion

The main objective in this study is to explore the dynamic topological properties of AD networks compared to healthy controls. Particularly, we focused on examining the shifting balance between brain network integration and segregation in Alzheimer's disease. For this end, resting state EEG signals

were recorded from 20 participants (10 AD patients and 10 controls). The cortical functional networks were reconstructed from scalp signals using the EEG source connectivity method. A sliding window approach was used to track the dynamics of networks. To examine the differences between the two groups (AD versus controls), several network measures were extracted. The measures used to quantify the integration of networks are: the network global efficiency, the inter-modular connections and the connector hubs. To quantify segregation we extracted the clustering coefficient, the intra-modular connections and the provincial hubs. The nodes resilience against attacks was also analyzed in order to identify the main brain regions potentially affected by AD. Interestingly, a general trend is that all metrics showed that AD networks tend to have improved segregation (higher local information processing) and reduced integration (lower global information processing). Results also showed a significant correlation between patients' cognitive performance (as measured by the MMSE score) and network measures. Results are discussed in detail hereafter.

#### AD networks: high segregation and low integration

Results indicated that AD networks are characterized by lower integration (revealed by a decrease in the network global efficiency, the number of connector hubs and the integration measure), and higher segregation (revealed by an increase

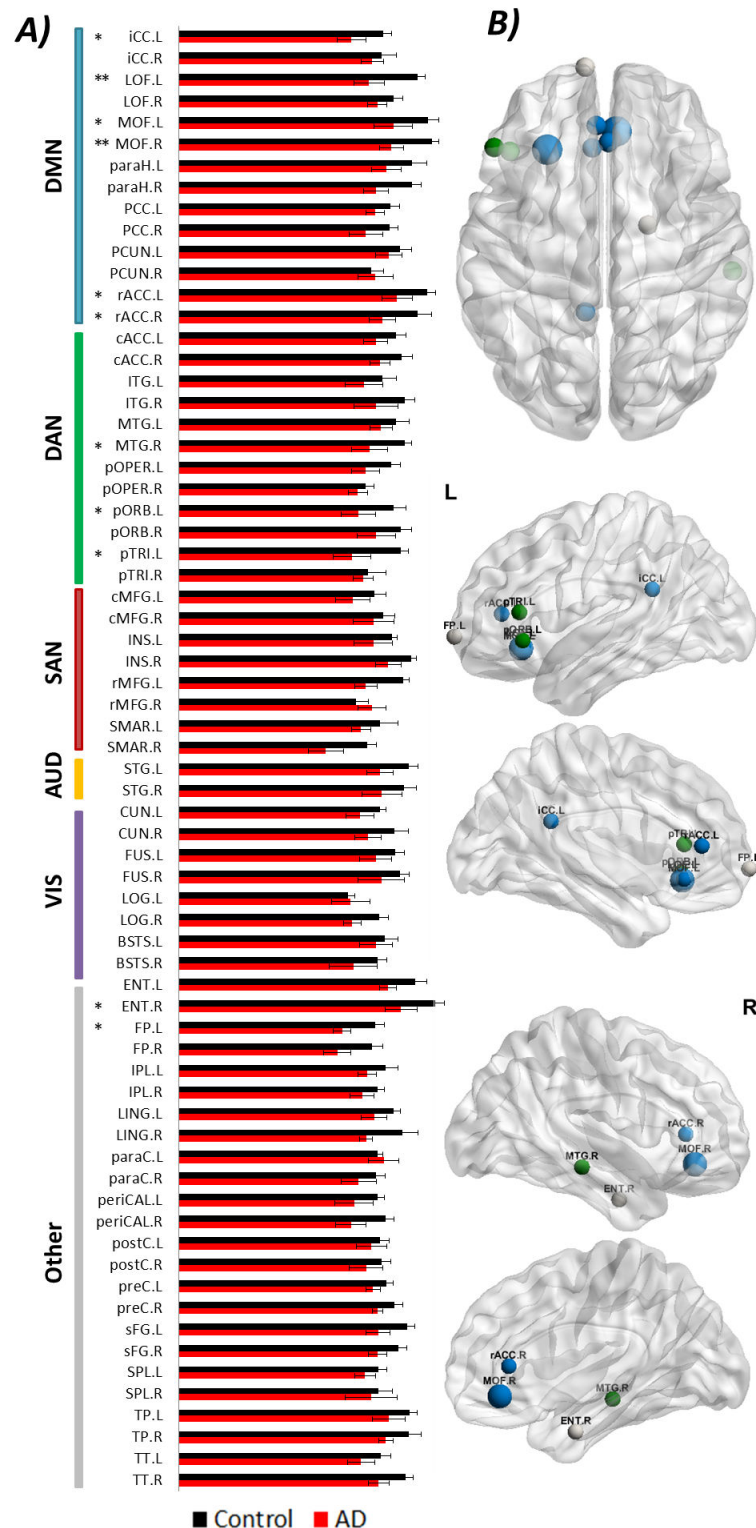


**Figure 4.** Difference between healthy subjects and AD patients in term of node vulnerability. (A) Distribution of vulnerability values for the 68 ROIs in healthy control networks (black color) and in AD networks (red color). A node is marked with \* if it shows significant difference between groups ( $p < 0.05$ , uncorrected) and with \*\* if it shows significant difference after correction for multiple comparisons. (B) Cortical distribution of the 11 significant nodes. The node color corresponds to the matching RSN (see table 1 for ROI names and abbreviations). The nodes with larger size are those who resisted the multiple comparison adjustment.

in clustering coefficient, in the number of provincial hubs and in the recruitment measure) compared to healthy control networks. One possible interpretation of the increased local connectivity is a possible compensatory mechanism that is

triggered by the dysfunctional integration in the AD brain networks (Afshari and Jalili 2017). These findings are in line with studies that revealed decrease in the network global efficiency (Stam et al 2009, Lo et al 2010, Douw et al 2011, Stam



and van Straaten 2012, Zhao *et al* 2012, Tijms *et al* 2013a, Afshari and Jalili 2017) and the participation coefficient (De Haan *et al* 2012) in AD networks. In line with these studies, Debeuck and coll. Delbeuck *et al* (2003) studied the McGurk effect in AD and reported that the integration between auditory and visual speech information was disrupted. The increased segregation observed in AD was reported using the local efficiency and the clustering coefficient (Zhao *et al* 2012, Afshari and Jalili 2017). More importantly, and in line with our findings, a longitudinal EEG study reported reduced global efficiency and increased clustering coefficient during AD progression (Morabito *et al* 2015).

### EEG frequency bands

EEG is increasingly used to detect cognitive deficits in neurodegenerative disorders. One of the main and consistent findings is the shift to lower frequencies in Alzheimer's disease, using resting-state recordings (Bennys *et al* 2001). A slowing of EEGs in the theta power was also observed in Alzheimer's disease at early stage of the disease (Benz *et al* 2014). Several previous studies have confirmed the importance of the theta band with regards to cognition, see Klimesch (1999) and Axmacher *et al* (2006) for two reviews. Moreover, the importance of theta activity in controlling the working memory processes was widely reported (Sarnthein *et al* 1998, Klimesch 1999, Stam 2000, Stam and Van Dijk 2002, Sauseng *et al* 2010). Our findings are in accordance with these studies. A potential interpretation of these findings is that disruption of lower frequencies such as theta rhythms is due to degeneration processes in the attentional system (Hassan *et al* 2017b, Klimesch 1999).

Compared to other frequency bands, here we found significant differences in theta band network characteristics in AD networks, namely, lower integration (low global efficiency), higher segregation (high recruitment and average clustering), a lower number of hubs, a lower effect of nodes' removal and a disrupted function of DMN. Abnormal EEG correlations in parietal and frontal regions within alpha and theta bands were reported in early AD stage (Montez *et al* 2009). Using brain network analysis, several previous studies have observed alterations in the lower frequency bands in patients with dementia. These findings revealed loss in hubs, disruption in functional connectivity (Bosboom *et al* 2009), reduction in network efficiency (van Dellen *et al* 2015) and a decrease in local integration (Utianski *et al* 2016) in the alpha2 band.

Results also depict an opposite influence of the lower frequency bands (theta, alpha1, alpha2) on the balance of integration/segregation compared to the higher frequency band (beta). A possible explanation is the complementary role of frequencies in conducting long/short range connections. In fact, while integrated information is mediated by low frequency bands, local information processing is mediated by high frequency bands (Von Stein and Sarnthein 2000, Buzsáki and Draguhn 2004, Schroeder and Lakatos 2009, Canolty and Knight 2010, Siegel *et al* 2012).

### Altered brain networks/regions in Alzheimer's disease

On the one side, the detection of nodal changes can reveal important insights about which brain regions are severely altered by the disease. Our results show a change in hub properties for R MOF, L rACC, R TT, L/R pCC and L pCUN (see table 1 for abbreviations). We also hypothesized that the removal of an important brain region will affect the information processing in the whole network, while an attack to a less critical region will have a smaller influence on the global network efficiency. We found 13 brain regions that have more importance in healthy network than in AD networks. One can realize that some of the affected hubs (figure 3) coincide with the 13 nodes (rACC, MOF, pCUN, TT). These affected nodes were also reported in Sorg *et al* (2007), Bai *et al* (2009), Buckner *et al* (2009), Mormino *et al* (2011), De Haan *et al* (2012), Vemuri *et al* (2012) and Tijms *et al* (2013b). Other studies also reported that amyloid decomposition in AD coincide with hubs location (Buckner *et al* 2009).

On the other side, alterations in the default mode network (DMN) connectivity in AD patients were reported in several studies (Li *et al* 2002, Greicius *et al* 2004, Wang *et al* 2006, Sorg *et al* 2007, Hedden *et al* 2009, Sheline *et al* 2010, Drzezga *et al* 2011, Mormino *et al* 2011, Vemuri *et al* 2012). Our results showed that the majority of the affected nodes in terms of vulnerability and hub dys-functionality are associated to the DMN. The disruption of DMN was also demonstrated by its reduced intrinsic connectivity as reported in table 1. The increased connectivity of DAN and SAN shown in table 1 may be interpreted as a compensatory mechanism due to the DMN alteration (Bai *et al* 2011, Damoiseaux *et al* 2012).

### Correlation between network measures and AD patient's cognitive scores

Single-subject analyses showed significant correlation between the MMSE score (used here to provide an overall measure of cognitive impairment) and network global efficiency, average clustering coefficient and vulnerability. Although the MMSE test has received good acceptance as a diagnostic test in the clinical and research community (Nieuwenhuis-Mark 2010), it is recommended not to be used as a stand-alone single administration test (Arevalo-Rodriguez *et al* 2015). Previous studies have shown that age, education and socio-cultural variables affect the effectiveness of MMSE to detect cognitive impairment (Bleecker *et al* 1988, Brayne and Calloway 1990, Crum 1993). Hence, the demand is high for other tests that provide higher detection accuracy (Carnero-Pardo *et al* 2011, 2014), as well as more specific scores (semantic, memory related... etc). In addition, the use of cognitive tasks that stimulate the affected networks in the case of AD (the memory network for instance) may improve the correlations with network based metrics. It is worth noting that the MMSE is not the unique test for AD diagnosis. It is currently used within a set of other tests including clinical examination (reflexes, muscle tone, balance) and brain imaging (such MRI and CT scan) aimed to

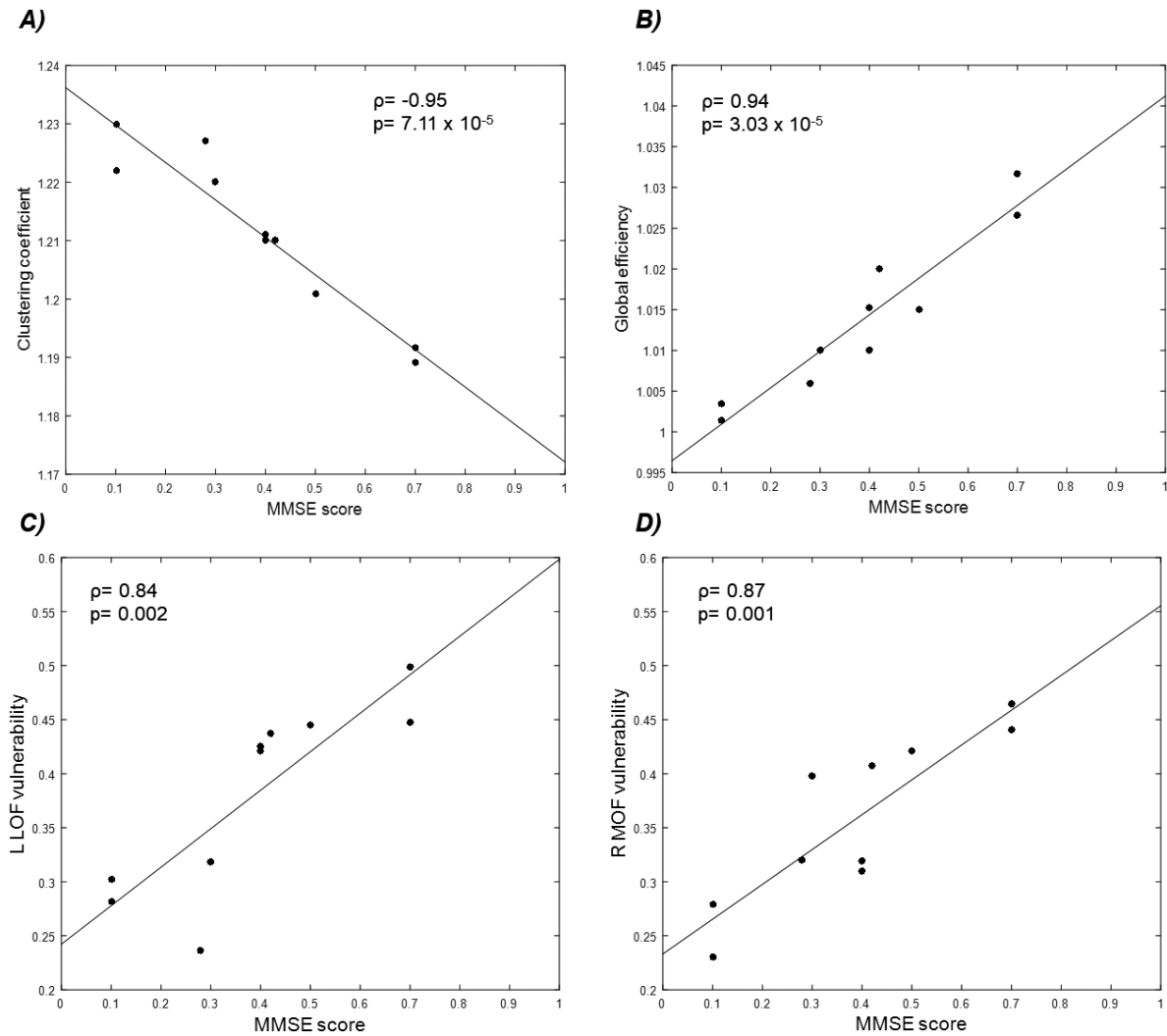


**Figure 5.** Correlation between the cognitive score (MMSE) and the graph measures for AD patients. (A) Clustering coefficient and (B) Global efficiency. (C) Vulnerability of the left lateral orbito-frontal region. (D) Vulnerability of the right middle orbito-frontal region.

pinpoint visible abnormalities related to conditions other than AD (stroke, trauma, etc). However, when MRI is negative (no visible anatomical damages), the screening of cognitive performance using clinical tests such as MMSE (or other specific cognitive scores) is mandatory. The proposed network-based metrics provides additional quantitative indications potentially useful for neurologists to complement diagnosis based on neuropsychological tests.

### Limitations

First, one of the main limitations of this study is the relatively low number of patients. Our intent was to show the difference between two groups: totally normal (control group) and AD patients with ‘severe’ cognitive impairment. Nevertheless, we are aware that the AD is very heterogeneous and may have different stages including patients with moderate or mild cognitive impairment. Detecting these ‘early’ cognitive deficits is on the major challenges in AD and will certainly be the subject of future investigation. These investigations should be performed on larger cohorts of patients in different AD stages,

using other experimental paradigms and additional cognitive scores, in order to be able to generalize the conclusions of the reported analysis.

Second, the EEG source connectivity was applied here to 32 scalp EEG channels. This method has previously proved its robustness in exploring resting-state topology using dense-EEG (>128 electrodes) (Kabbara *et al* 2016, 2017, Hassan *et al* 2017b). As reported in Hassan *et al* (2014), the use of a smaller number of electrodes (in the context of cognitive task) will result in a reduction in the accuracy of the obtained results. Nevertheless, several studies showed the possible extraction of useful information using low number of electrodes (19, 32, 64) (Canuet *et al* 2012, Vecchio *et al* 2014, 2017, Hata *et al* 2016). This can be explained by the facts that these studies (as the presented study) focus on the investigation of ‘large-scale’ networks to compare two groups with the same conditions. In addition, we conjecture that a compromise between the number of channels and the number of ROIs should be necessarily respected. Our very recent findings showed that a high number of electrodes (>32) is mandatory in the case of applications that require higher ‘granularity’, i.e.

spatial precision and accurate characterization of the network local properties, such as the identification of epileptogenic networks (*unpublished data*).

Third, it is important to keep in mind that measuring the functional connectivity is generally corrupted by the volume conduction problem (Schoffelen and Gross 2009). While the effects of this problem are reduced by the analysis of connectivity at source level, some ‘mixing effects’ remain (Brookes et al 2014). At the source level, few strategies have been suggested (Brookes et al 2012, Colclough et al 2015). The proposed approaches are all based on ignoring zero-lag interactions among signals, by supposing that their contributions are only due to the source leakage. Although these approaches have some advantages, they may also remove true communications that occur at zero lag (Finger et al 2016). In our study, we used the phase locking value measure. In a previous study, we showed that the metrics extracted from the networks constructed using PLV (including the within-module degree, clustering coefficient, betweenness centrality and the participation coefficient) were not affected by the spurious short connections (Kabbara et al 2017). Nevertheless, we believe that further methodological efforts are needed to completely solve the spatial leakage problem.

Fourth, a proportional threshold of 10% was used to remove the spurious connections from the connectivity matrices. Here, we preferred using a proportional threshold to absolute threshold to ensure equal density between groups, as recommended by van den Heuvel et al (2017). Moreover, Garrison et al (2015) showed that network measures are stable across proportional thresholds, in contrast to absolute thresholds. A variety of thresholding methods are available, but no method is free of bias. It is then recommended to perform studies across different values of thresholds (in addition to the use of alternative strategies) to ensure that the obtained findings are robust to this methodological factor.

Fifth, the choice of the inverse solution/connectivity combination was supported by two comparative studies using simulated data from a biophysical/physiological model (Hassan et al 2017a) and real data recorded during a cognitive task (Hassan et al 2014). In both analyses, the combination that showed the highest similarity between reference (ground truth) and estimated networks was the wMNE/PLV, used in the present paper. Nevertheless, other combinations or strategies that showed accurate construction of cortical networks from sensor level recordings could be also investigated and compared such as the use of beamforming combined with amplitude correlation between band-limited power envelopes as reported in several studies (Brookes et al 2011, Brookes et al 2012, Colclough et al 2015, 2016, O’Neill et al 2016).

## Conclusions

We reported a study using EEG connectivity at the source level in AD patients and healthy controls. We showed that AD networks are characterized by a reduction in their global performance (integration) associated with an enhancement in

their local performance (segregation). We also showed that these network topologies are correlated with the patient’s cognitive scores. We speculate that our findings, when validated on larger cohort, could contribute to the development of EEG-based tests that could consolidate results of currently-used neurophysiological tests.

## Acknowledgments

This study was funded by the National Council for Scientific Research (CNRS) in Lebanon. The work has also received a French government support granted to the CominLabs excellence laboratory and managed by the National Research Agency in the ‘Investing for the Future’ program under reference ANR-10-LABX-07-01. It was also financed by AZM Center for research in biotechnology and its applications.

## ORCID iDs

M Hassan  <https://orcid.org/0000-0003-0307-5086>

## References

- Afshari S and Jalili M 2017 Directed functional networks in Alzheimer’s disease: disruption of global and local connectivity measures *IEEE J. Biomed. Health Inform.* **21** 949–55
- Arevalo-Rodriguez I et al 2015 Mini-mental state examination (MMSE) for the detection of Alzheimer’s disease and other dementias in people with mild cognitive impairment (MCI) *Cochrane Database Syst. Rev.* **21** CD010783
- Axmacher N et al 2006 Memory formation by neuronal synchronization *Brain Res. Rev.* **52** 170–82
- Bai F et al 2009 Abnormal resting-state functional connectivity of posterior cingulate cortex in amnesic type mild cognitive impairment *Brain Res.* **1302** 167–74
- Bai F et al 2011 Specifically progressive deficits of brain functional marker in amnesic type mild cognitive impairment *PLoS One* **6** e24271
- Bassett D S et al 2013 Robust detection of dynamic community structure in networks *Chaos* **23** (<https://doi.org/10.1063/1.4790830>)
- Bassett D S et al 2015 Learning-induced autonomy of sensorimotor systems *Nat. Neurosci.* **18** 744–51
- Bennys K, Rondouin G, Vergnes C and Touchon J 2001 Diagnostic value of quantitative EEG in Alzheimer’s disease *Neurophysiol. Clin./Clin. Neurophysiol.* **31** 153–60
- Benz N, Hatz F, Bousleiman H, Ehrensperger M M, Gschwandtner U, Hardmeier M, Ruegg S, Schindler C, Zimmermann R and Monsch A U 2014 Slowing of EEG background activity in Parkinson’s and Alzheimer’s disease with early cognitive dysfunction *Front. Aging Neurosci.* **6** 314
- Bleecker M L et al 1988 Age-specific norms for the mini-mental state exam *Neurology* **38** 1565–8
- Blondel V D et al 2008 Fast unfolding of communities in large networks *J. Stat. Mech.: Theory Exp.* **2008** P10008
- Bosboom J L W et al 2009 MEG resting state functional connectivity in Parkinson’s disease related dementia *J. Neural Trans.* **116** 193–202
- Brayne C and Calloway P 1990 The association of education and socioeconomic status with the mini mental state examination



- and the clinical diagnosis of dementia in elderly people *Age Ageing* **19** 91–6
- Brookes M J *et al* 2011 Measuring functional connectivity using MEG: methodology and comparison with fMRI *NeuroImage* **56** 1082–104
- Brookes M J, Woolrich M W and Barnes G R 2012 Measuring functional connectivity in MEG: a multivariate approach insensitive to linear source leakage *NeuroImage* **63** 910–20
- Brookes M J, Woolrich M W and Price D 2014 An introduction to MEG connectivity measurements *Magnetoencephalography*, ed Supek S and Aine C (Berlin: Springer) pp 321–58
- Buckner R L *et al* 2009 Cortical hubs revealed by intrinsic functional connectivity: mapping, assessment of stability, and relation to Alzheimer's disease *J. Neurosci.* **29** 1860–73
- Bullmore E *et al* 2009 Complex brain networks: graph theoretical analysis of structural and functional systems *Nat. Rev. Neurosci.* **10** 186–98
- Buzsáki G and Draguhn A 2004 Neuronal oscillations in cortical networks *Science* **304** 1926–9
- Canolty R T and Knight R T 2010 The functional role of cross-frequency coupling *Trends Cogn. Sci.* **14** 506–15
- Canuet L *et al* 2012 Resting-state network disruption and APOE genotype in Alzheimer's disease: a lagged functional connectivity study *PLoS One* **7**
- Carnero-Pardo C *et al* 2011 Diagnostic accuracy, effectiveness and cost for cognitive impairment and dementia screening of three short cognitive tests applicable to illiterates *PLoS One* **6**
- Carnero-Pardo C *et al* 2014 A systematic review and meta-analysis of the diagnostic accuracy of the Phototest for cognitive impairment and dementia *Dement. Neuropsychol.* **8** 141–7
- Colclough G L *et al* 2015 A symmetric multivariate leakage correction for MEG connectomes *NeuroImage* **117** 439–48
- Colclough G L *et al* 2016 How reliable are MEG resting-state connectivity metrics? *NeuroImage* **138** 284–93
- Crum R M 1993 Population-based norms for the mini-mental state examination by age and educational level *J. Am. Med. Assoc.* **269** 2386–91
- Damoiseaux J S *et al* 2012 Functional connectivity tracks clinical deterioration in Alzheimer's disease *Neurobiol. Aging* **33**
- De Haan W *et al* 2012 Disrupted modular brain dynamics reflect cognitive dysfunction in Alzheimer's disease *NeuroImage* **59** 3085–93
- de Pasquale F *et al* 2010 Temporal dynamics of spontaneous MEG activity in brain networks *Proc. Natl Acad. Sci. USA* **107** 6040–5
- Delbeuck X *et al* 2003 Alzheimer's disease as a disconnection syndrome? *Neuropsychol. Rev.* **13** 79–92
- Delorme A and Makeig S 2004 EEGLAB: an open source toolbox for analysis of single-trial EEG dynamics including independent component analysis *J. Neurosci. Methods* **134** 9–21
- Desikan R S *et al* 2006 An automated labeling system for subdividing the human cerebral cortex on MRI scans into gyral based regions of interest *NeuroImage* **31** 968–80
- Douw L *et al* 2011 Cognition is related to resting-state small-world network topology: a magnetoencephalographic study *Neuroscience* **175** 169–77
- Drzezga A *et al* 2011 Neuronal dysfunction and disconnection of cortical hubs in non-demented subjects with elevated amyloid burden *Brain* **134** 1635–46
- Eickhoff S B *et al* 2005 A new SPM toolbox for combining probabilistic cytoarchitectonic maps and functional imaging data *NeuroImage* **25** 1325–35
- Engels M M A *et al* 2017 'Alzheimer's disease: the state of the art in resting-state magnetoencephalography *Clin. Neurophysiol.* **128** 1426–37
- Finger H *et al* 2016 Modeling of large-scale functional brain networks based on structural connectivity from DTI: comparison with EEG derived phase coupling networks and evaluation of alternative methods along the modeling path *PLoS Comput. Biol.* **12**
- Folstein M F, Folstein S E and McHugh P R 1975 'Mini-mental state'. A practical method for grading the cognitive state of patients for the clinician *J. Psychiatric Res.* **12** 189–98
- Garrison K A *et al* 2015 The (in)stability of functional brain network measures across thresholds *NeuroImage* **118** 651–61
- Gol'dshtein V, Koganov G A and Surdutovich G I 2004 Vulnerability and hierarchy of complex networks *Physics* (arXiv:cond-mat/0409298)
- Gramfort A *et al* 2010 OpenMEEG: opensource software for quasistatic bioelectromagnetics *Biomed. Eng. Online* **9** 45
- Greicius M D *et al* 2004 Default-mode network activity distinguishes Alzheimer's disease from healthy aging: evidence from functional MRI *Proc. Natl Acad. Sci. USA* **101** 4637–42
- Guimerà R and Nunes Amaral L A 2005 Functional cartography of complex metabolic networks *Nature* **433** 895–900
- Hamalainen M S and Ilmoniemi R J 1994 Interpreting magnetic fields of the brain: minimum norm estimates *Med. Biol. Eng. Comput.* **32** 35–42
- Hassan M *et al* 2014 EEG source connectivity analysis: from dense array recordings to brain networks *PLoS One* **9** (<https://doi.org/10.1371/journal.pone.0105041>)
- Hassan M *et al* 2015 Dynamic reorganization of functional brain networks during picture naming *Cortex* **73** 276–88
- Hassan M *et al* 2017a Identification of interictal epileptic networks from dense-EEG *Brain Topogr.* **30** 60–76
- Hassan M *et al* 2017b Functional connectivity disruptions correlate with cognitive phenotypes in Parkinson's disease *NeuroImage* **14** 591–601
- Hata M *et al* 2016 Functional connectivity assessed by resting state EEG correlates with cognitive decline of Alzheimer's disease—an eLORETA study *Clin. Neurophysiol.* **127** 1269–78
- Hedden T *et al* 2009 Disruption of functional connectivity in clinically normal older adults harboring amyloid burden *J. Neurosci.* **29** 12686–94
- Hipp J F *et al* 2012 Large-scale cortical correlation structure of spontaneous oscillatory activity *Nat. Neurosci.* **15** 884–90
- Ismail Z, Rajji T K and Shulman K I 2010 Brief cognitive screening instruments: an update *Int. J. Geriatr. Psychiatry* **25** 111–20
- Kabbara A *et al* 2016 Graph analysis of spontaneous brain network using EEG source connectivity *Int. Conf. on Bio-engineering for Smart Technologies (BioSMART)* (Dubai, UAE, 4–7 December 2016) (arXiv:1607.00952)
- Kabbara A *et al* 2017 The dynamic functional core network of the human brain at rest *Scientific Reports* **7** 2936
- Klem G H, Lüders H O, Jasper H H and Elger C 1999 The twenty electrode system of the International Federation. The International Federation of Clinical Neurophysiology *Electroencephalogr. Clin. Neurophysiol. Suppl.* **52** 3–6
- Klimesch W 1999 EEG alpha and theta oscillations reflect cognitive and memory performance: a review and analysis *Brain Res. Rev.* **29** 169–95
- Korjus K *et al* 2015 Personality cannot be predicted from the power of resting state EEG *Front. Human Neurosci.* **9**
- Lachaux J P *et al* 1999 Measuring phase synchrony in brain signals *Human Brain Mapp.* **8** 194–208
- Lachaux J-P *et al* 2000 Studying single-trials of phase synchronous activity in the brain *Int. J. Bifurcation Chaos* **10** 2429
- Lancichinetti A and Fortunato S 2012 Consensus clustering in complex networks *Sci. Rep.* **2** 336
- Latora V and Marchiori M 2001 Efficient behavior of small world networks *Phys. Rev. Lett.* **87** 198701
- Li F *et al* 2015 Relationships between the resting-state network and the P3: evidence from a scalp EEG study *Sci. Rep.* **5** 15129
- Li S-J *et al* 2002 Alzheimer disease: evaluation of a functional MR imaging index as a marker *Radiology* **225** 253–9

- Lo C *et al* 2010 Diffusion tensor tractography reveals abnormal topological organization in structural cortical networks in Alzheimer's disease *J. Neurosci.* **30** 16876–85
- Mehrkanoon S *et al* 2014 Intrinsic coupling modes in source-reconstructed electroencephalography *Brain Connect.* **4** 812–25
- Montez T *et al* 2009 Altered temporal correlations in parietal alpha and prefrontal theta oscillations in early-stage Alzheimer disease *Proc. Natl Acad. Sci.* **106** 1614–9
- Morabito F C *et al* 2015 A longitudinal EEG study of Alzheimer's disease progression based on a complex network approach *Int. J. Neural Syst.* **25** 1550005
- Mormino E C *et al* 2011 Relationships between beta-amyloid and functional connectivity in different components of the default mode network in aging *Cerebral Cortex* **21** 2399–407
- Mungas D 1991 In-office mental status testing: a practical guide *Geriatrics* **46** 54–8, 63, 66
- Nieuwenhuis-Mark R E 2010 The death knoll for the MMSE: has it outlived its purpose? *J. Geriatr. Psychiatry Neurol.* **23** 151–7
- O'Neill G C *et al* 2016 Measurement of dynamic task related functional networks using MEG *NeuroImage* accepted (<https://doi.org/10.1016/j.neuroimage.2016.08.061>) (Elsevier)
- Onton J *et al* 2006 Imaging human EEG dynamics using independent component analysis *Neurosci. Biobehav. Rev.* **30** 808–22
- Pievani M *et al* 2011 Functional network disruption in the degenerative dementias *Lancet Neurol.* **10** 829–43
- Rubinov M and Sporns O 2011 Weight-conserving characterization of complex functional brain networks *NeuroImage* **56** 2068–79
- Sales-Pardo M *et al* 2007 Correction for Sales-Pardo *et al* extracting the hierarchical organization of complex systems *Proc. Natl Acad. Sci. USA* **104** 18874
- Sarnthein J *et al* 1998 Synchronization between prefrontal and posterior association cortex during human working memory *Proc. Natl Acad. Sci. USA* **95** 7092–6
- Sauseng P *et al* 2010 Control mechanisms in working memory: a possible function of EEG theta oscillations *Neurosci. Biobehav. Rev.* **34** 1015–22
- Schoffelen J M and Gross J 2009 Source connectivity analysis with MEG and EEG *Hum. Brain Mapp.* **30** 1857–65
- Schroeder C E and Lakatos P 2009 Low-frequency neuronal oscillations as instruments of sensory selection *Trends Neurosci.* **32** 9–18
- Sheline Y I *et al* 2010 Amyloid plaques disrupt resting state default mode network connectivity in cognitively normal elderly *Biol. Psychiatry* **67** 584–7
- Shirer W R *et al* 2012 Decoding subject-driven cognitive states with whole-brain connectivity patterns *Cerebral Cortex* **22** 158–65
- Siegel M, Donner T H and Engel A K 2012 Spectral fingerprints of large-scale neuronal interactions *Nat. Rev. Neurosci.* **13** 20–5
- Sorg C *et al* 2007 Selective changes of resting-state networks in individuals at risk for Alzheimer's disease *Proc. Natl Acad. Sci. USA* **104** 18760–5
- Sporns O 2010 *Networks of the Brain* (Cambridge, MA: The MIT Press)
- Stam C J 2000 Brain dynamics in theta and alpha frequency bands and working memory performance in humans *Neurosci. Lett.* **286** 115–8
- Stam C J and Van Dijk B W 2002 Synchronization likelihood: an unbiased measure of generalized synchronization in multivariate data sets *Physica D* **163** 236–51
- Stam C J and van Straaten E C W 2012 The organization of physiological brain networks *Clin. Neurophysiol.* **123** 1067–87
- Stam C J *et al* 2009 Graph theoretical analysis of magnetoencephalographic functional connectivity in Alzheimer's disease *Brain* **132** 213–24
- Supekar K *et al* 2008 Network analysis of intrinsic functional brain connectivity in Alzheimer's disease *PLoS Comput. Biol.* **4**
- Tadel F *et al* 2011 Brainstorm: a user-friendly application for MEG/EEG analysis *Comput. Intell. Neurosci.* **2011** (<https://doi.org/10.1155/2011/879716>)
- Tijms B M *et al* 2013a 'Alzheimer's disease: connecting findings from graph theoretical studies of brain networks *Neurobiol. Aging* **34** 2023–36
- Tijms B M *et al* 2013b Single-subject grey matter graphs in Alzheimer's disease *PLoS One* **8** (<https://doi.org/10.1371/journal.pone.0058921>)
- Utianski R L *et al* 2016 Graph theory network function in parkinson's disease assessed with electroencephalography *Clin. Neurophysiol.* **127** 2228–36
- van Dellen E *et al* 2015 Loss of EEG network efficiency is related to cognitive impairment in dementia with lewy bodies *Mov. Disord.* **30** 1785–93
- van den Heuvel M P and Sporns O 2013 Network hubs in the human brain *Trends Cogn. Sci.* **17** 683–96
- van den Heuvel M P *et al* 2017 Proportional thresholding in resting-state fMRI functional connectivity networks and consequences for patient-control connectome studies: issues and recommendations *NeuroImage* **152** 437–49
- Vecchio F *et al* 2014 Human brain networks in cognitive decline: a graph theoretical analysis of cortical connectivity from EEG data *J. Alzheimer's Dis.* **41** 113–27
- Vecchio F *et al* 2017 'Small World' architecture in brain connectivity and hippocampal volume in Alzheimer's disease: a study via graph theory from EEG data *Brain Imaging Behav.* **11** 473–85
- Vemuri P, Jones D T and Jack C R Jr 2012 Resting state functional MRI in Alzheimer's disease *Alzheimers Res. Ther.* **4** 2
- Von Stein A and Sarnthein J 2000 Different frequencies for different scales of cortical integration: from local gamma to long range alpha/theta synchronization *Int. J. Psychophysiol.* **38** 301–13
- Wang L *et al* 2006 Changes in hippocampal connectivity in the early stages of Alzheimer's disease: evidence from resting state fMRI *NeuroImage* **31** 496–504
- Watts D J and Strogatz S H 1998 Collective dynamics of 'small-world' networks *Nature* **393** 440–2
- World Health Organization 2012 Dementia: a public health priority *Dementia* (Geneva, Switzerland: World Health Organization) p 112
- Zhao X *et al* 2012 Disrupted small-world brain networks in moderate Alzheimer's disease: a resting-state fMRI study *PLoS One* **7**
- Zhou J *et al* 2010 Divergent network connectivity changes in behavioural variant frontotemporal dementia and Alzheimer's disease *Brain* **133** 1352–67

# Reduced integration and improved segregation of functional brain networks in Alzheimer's disease

Kabbara A.<sup>1, 2, 3, 4\*</sup>, EL Falou W.<sup>3, 4</sup>, Eid H.<sup>5</sup>, Khalil M.<sup>3, 4</sup>, Hassan M.<sup>1, 2</sup>

<sup>1</sup> INSERM, U1099, F-35000 Rennes, France

<sup>2</sup> University of Rennes 1, LTSI, F-35000 Rennes, France

<sup>3</sup> Azm Center for Research in Biotechnology and its Application, EDST, Lebanese University, Lebanon

<sup>4</sup> CRSI research center, Faculty of Engineering, Lebanese University, Lebanon

<sup>5</sup> Mazloun Hospital, Tripoli, Lebanon

\* Corresponding author: [mahmoud.hassan@univ-rennes1.fr](mailto:mahmoud.hassan@univ-rennes1.fr)

Acronyms	Name	RSN
iCC L	isthmuscingulate L	DMN
iCC R	isthmuscingulate R	DMN
MOF L	medialorbitofrontal L	DMN
MOF R	medialorbitofrontal R	DMN
PCC L	posteriorcingulate L	DMN
PCC R	posteriorcingulate R	DMN
PCUN L	precuneus L	DMN
PCUN R	precuneus R	DMN
rACC L	rostralanteriorcingulate L	DMN
rACC R	rostralanteriorcingulate R	DMN
LOF L	lateralorbitofrontal L	DMN
LOF R	lateralorbitofrontal R	DMN
paraH L	parahippocampal L	DMN
paraH R	parahippocampal R	DMN
cACC L	cAUDalanteriorcingulate L	DAN
cACC R	cAUDalanteriorcingulate R	DMN
ITG L	inferiortemporal L	DAN
ITG R	inferiortemporal R	DAN
MTG L	middletemporal L	DAN
MTG R	middletemporal R	DAN
pOPER L	parsopercularis L	DAN
pOPER R	parsopercularis R	DAN
pORB L	parsorbitalis L	DAN
pORB R	parsorbitalis R	DAN
pTRI L	parstriangularis L	DAN
pTRI R	parstriangularis R	DAN
INS L	insula L	SAN
INS R	insula R	SAN
rMFG L	rostralmiddlefrontal L	SAN
rMFG R	rostralmiddlefrontal R	SAN
SMAR L	supramarginal L	SAN
SMAR R	supramarginal R	SAN
cMFG L	caudalmiddlefrontal L	SAN
cMFG R	caudalmiddlefrontal R	SAN

Acronyms	Name	RSN
STG L	superiortemporal L	AUD
STG R	superiortemporal R	AUD
CUN L	cuneus L	VIS
CUN R	cuneus R	VIS
LOG L	lateraloccipital L	VIS
LOG R	lateraloccipital R	VIS
FUS R	fusiform R	VIS
FUS L	fusiform L	VIS
LING L	lingual L	VIS
LING R	lingual R	VIS
BSTS L	bankssts L	other
BSTS R	bankssts R	other
ENT L	entorhinal L	other
ENT R	entorhinal R	other
FP L	frontalpole L	other
FP R	frontalpole R	other
IPL L	inferiorparietal L	other
IPL R	inferiorparietal R	other
sFG L	superiorfrontal L	other
sFG R	superiorfrontal R	other
paraC L	paracentral L	other
paraC R	paracentral R	other
periCAL L	pericalcarine L	other
periCAL R	pericalcarine R	other
postC L	postcentral L	other
postC R	postcentral R	other
preC L	precentral L	other
preC R	precentral R	other
SPL L	superiorparietal L	other
SPL R	superiorparietal R	other
TP L	temporalpole L	other
TP R	temporalpole R	other
TT L	transversetemporal L	other
TT R	transversetemporal R	other

**Table S1. Anatomic regions-of-interest (ROIs) included in the analysis, as derived from the Desikan Killiany atlas, and their affiliation to RSNs. Abbreviations: Default mode network=DMN, Dorsal attention network=DAN, Salience attention network=SAN, Auditory network=AUD, Visual network=VIS.**

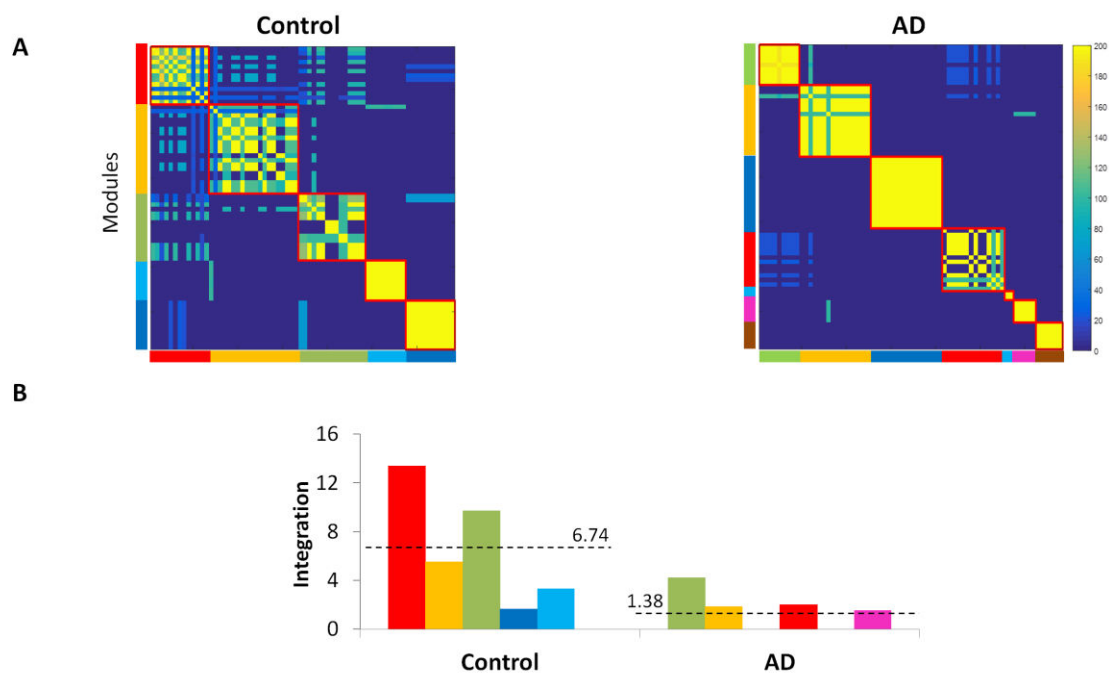


**Figure S1. A)** The association matrices obtained by the multi-slice modularity method for healthy controls and AD patients in the alpha1 band. **B)** The bar plots show the integration values of each group's modules. The dotted line presents the average integration value across modules.



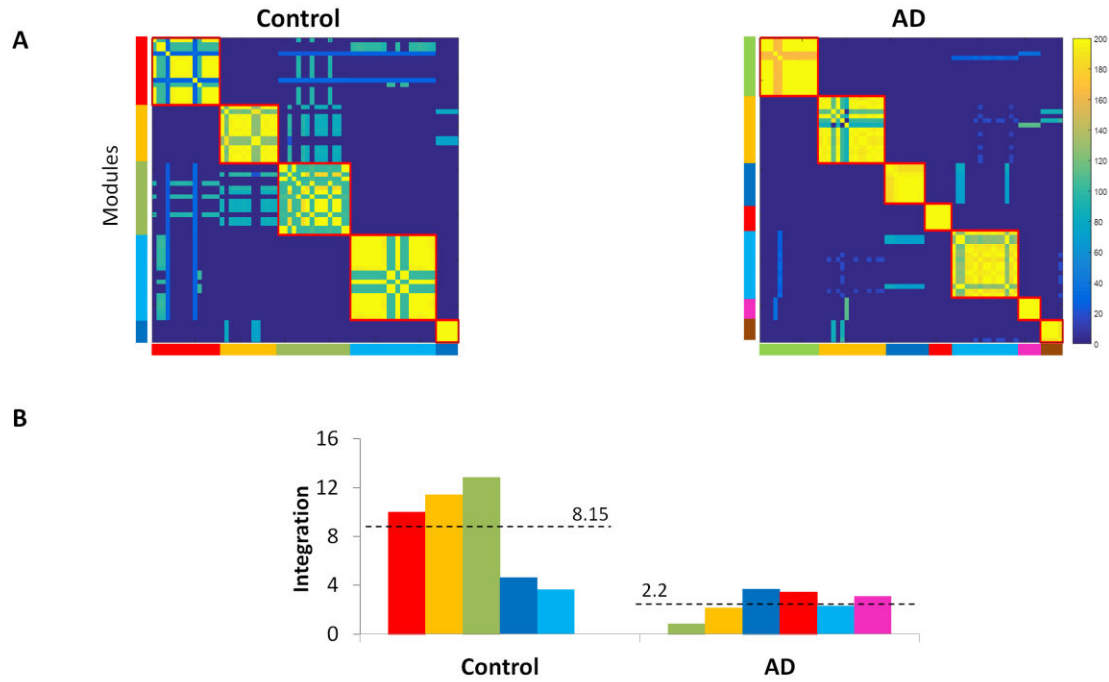


**Figure S2. A)** The association matrices obtained by the multi-slice modularity method for healthy controls and AD patients in the alpha2 band. **B)** The bar plots show the integration values of each group's modules. The dotted line presents the average integration value across modules.

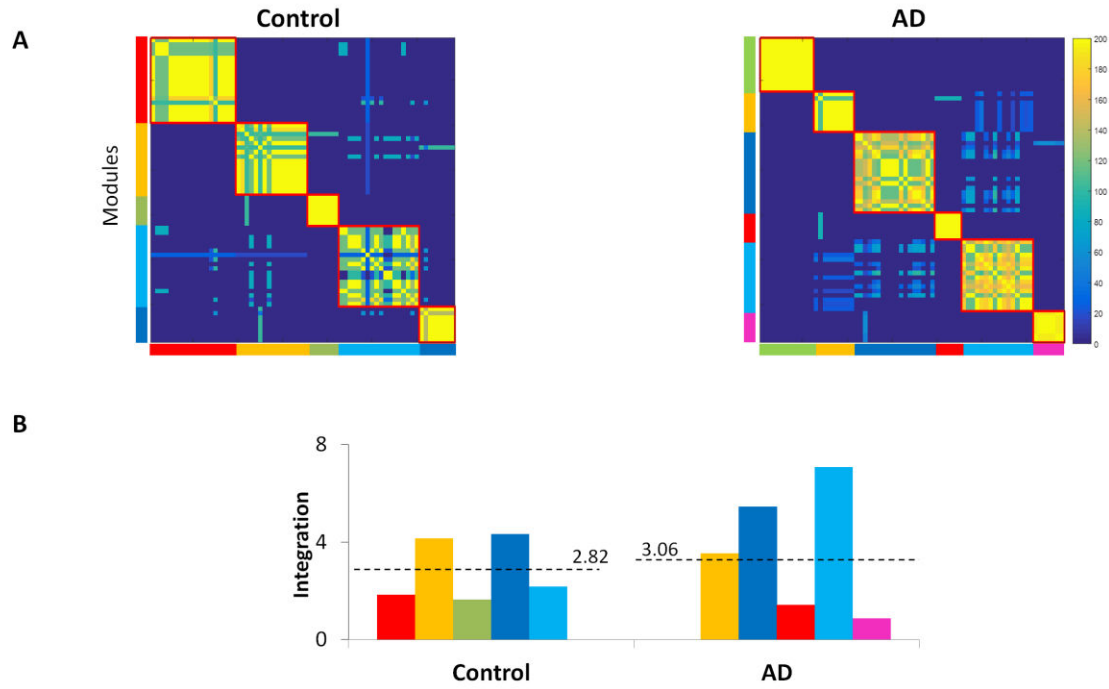


**Figure S3. A)** The association matrices obtained by the multi-slice modularity method for healthy controls and AD patients in the beta band. **B)** The bar plots show the integration values of each group's modules. The dotted line presents the average integration value across modules.

# **Study 4: Dense scalp-EEG source connectivity predicts depth-EEG exploration in epilepsy**

Aya Kabbara, Mahmoud Hassan, Mohamad Khalil, Arnaud Biraben, Anca Nica,  
Isabelle Merlet and Fabrice Wendling

*Submitted*

# Matching between depth-EEG locations and EEG source-space networks in epilepsy

## Authors

Aya Kabbara<sup>1, 3</sup>, Mahmoud Hassan<sup>1</sup>, Mohamad Khalil<sup>3</sup>, Arnaud Biraben<sup>1, 2</sup>, Anca Nica<sup>2</sup>, Isabelle Merlet<sup>1\*</sup> and Fabrice Wendling<sup>1\*</sup>

<sup>1</sup> Univ Rennes, LTSI – U1099, F-35000 Rennes, France

<sup>2</sup> Neurology department, CHU, Rennes, France

<sup>3</sup> Azm Center for Research in Biotechnology and its Application, EDST, Lebanese University, Lebanon

\*These authors contributed equally to this work.

## (1) Corresponding author

Mahmoud Hassan  
Campus de Beaulieu - Bât. 22 - LTSI  
35042 Rennes Cedex - France -  
[mahmoud.hassan@univ-rennes1.fr](mailto:mahmoud.hassan@univ-rennes1.fr)

# Abstract

---

**Objective:** Most brain disorders, including drug-resistant epilepsies, are network diseases. Thus, from a clinical perspective, the demand is high for non-invasive, network-based and easy-to-use methods to identify these pathological brain networks.

**Methods:** In this paper, we introduce a novel methodological framework to identify epileptogenic networks from scalp dense-electroencephalography (EEG). The proposed approach combines the emerging technique called ‘EEG source connectivity’ with graph theory. We used depth-EEG and scalp dense-EEG data at rest (regardless of the presence/absence of epileptiform activity) from 18 patients. Depth-EEG data were used to evaluate the accuracy of epileptogenic networks identified from scalp data. The method performance was quantified by its capacity to identify pathological brain networks in the region explored by depth-EEG in epileptic patients. This quantification was done using hemispherical and lobar accuracies as well as the distance between depth-EEG electrode positions and estimated networks.

**Results:** Results showed that the proposed approach was able to predict the brain hemisphere ( $accuracy = 97 \pm 9\%$ ) and the lobe ( $accuracy = 91 \pm 19\%$ ) where SEEG exploration was performed a posteriori ( $average\ distance = 13 \pm 11\ mm$ ). Results showed also the high advantage of network segregation measures (local functional connectivity) compared to global measures ( $p < 0.01$ , *corrected*) in revealing epileptogenic networks.

**Interpretation:** These results may promote the noninvasive dense-EEG as a complementary tool in pre-surgical evaluation in order i) to define of the best depth-electrode placement (hemisphere and lobe) and ii) to highlight cortical regions that may be overlooked during pre-surgical planning.

# Introduction

---

Drug-resistant epilepsies, which represent 30% of epilepsies, are most often partial or focal, i.e. characterized by an epileptogenic zone (EZ) that is relatively circumscribed in one of the two cerebral hemispheres. Resective surgery is currently the only treatment capable of suppressing drug-resistant seizures (ANAES, 2004). However, prior to surgery, the crucial issue to be solved is the identification of epileptogenic networks, in the specific context of each patient. Indeed, the outcome of this therapeutic approach directly depends on the capacity to accurately localize epileptogenic networks and subsequently define the optimal resection which maximizes benefit/deficit ratio for the patient.

Among pre-surgical investigations, intracranial electroencephalography represents, so far, the ‘gold standard’ for identifying epileptogenic networks and for accurately localizing the EZ (Bartolomei et al., 2017). Nevertheless, it remains an invasive technique with limited spatial resolution and the demand is high for non-invasive, easy-to-use and clinically available methods able to reveal epileptogenic brain networks. To some extent, functional (fMRI, SPECT) neuroimaging methods (Schneider et al., 2013; Tavares et al., 2017), including electrical source imaging (ESI) (Brodbeck et al., 2010; Lantz et al., 2001; Lascano et al., 2012; Michel et al., 1999), are intended to respond to this demand. However, and despite the substantial progress accomplished in this field (Chiang et al., 2017), information provided by these techniques is not routinely used during pre-surgical evaluation due to intricate interpretation of localization results.

In this study, we propose a novel framework combining the emergent method called EEG source connectivity with graph theory. Previous studies already revealed that the brain networks of temporal lobe epilepsy patients are characterized by small-world topology compared to those of

healthy controls (Bernhardt et al., 2011). Other studies showed alterations in network hubs (highly connected nodes) around brain regions belonging to the epileptogenic zone (Nissen et al., 2016; Zhang et al., 2011). However, these studies suffer from three main limitations: i) the empirical choice of graph metrics used to characterize identified networks, ii) the user-dependent selection of ictal or interictal periods which requires a demanding preprocessing step and iii) the lack of ground truth for validating the networks identified from scalp EEG.

These issues were addressed in the present study. First, we devised a ‘local functional connectivity’ network metrics inspired from the pathophysiology of partial epilepsies which dramatically increases the method performance. Second, epileptogenic networks are identified from EEG signals recorded from spontaneous brain activity regardless of the presence/absence of epileptiform events. And third, intracerebral SEEG recordings are being used to evaluate the accuracy of epileptogenic networks identified from scalp EEG data. The proposed method was evaluated in 18 patients with partial epilepsy who underwent both dense-EEG (256 electrodes) and SEEG recordings. Results show excellent spatial concordance between networks identified from non-invasive data, on the one side, with the region explored by SEEG electrodes, on the other side, suggesting that proper processing of resting-state dense-EEG epochs can provide substantial information about the localization of the epileptogenic zone.

# Materials and methods

---

The full pipeline of our study is summarized in Figure 1.

## **Patients**

In total, the study included eighteen patients with drug resistant epilepsy (13 males and 5 females, age 16-40 y). Detailed information about the seizure type, seizure onset, surgery, and MRI abnormalities of each patient is provided in Table 1.

These patients were diagnosed with drug resistant epilepsy. They underwent full presurgical evaluation including neurological examination, neuropsychological testing, standard long-term video EEG recording, structural MRI, dense scalp EEG recording with video recordings, CT scan and intracerebral EEG recordings. All acquisitions were performed in accordance with the relevant guidelines and regulations of the National Ethics Committee for the Protection of Persons (CPP), (agreement number 2012-A01227-36, promoter: Rennes University Hospital), which approved all experimental protocols and procedures. Written consent was obtained from patients who were informed that collected data might be used for research purpose.

## **Data**

Dense-EEG signals (256 channels, EGI, Electrical Geodesic Inc.) were recorded at 1000 Hz, band-pass filtered within 0.3-45 Hz. All subjects underwent resting-state in which they were asked to relax and keep their eyes closed without falling asleep. For each participant, three non-overlapping 40-seconds epochs were selected. All epochs were chosen free of artifacts, during periods of quiet resting. For some patients, few electrodes with poor signal quality could be identified. For these electrodes, signals were reconstructed by interpolation of signals collected at the level of the surrounding electrodes.



SEEG recordings (Micromed Inc.) were performed using multi-contact intracerebral electrodes ( $10\pm 18$  leads; length, 2 mm, diameter, 0.8 mm; 1.5 mm apart) implanted according to Talairach's stereotactic method (Bancaud et al., 1970). The patient-specific position of depth electrodes was determined by the neurological team, after detailed analysis of clinical, functional and anatomical data recorded for each patient. The exact 3D coordinates of each electrode contact were determined after co-registering the CT scan showing the intracerebral leads onto the structural MRI image using a 6-parameter rigid-body transformation (Eickhoff et al., 2005; Studholme et al., 1998).

## **Reconstruction of functional networks**

The functional networks were reconstructed using the EEG source connectivity method. Readers may refer to (Hassan et al., 2014) for detailed information. In brief, this method requires two main steps: i) solving the EEG inverse problem to reconstruct the temporal dynamics of the cortical regions at source level and ii) measuring the functional connectivity between the reconstructed regional time series. Here, the weighted Minimum Norm Estimate (wMNE) was used to reconstruct the dynamics of the cortical sources (Hamalainen and Ilmoniemi, 1994). Then, the functional connectivity was computed using the phase locking value (PLV) method (Lachaux et al., 1999). This combination of wMNE/PLV was previously shown to outperform procedures combining other inverse/connectivity methods, in terms of accuracy and relevance of cortical brain networks identified from scalp EEG data (Hassan et al., 2016, Hassan et al., 2014). This combination was also used in the context of Parkinson diseases (Hassan et al., 2017), cognitive task (Hassan et al., 2014; Mahmoud Hassan et al., 2015) and recently resting state (Kabbara et al., 2017).

The steps performed to reconstruct the functional brain networks from dense-EEG signals can be summarized as follows:

- Segment the T1-weighted anatomical MRI of each patient to build the cortical surface mesh using FreeSurfer (Fischl, 2012). This latter was then down-sampled into 15000 vertices using Brainstorm (Tadel et al., 2011).
- Compute the lead field matrix using the boundary element method (BEM). Here, we used the OpenMEEG package (Gramfort et al., 2010) available in Brainstorm.
- For each patient, the noise covariance matrix was estimated using one minute resting segment.
- Reconstruct the dynamics of EEG sources using the wMNE algorithm where the regularization parameter was set relatively to the signal to noise ratio ( $\lambda \sim 0.1$  in our analysis).
- Project the EEG sources onto an anatomical atlas. Here, we used the Desikan-Killiany atlas (Desikan et al., 2006) sub-divided into 221 regions as described in (Hagmann et al., 2008). The signals of the sources that belong to each ROI were averaged. This parcellation produced 221 regional time-series.
- Compute the functional connectivity between the regional time-series using the PLV (Lachaux et al., 1999). This measure, ranging from 0 (no synchronization) to 1 (full synchronization), reflects statistical dependences between two oscillatory signals through the quantification of the phase synchrony. To explore the time dynamics of brain networks, we used a sliding window over which PLV was calculated. Here, at broad band. Considering the investigated frequency range (0.3-45 Hz), the duration of the smallest time window that contains a sufficient number of cycles for PLV computation is

0.3 s, as recommended in (Lachaux et al., 1999). This value of 0.3s was thus retained for the sliding window.

- Threshold the connectivity matrix using the automatic thresholding algorithm described in (Genovese et al., 2002). According to this method, the connectivity matrix was converted into a  $p$ -value map based on the  $t$ -statistics. The computed  $p$ -values were corrected for multiple comparisons using the False Discovery Rate (FDR) approach of  $p < 0.05$ . Then, the connectivity values whose  $p$ -values passed the statistical FDR threshold were retained (their values remained unchanged). Otherwise, the values were set to zero.

Consequently, at each time window, these steps produce a thresholded weighted connectivity matrix that is formally equivalent to an undirected weighted functional network.

## **From graph theory to epileptogenic networks**

While functional connectivity provides crucial information about how the different brain regions are connected, graph theory offers a framework to characterize the network topology and organization. In practice, many graph measures can be extracted from networks to characterize global and local network properties. Here, we focused on measures quantifying the local connectivity of brain regions able to reveal clusters or modules in functional networks characterized by abnormal segregated neural processing. This choice was motivated by mechanistic hypotheses regarding the pathophysiology of epileptogenic networks. In particular, these “hyperexcitable networks” are likely characterized by abnormally high local “intra-connectivity” and weaker “inter-connectivity”, as reported in a number of studies which provided both theoretical (Bartolomei et al., 2013; Netoff, 2004) and empirical (Bettus et al., 2011; Ponten et al., 2009; van Dellen et al., 2009; Van Mierlo et al., 2013) evidence.

Based on this assumption, recently summarized in (Bernasconi, 2017) and illustrated in Figure 2A, we hypothesized that an approach aimed at characterizing the modularity of brain networks (Sporns and Betzel, 2016a) could be relevant for revealing hyperexcitable epileptogenic sub-networks in large-scale networks. Such a modularity-based approach is illustrated in Figure 2B.

### ***Local network measures (segregation)***

1. **Within-module degree (Z)**: As depicted, the computation of the network modularity firstly includes the decomposition of network into modules, i.e clusters of nodes that are internally strongly connected, but externally weakly connected. To proceed, many algorithms were proposed to decompose a network into modules. Given the inter- and intra- algorithm variability, dissimilar partitions may be obtained when changing the clustering algorithms. To tackle this issue, it is recommended to combine multiple algorithms of community detection and multiple runs to obtain the consensus (or the average) representative partition (Sporns et al., 2016). Here, we adopted the consensus clustering approach: given an ensemble of partitions acquired from Newman algorithm (Girvan and Newman, 2002) and Louvain algorithm (Blondel et al., 2008) repeated for 200 runs, we obtained a  $N \times N$  association matrix ( $N$  is the number of nodes), which element  $a_{i,j}$  represents the number of times the nodes  $i$  and  $j$  are assigned to the same module across all runs and algorithms. To obtain consensus communities, we re-clustered the association matrix using Louvain algorithm after comparing it to a null model association matrix generated from a permutation of the original partitions (Bassett et al., 2013) and keeping its significant values (Bassett et al., 2013). Once modules are detected, the within-module degree ( $Z$ ) is extracted to measure how well a node is connected to other nodes within the same module (Guimera et al., 2005). The within-module degree ( $Z$ ) is defined as follows:

$$Z_i = \frac{K_i(m_i) - \overline{K(m_i)}}{\sigma_{k(m_i)}}$$

Where  $K_i(m_i)$  is the within-module degree of the node  $i$ ,  $\overline{K(m_i)}$  is the mean of within module degree of nodes assigned to the same community as node  $i$ , and  $\sigma_{k(m_i)}$  is the standard deviation.

2. **Clustering coefficient (CC)**: We have also extracted the clustering coefficient (CC) which represents one of the most used metrics to measure the local connectedness of a node within a network. This measure quantifies how close the nodes' neighbors are inter-connected (Watts and Strogatz, 1998).

### ***Global network measures (integration)***

In order to comparatively assess the performance of the above-described local measures, other network measures quantifying the global information processing (integration) and the importance of a node within a network were also computed:

- 1- **The participation coefficient (P)**: This metric quantifies the integration of a node by measuring how its edges are distributed across modules:

$$P_i = 1 - \sum_{c=1}^C \left( \frac{K_i(M)}{K_i} \right)^2$$

Where  $C$  is the number of modules and  $K_i(m)$  is the number of edges between node  $i$  and nodes in module  $M$ .

- 2- **Betweenness Centrality (C)**: The importance of a node is proportional to its betweenness centrality (Freeman, 1977).  $C$  measures the proportion of the number of shortest paths in which the node participates:

$$C_i = \sum_{i,j} \frac{\sigma(i,u,j)}{\sigma(i,j)}$$

Where  $\sigma(i,u,j)$  is the number of shortest paths between nodes  $i$  and  $j$  that pass through node  $u$ ,  $\sigma(i,j)$  is the total number of shortest paths between  $i$  and  $j$ , and the sum is over all pairs  $i, j$  of distinct nodes.

All extracted network measures were normalized with respect to random networks. Thus, for each time window, we generated 500 surrogate random networks derived from the original network by randomly reshuffling the edge weights. The normalized values were computed by dividing the original values by the average values computed on the randomized graphs.

## Statistical tests

For each patient, we concatenated the distribution of the nodal metrics of the three epochs, which led to a distribution of 400 values (number of epochs \* number of windows) corresponding to each of the metrics extracted. To statistically identify the significant nodes in terms of local network measures (within-module degree ( $Z$ ), clustering coefficient ( $CC$ )) and global network measures (centrality ( $C$ ), and participation coefficient ( $P$ )), we quantified the difference between nodes metrics' distributions using a Wilcoxon Mann–Whitney  $U$  test. Thus, a  $221 \times 221$   $p$ -value matrix was generated, where the element  $p_{i,j}$  represents the statistical difference between the distributions of nodes  $i$  and  $j$ . The  $p$ -values were then corrected for multiple comparisons using

Bonferroni correction method. Afterwards, the nodes that have a number of  $p$ -values above 99% of the confidence interval were considered as significant.

## Noninvasive vs. invasive data

For each patient, significant nodes, as obtained using the EEG source connectivity method described, above were compared to the position of intracerebral electrode contact positions, as defined by the epileptologist during the pre-surgical planning procedure. To proceed, the SEEG electrode contacts were first projected into the same atlas of 221 ROIs: to each intracerebral contact we assigned the closest ROI from the 221 regions of atlas. Based on this co-registration in the grey matter, the position of scalp-EEG based significant nodes could be compared to that of SEEG contacts. This comparison gives an overall indication of the matching between noninvasive and invasive recordings (same hemisphere, same lobe, same sub-lobar region).

The qualitative results were also quantified using several performance measures:

- **The average distance (mm)** between SEEG nodes and EEG nodes. AD is defined as follows:

$$AD = \frac{\sum_k d(N_k, N_v)}{M} \quad k \in [1, M]; v \in [1, W]$$

Where  $d(N_k, N_v)$  is the euclidian distance between the node  $N_k$  detected by EEG method and the nearest SEEG contact  $N_v$ .  $M$  denotes the total number of detected EEG nodes, and  $W$  denotes the total number of SEEG contacts.

- **The closeness accuracy (%)** which is defined as:

$$CA = \frac{\sum_k x_k}{M} \quad ; \quad x_k = 1 - \frac{d(N_k, N_v)}{\bar{d}}$$

where  $\bar{d}$  is the mean Euclidian distance between EEG and SEEG nodes.

- **The hemispherical accuracy (%)** which represents the proportion of the EEG nodes detected in the same hemisphere with the SEEG contacts.
- **The lobar accuracy (%)** which represents the proportion of the EEG nodes detected in the same lobe with the SEEG contacts. The lobar partition is illustrated in Figure S5.
- **The overall accuracy (%)** defined as the arithmetic mean of the three above-described accuracy values (closeness, hemispherical and lobar).

## Software

FreeSurfer (Fischl, 2012) was used for surface parcellation, Brainstorm open MATLAB toolbox (Tadel et al., 2011) for source reconstruction and EEG preprocessing, OpenMEEG package for lead field matrix computation (Gramfort et al., 2010), SPM8 (Eickhoff et al., 2005) for the co-registration of the MRI and CT scan images, IEElectrodes (Blenkman et al., 2017) for contacts positions extraction, Brain Connectivity Toolbox (BCT) <https://sites.google.com/site/bctnet/> for graph measures computation (Rubinov and Sporns, 2010) and BrainNetViewer (BNV) (Xia et al., 2013) for networks visualization. Other homemade codes were also developed for modules generation, statistical tests, and quantitative evaluation.

## Results

---

For each network measure, we quantified the matching between the scalp-EEG-based networks and the depth-EEG electrodes positions in terms of spatial Euclidian distance (mm), hemispherical accuracy (%), lobar accuracy (%), closeness accuracy (%) and the overall accuracy (%), which is a combination of the three previous features.

The quantitative comparison between the local and global network measures is presented in Figure 3. Results demonstrate that the local network measures (Z and CC) achieve higher spatial



precision (reflected by high accuracies associated with low distances between EEG and SEEG) compared to the global measures (C and P). Particularly, significant differences were found between Z and both global measures in hemispherical accuracy ( $p_{Z,C} = 0.0008$ ;  $p_{Z,P} = 0.0002$ ), lobar accuracy ( $p_{Z,C} = 0.0009$ ;  $p_{Z,P} = 0.0003$ ), closeness accuracy ( $p_{Z,C} = 0.001$ ;  $p_{Z,P} = 0.0006$ ), overall accuracy ( $p_{Z,C} = 0.0006$ ;  $p_{Z,P} = 0.0002$ ) and Euclidian distance ( $p_{Z,C} = 0.005$ ;  $p_{Z,P} = 0.0006$ ). In addition, the closeness accuracy rate is statistically higher using CC than C ( $p_{CC,C} = 0.004$ ). Figure 3 also reveals a difference between CC and P with respect to the distance between identified EEG regions and SEEG contacts ( $p_{CC,P} = 0.003$ ). However, no significant difference was observed between the local network measures, neither between the global network measures. Tables S1, S2, S3, S4 and S5 report the detailed distance and accuracy values obtained using the network measures for the 18 patients.

In figure 4 and figure 5, we show the individual results obtained in two patients (P1 and P2) chosen according to the accuracy detection: patient P1 is characterized by an excellent accuracy detection (overall accuracy = 95 %) while patient P2 is characterized by low accuracy detection (overall accuracy = 61 %). Concerning the patient P1, all regions that showed significant CC and Z values ( $p < 0.01$ , *Bonferroni corrected*) were located in the same hemisphere and in the same lobe where SEEG exploration was performed (hemispherical accuracy=100%, lobar accuracy=100%). In contrast, the hemispherical accuracy achieved using the global network measures dropped down to 60% for C and to 57% for P. Results also indicated that the lobar accuracies obtained using C and P measures were 40% and 0% respectively. Moreover, one can state that four EEG nodes detected using local metrics (Z), overlapped with depth-EEG contacts while six other nodes were found to be close to SEEG contact positions (AD= 5.13 mm, CA=80%). Using CC, the distance between scalp-EEG-based and depth-EEG-based nodes was

equal to 0 mm leading to a closeness accuracy of 100%. Concerning the global metrics, nodes by both measures (C and P) were found to be distant from the SEEG contact positions (AD=53.85 mm, 85.95 mm; CA= 37.95%, 22.07%, respectively).

Figure 5 shows results obtained in Patient P2, characterized by poorer results, to some extent. It is worth noting that this patient had bilateral implantation, indicative of “clinically-difficult” cases. In this patient P2 the hemispherical accuracy using the first local measure (Z) was 60%. Nevertheless, the second local measure (CC) was found to exhibit higher performance. As illustrated, all the identified EEG nodes obtained using the CC measure were located in the right hemisphere (hemispherical accuracy=100%), and near the SEEG contacts implanted (lobar accuracy=100%). In contrast, and as in patient P1, the global network measures revealed hemispherical accuracy rates of 50% for C, and 0% for P. Concerning C, only one of four identified significant nodes was located in the same lobe of SEEG implantation (lobar accuracy=25%). The barplots in Figure 5 show that CC yields to the lowest distance and highest closeness accuracy (AD=16.8 mm, CA=73%) compared to Z (AD=23.38 mm, CA=62.5%), C (AD=21 mm, CA=67%) and P (AD=39 mm, CA=54%). In other words, results obtained in P2 showed that C led to one EEG node overlapping a SEEG contact while three other detected nodes were remarkably far from the location of SEEG contacts.

For all other patients (P3 → P18), the cortical regions that were identified using the local network measures are illustrated in supplementary Figures S1, S2, S3, S4. Using Z, it is noteworthy that for all patients (n=10) who underwent unilateral SEEG implantation (P1, P3, P4, P8, P10, P13, P15, P16, P17 and P18), the significant ROIs detected from scalp EEG were in the same hemisphere than SEEG contacts (100% hemispherical accuracy). In patients (n=8) who underwent bilateral intracerebral electrode implantation (P2, P5, P6, P7, P9, P11, P12 and P14),

the EEG-based method highlights, in six of eight patients, the predominance of one hemisphere (w.r.t to contra-lateral hemisphere) in terms of Z. For P12, significant EEG nodes were positioned in both right and left hemispheres. Overall, the average hemispherical accuracy obtained is  $97.78 \pm 9.42\%$  (Table S1). In terms of lobar accuracy, EEG nodes were detected in the same lobe of intracerebral electrodes in P1, P3, P5, P6, P7, P8, P9, P10, P11, P13, P15, P16, P17 and P18 (100% lobar accuracy). Across all patients, the mean lobar accuracy obtained is  $91.67\% \pm 19.85\%$  (Table S2). Figures S1, S2 show also that for the patient P3, all EEG nodes that have high Z values matched the SEEG contacts positions (AD=0 mm). For the patients P4, P5, P6, P7, P8, P9, P11, P12, P15, P16, P17 and P18, a considerable number of the identified EEG nodes matched with a number of SEEG contacts, while the rest of nodes were observed near the positions of the SEEG electrodes (AD=10.34 mm, 16.05 mm, 12.57 mm, 3.21 mm, 4.12 mm, 23.95 mm, 22.28 mm, 15 mm, 6.21 mm, 6.14 mm, 5.71 mm; respectively). Concerning the patients P10, P13, P14, although no EEG node coincided with a SEEG contact position, all the identified nodes were located just in proximity of the depth-EEG electrode contacts (AD=16.43 mm, 30.12 mm, 43.01 mm; respectively).

The quantitative evaluation reported an averaged closeness accuracy value equal to  $76.23 \pm 16.14\%$  (supplementary Table S3), as well as an averaged overall accuracy value of  $88.55 \pm 11.85\%$  (supplementary Table S4). The mean distance between EEG-identified nodes and SEEG contacts was  $14.01 \pm 11.44$  mm (Table S5). Using CC, 12 of the 18 patients (P1, P2, P4, P5, P6, P7, P9, P12, P13, P14, P15, and P16) revealed hemispherical accuracy of 100%. Among these patients, seven patients (P1, P2, P4, P5, P14, P15, and P16) showed a lobar accuracy of 100%. Across all patients, the averaged hemispherical accuracy was  $86.6 \pm 24.04\%$  (supplementary Table S1), the averaged lobar accuracy was  $65.11 \pm 38.7\%$  (Table S2), the average overall

accuracy was  $85.59 \pm 4.96$  % (Table S4) and an average distance was  $25.7 \pm 17.75$  mm (supplementary Table S5).

## Discussion

---

Identification of brain functional networks from scalp-EEG signals has been a topic of increasing interest over the two past decades (Hassan and Wendling, 2018). Emerging evidence shows the importance of identifying such networks at the cortical level (in the source space, in contrast with electrode space) using dense-EEG data (Hassan and Wendling, 2018). The approach, called “EEG source connectivity”, has led to novel findings regarding the spatio-temporal dynamics of functional brain networks, estimated from scalp-EEG data (Coito et al., 2015; M. Hassan et al., 2015; Lu et al., 2012). Here, we studied the applicability of network science applied to brain networks identified from non-invasive dense-EEG recordings at rest, in the aim of predicting stereo-EEG (SEEG) exploration in patients with refractory epilepsy. Inspired from the current understanding of epileptogenic networks characterized by hyperexcitability and hypersynchronization (review in (Bartolomei et al., 2017)), our approach was guided by the following hypothesis: can we identify sub-networks, referred to as “significant nodes”, characterized by significantly high local functionality while showing low interdependence level with large-scale networks at rest. Eventually, we substantiate the usefulness of our hypothesis by comparing the positions of nodes detected by scalp EEG to those of SEEG electrode. We found that the proposed approach has succeeded to identify significant nodes in the vicinity of the zone where SEEG implantation was performed. The major advantages of the presented approach are: i) the non-invasiveness of EEG, ii) the exploration of network dynamics at short time scale (hundreds of millisecond) and iii) the use of raw interictal recordings without pre-processing aimed at detecting epileptic events (like spikes or spike-waves). Results are discussed hereafter.

## **Epilepsy is a network disorder**

Source localization methods have been extensively used for the identification of the epileptic focus (Baumgartner et al., 1995; Boon et al., 1997; Boon and D'Havé, 1995; Merlet et al., 1996; Michel et al., 2004). However, it is now well admitted that epilepsy is a network disorder, characterized by an epileptogenic zone most often organized as a large-scale dysfunctional network involving multiple regions rather than a single focus (Bartolomei et al., 2001; Engel et al., 2013; Wang et al., 2014). Recent studies that compared network-based and localization-based approaches showed the advantage of the network approach (Coito et al., 2016; Hassan et al., 2016; Staljanse et al., 2017). These studies showed that localization-based approach can lead to spurious sources (Hassan et al., 2016) and lower accuracy in localizing the seizure onset zone (Staljanse et al., 2017). Our findings support that EEG source connectivity complemented by graph theory leads to sparser networks which are more specific to epileptogenic networks. One explanation is that the source localization methods ignore the functional connectivity between brain regions, on one side, and ignore the possible contribution of brain sources with low energies, on the other side. In contrast, the network approach accounts for the communication dynamics between regions regardless of their energies.

The current shift from 'focus' to 'network' in epilepsy research has motivated many researchers to explore the epileptogenic networks by investigating the interactions between the brain sources reconstructed from MEG/EEG (Coito et al., 2015; Dai et al., 2012; Ding et al., 2007; Hassan et al., 2016; Jmail et al., 2016; Lu et al., 2012; Nissen et al., 2016; Song et al., 2013; Vecchio et al., 2016). Interestingly, a recent work with interictal MEG networks attempted to identify the epileptogenic zone on the basis of the betweenness centrality graph measure (Nissen et al., 2016).

In this study, we showed how local network measures may have a potential relation with the pathophysiology of epileptogenic networks. Indeed, based on the metrics introduced here (within-module degree (Z) and clustering coefficient (CC)), significant nodes correspond to pathological regions with high local connectivity. Indeed, both metrics quantify the implication of nodes within a local network and were able to localize the hemisphere and the lobe of stereo-EEG sites in most patients (17 of 18 patients for Z, and 15 of 18 patients for CC). To emphasize that a good identification of epileptogenic network is related to the local properties of the network, we examined the results obtained by other graph measures related to network global properties: i) the betweenness centrality (C) which measures the importance of the node, and ii) the participation coefficient (P) which measures the global functionality of the node. Our results showed that the identified regions using P and C global measures were distant from the SEEG contacts positions.

## **Clinical impact**

Stereo-electroencephalography (SEEG) is a gold-standard for pre-surgical evaluation of drug-resistant epilepsies (Bancaud and Talairach, 1973). Despite the fact that SEEG has dramatically improved the identification of the area to be resected to maximize the benefit/risk ratio after surgery, it requires *a priori* knowledge about the lateralization and the lobar position of epileptogenic networks in order to adequately place the electrodes. This decision is usually based on multiple parameters obtained from clinical (patient history, semiology of seizures), anatomical (MRI, CT) and non-invasive functional investigations (video-EEG, fMRI, PET). (Gilard et al., 2016; Kovac et al., 2017). Still in many cases, interpretation of multi-modal data coming from such investigations may be ambiguous and difficult to interpret, which make the localization of epileptogenic zones an open and often hard issue. Overall, there is a growing

clinical demand for non-invasive and easy-to-use pre-surgical network identification tools. The proposed approach meets this demand.

Another clinical need is to investigate the epileptogenic networks through recordings that do not directly depend on ictal activity. This could dramatically reduce the monitoring period and the preprocessing steps required to select, segment and clean the epileptiform activity such as epileptic spikes (Khambhati et al., 2016). Interestingly, an analysis of the brain networks derived from both ictal and interictal recordings has identified topological similarities, suggesting that interictal networks topology can predict the brain regions that generate seizures (Khambhati et al., 2016), even in the absence of interictal spikes (Coito et al., 2016). These findings militate in favor of pushing the identification of epileptogenic networks using EEG recordings for which the presence epileptiform events are not a prior.

Thereby, given the above described advantages (i.e. the non-invasiveness, minimal pre-processing of EEG signals recorded during resting state periods with no absolute necessity of including interictal epileptiform events), we believe that the proposed approach can bring relevant and complementary information in the context of pre-surgical evaluation. In particular, the additional clues provided by the method can be used by epileptologists in the definition of the best depth-electrode placement (hemisphere and lobe). In addition, due to the fact that SEEG cannot cover the whole surface of the brain in contrast to EEG, the proposed method may also highlight cortical regions that may be overlooked by the traditional pre-surgical evaluation.

## **Limitations and methodological considerations**

First, in the current study we restrictedly looked at the positions of SEEG contacts, without performing any analysis on the underlying networks, as identified from SEEG signals. Our main motivation was to analyze the matching between the networks identified from scalp-EEG

recordings with the spatial locations of the SEEG contacts decided by epileptologists. Results indicate that dense-EEG combined with appropriate signal processing could become a tool for guiding to the SEEG electrodes position. However, we did not investigate the correspondence between scalp-EEG-based networks and depth-EEG-based networks; this is an important topic for future study, that can be addressed using data without epileptiform activity (resting state) or with epileptiform activity (spikes for instance).

Second, while EEG source connectivity has extremely improved the spatial resolution of EEG (Hassan and Wendling, 2018), the networks identified are still limited to the cortical grey matter. In fact, the localization of subcortical structures remains difficult using EEG technology, namely due to anatomical and analytical reasons. Unlike the layered cortex, a subcortical region would not have the necessary organization of pyramidal cells to give rise to localizable scalp-recorded EEG (Cohen et al., 2011).

Third, the weighted minimum norm estimate was used to reconstruct the source signals combined with the phase locking value to compute the functional connectivity. The use of wMNE/PLV combination has previously shown its ability to “re-estimate” the reference epileptogenic networks modelled at neocortical level (Hassan et al., 2016) and to reveal relevant resting state networks from dense-EEG in two recent studies (Hassan et al., 2017; Kabbara et al., 2017). The good performance of the wMNE/PLV combination (compared to other combinations as reported in (Hassan et al., 2016) might be related to the fact that wMNE relies on reasonable “physiological” hypothesizes (sources position and orientation). The only “mathematical” assumption is that the solution should have lowest energy. It is worth noting that this assumption could be considered as physiological in term of minimal energetic cost in the brain during rest (Achard and Bullmore, 2007). Regarding the second step, the PLV method estimates the phase



synchronization between EEG oscillations. Therefore, this method is in line with the concept that (hyper)synchronization between locally-generated signals is a crucial mechanism in brain (dys)function. In the context of EEG source connectivity, the PLV method in particular, and more generally the phase synchronization methods precisely reflect the underlying synchronization between the brain signals generated by distant sources. Altogether, these features may explain the good performance of this combination of methods in the assessment of brain epileptogenic networks at rest.

Fourth, a recurrent problem in the field of M/EEG source space functional connectivity is the volume conduction effects (Brookes et al., 2014). Connectivity analysis at source level was shown to reduce the effect of volume conduction as connectivity methods are applied to “local” time-series (analogous to local field potentials) generated by cortical neuronal assemblies modelled as current dipole sources. Nevertheless, these so-called “mixing effects” can also occur in the source space but can be reduced by an appropriate choice of connectivity measures. Indeed, false functional couplings can be generated by some connectivity methods when applied to mixed signals such as estimated brain sources. To address this issue, a number of methods were developed based on the rejection of zero-lag correlation. In particular, “unmixing” methods, called “leakage correction”, have been reported which force the reconstructed signals to have zero cross-correlation at lag zero (Colclough et al., 2015). Although handling this problem -theoretically- helps interpretation, a very recent study showed that the current correction methods also produce erroneous human connectomes under very broad conditions (Pascual-marqui et al., 2017). In addition, we also showed recently that the graph metrics including the Z, CC, C and P extracted from the networks constructed using the PLV were not affected by the spurious short connections problem (Kabbara et al., 2017).

# Acknowledgement

---

This work has received a French government support granted to the CominLabs excellence laboratory and managed by the National Research Agency in the "Investing for the Future" program under reference ANR-10-LABX-07-01. It was also financed by the Rennes University Hospital (COREC Project named *conneXion*, 2012-14). The study was also funded by the National Council for Scientific Research (CNRS) in Lebanon.

## Author contributions

---

A.K., M.H., M.K., A.B., A.N., I.M. and F.W. took part in the conception and design of the study. A.N. and I.M. contributed in acquiring the data, and A.K., M.H., M.K., A.B., A.N., I.M. and F.W. analyzed the data. A.K. drafted the manuscript and the figures.

## References

---

- Achard, S., Bullmore, E., 2007. Efficiency and cost of economical brain functional networks. *PLoS Comput. Biol.* 3, 0174–0183.
- ANAES, 2004. [Proceedings of the Consensus Conference on Management of Drug-Resistant Partial Epilepsy. 3-4 March 2004]. *Rev. Neurol. (Paris)*.
- Bancaud, J., Angelergues, R., Bernouilli, C., Bonis, A., Bordas-Ferrer, M., Bresson, M., Buser, P., Covelto, L., Morel, P., Szikla, G., Takeda, A., Talairach, J., 1970. Functional stereotaxic exploration (SEEG) of epilepsy. *Electroencephalogr. Clin. Neurophysiol.* 28, 85–86.
- Bancaud, J., Talairach, J., 1973. Methodology of stereo EEG exploration and surgical intervention in epilepsy. *Rev. Otoneuroophthalmol.* 45, 315.
- Bartolomei, F., Guye, M., Wendling, F., 2013. Abnormal binding and disruption in large scale networks involved in human partial seizures. *EPJ Nonlinear Biomed. Phys.* 1, 4.
- Bartolomei, F., Lagarde, S., Wendling, F., McGonigal, A., Jirsa, V., Guye, M., Bénar, C., 2017. Defining epileptogenic networks: Contribution of SEEG and signal analysis. *Epilepsia*.
- Bartolomei, F., Wendling, F., Bellanger, J.J., Régis, J., Chauvel, P., 2001. Neural networks involving the medial temporal structures in temporal lobe epilepsy. *Clin. Neurophysiol.* 112, 1746–1760.
- Bassett, D.S., Porter, M.A., Wymbs, N.F., Grafton, S.T., Carlson, J.M., Mucha, P.J., 2013. Robust detection of dynamic community structure in networks. *Chaos* 23.
- Baumgartner, C., Lindinger, G., Ebner, A., Aull, S., Serles, W., Olbrich, A., Lurger, S., Czech, T., Burgess, R., Luders, H., 1995. Propagation of interictal epileptic activity in temporal lobe epilepsy. *Neurology* 45, 118–122.
- Bernasconi, A., 2017. Connectome-based models of the epileptogenic network: A step towards epileptomics? *Brain*.
- Bernhardt, B.C., Chen, Z., He, Y., Evans, A.C., Bernasconi, N., 2011. Graph-theoretical analysis reveals disrupted

- small-world organization of cortical thickness correlation networks in temporal lobe epilepsy. *Cereb. Cortex* 21, 2147–2157.
- Bettus, G., Ranjeva, J.P., Wendling, F., Bénar, C.G., Confort-Gouny, S., Régis, J., Chauvel, P., Cozzone, P.J., Lemieux, L., Bartolomei, F., Guye, M., 2011. Interictal functional connectivity of human epileptic networks assessed by intracerebral EEG and BOLD signal fluctuations. *PLoS One* 6.
- Blenkemann, A.O., Phillips, H.N., Princich, J.P., Rowe, J.B., Bekinschtein, T.A., Muravchik, C.H., Kochen, S., 2017. iElectrodes: a comprehensive open-source toolbox for depth and subdural grid electrode localization. *Front. Neuroinform.* 11, 14.
- Blondel, V.D., Guillaume, J.-L., Lambiotte, R., Lefebvre, E., 2008. Fast unfolding of communities in large networks. *J. Stat. Mech. Theory Exp.* 10008, 6.
- Boon, P., D'Havé, M., 1995. Interictal and ictal dipole modelling in patients with refractory partial epilepsy. *Acta Neurol. Scand.* 92, 7–18.
- Boon, P., D'Havé, M., Adam, C., Vonck, K., Baulac, M., Vandekerckhove, T., De Reuck, J., 1997. Dipole modeling in epilepsy surgery candidates. *Epilepsia* 38, 208–218.
- Brodbeck, V., Spinelli, L., Lascano, A.M., Pollo, C., Schaller, K., Vargas, M.I., Wissmeyer, M., Michel, C.M., Seeck, M., 2010. Electrical source imaging for presurgical focus localization in epilepsy patients with normal MRI. *Epilepsia* 51, 583–591.
- Brookes, M.J., Woolrich, M.W., Price, D., 2014. An Introduction to MEG connectivity measurements, in: *Magnetoencephalography: From Signals to Dynamic Cortical Networks*. pp. 321–358.
- Chiang, S., Haneef, Z., Stern, J.M., Engel, J., 2017. Use of resting-state fMRI in planning epilepsy surgery. *Neurol. India* 65, S25–S33.
- Cohen, M.X., Cavanagh, J.F., Slagter, H.A., 2011. Event-related potential activity in the basal ganglia differentiates rewards from nonrewards: Temporospatial principal components analysis and source localization of the feedback negativity: Commentary. *Hum. Brain Mapp.*
- Coito, A., Genetti, M., Pittau, F., Iannotti, G.R., Thomschewski, A., Höller, Y., Trinka, E., Wiest, R., Seeck, M., Michel, C.M., Plomp, G., Vulliemoz, S., 2016. Altered directed functional connectivity in temporal lobe epilepsy in the absence of interictal spikes: A high density EEG study. *Epilepsia* 57, 402–411.
- Coito, A., Plomp, G., Genetti, M., Abela, E., Wiest, R., Seeck, M., Michel, C.M., Vulliemoz, S., 2015. Dynamic directed interictal connectivity in left and right temporal lobe epilepsy. *Epilepsia* 56, 207–217.
- Colclough, G.L., Brookes, M.J., Smith, S.M., Woolrich, M.W., 2015. A symmetric multivariate leakage correction for MEG connectomes. *Neuroimage* 117, 439–448.
- Dai, Y., Zhang, W., Dickens, D.L., He, B., 2012. Source connectivity analysis from MEG and its application to epilepsy source localization. *Brain Topogr.* 25, 157–166.
- Desikan, R.S., Sugonne, F., Fischl, B., Quinn, B.T., Dickerson, B.C., Blacker, D., Buckner, R.L., Dale, A.M., Maguire, R.P., Hyman, B.T., Albert, M.S., Killiany, R.J., 2006. An automated labeling system for subdividing the human cerebral cortex on MRI scans into gyral based regions of interest. *Neuroimage* 31, 968–980.
- Ding, L., Worrell, G.A., Lagerlund, T.D., He, B., 2007. Ictal source analysis: Localization and imaging of causal interactions in humans. *Neuroimage* 34, 575–586.
- Eickhoff, S.B., Stephan, K.E., Mohlberg, H., Grefkes, C., Fink, G.R., Amunts, K., Zilles, K., 2005. A new SPM toolbox for combining probabilistic cytoarchitectonic maps and functional imaging data. *Neuroimage* 25, 1325–1335.
- Engel, J., Jr., Thompson, P.M., Stern, J.M., Staba, R.J., Bragin, A., Mody, I., 2013. Connectomics and epilepsy. *Curr. Opin. Neurol.* 26, 186–194.
- Fischl, B., 2012. FreeSurfer. *Neuroimage*.
- Freeman, L.C., 1977. A Set of Measures of Centrality Based on Betweenness. *Sociometry*.
- Genovese, C.R., Lazar, N.A., Nichols, T., 2002. Thresholding of statistical maps in functional neuroimaging using the false discovery rate. *Neuroimage* 15, 870–878.
- Gilard, V., Proust, F., Gerardin, E., Lebas, A., Chastan, N., Fréger, P., Parain, D., Derrey, S., 2016. Usefulness of multidetector-row computerized tomographic angiography for the surgical planning in stereoelectroencephalography. *Diagn. Interv. Imaging* 97, 331–335.
- Girvan, M., Newman, M.E.J., 2002. Community structure in social and biological networks. *Proc. Natl. Acad. Sci. U. S. A.* 99, 7821–6.
- Gramfort, A., Papadopoulos, T., Olivi, E., Clerc, M., 2010. OpenMEEG: opensource software for quasistatic bioelectromagnetics. *Biomed. Eng. Online* 9, 45.
- Guimera, R., Guimerà, R., Nunes Amaral, L. a, 2005. Functional cartography of complex metabolic networks. *Nature* 433, 895–900.

- Hagmann, P., Cammoun, L., Gigandet, X., Meuli, R., Honey, C.J., Van Waden, J., Sporns, O., 2008. Mapping the structural core of human cerebral cortex. *PLoS Biol.* 6, 1479–1493.
- Hamalainen, M.S., Ilmoniemi, R.J., 1994. Interpreting magnetic fields of the brain: minimum norm estimates. *Med. Biol. Eng. Comput.* 32, 35–42.
- Hassan, M., Benquet, P., Biraben, A., Berrou, C., Dufor, O., Wendling, F., 2015. Dynamic reorganization of functional brain networks during picture naming. *Cortex* 73, 276–288.
- Hassan, M., Chaton, L., Benquet, P., Delval, A., Leroy, C., Plomhause, L., Moonen, A.J.H., Duits, A.A., Leentjens, A.F.G., van Kranen-Mastenbroek, V., Defebvre, L., Derambure, P., Wendling, F., Dujardin, K., 2017. Functional connectivity disruptions correlate with cognitive phenotypes in Parkinson's disease. *NeuroImage Clin.* 14, 591–601.
- Hassan, M., Dufor, O., Merlet, I., Berrou, C., Wendling, F., 2014. EEG source connectivity analysis: From dense array recordings to brain networks. *PLoS One* 9.
- Hassan, M., Merlet, I., Mheich, A., Kabbara, A., Biraben, A., Nica, A., Wendling, F., 2016. Identification of Interictal Epileptic Networks from Dense-EEG. *Brain Topogr.* 1–17.
- Hassan, M., Wendling, F., 2018. Electroencephalography source connectivity : toward high time / space resolution brain networks. *IEEE Signal Process. Mag.* 1–25.
- Jmail, N., Gavaret, M., Bartolomei, F., Chauvel, P., Badier, J.M., Bunar, C.G., 2016. Comparison of Brain Networks During Interictal Oscillations and Spikes on Magnetoencephalography and Intracerebral EEG. *Brain Topogr.* 29, 752–765.
- Kabbara, A., Falou, W.E.L., Khalil, M., Wendling, F., Hassan, M., 2017. The dynamic functional core network of the human brain at rest. *Sci Rep.* 1–16.
- Khambhati, A.N., Bassett, D.S., Oommen, B.S., Chen, Stephanie, H., Lucas, T.H., Davis, K.A., Litt, B., 2016. Recurring functional interactions predict network architecture of interictal and ictal states in neocortical epilepsy. *Revis. eNeuro.*
- Kovac, S., Vakharia, V.N., Scott, C., Diehl, B., 2017. Invasive epilepsy surgery evaluation. *Seizure.*
- Lachaux, J.P., Rodriguez, E., Martinerie, J., Varela, F.J., 1999. Measuring phase synchrony in brain signals. *Hum. Brain Mapp.* 8, 194–208.
- Lantz, G., Michel, C.M., Seeck, M., Blanke, O., Spinelli, L., Thut, G., Landis, T., Rosén, I., 2001. Space-oriented segmentation and 3-dimensional source reconstruction of ictal EEG patterns. *Clin. Neurophysiol.* 112, 688–697.
- Lascano, A.M., Vulliemoz, S., Lantz, G., Spinelli, L., Michel, C., Seeck, M., 2012. A Review on Non-Invasive Localisation of Focal Epileptic Activity Using EEG Source Imaging \* 80–89.
- Lu, Y., Yang, L., Worrell, G.A., He, B., 2012. Seizure source imaging by means of FINE spatio-temporal dipole localization and directed transfer function in partial epilepsy patients. *Clin. Neurophysiol.* 123, 1275–1283.
- Merlet, I., Garcia-Larrea, L., Grégoire, M.C., Lavenne, F., Mauguière, F., 1996. Source propagation of interictal spikes in temporal lobe epilepsy. Correlations between spike dipole modelling and [18F]fluorodeoxyglucose PET data. *Brain* 119 ( Pt 2, 377–92.
- Michel, C.M., De Peralta, R.G., Lantz, G., Andino, S.G., Spinelli, L., Blanke, O., Landis, T., Seeck, M., 1999. Spatiotemporal EEG analysis and distributed source estimation in presurgical epilepsy evaluation. *J. Clin. Neurophysiol.*
- Michel, C.M., Murray, M.M., Lantz, G., Gonzalez, S., Spinelli, L., Grave De Peralta, R., 2004. EEG source imaging. *Clin. Neurophysiol.*
- Netoff, T.I., 2004. Epilepsy in Small-World Networks. *J. Neurosci.* 24, 8075–8083.
- Nissen, I.A., Stam, C.J., Reijneveld, J.C., van Straaten, I.E., Hendriks, E.J., Baayen, J.C., De Witt Hamer, P.C., Idema, S., Hillebrand, A., 2016. Identifying the epileptogenic zone in interictal resting-state MEG source-space networks. *Epilepsia* 1–12.
- Pascual-marqui, R.D., Biscay, R.J., Bosch-bayard, J., Faber, P., 2017. Innovations orthogonalization : a solution to the major pitfalls of EEG / MEG “ leakage correction ” 1–20.
- Ponten, S.C., Douw, L., Bartolomei, F., Reijneveld, J.C., Stam, C.J., 2009. Indications for network regularization during absence seizures: Weighted and unweighted graph theoretical analyses. *Exp. Neurol.* 217, 197–204.
- Rubinov, M., Sporns, O., 2010. Complex network measures of brain connectivity: Uses and interpretations. *Neuroimage* 52, 1059–1069.
- Schneider, F., Irene Wang, Z., Alexopoulos, A. V., Almubarak, S., Kakisaka, Y., Jin, K., Nair, D., Mosher, J.C., Najm, I.M., Burgess, R.C., 2013. Magnetic source imaging and ictal SPECT in MRI-negative neocortical epilepsies: Additional value and comparison with intracranial EEG. *Epilepsia* 54, 359–369.
- Song, J., Tucker, D.M., Gilbert, T., Hou, J., Mattson, C., Luu, P., Holmes, M.D., 2013. Methods for examining

- electrophysiological coherence in epileptic networks. *Front. Neurol.* 4 MAY.
- Sporns, O., Betzel, R.F., 2016. Modular Brain Networks. *Annu. Rev. Psychol.* 67, 613–640.
- Staljanssens, W., Strobbe, G., Van Holen, R., Keereman, V., Gadeyne, S., Carrette, E., Meurs, A., Pittau, F., Momjian, S., Seeck, M., Boon, P., Vandenberghe, S., Vulliemoz, S., Vonck, K., van Mierlo, P., 2017. EEG source connectivity to localize the seizure onset zone in patients with drug resistant epilepsy. *NeuroImage Clin.* 16, 689–698.
- Studholme, C., Hawkes, D.J., Hill, D.L., 1998. Normalized entropy measure for multimodality image alignment. *Proc. SPIE* 3338, 132–143.
- Tadel, F., Baillet, S., Mosher, J.C., Pantazis, D., Leahy, R.M., 2011. Brainstorm: A user-friendly application for MEG/EEG analysis. *Comput. Intell. Neurosci.* 2011.
- Tavares, V., Ribeiro, A.S., Capela, C., Cerqueira, L., Ferreira, H.A., 2017. Epileptogenic focus localization using complexity analysis of BOLD signals, in: ENBENG 2017 - 5th Portuguese Meeting on Bioengineering, Proceedings.
- van Dellen, E., Douw, L., Baayen, J.C., Heimans, J.J., Ponten, S.C., Vandertop, W.P., Velis, D.N., Stam, C.J., Reijneveld, J.C., 2009. Long-Term Effects of Temporal Lobe Epilepsy on Local Neural Networks: A Graph Theoretical Analysis of Corticography Recordings. *PLoS One* 4.
- Van Mierlo, P., Carrette, E., Hallez, H., Raedt, R., Meurs, A., Vandenberghe, S., Van Roost, D., Boon, P., Staelens, S., Vonck, K., 2013. Ictal-onset localization through connectivity analysis of intracranial EEG signals in patients with refractory epilepsy. *Epilepsia* 54, 1409–1418.
- Vecchio, F., Miraglia, F., Quaranta, D., Granata, G., Romanello, R., Marra, C., Bramanti, P., Rossini, P.M., 2016. Cortical connectivity and memory performance in cognitive decline: A study via graph theory from EEG data. *Neuroscience* 316, 143–150.
- Wang, J., Qiu, S., Xu, Y., Liu, Z., Wen, X., Hu, X., Zhang, R., Li, M., Wang, W., Huang, R., 2014. Graph theoretical analysis reveals disrupted topological properties of whole brain functional networks in temporal lobe epilepsy. *Clin. Neurophysiol.* 125, 1744–1756.
- Watts, D.J., Strogatz, S.H., 1998. Collective dynamics of “small-world” networks. *Nature* 393, 440–2.
- Xia, M., Wang, J., He, Y., 2013. BrainNet Viewer: A Network Visualization Tool for Human Brain Connectomics. *PLoS One* 8.
- Zhang, Z., Liao, W., Chen, H., Mantini, D., Ding, J.R., Xu, Q., Wang, Z., Yuan, C., Chen, G., Jiao, Q., Lu, G., 2011. Altered functional-structural coupling of large-scale brain networks in idiopathic generalized epilepsy. *Brain* 134, 2912–2928.

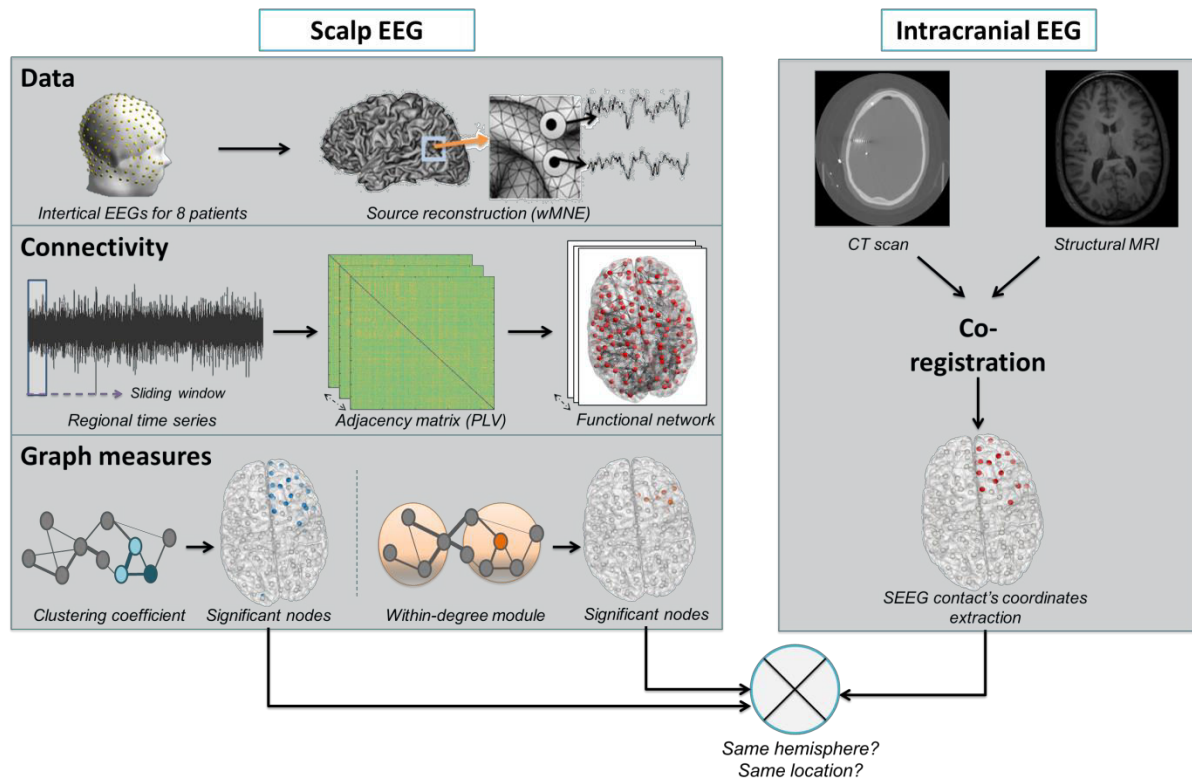


**Figure 1.** The full pipeline of the study. *On the left:* the steps performed to identify the pathological nodes using EEG network analysis. First, we reconstructed the regional time series using the weighted minimum norm estimate (wMNE) inverse solution. The dynamic functional connectivity matrices were then computed using a sliding window approach combined with the phase locking value (PLV) connectivity measure. After that, the within-degree module and the clustering coefficient were used to quantify the local network property. *On the right:* the steps performed to extract the SEEG contacts' coordinates using the CT scan and the structural MRI images. Finally, the significant nodes obtained using EEG approach were compared to the positions of SEEG contacts in terms of hemispherical, lobar and epileptogenic zone detection.

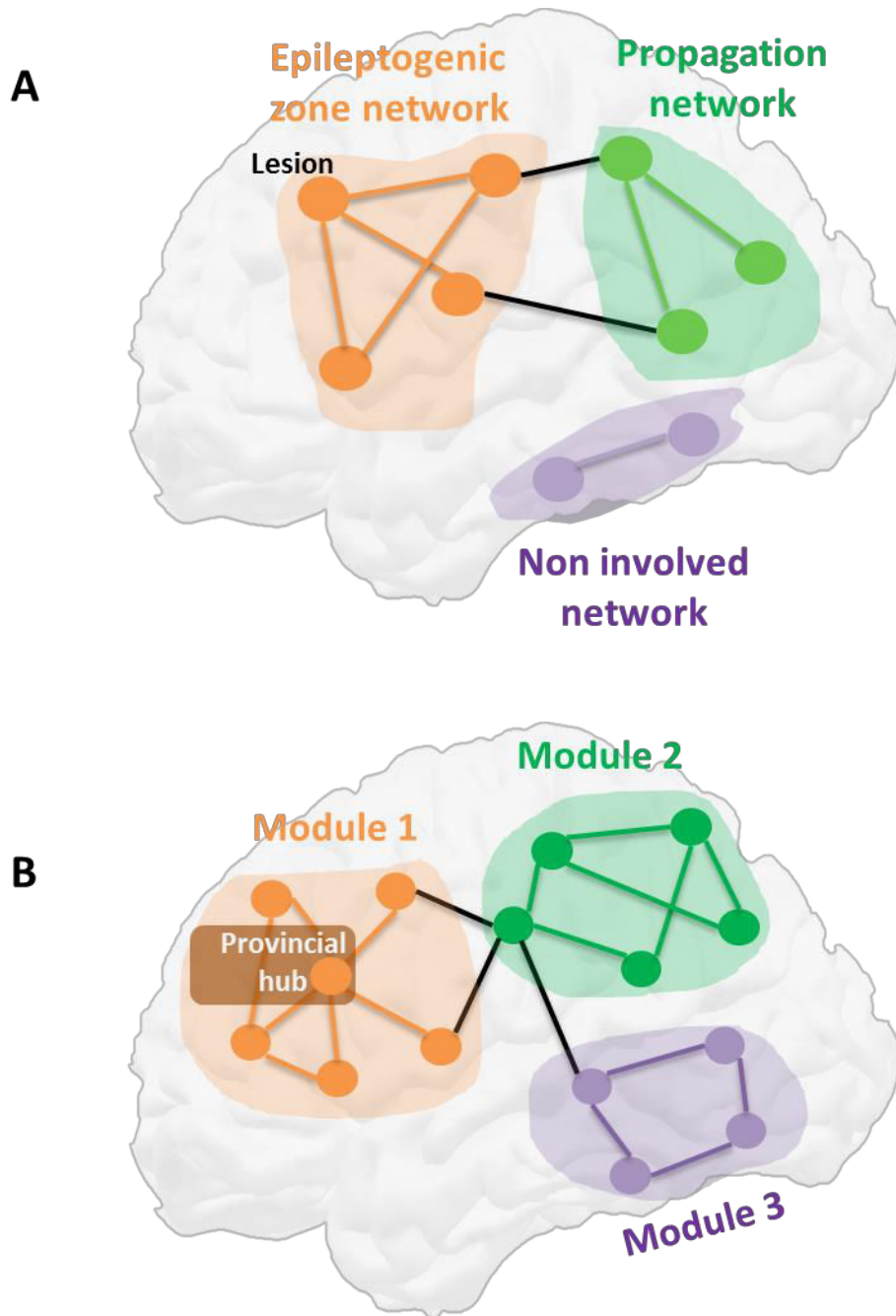


**Figure 2. (Up) Organization of the epileptogenic networks in focal epilepsy. The epileptogenic zone (EZ) network contains brain regions (orange nodes) that may generate seizures. This EZ prompts another set of brain regions forming the propagation zone network (Green nodes). Adapted from (Bernasconi, 2017)**

**(Bottom) Organization of the brain networks into modules. Networks can be decomposed into modules. Edges are either linking nodes within modules (Orange, green or purple) or between modules (black edges). Highly connected nodes with other nodes in the same modules nodes are called provincial hub. Adapted from (Sporns and Betzel, 2016b).**

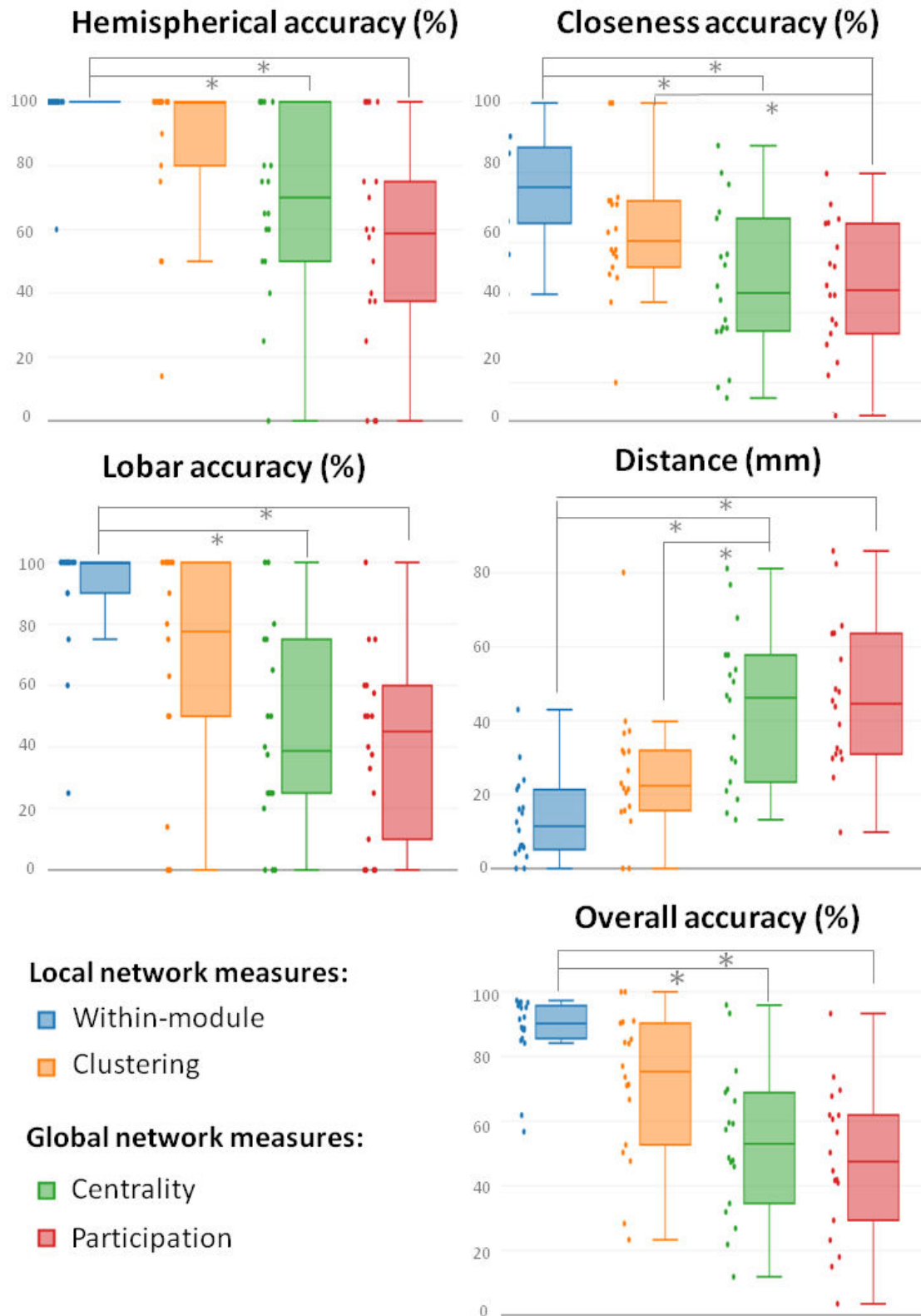
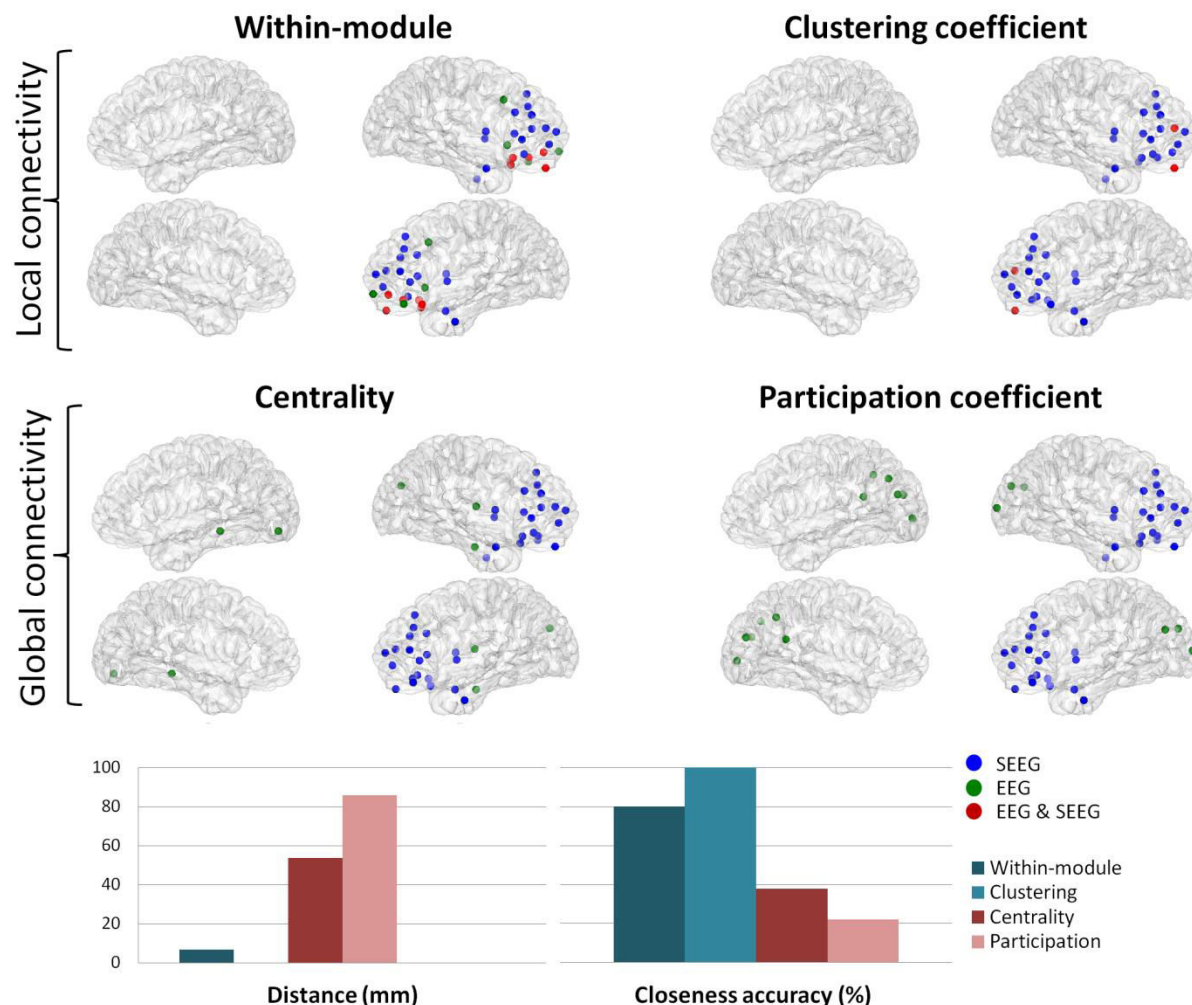


Figure 3. Comparison between the local and global network measures in terms of hemispherical, lobar, closeness, global accuracies and Euclidian distance. \* denotes significant difference for  $p < 0.01$ .





**Figure 4. Patient P1 (Excellent overall accuracy)**

**Top)** The cortical surface representations of the regions that showed high significant values ( $p < 0.01$ , Bonferroni corrected) in local network measures (within-degree module, clustering coefficient) and in global network measures (centrality, and participation coefficient) for the patient P1. A blue node represents SEEG contact, not detected by EEG approach. A green node represents a node detected by EEG approach. A node colored in red represents a node that overlaps between SEEG contact and EEG approach. The barplots of the distance between scalp and depth EEG and the closeness accuracy for the four network measures.

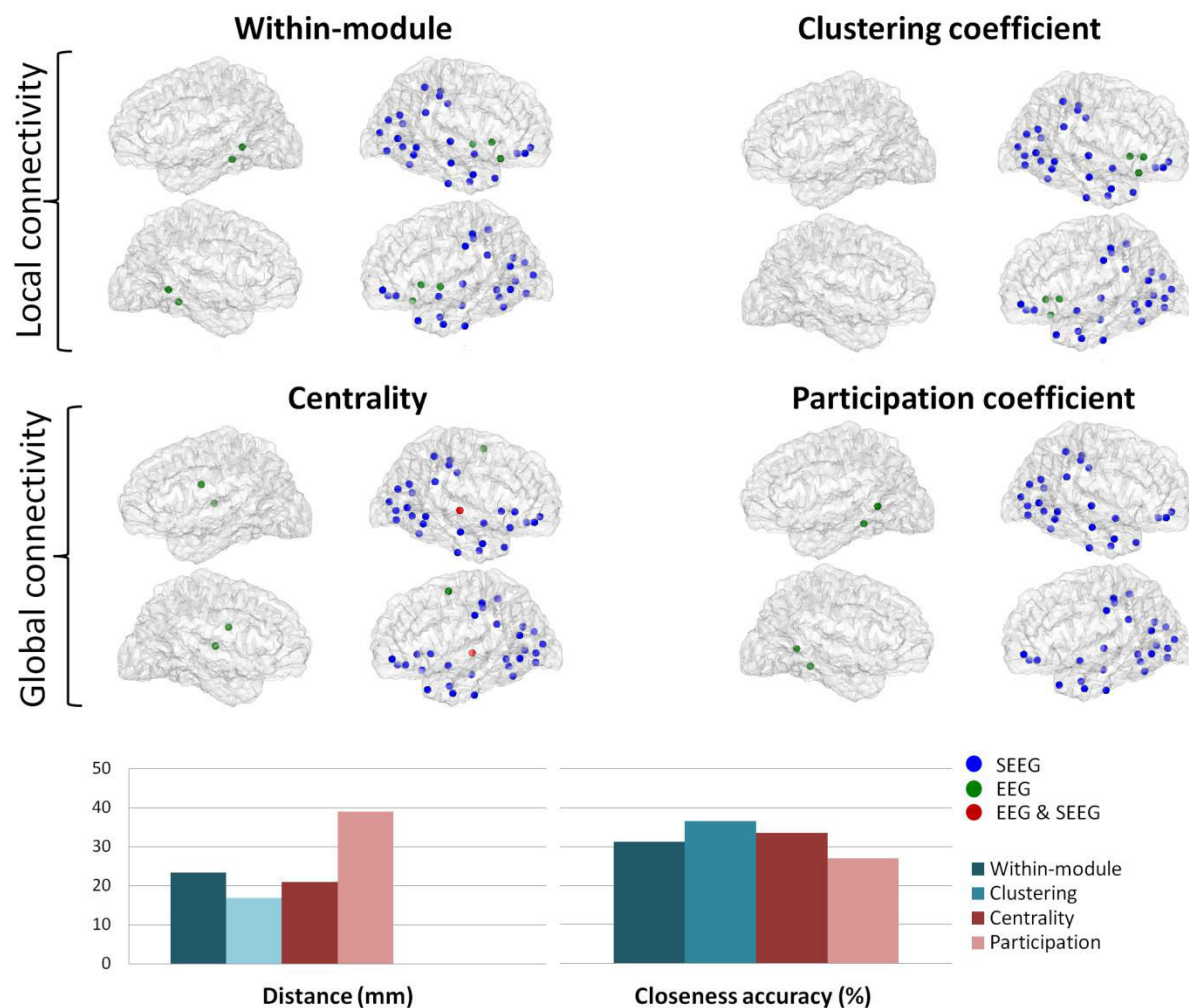


**Figure 5. Patient P2 (good overall accuracy)**

**Top)** The cortical surface representations of the regions that showed high significant values ( $p < 0.01$ , Bonferroni corrected) in local network measures (within-degree module, clustering coefficient) and in global network measures (centrality, and participation coefficient) for the patient P2. A blue node represents SEEG contact not detected by EEG approach. A green node represents a node detected by EEG approach. A node colored in red represents a node that overlaps between SEEG contact and EEG approach. The barplots of the distance between scalp and depth EEG and the closeness accuracy for the four network measures.

Patient	Age	EZ	SEEG implantation		MRI
			Side (nb electrodes)	Brain areas	
P1 (F)	28	R Fr	R(9)	iFr, mFr, sFr, IOFr, mesOFr, preC, aCing, mCing, Ins, mTe, Amy	R sFr FCD
P2 (M)	36	R Te-Occ	R(10)	MesFr, iFr, mesOFr, EC, iTe, mTe, sT, Ins, Amy, Hipp, paraHipp, Ling, Fus, Cun, pCing, IOcc, iPA	R iTe and Te-Occ DNET
P3 (M)	27	R Fr	R (11)	iFr, mFr, sFr, mesFr, aCing, mCing, preC, pC	Right mFr DNET
P4 (F)	35	L Te +Ins	L(12)	mFr, TeP, sTe, mTe, iTe, EC Amy, Hipp, Fus, Ins, preC, iPa,	T2 signal abnormality in L TeP and Ins
P5 (M)	19	L Pa-Occ	L(10) R(2)	paraC, pC, mTe, Hipp, Fus, iPa, sPa, preCun, pCing, IOcc, Ling, Calc, Cun sPa, iPa, pCing	L mes Pa-Occ FCD
P6(M)	30	L Pa-Occ	L(6)	mT, sTe, Hipp, Fus, iPa, sPa, pC, preCun, pCing	L Pa-Occ post-surgery cavity
P7 (F)	16	L Fr	L(9)	iFr, mFr, sFr, mesFr, IOFr, mesOFr aCing, mTe, Amy	L mesOFr FCD
P8 (M)	19	L C	L(11)	iFr, mFr, sFr, mesFr, preC, pC, aCing, mCing, pCing, Ins	-
P9 (M)	26	R Te + Ins	R(9) L(3)	mFr, preC, iTe, mTe, sTe, Hipp, Amy, EC, Ins, Fus mFr, mTe, preC, Amy, Hipp, Ins	-
P10 (F)	35	L Te	L(5)	mTe, sTe, Hipp, Amy, paraHipp	Previous L TeP, Amy and aTe resection
P11 (M)	26	R Fr	R(13)	iFr, mFr, sFr, mesFr, preC, pC, aCing, mCing, pCing, Ins	-
P12 (M)	33	L Fr	R(10)	iFr, mFr, sFr, mesFr, aCing, iTe, mTe, sTe, EC,	L iFr FCD

		+ R Te +R Ins	L(4)	Amy, Hipp, Ins, aCing, preC, mTe, Amy, Hipp, Ins	
P13 (M)	25	R C	R(10)	iFr, mFr, sFr, mesFr, preC, pC, paraC, aCing, mCing, pCing, Ins, iPa, preCun	-
P14 (M)	28	R Fr-Te + R Ins	R(14)	iFr, mFr, sFr, mesFr, IOFr, mesOFr, preC, pC, mTe, sTe, Amy, paraHipp, Hipp, Ins	-
P15 (F)	22	L Te + L Ins	L(11)	mesOFr, preC, TeP, iTe, mTe, sTe, Hipp, EC, paraHipp, Amy, Ins, iPa	-
P16 (M)	23	R Te-Occ	R(13)	sFr, sTe, mTe, Hipp, paraHipp mCing, pCing, iPa, sPa, preCun, IOcc, Ling, Calc, Cun	-
P17 (M)	29	R Te	R(12)	iTe, mTe, sTe, Amy, Hipp, ParaHipp, Ling, IOcc, Calc, pCing, iPa	-
P18 (M)	40	L Fr	L(11)	iFr, mFr, sFr, mesFr, preC, pC, paraC, aCing, pCing, Ins, Thal	L sFr abnormal sulcus

**Table1. Demographic of the 18 patients.**

**Abbreviations:** L: left; R: right; i: inferior; m: middle; s: superior; a: anterior, p: posterior; mes: mesial; l: lateral; Fr: frontal; OFr: orbito-frontal; Cing: cingulate gyrus; C: central; Ins: Insula; Te: temporal; TeP: temporal pole, Pa: Parietal; Occ: Occipital; Amy: amygdala; Hipp: hippocampus; EC: entorhinal cortex; Fus: fusiform gyrus; Ling: Lingual gyrus; Calc: calcarin sulcus; Cun: cuneus; DNET: Dysembryplastic Neuroepithelial Tumor; FCD : Focal Cortical dysplasia.

# **Study 5: Tracking fast modular brain states in rest and task**

A. Kabbara, M. Khalil, F. Wendling & M. Hassan

*Submitted*

# Detecting modular brain states in rest and task

Kabbara A.<sup>1,2</sup>, Khalil M.<sup>2</sup>, O'Neill G.<sup>3</sup>, Dujardin K.<sup>4,5,6</sup>, Wendling F.<sup>1</sup> and Hassan M.<sup>1</sup>

<sup>1</sup> Univ Rennes, LTSI - U1099, F-35000 Rennes, France

<sup>2</sup> Azm Center for Research in Biotechnology and its Application, EDST, Lebanese University, Lebanon

<sup>3</sup> Sir Peter Mansfield Imaging Centre, School of Physics and Astronomy, University of Nottingham, University Park, Nottingham, UK

<sup>4</sup> INSERM, U1171, F-59000 Lille, France

<sup>5</sup> CHU Lille, Clinical Neurophysiology Department, F-59000 Lille, France

<sup>6</sup> CHU Lille, Neurology and Movement Disorders Department, F-59000 Lille, France

# Abstract

---

The human brain is a dynamic networked system that continually reconfigures its connectivity patterns over time. Thus, developing approaches able to adequately detect fast brain dynamics is critical. Of particular interest are the methods that analyze the modular structure of brain networks, i.e. the presence of clusters of regions that are densely inter-connected. In this paper, we propose a novel framework to identify fast modular states that dynamically fluctuate over time during rest and task. We validate our method using MEG data recorded during a finger movement task, identifying modular states linking somatosensory and primary motor regions. The algorithm was also validated on dense-EEG data recorded during picture naming task, revealing the sub-second transition between several modular states which relate to visual processing, semantic processing and language. Next, we validate our method on a dataset of resting state dense-EEG signals recorded from 124 parkinsonians patients of different cognitive phenotypes. Results disclosed brain modular states that differentiate cognitively intact patients, patients with moderate cognitive deficits and patients with severe cognitive deficits. Our new approach tracks the brain modular states on an adequate task-specific timescale.

# Introduction

---

The human brain is a modular dynamic system. Following fast neuronal activity<sup>1,2</sup>, the functional organization of resting<sup>3-7</sup> and task-evoked connectivity<sup>8-11</sup> are in constant flux. Hence, an appropriate description of time-varying connectivity is of utmost importance to understand how cognitive and behavioral functions are supported by networks.

Electro/magneto-encephalography (EEG/MEG) are unique noninvasive techniques, which allow for the tracking of brain dynamics on a millisecond time-scale, a resolution not reachable using other techniques such as the functional Magnetic Resonance Imaging (fMRI)<sup>12-14</sup>. In this context, several methods have been proposed to reveal when, and how the functional connections between brain regions vary during short-time (sub-second) experiments. Some of these studies proposed to group the temporal networks into states, where each state reflect unique spatial connectivity pattern. These brain states were mainly generated using Hidden Markov model approaches<sup>6,15</sup>, K-means clustering<sup>3,16,17</sup> or independent component analysis<sup>9</sup>. Other studies have tried to investigate the dynamic topological changes using graph theoretical analysis<sup>5,7</sup>.

Due to the modular organization of the human brain network<sup>18</sup>, methods for detecting network communities (or modules) are of particular interest<sup>19</sup>. These methods decompose the network into building blocks or modules that are internally strongly connected, often corresponding to specialized functions. Importantly, brain modularity has been revealed to be related to behavior involved in learning<sup>20</sup>, remembering, attention and integrated reasoning<sup>21</sup>.

To detect modules, many community detection methods have been proposed<sup>22,23</sup>. Using the most widely applied community detection methods, brain networks are often analyzed as static arrangements of nodes and edges with a number of studies starting to explore how the modular



organization shapes the dynamics of neural activity<sup>19,20,24,25</sup>. One of the algorithms used to characterize the flow of communities across time is multi-slice modularity (also called multi-layer modularity)<sup>26</sup>, which has been used to follow changes of the modular architecture across time<sup>20 27</sup>. However, it does not automatically decipher functional modular brain states i.e. subset of brain modules implicated in a given brain function at a given time period.

Here, we propose a novel framework aiming to elucidate the main modular brain structures, called ‘modular states’ (MS), which fluctuate over time during rest and task. The new method is based on temporally categorizing the modular structures that share the same topology by quantifying the similarity between their partitions (Figure 1). The proposed framework was validated in simulation and on three different MEG/EEG datasets, recorded in rest and task from healthy and/or patients. Our method revealed both time-varying functional connectivity and the corresponding spatial patterns. We are able to track the space/time dynamic of brain networks in task-adapted timescale.

# Results

---

The proposed algorithm is illustrated in Figure 1. The dynamic functional connectivity matrices were obtained using a sliding window approach giving a weighted network at each time window. By applying a community detection algorithm (Louvain method), each network was then decomposed into modules (i.e clusters of nodes that are internally strongly connected, but externally weakly connected). The similarity between the temporal modular structures was then calculated (Figure 1B). Finally, the modular states (MS) were obtained by applying community detection algorithm to the similarity matrix (Figure 1 C).

We propose two different frameworks i) “categorical” where the objective is to find the main modular structures over time, without any interest in their sequential order and ii) “consecutive” where the objective to find the modular structures in a successive way.

## **Validation on simulated data**

We first evaluate the performance and the space/time precision of the algorithm using simulated data. Briefly, an adjacency tensor was simulated over a time-course spanning 60 seconds by combining four network structures: M1, M2, M3 and M4 (illustrated in Figure 2.A). The onset as well as the duration of each modular structure is illustrated in Figure 2.B. Random Gaussian noise was added to the adjacency tensor, and the standard deviation of the noise was allowed to vary between 0.2 and 0.5 (see Methods section for more details about the simulation).

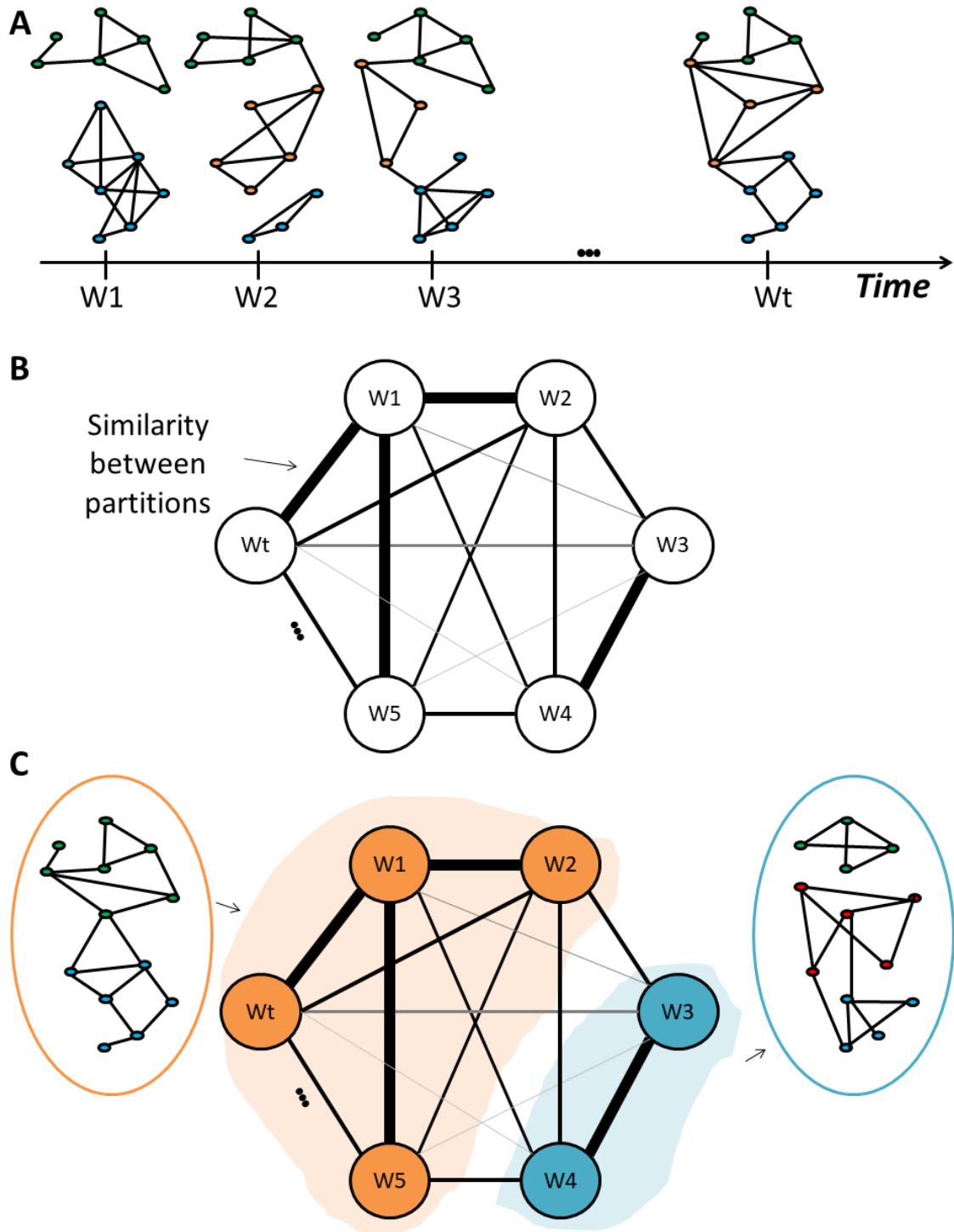


**Figure 1. The algorithm procedure.** A) Computation of modules for each temporal network. B) Assessment of the similarity between the dynamic modular structures. C) Clustering the similarity matrix into “categorical Modules”.

Figure 3 shows the results of the categorical method applied on the dynamic networks generated by the simulation scenario ( $STD_{noise} = 0.2$ ). Four modular states were obtained: MS1, MS2, MS3 and MS4. Figure 3.A illustrates the modular states' time courses, showing the most likely state at each time-window whilst Figure 3.B shows the 3D representation of the MS. Clearly, the four simulated modular structures have been successfully reconstructed. However, one time window that actually belongs to the background (i.e. random) has been wrongly affiliated to MS2. Moreover, MS3 state time course presented two false time window detection: one belongs to MS4, and the other belongs to the background. To quantitatively validate the obtained results, we compared the simulated structures (M1, M2, M3 and M4) to the reconstructed structures (MS1, MS2, MS3 and MS4) in terms of spatial and temporal similarities. The spatial similarities between the simulated and the reconstructed data are 0.99, 0.98, 0.99 and 0.98 for MS1, MS2, MS3, and MS4 respectively. The temporal similarities are 0.79, 0.83, 0.9 and 0.71 for MS1, MS2, MS3, and MS4 respectively.

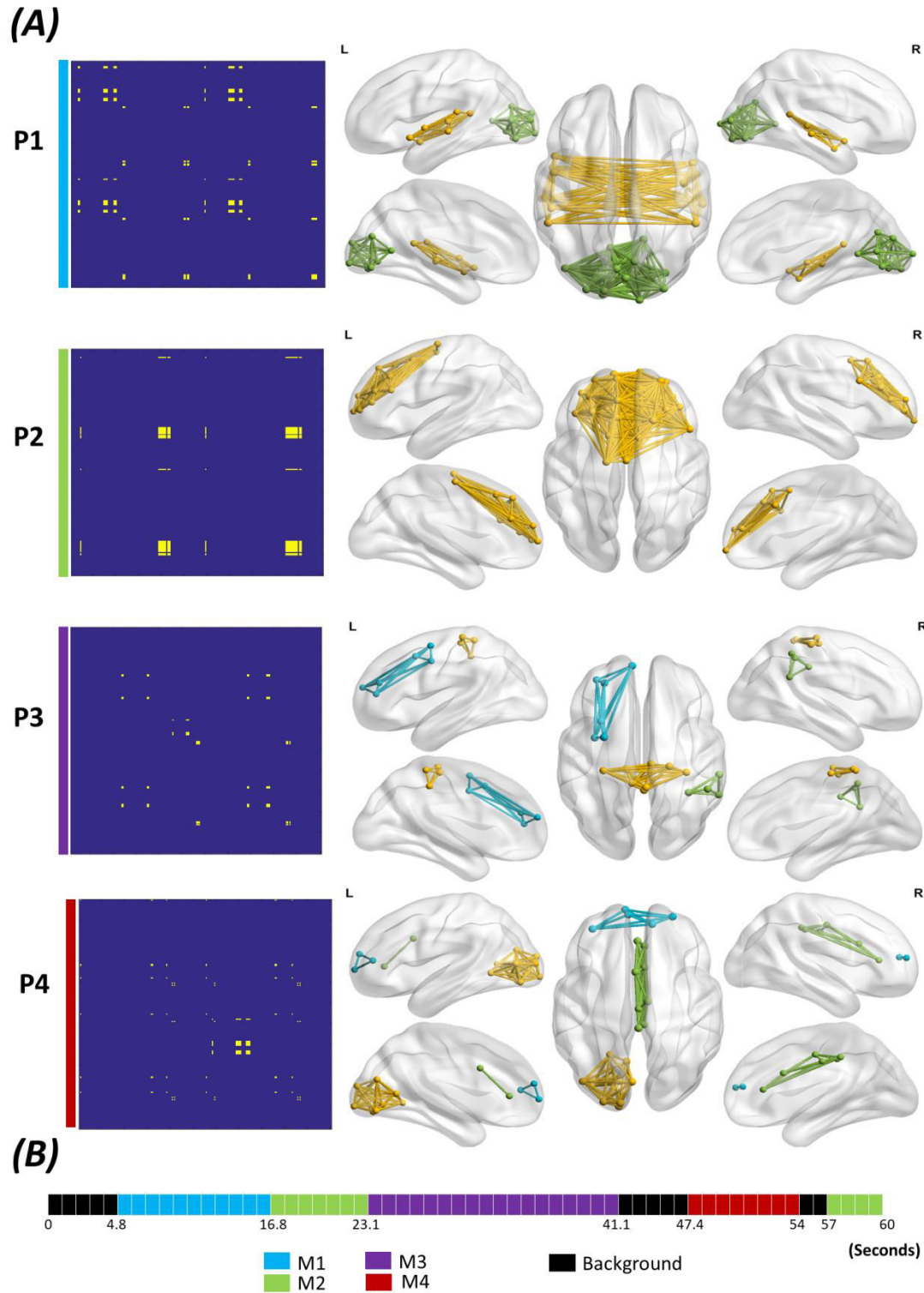


**Figure 2. The simulation scenario.** A) Left: the adjacency matrix of the constructed networks, Right: the 3D cortical presentation of the modular structures of the simulated networks. B) the time axis showing the beginning and the end of each network.

Using the consecutive method, the algorithm has successfully segmented the similarity matrix yielding to the detection of five modular states (Figure 4.A). Their 3D representations are shown in Figure 4.B. One can remark that MS1 (spatial similarity=0.94; temporal similarity=0.88), MS2 (spatial similarity=0.99; temporal similarity=0.94), MS3 (spatial similarity=0.97; temporal similarity=0.77), MS4 (spatial similarity=1; temporal similarity=0.88), and MS5 (spatial similarity=0.95; temporal similarity=1) matched, temporally and spatially, the simulated networks generated at the corresponding time-windows.

Results corresponding to  $STD_{noise} = 0.35$ ;  $STD_{noise} = 0.5$  are illustrated in the supplementary materials. In brief, results show that using the categorical algorithm, the spatial characterizations of the four modular states were successfully detected. However, the state time-course of MS3 failed to detect the second corresponding segment (Figure S1, S2). Using the consecutive algorithm, the five MS were temporally detected (Figure S3, S4).

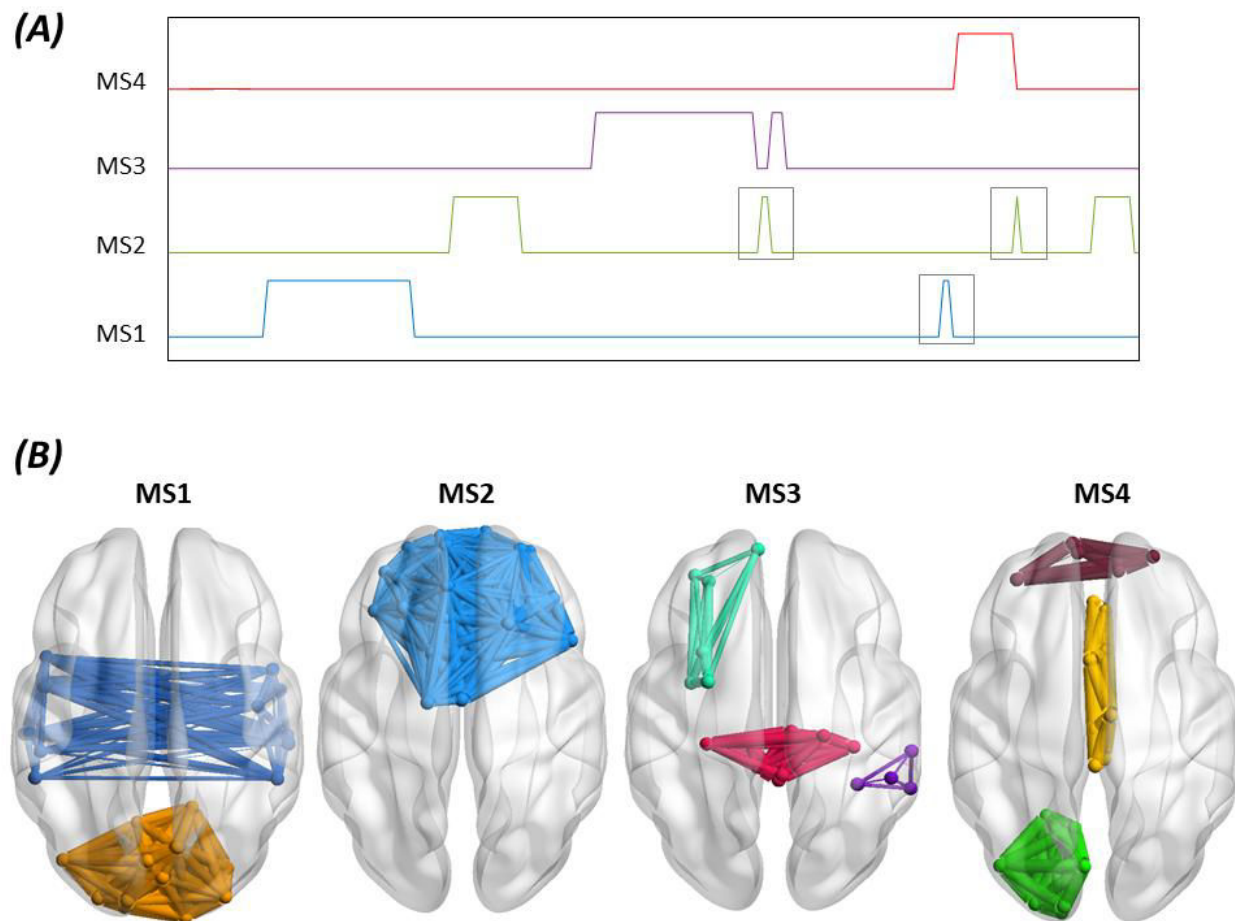


**Figure 3. Results of the categorical method applied on simulated data.** A) the time course of the four modular structures reconstructed. The grey square indicates false time-window detection. B) 3D representation of the four modular structures states.

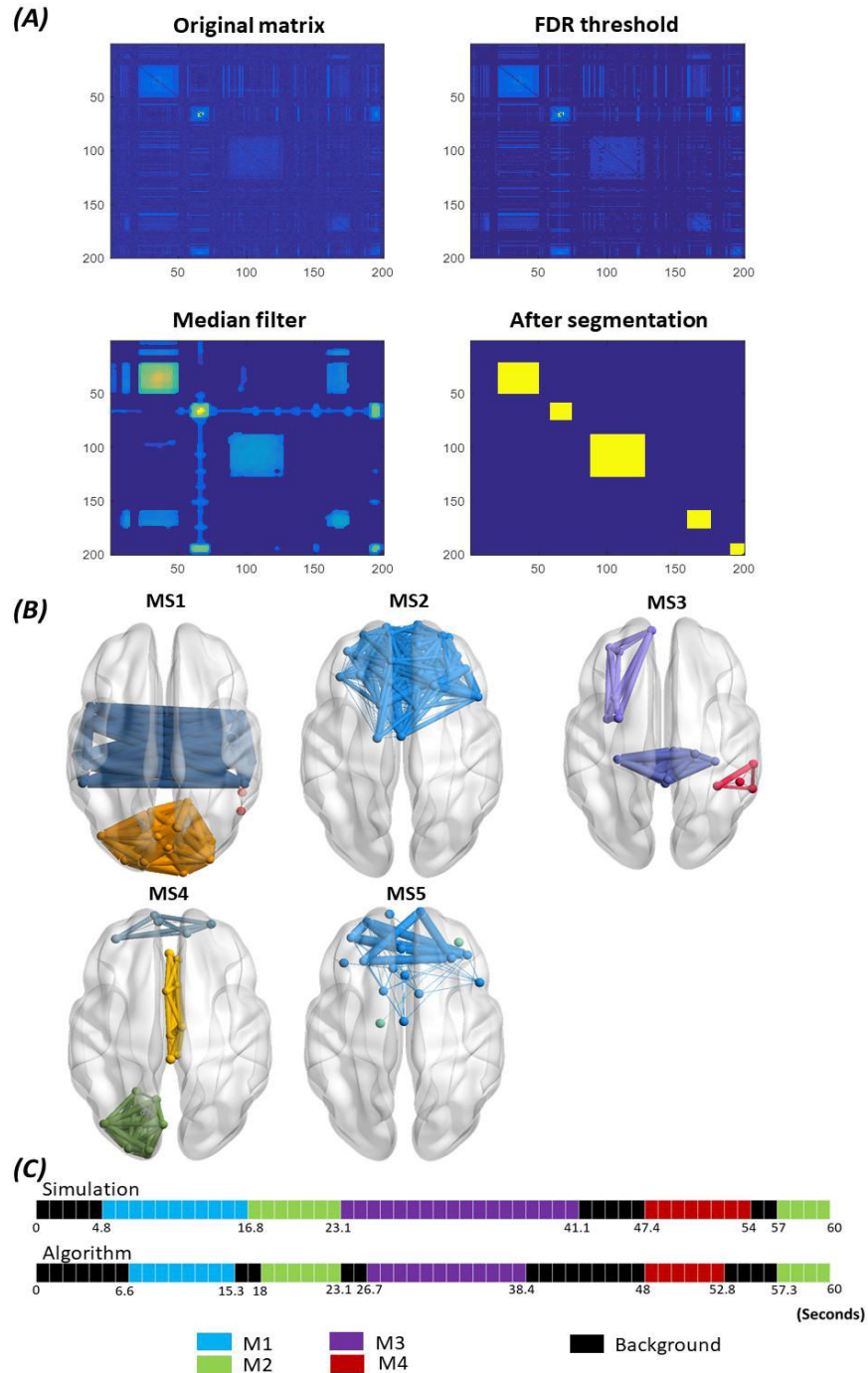


**Figure 4. Results of the consecutive method applied on simulated data.** A) The results of the segmentation algorithm used to derive the consecutive modular structures from the similarity matrix by: 1) Thresholding the matrix using FDR, 2) applying a median filter on the thresholded matrix and 3) extracting the most significant segments (See methods section for more details about the consecutive algorithm steps). B) The 3D representation of the five consecutive modular structures obtained. C) The difference between the simulated time axis and the obtained time axis.



## Real data

### **Dataset 1-** *self paced motor task for healthy participants (MEG data):*

Here, MEG data were recorded from 15 participants during a self-paced motor task, i.e. participants that were asked to periodically press a button. The source time courses were reconstructed using a beamforming approach. The consecutive algorithm was also applied on the computed dynamic connectivity matrices averaged over all trials and subjects. The dynamic functional connectivity matrices were calculated using a sliding window approach based on envelope correlation (see Methods section). The same dataset and methods was previously used in <sup>9,28,29</sup>. The algorithm results in one significant MS found between -0.5s and 1.5 s (Figure 5). As illustrated, this module implicates the sensory motor area, the post and pre-central regions of both hemispheres.

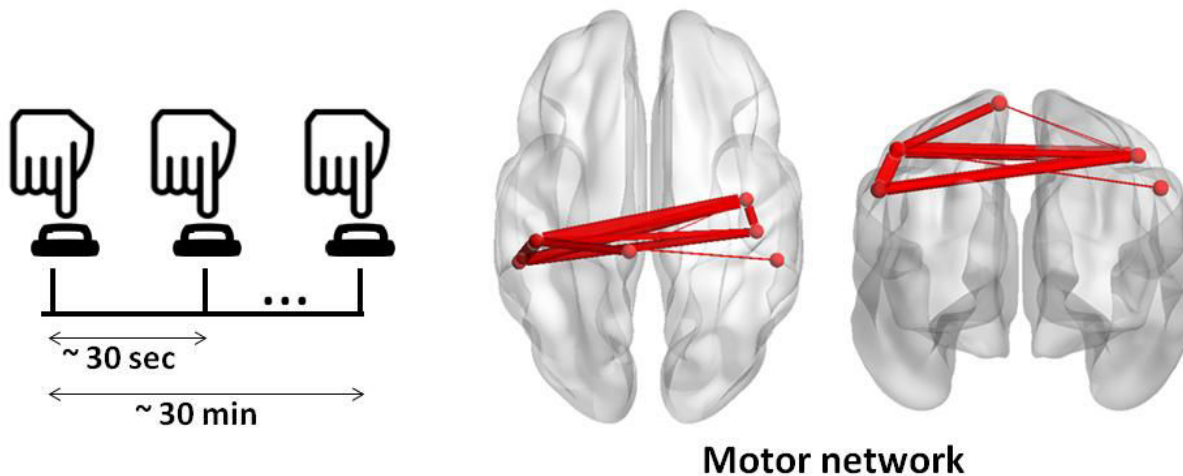


**Figure 5.** The MS of the MEG motor task obtained using the ‘consecutive’ method.

**Dataset 2-** *picture naming task for healthy participants (dense-EEG data):*

This dataset consists of dense-EEG (256 channels) data recorded from 21 healthy subjects asked to name displayed pictures. The objective of using this dataset was to track the fast space/time dynamics of functional brain networks at sub-second time scale from the onset (presentation of the visual stimuli) to the reaction time (articulation). Hence, the consecutive version was applied on the dynamic connectivity matrices averaged over subjects.

The same dataset was previously used by Hassan et al <sup>8</sup> and it consists of dense-EEG data recorded. The source time series were reconstructed using the weighted minimum norm solution (wMNE). The dynamic functional connectivity matrices were computed using the inter-trial version of the phase locking value (see Methods section for more details). Figure 6A shows the obtained results revealing that the cognitive process can be divided into five modular structures: The first MS corresponds to the time period ranging from the stimulus onset to 130 ms and presents one module located mainly in the occipital region. The second MS is observed between 131 and 187 ms, and involves one module showing occipito-temporal connections. The third MS is identified between 188 and 360 ms, and illustrates a module located in the occipito-temporal region, and another module located in the fronto-central region. This structure was then followed by a fourth MS, found over the period 361-470 ms. MS4 was very similar to the previous MS but with additional fronto-central connections. The last MS is observed between 471 and 500 ms and it shows a module connecting the frontal, the central and the temporal regions. It is worth noting that these MS denotes the transitions from the visual processing and recognition the semantic processing and categorization to the preparation of the articulation process <sup>8,30,31</sup>.

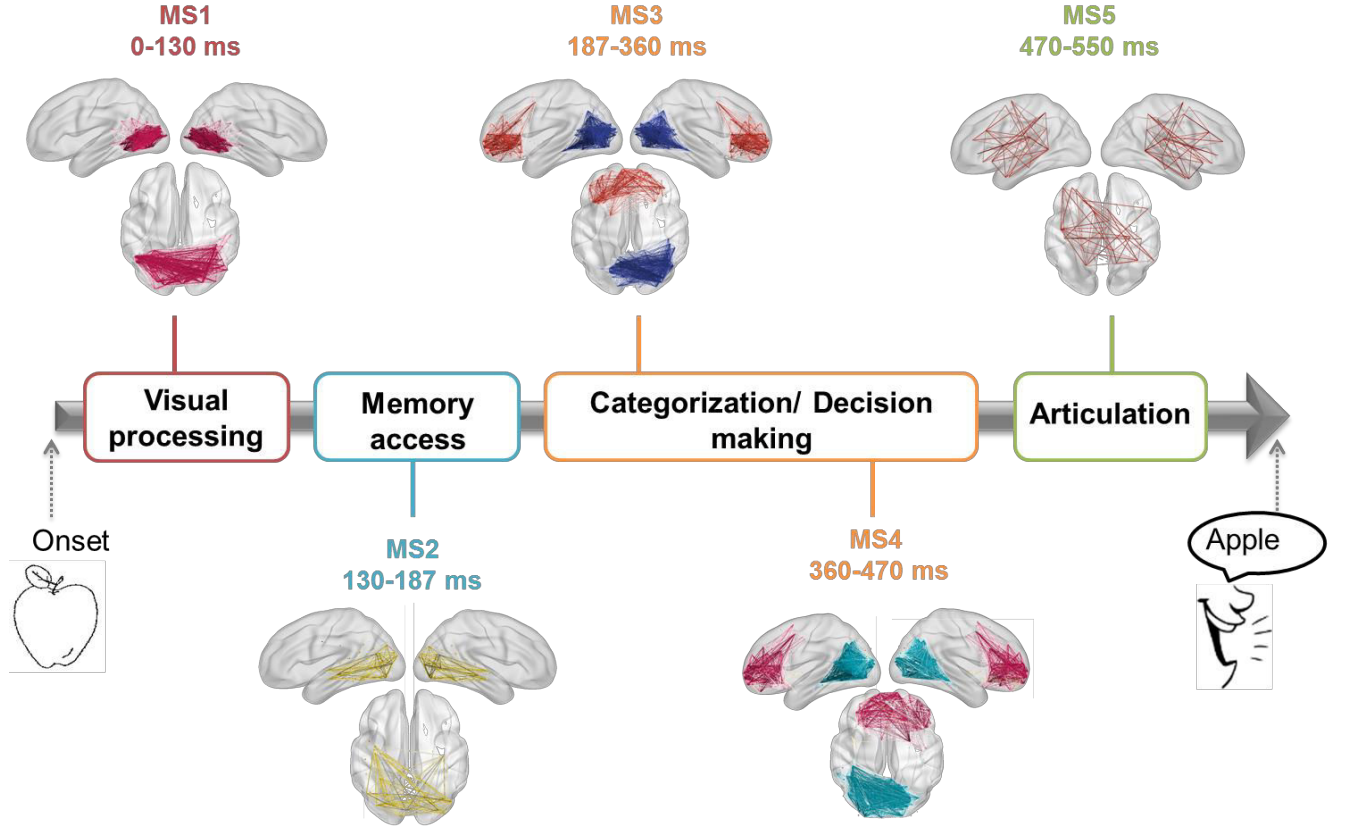


**Figure 6.** The sequential MSs of the EEG picture naming task obtained using the consecutive method and their corresponding cognitive functions.

**Dataset 3-** *resting state in Parkinson's disease patients (dense-EEG data):*

This dataset consists of dense-EEG data recorded from 124 patients with idiopathic Parkinson's disease and separated (based on their neuropsychological tests) into three groups: G1) cognitively intact patients (N=63), G2) patients with mild cognitive deficits (N=46) and G3) patients with severe cognitive impairment (N=15). See <sup>32,44,45</sup> for more details about the database.

Our objective here is to validate the usefulness of the categorical version in detecting the modular alterations between G1, G2 and G3. To do that, the dynamic functional connectivity of each patient was calculated using a sliding window approach automatically selected based on phase locking value (see Methods for more details). Then, the dynamic connectivity matrices of the three groups were concatenated over time, forming a single data tensor of dimension  $N \times N \times$

T, where N is the number of ROIs, and T is equal to the number of time-windows \* the number of patients (Figure 4). The algorithm was then applied to identify the modular structures that are common to the three groups, and those who are specific to each group.

Results are illustrated in Figure 7. Five modular structures were identified (MS1, MS2, MS3, MS4 and MS5). Three MSs were found for G1 and G2. However, the number of MS decreased from three to two MSs in G3. Results revealed that MS1 was found to be present in the three groups while MS1 and MS2 were present only in G1 and G2. The modular structure MS2 (absent in G3) is illustrated in Figure 7 and includes two modules involving mainly fronto-central and occipito-temporal connections. The difference between G1 and G2 was reflected by the absence of the structure MS3 replaced by the structure MS4 in G2. Results in Figure 7 showed that the difference is mainly the fronto-temporal. The difference between G2 and G3 was reflected by the absence of the structure MS4 from G2 and the presence of the structure MS5 in G3. Figure 7 showed that the functional disruptions between G2 and G3 are mainly fronto-temporal connections. It is worth noting that the fronto-temporal disruptions were widely reported in mild cognitive impairments<sup>33,34,35,36</sup> while the central disruptions are widely observed in severe cognitive impairments<sup>32</sup> and dementia<sup>34</sup>.

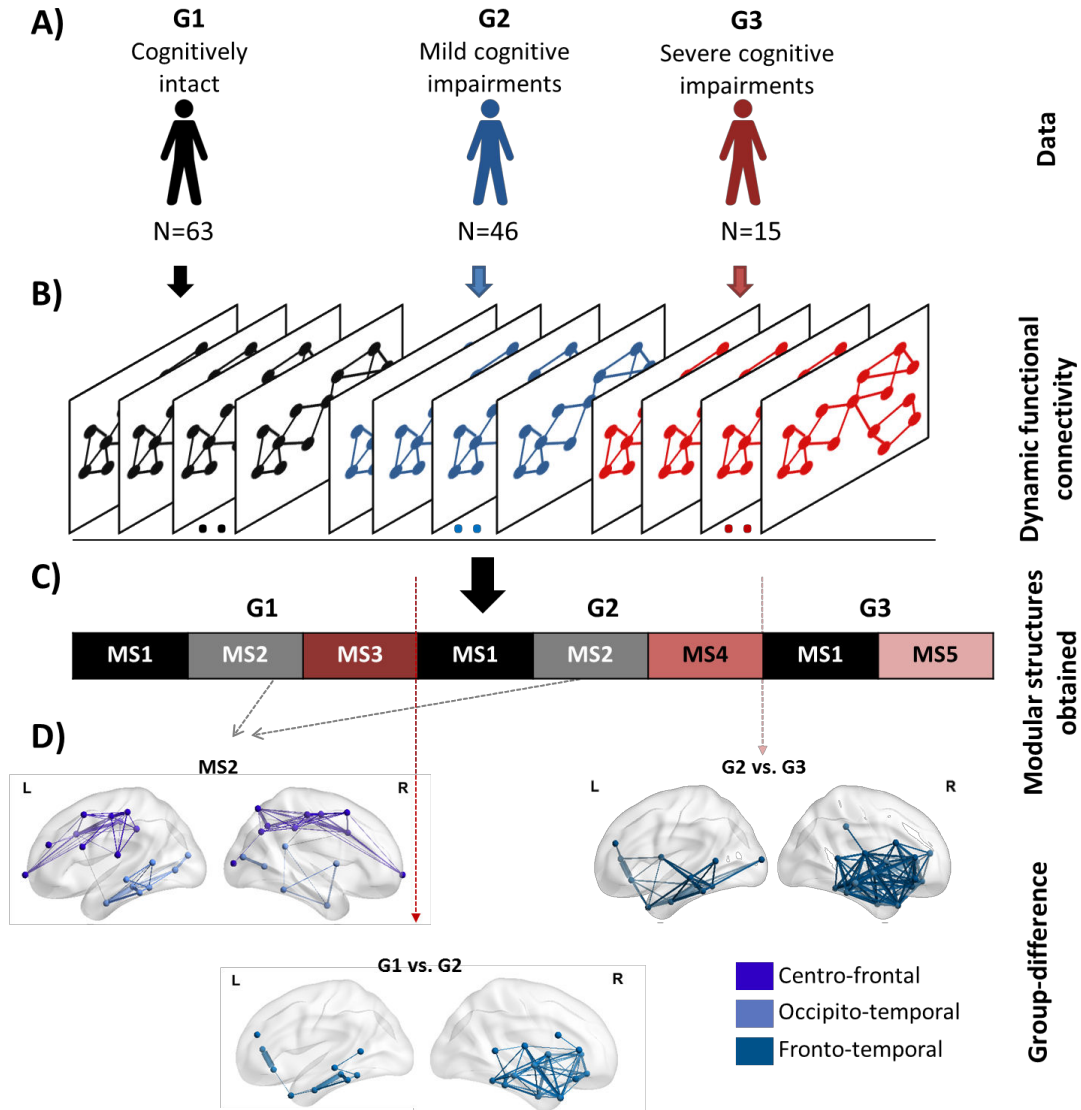


**Figure 7. The analysis pipeline and the results of the categorical method applied on Parkinson's disease EEG dataset.** A) The dataset composed of 124 patients partitioned into three groups: G1) cognitively intact patients (N=63), G2) patients with mild cognitive deficits (N=46) and G3) patients with severe cognitive impairment (N=15). B) The functional dynamic connectivity matrices of the three groups concatenated over time. C) The five modular structures obtained after applying the categorical algorithm on the concatenated tensor. D) The modular differences between G1 and G2, G1 and G3, G2 and G3.

# Discussion

---

In this paper, we have developed a novel framework aims to explore the fast reconfiguration of the functional brain networks during rest and task. The new method can be used to track the sequential evolution of brain modules during a task-directed paradigm or to identify the dominant brain modules that arise at rest. The simulation-based analysis showed clearly the ability of the method to “re-estimate” the modular network structures over time.

The new framework was validated in simulation and on three different EEG/MEG datasets i) MEG data recorded from 15 healthy subjects during a self-paced motor task , ii) Dense-EEG data recorded from 21 healthy subjects during a picture naming task and iii)Dense-EEG data recorded at rest from 120 Parkinson’s disease patients with different cognitive phenotypes.. Our results show that our method has the flexibility to not only track the fast modular states of the human brain network at sub-second time scale, but also highlights its potential clinical applications, such as the detection of the early cognitive decline in the Parkinson’s disease.

## **“Categorical” and “consecutive” processing schemes**

The two processing schemes proposed here are both derived from the similarity matrix between the temporal modules (Step 1→3 in Methods section). However, each version highlights a specific characterization of the modular structures, which can be then exploited depending on the application (time/condition dependent). . In particular, the results of the categorical algorithm on the simulated data reveal high spatial resolution and relatively low temporal resolution compared to those obtained using the consecutive algorithm. The low temporal resolution of the categorical version is reflected by the false (Figure 2) as well as the missed time-windows detection (Figure S1, Figure S2). In contrast, these time-windows were correctly detected by the consecutive

version despite their short length (Figure 3, Figure S3 and Figure S4). Yet, the low spatial resolution of the consecutive version can be illustrated by MS5 (Figure 3, Figure S3, Figure S4) that should represent M2 (Figure 1). This is probably due to the categorical version using the maximum number of available data points to generate their corresponding MS, whilst the consecutive version treats each temporal segment solely.

We suggest using the consecutive version where sequential order of MSs is interesting to investigate such as the tracking of cognitive tasks. When the temporal aspects are not necessary, we would recommend the categorical version.

## **Tracking of fast cognitive functions**

As many brain responses only last on the order of milliseconds to seconds, the brain dynamically reconfigures its functional network structure on sub-second temporal scales to guarantee efficient cognitive and behavioral functions<sup>37</sup>. Tracking the spatiotemporal dynamics of large scale networks over this short time duration is a very challenging issue<sup>11,17</sup>. In this paper, we aimed at examining how fast changes in the modular architecture shape the information processing and distribution in i) motor task and ii) picture naming task.

Concerning the self-paced motor task, it is a simple task where only motor areas are expected to be involved over time. Our results showed indeed that motor module is clearly elucidated related to the tactile movement of the button press. The spatial and the temporal features of the obtained module are very close to the significant component obtained by O'Neill et al.<sup>9</sup> using the temporal ICA method.

The different MSs obtained in the EEG picture naming task are temporally and spatially analogous to the network brain states detected using other approaches such as K-means clustering by<sup>8</sup>. In particular, the first MS representing the visual network is probably modulated

by the visual processing and recognition processes <sup>30,31</sup>. The second MS reflects the memory access reflected by the presence of the occipital-temporal connections <sup>38</sup>. In other words, the brain tries to retrieve the information related to the picture illustrated from the memory <sup>38</sup>. In the third and the fourth MSs, we notice the implication of a separated frontal module. This module may be related to the object category recognition (tools vs. animals) and the decision making process <sup>39–41</sup>. After taking the decision, the speech articulation and the naming process is prepared and started <sup>42</sup>. This is reflected by the MS5 that combines the frontal, the motor and the temporal brain areas.

## **Modular brain states and cognitive phenotypes in Parkinson's disease**

Emerging evidence show that Parkinson's disease (PD) is associated with alteration in structural and functional brain networks <sup>43</sup>. Hence, from a clinical perspective, the demand is high for a network-based technique to identify the pathological networks and to detect early cognitive decline in PD.

Here, we used a dataset with a large number (N=124) of PD patients categorized in three groups in term of their cognitive performance :G1- cognitively intact patients, G2- patients with mild to moderate cognitive deficits and G3- patients with severe cognitive deficits in all cognitive domains. See <sup>32,44,45</sup> for more information about this database.

The obtained MSs presented in Figure 7 show that while some MSs remain unchangeable during cognitive decline from G1 to G3, others are altered and replaced by new MS. More specifically, the number of MS detected in G3 has decreased compared to G1 and G2, MS3 in G1 was replaced by MS4 in G2 while MS4 in G2 was replaced by MS5 in G3. In addition, the alterations



in G3 involve more distributed modules (central, fronto-temporal) than the alterations occurring between G1 and G2 (fronto-temporal modules) where the impairment still moderate.

Interestingly, the underlying modular differences between the MSs of groups are consistent with the previously reported studies that explored the networks changes in PD<sup>32–34,36,46,47</sup>. Particularly, the loss of fronto-temporal connections in PD is supported by several EEG and MEG studies<sup>32,36,47</sup>. Similarly, results of structural MRI studies reveal frontal and temporal atrophies in PD with mild cognitive impairment<sup>33,34</sup>. Other functional<sup>35</sup> and structural<sup>36</sup> studies showed that Alzheimer’s disease networks are characterized by fronto-temporal alterations. In addition, the brain regions involved in the modular alterations in G3 found in our study are in line with findings obtained by EEG edge-wise analysis<sup>32</sup>, and by structural MRI studies showing widespread atrophy associated with PD patients related dementia<sup>34</sup>.

## **Methodological considerations**

First, we used a template anatomical image generated from MRIs of healthy controls for EEG/MEG source functional connectivity analysis. The template-based method is common practice in the absence of individual anatomical images and was previously employed by multiple EEG and MEG source reconstruction studies, because of non-availability of native MRIs<sup>5,32,48,49</sup>. Furthermore, a recent study showed that there are few potential biases introduced during the use of a template MRI compared to individual MRI co-registration

Second, the connectivity matrices in Dataset 3 (Parkinson’s disease analysis) were thresholded using a “proportional threshold” approach in contrast to other datasets (Picture naming and self-paced motor tasks) where a statistical threshold (FDR) approach was used (see Methods). The reason is that in dataset 3, three groups were analyzed and the proportional threshold approach, compared to other threshold approaches, ensures equal density between the analyzed groups<sup>50</sup>.

Moreover, studies suggests that FDR controlling procedures is effective for the analysis of neuroimaging data in the absence of inter-groups comparison<sup>25,51,52</sup>.

Third, in each dataset we adopted the same pipeline (from data processing to networks construction) used by the previous studies dealing with the same dataset. We did this to avoid influencing factors caused by changing the source connectivity method, the number of ROIs, the connectivity measure or the sliding window length. By relying on previous studies<sup>8,32,53</sup>, we provide appropriate input -already tested and validated - to the algorithm, regardless of how they were obtained.

## Methods

---

Our main objective is to develop a framework to track of the brain modules over time. We have developed two algorithm versions i) “categorical” where we aim to find the main modular structures over time, with no interest in their sequential order and ii) “consecutive” where the objective to find the modular structures in a successive way. The two versions are described hereafter.

### **Categorical version**

It includes four main steps:

- 1- Compute the dynamic functional connectivity matrices between the regional time-series using a sliding window approach<sup>7,11,17</sup>. Consequently, a weighted network is generated at each time window (Figure 1. A).
- 2- Decompose each network into modules (i.e clusters of nodes that are internally strongly connected, but externally weakly connected) (Figure 1. A). To do that, different

modularity algorithms were proposed in the literature <sup>23,54–56</sup>. In our study, we adopted the consensus clustering approach which was previously used in many studies <sup>7,25</sup>: Given an ensemble of partitions acquired from the Newman algorithm <sup>57</sup> and Louvain algorithm <sup>58</sup> repeated for 200 runs, an association matrix is obtained. This results in a  $N \times N$  matrix ( $N$  is the number of nodes) and an element  $A_{i,j}$  represents the number of times the nodes  $i$  and  $j$  are assigned to the same module across all runs and algorithms. The association matrix is then compared to a null model association matrix generated from a permutation of the original partitions, and only the significant values are retained <sup>25</sup>. To ultimately obtain consensus communities, we re-clustered the association matrix using Louvain algorithm.

- 3- Assess the similarity between the temporal modular structures (Figure 1. B). In this context, several methods have been suggested to compare community structures <sup>59</sup>. Here, we focused on the pair-counting method, which defines a similarity score by counting each pair of nodes drawn from the  $N$  nodes of a network according to whether the pair falls in the same or in different groups in each partition <sup>59</sup>. We considered the z-score of Rand coefficient, bounded between 0 (no similar pair placements) and 1 (identical partitions). This yield a  $T \times T$  similarity matrix where  $T$  is the number of time windows.
- 4- Cluster the similarity matrix into “categorical” modular states (MS) using the consensus clustering method (Figure 1. C). This step combine similar temporal modular structures in the same community. Hence, the association matrix of each “categorical” community is computed using the modular affiliations of its corresponding networks.

### Consecutive version:

The difference between the two versions of the algorithm is essentially in the fourth step, in which the final communities were defined. Particularly, the similarity matrix is segmented in a sequential way using the following steps:

- Threshold the similarity matrix using an automatic thresholding algorithm described in (Genovese et al) <sup>52</sup>. Briefly the matrix was converted into a  $p$ -value map which is then thresholded based on the false discovery rate (FDR) controlling.
- In order to get smoother presentation of the similarity matrix, a median filter is applied.
- Segment the matrix in a sequential way following the algorithm illustrated in the flowchart of Figure 8. In brief, the method group similar consecutive modular structures. As these modular structures show high similarity values with each other, the algorithm detect the squares located around the diagonal of the similarity matrix. As presented in Figure 8, the condition for which two consecutive structures are associated to the same state is the following:

$$S_{i,j} > \alpha$$

$$\text{Where } S_{i,j} = \sum_{k=0}^j a_{i+j,i+k} + \sum_{k=0}^j a_{i+k,i+j} - a_{i+j,i+j} \quad ; \quad i, j \in [1, T]$$

where  $a_{l,m}$  denotes the similarity value between the modular structure corresponding to the time window  $l$  and that corresponding to the time window  $m$ .

$\alpha$  is the “accuracy parameter”, strictly bounded between 0 and 1. It regulates the temporal-spatial accuracy of detected modular states. We recommend choosing an adaptive value of  $\alpha$ . In this paper, we choose  $\alpha$  equals to the average of the similarity matrix. A segment is considered as relevant if the number of included time-windows is greater than  $j_{min}$  (the minimal size allowed for a segment).

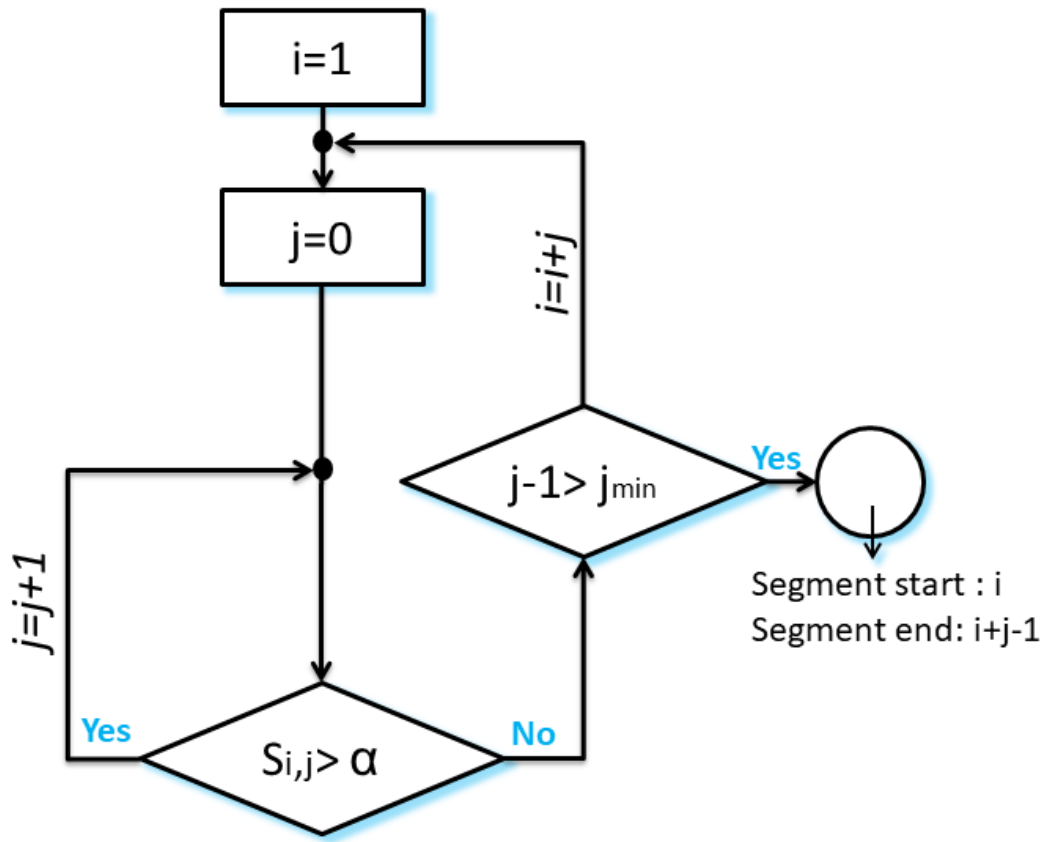


**Figure 8. The flowchart of the segmentation algorithm.**

The algorithm is illustrated in Figure 9. (I): starting with  $i = 1, j = 0$ ; and considering that  $a_{11}$  is lower than  $\alpha$ , we obtained  $S_{1,0} = a_{11} < \alpha$ , and the algorithm will move to the next time window  $i = 2$ . (II): as  $S_{2,0} = a_{22}$  is greater than  $\alpha$ ,  $j$  is incremented by 1. (III): having  $S_{2,1} = \frac{a_{23}+a_{23}+a_{33}}{3} > \alpha$ , the second and the third time windows are associated to the segment. (IV): the algorithm succeeded to add also the fourth time window as  $S_{2,2} = \frac{a_{24}+a_{42}+a_{34}+a_{43}+a_{44}}{5} > \alpha$ . (V): Then, for  $j = 3$ , we obtain  $S_{2,3} = \frac{a_{25}+a_{35}+a_{45}+a_{55}+a_{52}+a_{53}+a_{54}}{7} < \alpha$ . This means that the fifth time window differs from the previous windows in his modular structure. Afterwards, the algorithm moves toward finding another segment by incrementing  $i$  and repeating the process (IV).

- For each detected segment, the modular structure is obtained after computing the association matrix of the corresponding time windows modular affiliations.



Figure 9. An illustrative example describing the segmentation algorithm

## Simulated data

We simulated adjacency tensor data following the methodology applied in O'Neill et al.<sup>9</sup>. Briefly, four  $N \times N$  adjacency matrices  $P_j$  were constructed, where  $j \in [1,4]$  and  $N$  is the number of ROIs. We used an anatomical atlas of 221 ROIs with the mean of Desikan-Killiany atlas subdivided by Hagmann et al.<sup>60</sup>, yielding to  $N=221$ . The adjacency matrices and the 3D visualization of the networks are presented in Figure 2.A. Following this step, the time evolution of dynamic connectivity in each network is given by:

$$M_j(t) = a \cdot f_{1j}(t) + b \cdot f_{2j}(t)$$

$f_{1j}(t)$  is the modulation function, which was represented by Hanning window of unit amplitude.  $f_{2j}(t)$  represents uncorrelated Gaussian noise added to the simulated time-courses, and  $a$  and  $b$  are scalar values set to 0.45 and 0.15 as in O'Neill et al.<sup>9</sup>.

In our study,  $M_j(t)$  is sampled at  $3.3 \text{ Hz}$  (to obtain a sliding window of 0.3s as in real data). The onset as well as the duration of each module structure is illustrated in Figure 2.B. We then combined the four network matrices in order to generate single adjacency matrix at each time point  $t$  over a time-course spanning 60 seconds. As a final step, we added a random Gaussian noise to the adjacency tensor, and the standard deviation of the noise was allowed to vary between 0.2 and 0.5.

## Validation

On the simulated data, we evaluated the performance of the method by computing the similarity between the reconstructed and the simulated (reference) networks, taking into account both spatial and temporal similarities. The spatial similarity is given by the z-score of Rand coefficient between the simulated and the constructed modular structures, while the temporal similarity represents the rate of the correct affiliation of time windows.

## Real data

**Dataset 1- *Self paced motor task for healthy participants (MEG data)*:** Previously used in <sup>9,28,29</sup>, this dataset includes 15 participants (9 male, 6 female) asked to press a button using the index finger of their dominant hand, once every 30 seconds. Using a 275-channel CTF MEG system (MISL; Coquitlam, BC, Canada), MEG data were recorded at a sampling rate of 600Hz. MEG data were co-registered with a template MRI. The cortex was parcellated using the Desikan-Killiany atlas (68 regions). The pre-processing, the source reconstruction and the dynamic functional connectivity computations were performed similarly as in O'Neill et al. <sup>9</sup>. Briefly, the pre-processing comprises the exclusion of trials ( $t = -12s \rightarrow 12s$ ) contaminated by noise. Then, source time courses were reconstructed using a beamforming approach (please refer to <sup>9</sup> for more details). Afterwards, the regional time-series were symmetrically orthogonalized following the method proposed in <sup>61</sup> to remove the effects of “signal leakage”. The amplitude envelopes of the time courses were obtained using Hilbert transform. Finally, the dynamic connectivity was estimated by the Pearson correlation measure using a sliding window approach of 6 s of length. The sliding window was shifted by 0.5 s over time. The number of connectivity matrices obtained for each trial was then 49. The consecutive scheme of the proposed method was tested.

**Dataset 2- *Picture naming task for healthy participants (dense-EEG data)*:** Twenty one right-handed healthy subjects (11 women and 10 men), with no neurological disease participated in this study. In a session of about eight minutes, each participant was asked to name 148 displayed pictures on a screen using EPrime 2.0 software (Psychology Software Tools, Pittsburgh, PA) <sup>62</sup>. Oral responses were recorded to set the voice onset time. This study was approved by the National Ethics Committee for the Protection of Persons (CPP), *conneXion* study, agreement number (2012- A01227-36), and promoter: Rennes University Hospital. All participants provide



their written informed consent to participate in this study. A typical trial started with the appearance of an image during 3 sec followed by a jittered inter-stimulus interval of 2 or 3 sec randomly. Errors in naming were discarded from the analysis. A total of 2926 on 3108 events were considered.

Dense-EEG data were recorded using a system of 256 electrodes (EGI, Electrical Geodesic Inc.). EEGs were collected at 1 kHz sampling frequency and band-pass filtered between 3 and 45 Hz. The pre-processing and the computation of the functional connectivity followed the same pipeline applied in (Hassan et al.)<sup>8</sup>. In brief, each trial ( $t=0 \rightarrow 600\text{ms}$ ) was visually inspected, and epochs contaminated by eye blinks, muscle movements or other noise sources were rejected. As described in the previous study<sup>8</sup>, the source connectivity method was performed using the wMNE/PLV combination, and the dynamic functional connectivity was computed at each millisecond. Authors also used the Destrieux atlas sub-divided into 959 regions<sup>8</sup>. Finally, a tensor of dimension  $959 \times 959 \times 600$  was obtained and analyzed using the consecutive scheme of our algorithm.

**Dataset 3- *resting state in Parkinson's disease patients (dense-EEG data)*:** This dataset includes 124 patients with idiopathic Parkinson's disease defined according to the UK Brain Bank criteria for idiopathic Parkinson's disease<sup>63</sup>. These patients were separated into three groups: G1) cognitively intact patients (N=63), G2) patients with mild cognitive deficits (N=46) and G3) patients with severe cognitive impairment (N=15). All participants gave their informed consent to participation in the study, which had been approved by the local institutional review boards (CPP Nord-Ouest IV, 2012-A 01317-36, ClinicalTrials.gov Identifier: NCT01792843). Dense-EEG were recorded with a cap (Waveguard®, ANT software BV, Enschede, the Netherlands) with 122 scalp electrodes distributed according to the international system 10-05<sup>64</sup>. Electrodes

impedance was kept below 10 k $\Omega$ . Patients were asked to relax without performing any task. Signals were sampled at 512 Hz and band-pass filtered between 0.1 and 45 Hz.

The data were pre-processed according to (Hassan et al.)<sup>32</sup> dealing with the same dataset. Briefly, EOG artifact detection and correction was applied following the method developed in (Gratton et al)<sup>65</sup>. Afterwards, epochs with voltage fluctuation  $>+90$   $\mu$ V and  $<-90$   $\mu$ V were removed. For each participant, two artifact-free epochs of 40s lengths were selected. This epoch length was used previously and considered as a good compromise between the needed temporal resolution and the reproducibility of the results in resting state<sup>7</sup>.

To compute the dynamic functional connectivity, the steps adopted here are the same used in many previous studies<sup>7,32,48</sup>. First, EEG data were co-registered with a template MRI through identification of the same anatomical landmarks (left and right pre-auricular points and nasion). Second, the lead field matrix was computed for a cortical mesh with 15,000 vertices using OpenMEEG package<sup>66</sup> available in Brainstorm. The noise covariance was estimated using one minute resting segment. After that, the time-series of EEG sources were estimated using the wMNE algorithm where the regularization parameter was set according to the signal to noise ratio ( $\lambda=0.1$  in our analysis). An atlas-based segmentation approach was used to project EEGs onto an anatomical framework consisting of 68 cortical regions identified by means of Desikan-Killiany<sup>67</sup> atlas. The dynamic functional connectivity was then computed using a sliding window over which PLV was calculated<sup>68</sup>. In the previous study<sup>32</sup>, the disruptions of the functional connectivity were found in the alpha2 band (10-13 Hz). For this reason, we considered the same frequency band in our analysis. To obtain a sufficient number of cycles at the given frequency band, we chose the smallest window length that is equal to  $\frac{6}{\text{central frequency}}$  as recommended in (Lachaux et al)<sup>68</sup>. This yields to a sliding window of 0.52 s. We then adopted a

proportional threshold of 10% to remove spurious connections from the connectivity matrices. These steps produce, for each epoch, a connectivity tensor of dimension  $N \times N \times T$  where  $N$  is the number of ROIs (68 regions), and  $T$  is the number of time windows (77 time-windows). This tensor is formally equivalent to dynamic functional connectivity matrices, and was analyzed using the categorical version of the proposed algorithm.

## Author contributions

---

Conceptualization: A.K, M.H; Formal analysis: A.K, M.H, W.E.F.; Writing: A.K., M.H. and F.W; Funding Acquisition: F.W., M.K.; Resources: F.W, M.K.

## Acknowledgments

---

This work has received a French government support granted to the CominLabs excellence laboratory and managed by the National Research Agency in the "Investing for the Future" program under reference ANR-10-LABX-07-01. It was also financed by the Rennes University Hospital (COREC Project named *conneXion*, 2012-14). This work was financed by Azm center for research in biotechnology and its applications. GCO is funded by a Medical Research Council New Investigator Research Grant (MR/M006301/1).

## Additional information

---

Authors have no competing interests as defined by Nature Publishing Group, or other interests that might be perceived to influence the results and/or discussion reported in this paper.

# References

---

1. Pfurtscheller, G. & Lopes Da Silva, F. H. Event-related EEG/MEG synchronization and desynchronization: Basic principles. *Clinical Neurophysiology* **110**, 1842–1857 (1999).
2. Pfurtscheller, G. & Aranibar, A. Event-related cortical desynchronization detected by power measurements of scalp EEG. *Electroencephalogr. Clin. Neurophysiol.* **42**, 817–826 (1977).
3. Damaraju, E. *et al.* Dynamic functional connectivity analysis reveals transient states of dysconnectivity in schizophrenia. *NeuroImage Clin.* **5**, 298–308 (2014).
4. de Pasquale, F. *et al.* A Cortical Core for Dynamic Integration of Functional Networks in the Resting Human Brain. *Neuron* **74**, 753–764 (2012).
5. de Pasquale, F., Penna, S. Della, Sporns, O., Romani, G. L. & Corbetta, M. A Dynamic Core Network and Global Efficiency in the Resting Human Brain. *Cereb. Cortex* bhv185 (2015). doi:10.1093/cercor/bhv185
6. Baker, A. P. *et al.* Fast transient networks in spontaneous human brain activity. *Elife* **2014**, (2014).
7. Kabbara, A., Falou, W. E. L., Khalil, M., Wendling, F. & Hassan, M. The dynamic functional core network of the human brain at rest. *Sci. Rep.* **7**, 2936 (2017).
8. Hassan, M. *et al.* Dynamic reorganization of functional brain networks during picture naming. *Cortex* **73**, 276–288 (2015).
9. O'Neill, G. C. *et al.* Measurement of dynamic task related functional networks using MEG. *Neuroimage* **146**, 667–678 (2017).
10. Bola, M. & Sabel, B. A. Dynamic reorganization of brain functional networks during cognition. *Neuroimage* **114**, 398–413 (2015).
11. Hutchison, R. M. *et al.* Dynamic functional connectivity: Promise, issues, and interpretations. *Neuroimage* **80**, 360–378 (2013).
12. Nunez, P. L. & Srinivasan, R. Electroencephalogram. *Scholarpedia* **2**, 1348 (2007).
13. Cohen, D. Magnetoencephalography: Detection of the Brain's Electrical Activity with a Superconducting Magnetometer. *Science* (80-. ). **175**, 664–666 (1972).
14. Penfield, W. & Jasper, H. Epilepsy and the Functional Anatomy of the Human Brain. *JAMA J. Am. Med. Assoc.* **155**, 86–86 (1954).
15. Vidaurre, D. *et al.* Discovering dynamic brain networks from big data in rest and task. *NeuroImage* (2017). doi:10.1016/j.neuroimage.2017.06.077
16. Allen, E. A., Damaraju, E., Eichele, T., Wu, L. & Calhoun, V. D. EEG Signatures of Dynamic Functional Network Connectivity States. *Brain Topography* 1–16 (2017). doi:10.1007/s10548-017-0546-2
17. Allen, E. A. *et al.* Tracking whole-brain connectivity dynamics in the resting state. *Cereb. Cortex* **24**, 663–676 (2014).
18. Sporns, O. & Betzel, R. F. Modular Brain Networks. *Annu. Rev. Psychol.* **67**, 613–640 (2016).
19. Sporns, O. & Betzel, R. F. Modular Brain Networks. *Annu. Rev. Psychol.* **67**, 613–640 (2016).
20. Bassett, D. S. *et al.* Dynamic reconfiguration of human brain networks during learning. *Proc. Natl. Acad. Sci. U. S. A.* **108**, 7641–6 (2011).
21. Gallen, C. L. *et al.* Modular brain network organization predicts response to cognitive

- training in older adults. *PLoS One* **11**, (2016).
22. Newman, M. & Girvan, M. Finding and evaluating community structure in networks. *Phys. Rev. E* **69**, 1–16 (2004).
  23. Girvan, M. & Newman, M. E. J. Community structure in social and biological networks. *Proc. Natl. Acad. Sci.* **99**, 7821–7826 (2002).
  24. Bassett, D. S., Yang, M., Wymbs, N. F. & Grafton, S. T. Learning-Induced Autonomy of Sensorimotor Systems. *Nat. Neurosci.* **18**, 744–751 (2015).
  25. Bassett, D. S. *et al.* Robust detection of dynamic community structure in networks. *Chaos* **23**, (2013).
  26. Mucha, P. J., Richardson, T., Macon, K., Porter, M. A. & Onnela, J. P. Community structure in time-dependent, multiscale, and multiplex networks. *Science* (80-. ). **328**, 876–878 (2010).
  27. Bassett, D. S., Yang, M., Wymbs, N. F. & Grafton, S. T. Learning-induced autonomy of sensorimotor systems. *Nat. Neurosci.* **18**, 744–751 (2015).
  28. Vidaurre, D. *et al.* Spectrally resolved fast transient brain states in electrophysiological data. *Neuroimage* **126**, 81–95 (2016).
  29. O'Neill, G. C. *et al.* Dynamic recruitment of resting state sub-networks. *Neuroimage* **115**, 85–95 (2015).
  30. Thorpe, S., Fize, D. & Marlot, C. Speed of processing in the human visual system. *Nature* **381**, 520–522 (1996).
  31. VanRullen, R. & Thorpe, S. J. The Time Course of Visual Processing: From Early Perception to Decision-Making. *J. Cogn. Neurosci.* **13**, 454–461 (2001).
  32. Hassan, M. *et al.* Functional connectivity disruptions correlate with cognitive phenotypes in Parkinson's disease. *NeuroImage Clin.* **14**, 591–601 (2017).
  33. Beyer, M. K., Janvin, C. C., Larsen, J. P. & Aarsland, D. A magnetic resonance imaging study of patients with Parkinson's disease with mild cognitive impairment and dementia using voxel-based morphometry. *J Neurol Neurosurg Psychiatry* **78**, 254–259 (2007).
  34. Song, S. K. *et al.* The pattern of cortical atrophy in patients with Parkinson's disease according to cognitive status. *Mov. Disord.* **26**, 289–296 (2011).
  35. De Haan, W. *et al.* Disrupted modular brain dynamics reflect cognitive dysfunction in Alzheimer's disease. *Neuroimage* **59**, 3085–3093 (2012).
  36. Zhang, Y. *et al.* White matter damage in frontotemporal dementia and Alzheimer's disease measured by diffusion MRI. *Brain* **132**, 2579–92 (2009).
  37. O'Neill, G. C. *et al.* Dynamics of large-scale electrophysiological networks: A technical review. *NeuroImage* (2017). doi:10.1016/j.neuroimage.2017.10.003
  38. Martin, A. & Chao, L. L. Semantic memory and the brain: structure and processes. *Curr. Opin. Neurobiol.* **11**, 194–201 (2001).
  39. Rushworth, M. F. S., Noonan, M. A. P., Boorman, E. D., Walton, M. E. & Behrens, T. E. Frontal Cortex and Reward-Guided Learning and Decision-Making. *Neuron* **70**, 1054–1069 (2011).
  40. Andersen, R. A. & Cui, H. Intention, Action Planning, and Decision Making in Parietal-Frontal Circuits. *Neuron* **63**, 568–583 (2009).
  41. Clark, L. & Manes, F. Social and emotional decision-making following frontal lobe injury. *Neurocase* **10**, 398–403 (2004).
  42. Dronkers, N. F. A new brain region for coordinating speech articulation. *Nature* **384**, 159–161 (1996).

43. Fornito, A., Zalesky, A. & Breakspear, M. The connectomics of brain disorders. *Nature Reviews Neuroscience* **16**, 159–172 (2015).
44. Dujardin, K. *et al.* Cognitive disorders in Parkinson's disease: Confirmation of a spectrum of severity. *Park. Relat. Disord.* **21**, 1299–1305 (2015).
45. Lopes, R. *et al.* Cognitive phenotypes in parkinson's disease differ in terms of brain-network organization and connectivity. *Hum. Brain Mapp.* **38**, 1604–1621 (2017).
46. Haan, W. de & Pijnenburg, Y. Functional neural network analysis in frontotemporal dementia and Alzheimer's disease using EEG and graph theory. *BMC Neurosci.* **10**, 101 (2009).
47. Bosboom, J. L. W., Stoffers, D., Wolters, E. C., Stam, C. J. & Berendse, H. W. MEG resting state functional connectivity in Parkinson's disease related dementia. *J. Neural Transm.* **116**, 193–202 (2009).
48. Kabbara, A. *et al.* Reduced integration and improved segregation of functional brain networks in Alzheimer's disease. *J. Neural Eng.* **15**, (2018).
49. Lopez, M. E. *et al.* Alpha-Band Hypersynchronization in Progressive Mild Cognitive Impairment: A Magnetoencephalography Study. *J. Neurosci.* **34**, 14551–14559 (2014).
50. van den Heuvel, M. P. *et al.* Proportional thresholding in resting-state fMRI functional connectivity networks and consequences for patient-control connectome studies: Issues and recommendations. *Neuroimage* **152**, 437–449 (2017).
51. Patel, A. X. & Bullmore, E. T. A wavelet-based estimator of the degrees of freedom in denoised fMRI time series for probabilistic testing of functional connectivity and brain graphs. *Neuroimage* **142**, 14–26 (2016).
52. Genovese, C. R., Lazar, N. A. & Nichols, T. Thresholding of statistical maps in functional neuroimaging using the false discovery rate. *Neuroimage* **15**, 870–878 (2002).
53. O'Neill, G. C. *et al.* Measurement of Dynamic Task Related Functional Networks using MEG. *Neuroimage* **in press**, (2016).
54. Duch, J. & Arenas, A. Community detection in complex networks using extremal optimization. *Phys. Rev. E* **72**, 27104 (2005).
55. Blondel, V. D., Guillaume, J. L., Lambiotte, R. & Lefebvre, E. Fast unfolding of communities in large networks. *J. Stat. Mech. Theory Exp.* **2008**, (2008).
56. Guimerà, R. & Amaral, L. A. N. Functional cartography of complex metabolic networks. *Nature* **433**, 895–900 (2005).
57. Girvan, M. & Newman, M. E. J. Community structure in social and biological networks. *Proc. Natl. Acad. Sci. U. S. A.* **99**, 7821–6 (2002).
58. Blondel, V. D., Guillaume, J.-L., Lambiotte, R. & Lefebvre, E. Fast unfolding of communities in large networks. *J. Stat. Mech. Theory Exp.* **10008**, 6 (2008).
59. Traud, A. L., Kelsic, E. D., Mucha, P. J. & Porter, M. A. Comparing Community Structure to Characteristics in Online Collegiate Social Networks. **53**, 526–543 (2008).
60. Hagmann, P. *et al.* Mapping the structural core of human cerebral cortex. *PLoS Biol.* **6**, 1479–1493 (2008).
61. Colclough, G. L., Brookes, M. J., Smith, S. M. & Woolrich, M. W. A symmetric multivariate leakage correction for MEG connectomes. *Neuroimage* **117**, 439–448 (2015).
62. Schneider, W., Eschman, a & Zuccolotto, a. E-Prime reference guide. *Psychol. Softw. Tools* **3**, 1 (2002).
63. Gibb, W. R. G. & Lees, A. J. The relevance of the Lewy body to the pathogenesis of idiopathic Parkinson's disease. *Journal of Neurology, Neurosurgery and Psychiatry* **51**,

- 745–752 (1988).
64. Oostenveld, R. & Praamstra, P. The five percent electrode system for high-resolution EEG and ERP measurements. *Clin. Neurophysiol.* **112**, 713–719 (2001).
  65. Gratton, G., Coles, M. G. H. & Donchin, E. A new method for off-line removal of ocular artifact. *Electroencephalogr. Clin. Neurophysiol.* **55**, 468–484 (1983).
  66. Gramfort, A., Papadopoulos, T., Olivi, E. & Clerc, M. OpenMEEG: opensource software for quasistatic bioelectromagnetics. *Biomed. Eng. Online* **9**, 45 (2010).
  67. Desikan, R. S. *et al.* An automated labeling system for subdividing the human cerebral cortex on MRI scans into gyral based regions of interest. *Neuroimage* **31**, 968–980 (2006).
  68. Lachaux, J. P., Rodriguez, E., Martinerie, J. & Varela, F. J. Measuring phase synchrony in brain signals. *Hum. Brain Mapp.* **8**, 194–208 (1999).

# Supplementary materials

---

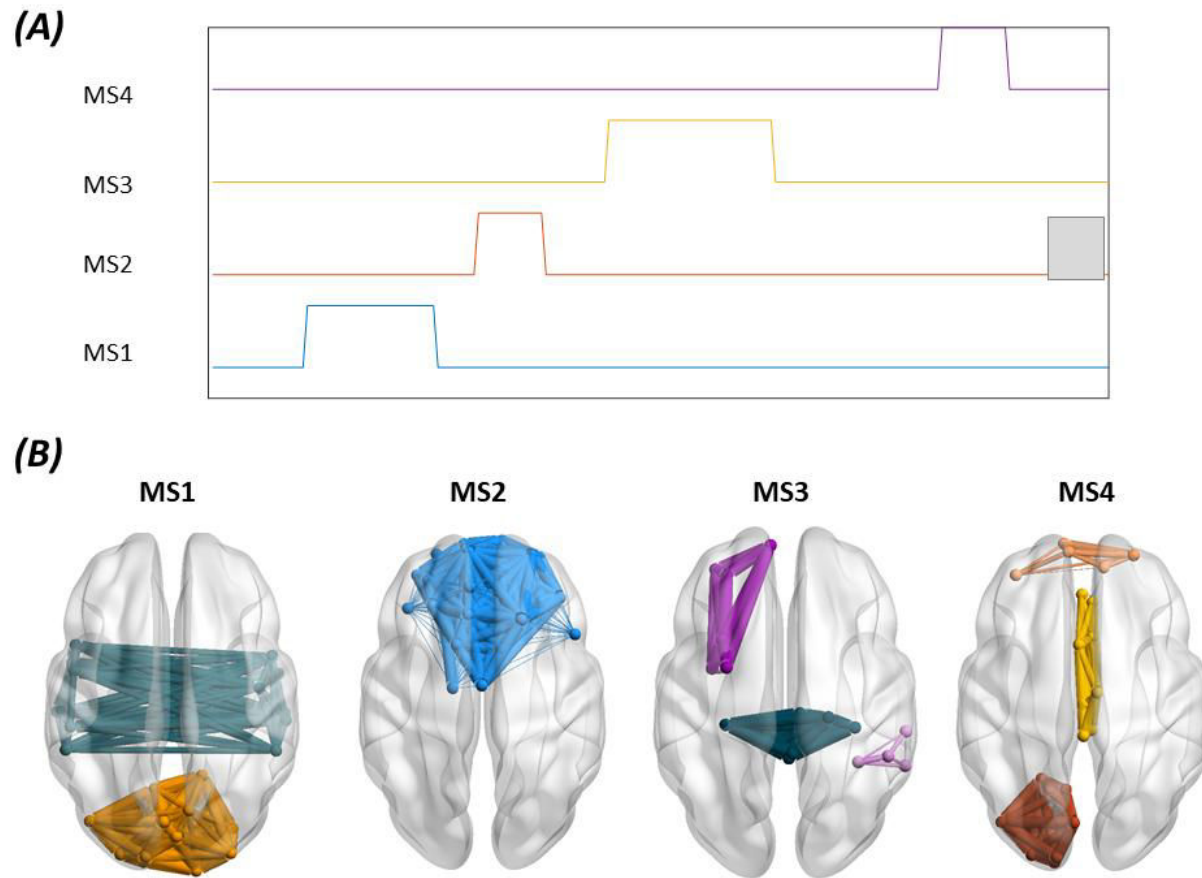
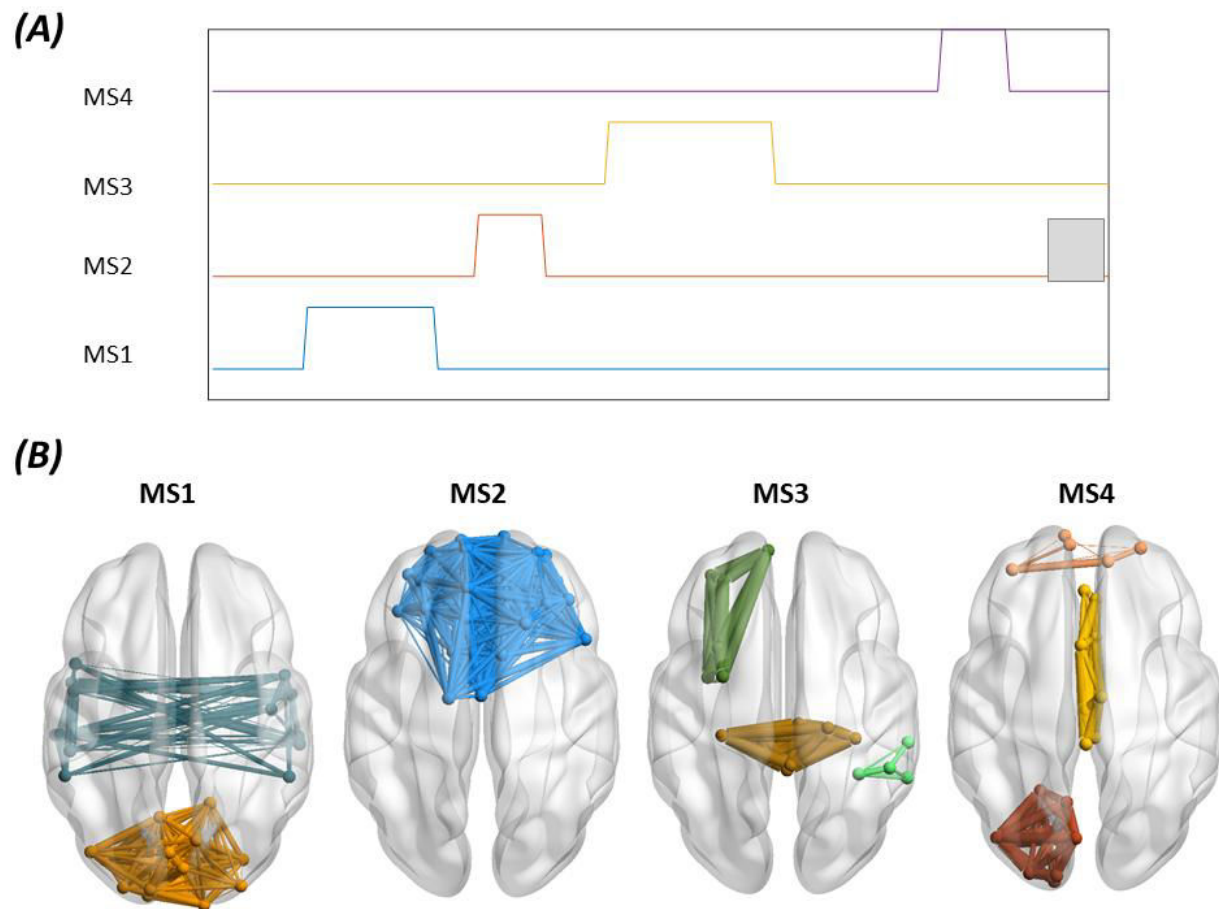
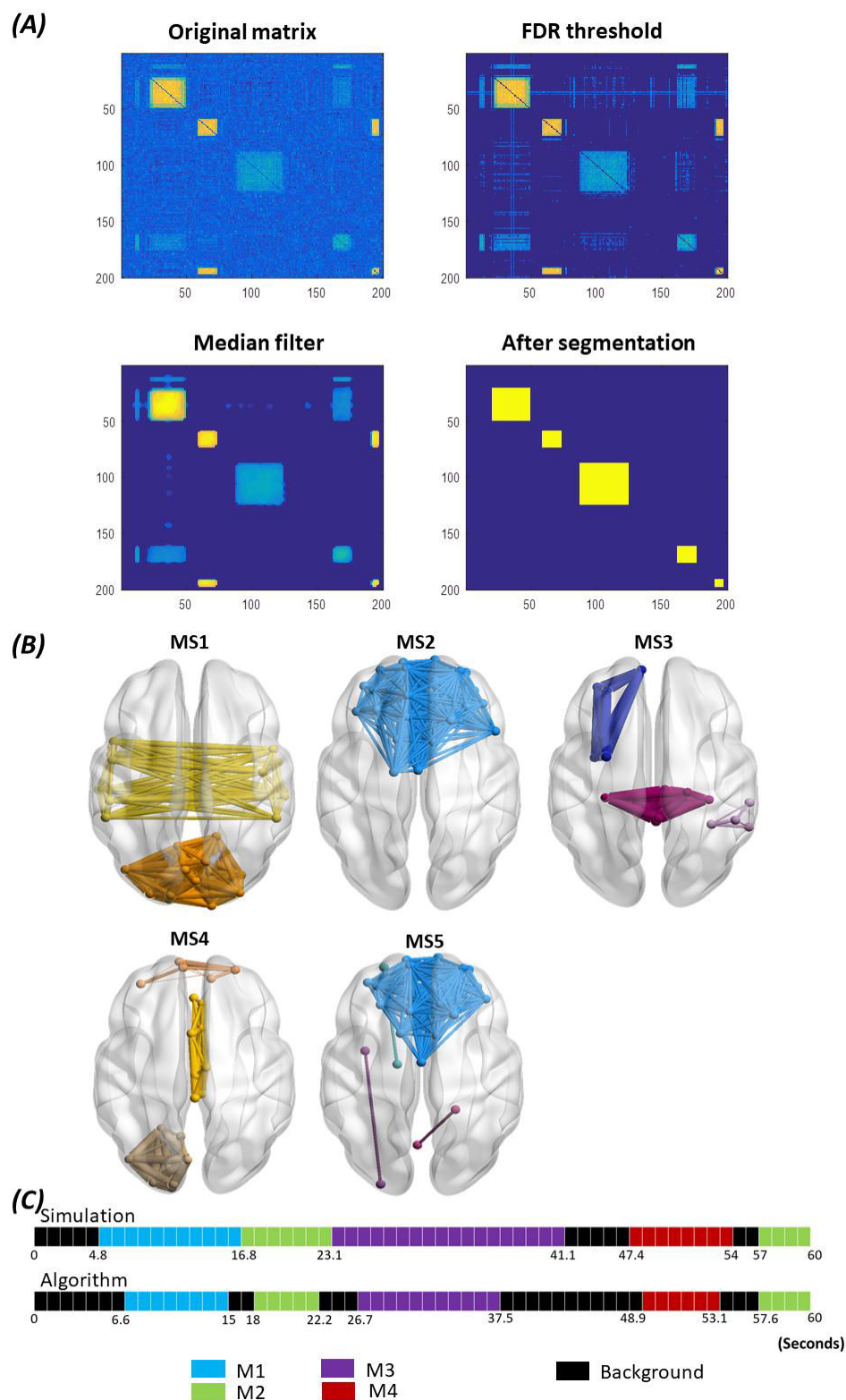


Figure 1. Results of the categorical method applied on simulated data ( $STD_{noise} = 0.35$ ). A) the time course of the four modular structures reconstructed. The grey square indicates the missed time-window detection. B) 3D representation of the four modular structures states.





**Figure 2. Results of the categorical method applied on simulated data ( $STD_{noise} = 0.5$ ). A) the time course of the four modular structures reconstructed. The grey square indicates the missed time-window detection. B) 3D representation of the four modular structures states.**



**Figure 3. Results of the consecutive method applied on simulated data ( $STD_{noise} = 0.35$ ). A) The different steps of the segmentation algorithm that ended to find 5 modular structures. B) The 3D representation of the six consecutive modular structures obtained. C) The difference between the simulated time axis and the obtained time axis.**

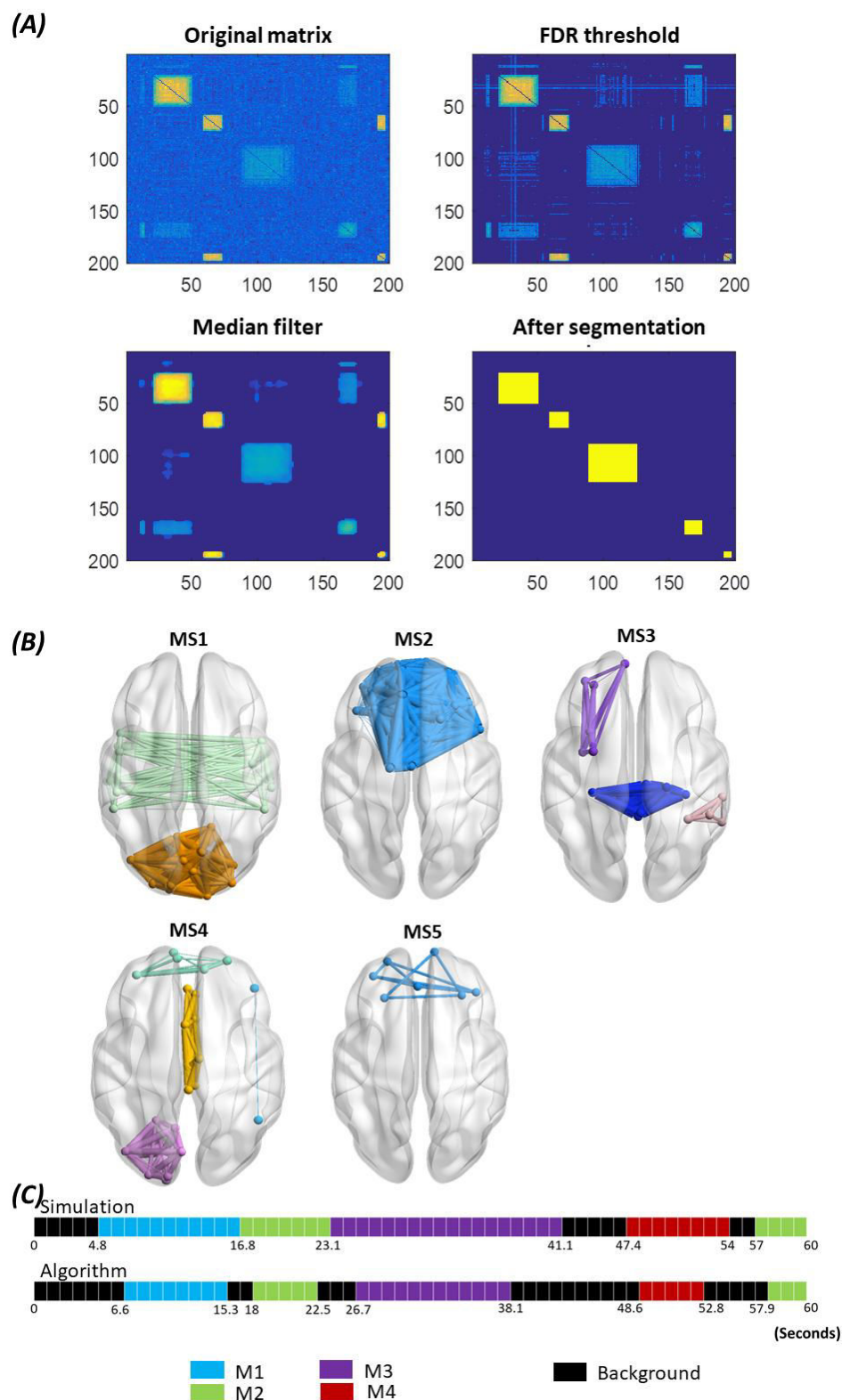


**Figure 4.** Results of the consecutive method applied on simulated data ( $STD_{noise} = 0.5$ ). **A)** The different steps of the segmentation algorithm that ended to find 5 modular structures. **B)** The 3D representation of the six consecutive modular structures obtained. **C)** The difference between the simulated time axis and the obtained time axis.